Université de Montréal

Kinesin-13, Tubulins and Their New Roles in DNA Damage Repair

Par

Mohammadjavad Paydar

Programme de Biologie Moléculaire, option Biologie des Systèmes

Faculté de Médecine

Thèse présentée en vue de l'obtention du grade de Philosophiae Doctor (Ph. D.)

en Biologie Moléculaire, option Biologie des Systèmes

December 2021

Université de Montréal

Faculté de Médecine

Cette thèse intitulée

Kinesin-13, Tubulins and Their New Roles in DNA Damage Repair

Présentée par

Mohammadjavad Paydar

A été évalué(e) par un jury composé des personnes suivantes

Laura Hulea
Président-rapporteur

Pascal Chartrand
Membre du jury

Greg Fitzharris
Représentant du doyen

Alexandre Orthwein
Examinateur externe

Benjamin H Kwok
Directeur de recherche

RÉSUMÉ

Les microtubules sont de longs polymères cylindriques de la protéine α, β tubuline, utilisés dans les cellules pour construire le cytosquelette, le fuseau mitotique et les axonèmes. Ces polymères creux sont cruciaux pour de nombreuses fonctions cellulaires, y compris le transport intracellulaire et la ségrégation chromosomique pendant la division cellulaire. Au fur et à mesure que les cellules se développent, se divisent et se différencient, les microtubules passent par un processus, appelé instabilité dynamique, ce qui signifie qu'ils basculent constamment entre les états de croissance et de rétrécissement. Cette caractéristique conservée et fondamentale des microtubules est étroitement régulée par des familles de protéines associées aux microtubules. Les protéines de kinésine-13 sont une famille de facteurs régulateurs de microtubules qui dépolymérisent catalytiquement les extrémités des microtubules.

Cette thèse traite d'abord des concepts mécanistiques sur le cycle catalytique de la kinésine-13. Afin de mieux comprendre le mécanisme moléculaire par lequel les protéines de kinésine-13 induisent la dépolymérisation des microtubules, nous rapportons la structure cristalline d'un monomère de kinésine-13 catalytiquement actif (Kif2A) en complexe avec deux hétérodimères αβ-tubuline courbés dans un réseau tête-à-queue. Nous démontrons également l'importance du « cou » spécifique à la classe de kinésine-13 dans la dépolymérisation catalytique des microtubules. Ensuite, nous avons cherché à fournir la base moléculaire de l'hydrolyse tubuline-guanosine triphosphate (GTP) et son rôle dans la dynamique des microtubules. Dans le modèle que nous présentons ici, l'hydrolyse tubuline-GTP pourrait être déclenchée par les changements conformationnels induits par les protéines kinésine-13 ou par l'agent chimique stabilisant paclitaxel. Nous fournissons également des preuves biochimiques montrant que les changements

conformationnels des dimères de tubuline précèdent le renouvellement de la tubuline-GTP, ce qui indique que ce processus est déclenché mécaniquement.

Ensuite, nous avons identifié la kinésine de microtubule Kif2C comme une protéine associée à des modèles d'ADN imitant la rupture double brin (DSB) et à d'autres protéines de réparation DSB connues dans les extraits d'œufs de Xenope et les cellules de mammifères. Les cassures double brin d'ADN (DSB) sont un type majeur de lésions d'ADN ayant les effets les plus cytotoxiques. En raison de leurs graves impacts sur la survie cellulaire et la stabilité génomique, les DSB d'ADN sont liés à de nombreuses maladies humaines, y compris le cancer. Nous avons constaté que les activités PARP et ATM étaient toutes deux nécessaires pour le recrutement de Kif2C sur les sites de réparation de l'ADN. Kif2C knockout ou inhibition de son activité de dépolymérisation des microtubules a conduit à l'hypersensibilité des dommages à l'ADN et à une réduction de la réparation du DSB via la jonction terminale non homologue et la recombinaison homologue.

Dans l'ensemble, notre modèle suggère que les protéines de kinésine-13 peuvent interagir avec les dimères de tubuline aux extrémités microtubules et modifier leurs conformations, moduler l'étendue des extrêmités tubuline-GTP dans les cellules et déclencher le désassemblage des microtubules. Ces deux modèles pourraient être des clés pour démêler les mécanismes impliqués dans le nouveau rôle de Kif2C dans la réparation de l'ADN DSB sans s'associer à des polymères de microtubules.

Mots-clés: microtubule, tubuline, hydrolyse du GTP, protéines motrices, kinésine-13, Kif2A, MCAK, KIF2C, paclitaxel, cassure double brin de l'ADN, réparation des lésions de l'ADN, foyers de cassure double brin de l'ADN, mobilité, dynamique.

ABSTRACT

Microtubules are long, cylindrical polymers of the proteins α, β tubulin, used in cells to construct the cytoskeleton, the mitotic spindle and axonemes. These hollow polymers are crucial for many cellular functions including intracellular transport and chromosome segregation during cell division. As cells grow, divide, and differentiate, microtubules go through a process, called dynamic instability, which means they constantly switch between growth and shrinkage states. This conserved and fundamental feature of microtubules is tightly regulated by families of microtubule-associated proteins (MAPs). Kinesin-13 proteins are a family of microtubule regulatory factors that catalytically depolymerize microtubule ends.

This thesis first discusses mechanistic insights into the catalytic cycle of kinesin-13. In order to better understand the molecular mechanism by which kinesin-13 proteins induce microtubule depolymerization, we report the crystal structure of a catalytically active kinesin-13 monomer (Kif2A) in complex with two bent αβ-tubulin heterodimers in a head-to-tail array. We also demonstrate the importance of the kinesin-13 class-specific "neck" in modulating Adenosine triphosphate (ATP) turnover and catalytic depolymerization of microtubules.

Then, we aimed to provide the molecular basis for tubulin-Guanosine triphosphate (GTP) hydrolysis and its role in microtubule dynamics. Although it has been known for decades that tubulin-GTP turnover is linked to microtubule dynamics, its precise role in the process and how it is driven are now well understood. In the model we are presenting here, tubulin-GTP hydrolysis could be triggered via the conformational changes induced by kinesin-13 proteins or by the stabilizing chemical agent paclitaxel. We also provide biochemical evidence showing that conformational changes of tubulin dimers precedes the tubulin-GTP turnover, which indicates that this process is triggered mechanically.

Next, we identified microtubule kinesin Kif2C as a protein associated with double strand break (DSB)-mimicking DNA templates and other known DSB repair proteins in *Xenopus* egg extracts and mammalian cells. DNA double strand breaks (DSBs) are a major type of DNA lesions with the most cytotoxic effects. Due to their sever impacts on cell survival and genomic stability, DNA DSBs are related to many human diseases including cancer. Here we found that PARP and ATM activities were both required for the recruitment of Kif2C to DNA repair sites. Kif2C knockdown/knockout or inhibition of its microtubule depolymerizing activity led to accumulation of endogenous DNA damage, DNA damage hypersensitivity, and reduced DSB repair via both non-homologous end-joining (NHEJ) and homologous recombination (HR). Interestingly, genetic depletion of KIF2C, or inhibition of its microtubule depolymerase activity, reduced the mobility of DSBs, impaired the formation of DNA damage foci, and decreased the occurrence of foci fusion and resolution.

Altogether, our findings shed light on the mechanisms involved in kinesin-13 catalyzed microtubule depolymerization. Our tubulin-GTP hydrolysis model suggests that kinesin-13 proteins may interact with tubulin dimers at microtubules ends and alter their conformations, modulate the extent of the GTP caps in cells and trigger microtubule disassembly. These two models could be keys to unravel the mechanisms involved in the novel role of Kif2C in DNA DSB repair without associating with microtubule polymers.

Keywords: microtubule, tubulin, GTP hydrolysis, motor proteins, kinesin-13, Kif2A, MCAK, KIF2C, paclitaxel, DNA double strand break, DNA damage repair, DNA DSB foci, mobility, dynamics

To Marie-Eve, with whom I recovered my true self

Not everything that can be counted counts, and not everything that counts can be counted.
Albert Einstein

ACKNOWLEDGEMENTS

First and foremost, I would like to thank my supervisor, Dr. Benjamin Kwok, for his patience, motivations and outstanding mentorship. His tireless answering of all my questions helped me a lot and made my PhD studies a great experience.

I also thank Dr. Sebastien Carreno, the member of my Supervisory Committee, for extending his full support whenever I required it. I am extremely grateful too, to Dr. Alexandre Orthwein, another member of my Thesis Committee, who helped shaping my project with his priceless comments. I would like to thank Dr. William Tsang and Dr. Alisa Piekny for their constructive advice during my committee meetings and qualification exam. I would also thank Dr. Julie Mantovani, Pascale Le Thérizien and Lucie Yan Liu for their contributions and follow-ups during the past five years.

Finally, I offer my deepest gratitude to my beloved wife, Marie-Eve for all her supports and encouragements. I thank William, who was constantly checking on my wellness during my thesis preparation. I also thank Evan, for his love and heartening words. Last but not least, I offer my thanks to my loving mother who has always been there for me, and I dedicate this thesis to my father, who I unfortunately lost recently.

TABLE OF CONTENT

RÉSUMÉ 3
ABSTRACT 5
ACKNOWLEDGEMENTS 9
TABLE OF CONTENT 10
LIST OF TABLES 14
LIST OF FIGURES 15
LIST OF ABREVIATIONS 16
CHAPTER 1. Introduction 18
1.1 Microtubules 18
1.1.1 MT polymerization and depolymerization dynamics 19
1.1.2 Tubulin guanosine triphosphate (GTP) hydrolysis & its relationship with MT polymerization 19
1.1.3 GTP cap and MT stability 21
1.1.4 Study of MT polymerization: the use of nucleotide analogs 22
1.1.5 Study of MT polymerization: the use of chemical stabilizing/destabilizing agents 23
1.1.6 MT poisons as cancer therapeutics 25
1.1.7 Structural study of tubulin/MT: The use of Antibody-Like engineered Polypeptides 26
1.2 MT dynamic instability in cells and Microtubule associated proteins 27
1.2.1 Kinesins 28
1.2.2 Kinesin-13 proteins and ATP-dependent catalytic depolymerization of MTs 31
1.2.3 Study of Kinesin-13 driven MT depolymerization: the use of ATP analogs 32
1.2.4 Kinesin-13 class specific neck and MT depolymerization 33
1.2.5 KIF2C and its roles during cell cycle 33
1.3 MT, Kinesin-13, DNA damage response (DDR) 34
1.3.1 DNA double strand break (DSB) and different repair mechanisms 36
1.3.2 Models to study HR & NHEJ repair mechanisms in cells 37
1.3.3 p53 & DDR 38
1.3.4 PARP1 and ATM in DNA repair mechanism 41
1.3.5 Possible involvements of microtubules and MAPs in DDR 43
1.4 Hypothesis & objectives 45

CHAPTER 2: Ternary complex of Kif2A-bound tandem tubulin heterodimers represents a kinesin-13-mediated microtubule depolymerization reaction intermediate 46
2.1. AUTHOR CONTRIBUTION 47
2.2 ABSTRACT 48
2.3 INTRODUCTION 49
2.4 RESULTS 53
2.4.1 Structure of the Kif2A-NM−tubulin tetramer complex 53
2.4.2 Interactions of the Kif2A neck with tubulin 59
2.4.3 Movement of the longitudinal tubulin interface 60
2.4.4 Conformation of the tubulin-bound Kif2A motor domain 63
2.4.5 Curvature of the Kif2A-NM-bound tubulin oligomer 66
2.4.6 ATP turnovers are modulated by neck binding to tubulin 69
2.4.7 microtubule-stimulated ATP turnover and tubulin disassembly 70
2.5 DISCUSSION 76
2.6 METHODS 80
2.6.1 Protein expression and purification 80
2.6.2 Kif2A-NM-tubulin-DARPin complex formation 82
2.6.3 Analytical size-exclusion chromatography 82
2.6.4 microtubule depolymerization assay 83
2.6.5 ATPase activity assay 83
2.6.6 Crystallization and X-ray structure determination 84
2.6.7 SEC-SAXS Data Collection and Analysis 85
2.7 Data availability 86
2.8 Acknowledgements 87
2.9 Competing interests 87
2.10 Supplementary Information 88
CHAPTER 3: Evidence for conformational change-induced hydrolysis of β-tubulin-GTP 104
3.1 AUTHOR CONTRIBUTION 105
3.2 ABSTRACT 106
3.3 INTRODUCTION 107
3.3.2 GTP cap and microtubule stability. 109
3.3.3 Microtubule dynamics in cells. 110
3.4 RESULTS 112
3.4.1 Tubulin-GTP hydrolysis can be triggered by binding and unbinding of kinesin-13 proteins. 112

3.4.2 Tubulin-GTP hydrolysis occurs via catalytic microtubule depolymerization by kinesin-13s, but not by non-catalytic means. 115
3.4.3 Interdependent relationship between kinesin-13 ATPase rate and tubulin-GTP turnovers 119
3.4.4 Conformational change-induced tubulin-GTP hydrolysis during microtubule polymerization. 124
3.4.5 Evidence for tubulin-GTP at microtubule ends – the "GTP Cap". 125
3.4.6 A model for conformational change driven tubulin-GTP hydrolysis. 132
3.5 DISCUSSION 135
3.6 MATERIALS AND METHODS 140
3.6.1 Materials 140
3.6.2 Microtubule Polymerization 140
3.6.3 Tubulin / Kinesin-13 mediated nucleotide hydrolysis assays 141
3.6.4 Nucleotide hydrolysis detection methods 142
3.6.5 Tubulin-Kinesin-13 Binding Assay 145
3.6.6 Negative staining of MTs by Transmission Electron Microscopy (TEM) 146
3.7 Acknowledgement 147
3.8 Declaration of Interests 147
3.9 SUPPLEMENTARY INFORMATION 148
CHAPTER 4: Kinesin Kif2C in Regulation of DNA Double Strand Break Dynamics and Repair 163
4.1 AUTHOR CONTRIBUTION 164
4.2 ABSTRACT 165
4.3 eLife Digest 166
4.4 INTRODUCTION 168
4.5 RESULTS 170
4.5.1 Kif2C associates with DSB-mimicking substrates and DNA repair proteins. 170
4.5.2 Kif2C undergoes two-stage recruitment to DNA damage sites. 172
4.5.3 Kif2C depletion or inhibition leads to accumulation of endogenous DNA damage. 177
4.5.4 Kif2C is required for efficient DSB repair via both HR and NHEJ. 181
4.5.5 Kif2C mediates the movement of DSBs, and the formation, fusion, and resolution of DNA damage foci 183
4.5.6 PARP1 and ATM regulate DSB dynamics largely via Kif2C. 188
4.6 DISCUSSION 191
4.6.1 Kif2C is a new player of the DNA damage response. 191
4.6.2 Kif2C mediates the mobility of DSBs, and the formation of DNA damage foci. 192

4.6.3 The emerging role of microtubule dynamics in DNA repair. 193
4.7 MATERIALS AND METHODS 196
4.7.1 Cell Culture, transfection and treatment 196
4.7.2 Cloning and mutagenesis 196
4.7.3 DNA binding assay 197
4.7.4 HR and NHEJ assays 197
4.7.5 Immunoblotting 198
4.7.6 Immunofluorescence and imaging 198
4.7.7 Microscopic analysis of DNA damage foci mobility and dynamics 199
4.7.8 Pull-down assay 200
4.7.9 Single cell gel electrophoresis (comet assay) 200
4.7.10 Xenopus egg extracts 200
4.8 ACKNOWLEDGEMENT 202
4.9 DECLARATION OF INTERESTS 202
4.10 SUPPLEMENTARY INFORMATION 203
CHAPTER 5. Discussion 217
5.1 Relationship between tubulin conformational change and GTP hydrolysis. 217
5.2 Conformational change-driven tubulin-GTP hydrolysis also occurs during MT polymerization 219
5.3 Implications of the newly discovered role of KIF2C inside the cell nucleus. 221
5.4 Possible roles of KIF2C in DNA DSB foci mobility and DNA damage repair 223
5.5 Concluding Remarks 225
REFERENCES 228

LIST OF TABLES

Table S 2.1 BioSAXS data collection and scattering-derived parameters. 102

Table 3.1 Stoichiometric and Interdependent relationship between Kinesin-13 ATPase rates and β-tubulin-GTP turnover rates..... 122

LIST OF FIGURES

Figure 1.1 Microtubule stabilizing and destabilizing agents, their effects on microtubule dynamics and their tubulin-binding sites.....24
Figure 1.2 Architecture of kinesins.....29
Figure 1.3 Association of KIF genes to different functions and relation to birth defect or monogenic phenotype groups.....30
Figure 1.4 Domain composition and structure of kinesin-13 KIF2C.....31
Figure 1.5 Overview of the DDR and p53 functional roles.....39
Figure 1.6 Interaction of 53BP1 and BRCA1 in repair pathway choice.....40
Figure 1.7 A model for the role of ALC1 in olaparib-mediated synthetic lethality.....42

Figure 2.1 Functional analysis of Kif2A constructs.....55
Figure 2.2 Structure of Kif2A-NM in complex with tubulin and DARPin.....58
Figure 2.3 Kif2A neck and loop 2 interactions with tubulin.....62
Figure 2.4 Conformation of the Kif2A motor domain.....65
Figure 2.5 Curvature and rotational displacement of tubulin induced by Kif2A-NM.....69
Figure 2.6 Microtubule-stimulated ATPase and microtubule-depolymerizing activities of kinesin-13s.....72
Figure 2.7 Nucleotide-dependent effect of DARPin on microtubule depolymerization by kinesin-13.....75

Figure 3.1 Binding dynamics of the Kinesin-13 KIF2A with tubulin dimers trigger β-tubulin-GTP hydrolysis.....114
Figure 3.2 Kinesin-13 mediated microtubule depolymerization, unlike non-catalytically induced depolymerization, triggers tubulin-GTP hydrolysis.....118
Figure 3.3 Stoichiometric relationship between kinesin-13 ATPase activity and the induced β-tubulin-GTP turnover.....123
Figure 3.4 Conformational change of tubulin dimers precedes GTP hydrolysis as they incorporate into microtubule polymers.....127
Figure 3.5 The level of GTP-bound tubulin dimers incorporation into microtubule polymers is directly proportional to the number of polymerizing microtubule ends.....131
Figure 3.6 A model of conformational change-driven β-tubulin-GTP hydrolysis.....134

Figure 4.1 Kif2C associates with DNA double strands breaks and DNA repair proteins.....171
Figure 4.2 Kif2C is recruited to DNA damage sites in a two-stage manner.....175
Figure 4.3 Kif2C suppression leads to accumulation of endogenous DNA damage and DNA damage hypersensitivity.....179
Figure 4.4 Kif2C is required for DNA double strand break repair.....183
Figure 4.5 Kif2C mediates DNA double strand break mobility and foci dynamics.....187
Figure 4.6 ATM and PARP inhibition impairs Kif2C-dependent foci mobility.....190

LIST OF ABREVIATIONS

53BP1	P53-Binding Protein 1
ADP	Adenosine DiPhosphate
AMPPNP	Adenosine5′-([β,γ]-imido)triphosphate
APTX	Aprataxin
ATM	Ataxia Telangiectasia Mutated
ATP	Adenosine TriPhosphate
bp	Base pair
DDR	DNA Damage Response
DLS	Dynamic Light Scattering
DSB	Double Strand Break
EB1	End-Binding Protein 1
EM	Electron Microscopy
G1	Gap 1 phase
G2	Gap 1 phase
GDP	Guanosine DiPhosphate
GFP	Green Fluorescent Protein
GMPCPP	Guanosine-5′-[(α,β)-methyleno]triphosphate
GTP	Guanosine TriPhosphate
GTPγS	Guanosine 5'-O-[gamma-thio]triphosphate
γH2AX	Phospho-Ser139 histone H2AX
HR	Homologous Recombination
IC50	Half-maximal Inhibitory Concentration
IR	Ionizing Radiation
kb	Kilo base
KD	Knock-Down
kDa	Kilo Dalton
KO	Knock-Out
MCAK	Mitotic centromere-associated kinesin
MSD	Mean Square Displacement
MT	Microtubule
NHEJ	Non-Homologous End-Joining
P53	Tumor protein p53
PARP	Poly (ADP-Ribose) Polymerase

PTM	Post-translational modification
TIRF	Total internal reflection fluorescence
UV	Ultraviolet
WT	Wild Type

CHAPTER 1. Introduction

1.1 Microtubules

Microtubules are major components and cytoskeletal filaments of eukaryotic cells that serve pivotal roles in many essential cellular functions. In non-dividing cells, migration, cell shape changes and intracellular cargo transportations are functionally dependent on microtubules (Bahmanyar et al., 2009; Bai et al., 2017; Barth et al., 2008; Bryantseva & Zhapparova, 2012; Francis et al., 2011; Hume & Seabra, 2011; Kaverina & Straube, 2011; Sarangapani & Asbury, 2014; Tanaka, 2012, 2013; Wakida et al., 2010). During cell division, a structure formed by microtubules called the mitotic spindle, is crucial for proper chromosome segregation into the daughter cells (Forth & Kapoor, 2017; Meunier & Vernos, 2012). Due to their key roles in cellular functions, several diseases can arise from the disruption or malfunction of microtubules, including cancer, infection, cardiovascular disease, and neurodegenerative disease. Microtubules are therefore often targeted by a number of chemotherapeutics, antiparasitic and antifungal medications (Chatterji et al., 2011; Dumontet & Jordan, 2010).

Microtubules are made up of α- and β-tubulin heterodimers, which interact with each other in a head-to-tail longitudinal style to form a protofilament. This interaction gives a polarity to microtubules, exposing α-tubulin at the minus end, and β-tubulin at the plus-end. The plus ends grow faster than minus ends and point towards the cell periphery, while the minus ends are typically embedded in the centrosome, the microtubule-organizing center (Akhmanova & Steinmetz, 2015; Desai & Mitchison, 1997). Lateral interaction of typically 13 of these protofilaments shapes a cylindrical hollow tube with an outer diameter of 25nm. However, the number of protofilaments in microtubules may vary between 11 – 16 protofilaments depending on

the species and tubulin isotypes (Chaaban & Brouhard, 2017; Desai & Mitchison, 1997; Evans et al., 1985; Fukushige et al., 1999; Savage et al., 1989).

1.1.1 MT polymerization and depolymerization dynamics

Microtubule polymerization is highly dynamic and often switches between growing and shrinking phases, a feature known as dynamic instability that is crucial for cell survival and growth. This characteristic of microtubules gives them the ability to reorganize quickly in order to perform their various functions. It allows them to rapidly fill the newly formed regions of cytoplasm, which is critical for the membrane systems recruitment via microtubule motor proteins (Desai & Mitchison, 1997; Tanaka & Kirschner, 1991). This feature of microtubules also gives them the ability to probe for specific targets within the cell, like the kinetochore regions of chromosomes during mitosis (Holy & Leibler, 1994), where the plus ends of centrosome-nucleated dynamically unstable microtubules search through the cytoplasm to capture sites on kinetochores (Hayden et al., 1990). Dynamic instability of microtubules also allows them to perform mechanical pushing and pulling forces during polymerization and depolymerization, respectively (Laan et al., 2012; Vleugel et al., 2016).

1.1.2 Tubulin guanosine triphosphate (GTP) hydrolysis & its relationship with MT polymerization

Tubulin contains two GTP-binding sites, one on α-tubulin, which is terminally bound in a non-exchangeable and non-hydrolyzable site and one on β-tubulin, which is exchangeable (Spiegelman et al., 1977). It is a widely held belief that both α- and β-tubulin must bind GTP in order to polymerize. It is known that microtubule dynamic instability is coupled to GTP hydrolysis

(Bowne-Anderson et al., 2013; Hyman, Middleton, et al., 1992; Zhang et al., 2015). The β-tubulin-GTP gets hydrolyzed to guanosine diphosphate (GDP) after the incorporation of the tubulin dimer into the microtubule lattice during polymerization (David-Pfeuty et al., 1977; MacNeal & Purich, 1978).

Dynamic instability of microtubules is a result of the capability of tubulin dimers to hydrolyze GTP to guanosine diphosphate (GDP). Each α- and β-tubulin monomer binds one GTP nucleotide. The GTPase activity of a free tubulin dimer is very low, but it can be stimulated by binding to other tubulin dimers (Roychowdhury et al., 1999). When another tubulin dimer is bound, the necessary residues for the hydrolysis are provided by the new α-tubulin subunit and the exposed GTP nucleotide on the β-tubulin surface is hydrolyzed to the GDP (Alushin et al., 2014). It is known that the hydrolysis of GTP affects the structure of the tubulin dimer (Horio & Murata, 2014). The tubulin dimer containing the GDP nucleotide experiences a mechanical strain that leads to a kink in the α-β- tubulin interface (Howard & Timasheff, 1986; Mitra & Sept, 2008), when the GTP containing tubulin dimer was previously thought to remain straight (Melki et al., 1989). This structure of GDP-tubulin dimers gives a curved shape to the whole protofilament. In the microtubule lattice, however, the protofilaments are forced to be straight by the lateral bonds between them (Brouhard & Rice, 2014).

The appearance of growing and shrinking microtubule ends exhibits significant differences (Mandelkow et al., 1991). Electron Microscopy (EM) studies have shown straight and outwardly tapered protofilaments with uneven lengths at the growing ends, vs curved and outwardly peeled protofilaments with no lateral contacts at the shrinking ends. These studies established the model proposing that GTP-tubulin adopts a straight curvature, which is a microtubule-compatible conformation, while GDP-tubulin exhibits a curved conformation (Melki et al., 1989). This model

provided a structural explanation for the necessity of GTP-binding for microtubule assembly and for the fact that GTP hydrolysis could depolymerize microtubules. It was indicated in a cryo-EM study that GTP-tubulin is not completely straight when it is incorporating into the microtubule lattice (Chrétien et al., 1995). It is known now, from crystal structures, that GTP-bound tubulin is curved (Ayaz et al., 2012; Nawrotek et al., 2011; Pecqueur et al., 2012).

1.1.3 GTP cap and MT stability

When the new tubulin dimers incorporate to the microtubule lattice faster than their β-tubulin-GTP gets hydrolyzed, a layer of GTP-bound-tubulin dimers will grow at the growing end of microtubules, forming a so-called "GTP cap". GTP-cap is widely believed to protect microtubules from depolymerization. Slower elongation of microtubules leads to erosion of the GTP cap and exposure of GDP tubulin, which is unstable. This will cause microtubule shrinkage or catastrophe (Caplow & Shanks, 1996; Chrétien et al., 1995; Howard & Hyman, 2003; Kueh & Mitchison, 2009; Mandelkow et al., 1991; Maurer et al., 2012; Roostalu et al., 2020; Westermann et al., 2006).

Insight into the size and nature of the GTP cap is fundamental to microtubule polymerization dynamics, as the size of the cap reports on the interplay of polymerization and GTP hydrolysis rates, and thus to the control of microtubules during cell proliferation and development. In the first attempts, the kinetic lifetime of the cap (Walker et al., 1991), or the smallest number of GMPCPP-tubulin subunits required to stabilize GDP microtubules (Drechsel & Kirschner, 1994) were utilized to measure the minimal cap size (Desai & Mitchison, 1997), however, the GTP cap itself was not directly observable. Microtubule end-binding (EB) proteins bind to the end of growing microtubules and form an extended 'comet'. It has been shown that EB proteins prefer to bind to the microtubules polymerized with slowly hydrolyzable and non-hydrolyzable GTP analogs, so

Seetapun et al. used a GFP-tagged EB1 binding as a read-out for the presence of the GTP cap at the growing ends of microtubules and measured the average cap size of 750 tubulin subunits, spread over 55 rows of tubulin (Brouhard & Sept, 2012; D. Seetapun et al., 2012). All these methods have used a probe to measure the length of the GTP cap, therefore finding a way to measure the length directly without relying on any binding probes or to quantify the GTP-tubulin dimers at the end of the growing end of microtubule would give a more accurate estimation of this important feature of microtubules.

If we could understand the biochemistry of the tubulin dimer conformational changes, we could predict the microtubule end structure. On the other hand, understanding the structure of microtubule end could help us figure out the biochemistry involved. Cryo-EM studies have shown that the growing ends of microtubule curve away from its long axis (Zhang et al., 2015). McIntosh et al. (2018) obtained electron tomograms of growing microtubules in cells from different species and also from samples of microtubules in vitro. Both in cells and in vitro, McIntosh et al. (2018) observed short (~40-80 nm), curved extensions on the ends of growing microtubules. The average curvature was comparable in magnitude to that seen in head-to-tail assemblies modeled from atomic structures of unpolymerized αβ-tubulin, so it likely reflects the intrinsic curvature of unpolymerized, GTP-bound αβ-tubulin (McIntosh et al., 2018). An interesting hypothesis here is if curved end of microtubule plus ends overlaps with the GTP cap. This could signify the impacts of tubulin conformational changes in accordance with GTP turnover in microtubule dynamics.

1.1.4 Study of MT polymerization: the use of nucleotide analogs

GMPCPP (guanosine-5′-[(α,β)-methyleno]triphosphate) is an analog of GTP which gets hydrolyzed slowly. Another non-hydrolyzable or slowly hydrolyzable analog of GTP is GTPγS

(guanosine 5'-O-[gamma-thio]triphosphate), which is a G-protein-activating nucleotide. Therefore, the microtubules that are generated using GMPCPP or GTPγS are more stable and resist depolymerization on their own at room temperature (Maurer et al., 2011; Yajima et al., 2012). So these nucleotides have been used in various microtubule studies, particularly the studies concerning GTP cap and GTP islands, which are not feasible using GTP. Different features of GMPCPP make it a proper alternative for GTP to analyze microtubule polymerization dynamics. GMPCPP has been shown to bind well to the tubulin E-site and to promote polymerization (Sandoval et al., 1978; Sandoval et al., 1977; Zhang et al., 2015; Zhang et al., 2018). It stimulates a large amount of nucleation and growth of unusually stable microtubules when injected in vivo (Wehland & Sandoval, 1983), effects that resemble those of the microtubule stabilizing drug taxol (De Brabander et al., 1981). Due to the fact that GMPCPP vigorously favours tubulin nucleation (Hyman, Middleton, et al., 1992), it is utilized to make short GMPCPP-stabilized microtubule "seeds" that can serve as nucleation sites for microtubule elongation, when added to polymerization reactions. This can surpass the rate-limiting nucleation step of microtubule assembly and specifically assess elongation (Roostalu & Surrey, 2017).

1.1.5 Study of MT polymerization: the use of chemical stabilizing/destabilizing agents

Microtubule-targeted drugs disrupt microtubule dynamics in distinct ways, and they are primarily classified into two groups: microtubule destabilizing agents, such as vinblastine, colchicine, and combretastatin-A4, and microtubule stabilizing agents, such as paclitaxel and epothilones (Figure 1.1) (Bates et al., 2016; Fanale et al., 2015; Mukhtar et al., 2014).

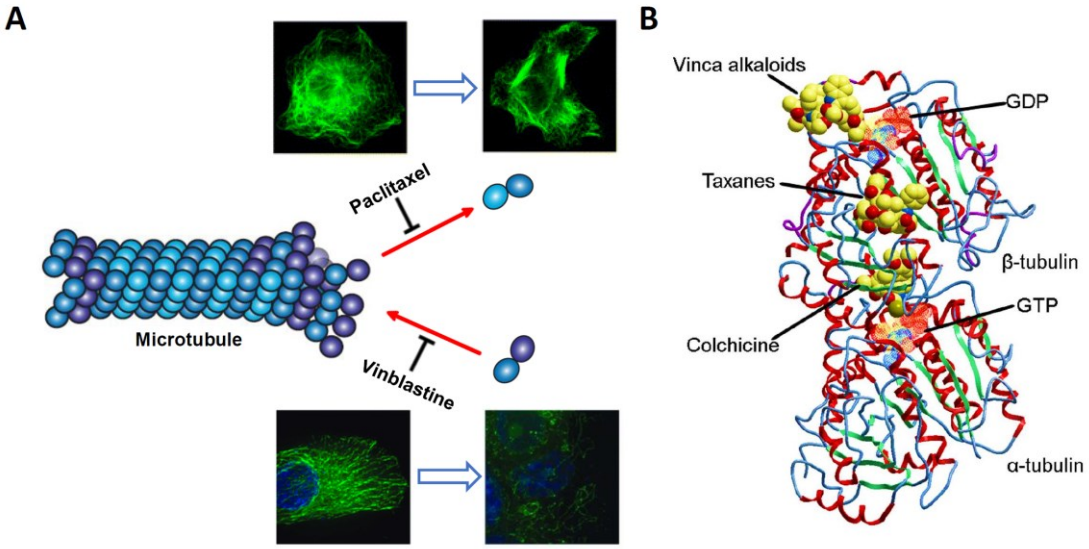

Figure 1.1 Microtubule stabilizing and destabilizing agents, their effects on microtubule dynamics and their tubulin-binding sites

(A) Paclitaxel promotes microtubule assembly and reduces their dynamicity, while vinblastine disrupts microtubule assembly and proper formation of the mitotic spindle and the kinetochore. Adapted with permission from (Harkcom et al., 2014; Shi & Sun, 2017). (B) Structure of the α/β-tubulin heterodimer showing binding sites for taxanes, vinca alkaloids, colchicine, GDP, and GTP. Adapted with permission from (Xie & Zhou, 2017).

Paclitaxel, an effective anticancer drug, binds stoichiometrically and specifically to the β-tubulin subunit in microtubules. The resulting microtubules are stable and resist depolymerization. The highly dynamic behavior of microtubules is greatly suppressed by paclitaxel, which induce abnormal mitosis and leads to cell death (Orr et al., 2003; Stanton et al., 2011). The question is: How does paclitaxel stabilize microtubules? It has been proposed that microtubule stabilization could be linked to a conformational change of the tubulin dimer that keeps the protofilaments straight and prevents the protofilament-curling at the microtubule ends that occurs during

microtubule disassembly. The structure of the tubulin dimer bound to paclitaxel was obtained by electron crystallography of zinc-induced tubulin sheets (Donhauser et al., 2018; Nogales et al., 1998). Also docking of this tubulin model reconstructed from cryoelectron microscopy images of microtubules indicated the nature of interdimer contacts within and between protofilaments. Although photoaffinity labeling and electron crystallography have localized the binding pocket for paclitaxel to a small region in β-tubulin, neither of these approaches gives access to conformational changes occurring in tubulin that are indicative of the mechanisms involved in microtubule stabilization, upon binding of paclitaxel (Snyder et al., 2001; Xiao et al., 2006).

Due to the conformational changes that these stabilizing and destabilizing agents induce in tubulin structure (Elie-Caille et al., 2007; Gigant et al., 2009; Mitra & Sept, 2008), the microtubules that are polymerized in their presence are structurally different than native ones. This discrepancy in the structure is sometimes troublesome, especially when the specific feature of microtubules that is being studied gets affected by the forced conformational changes. However, in some cases these agents could serve as unique tools to study microtubule polymerization mechanism. For instance, when there are changes of microtubule depolymerization during sample preparation, one solution is using paclitaxel-stabilized microtubules.

1.1.6 MT poisons as cancer therapeutics

In proliferating cells, microtubules are one of the essential components in the division process through the formation of the mitotic spindle. This event can take place because of the dynamic nature of microtubules through polymerization and depolymerization cycles. As a result of these functions, and due to the fact that cancer is basically a disease of uncontrolled cell division, tubulin and microtubules are targets for anticancer agents. Microtubule-targeting agents can be divided

into two groups: microtubule-stabilizing agents that stabilize microtubules, and microtubule-destabilizing agents that destabilize microtubules. Despite these differences, alteration of tubulin microtubule equilibrium leads to disruption of mitotic spindle, halting the cell cycle at the metaphase-anaphase transition and resulting in cell death (Fanale et al., 2015; Mukhtar et al., 2014; Yvon et al., 1999).

Paclitaxel and other taxanes have been used successfully to treat solid tumours, especially in ovarian, breast, prostate and lung cancers. Paclitaxel stabilizes microtubule cytoskeleton and inhibits depolymerization and therefore might block the cell cycle in its G2/M phases at high doses or in G1 phase at lower doses (Demidenko et al., 2008). It could also induce multipolar spindles and increase aneuploidy and chromosome missegregation at lower doses (Zasadil et al., 2014).

Vinca alkaloids, like vinblastine and vincristine are of the first microtubule-destabilizing agents to be discovered, which depolymerize microtubules by interacting with various β-tubulin sites. In particular, Vinca alkaloids interact with tubulin at specific binding sites, which differ from those of other agents, interfering with microtubule dynamics, blocking polymerization at the end of the mitotic spindle, and leading to metaphase arrest. Thanks to their peculiar mechanism of action, Vinca alkaloids have been widely used in anticancer therapy, usually in combination with other chemotherapeutic agents which do not have cross-resistance with them (Avendaño & Menéndez, 2015; Bates & Eastman, 2017; Mukhtar et al., 2014).

1.1.7 Structural study of tubulin/MT: The use of Antibody-Like engineered Polypeptides

In the past decades, single-chain short recombinant antibodies has replaced the conventional immunization methods. Various types of alternative scaffolds have been generated that are based

on proteins with repeating motifs, including leucine-rich repeats, ankyrin repeats, Armadillo repeats, and tetratricopeptide repeats (Grove et al., 2008; Shilova & Deyev, 2019).

DARPins are artificial proteins that are based on ankyrin repeats. In eukaryotic cell proteins that are generated from ankyrin repeats could bind to various targets to organize cytoskeleton and to regulate enzyme activities. The X-ray structure of DARPin complex with GTP-tubulin revealed that it can bind to the β-tubulin at microtubule plus ends. It has been shown by total internal reflection fluorescence (TIRF) microscopy that DARPin could specifically block the growth of microtubules at their plus end and it favors disassembly of tubulin subunits via a selective end-capping mechanism (Knossow et al., 2020; Plückthun, 2015; Shilova & Deyev, 2019). By binding to the β-tubulin surface exposed at microtubule plus ends, DARPin in fact competes with the binding of the α-tubulin of another tubulin dimer (Pecqueur et al., 2012). This specific characteristic enables DARPins to serve as designable tools for the dissection of microtubule dynamic properties selective for either of their two different ends.

1.2 MT dynamic instability in cells and Microtubule associated proteins

In cells, microtubule dynamics are regulated by different microtubule associated proteins (MAPs), which have distinct functions in the cytoplasm and in the nucleus. These proteins promote either the polymerization or depolymerization of microtubules (Rutten et al., 1997; Sandoval & Weber, 1980a, 1980b). They can also attach various cellular components and proteins to MTs and transport them along the MT lattice.

Microtubule motor proteins are specialized MAPs which localize to the sites that include mitotic spindles, spindle poles and centromeres/kinetochores (Gatlin & Bloom, 2010; Manning et al., 2010; Manning et al., 2007; Scholey et al., 1985; Vale et al., 1985). They act at the cortex to

generate sliding forces, attach MTs to cortical sites or kinetochores during growth and shortening, and to transport proteins along the lattice (Adames & Cooper, 2000; Carvalho et al., 2004; Maddox et al., 2003; Maekawa & Schiebel, 2004; Maekawa et al., 2003; Tanaka et al., 2005). Non-motor MAPs localize to specific sites along the MT by binding to newly polymerized or depolymerized ends, by motor transport, or by phosphorylation that targets these proteins to the correct sites (Akhmanova & Hoogenraad, 2005). They often regulate MT stability and function in nuclear movements or kinetochore-MT attachments (Berlin et al., 1990; McAinsh et al., 2003; Miller et al., 1998).

1.2.1 Kinesins

Kinesins are a group of molecular motor proteins that interact with microtubules in order to transport cargo or regulate the dynamics and structure of the microtubules (Figure 1.2). Kinesins are categorized into 14 families, which are in fact mechanochemical enzymes that utilize the energy released from hydrolysis of Adenosine triphosphate (ATP) to Adenosine diphosphate (ADP) to generate force and perform various types of work related to microtubule functions (Brady, 1985; Vale et al., 1985). Most conventional kinesins use this energy to transport cargo within a cell by moving along microtubules tracks in a step-wise fashion (Svoboda et al., 1993). Other kinesins use the energy to promote microtubule depolymerization, which is important for modulating microtubule dynamics (Desai et al., 1999; Walczak & Mitchison, 1996).

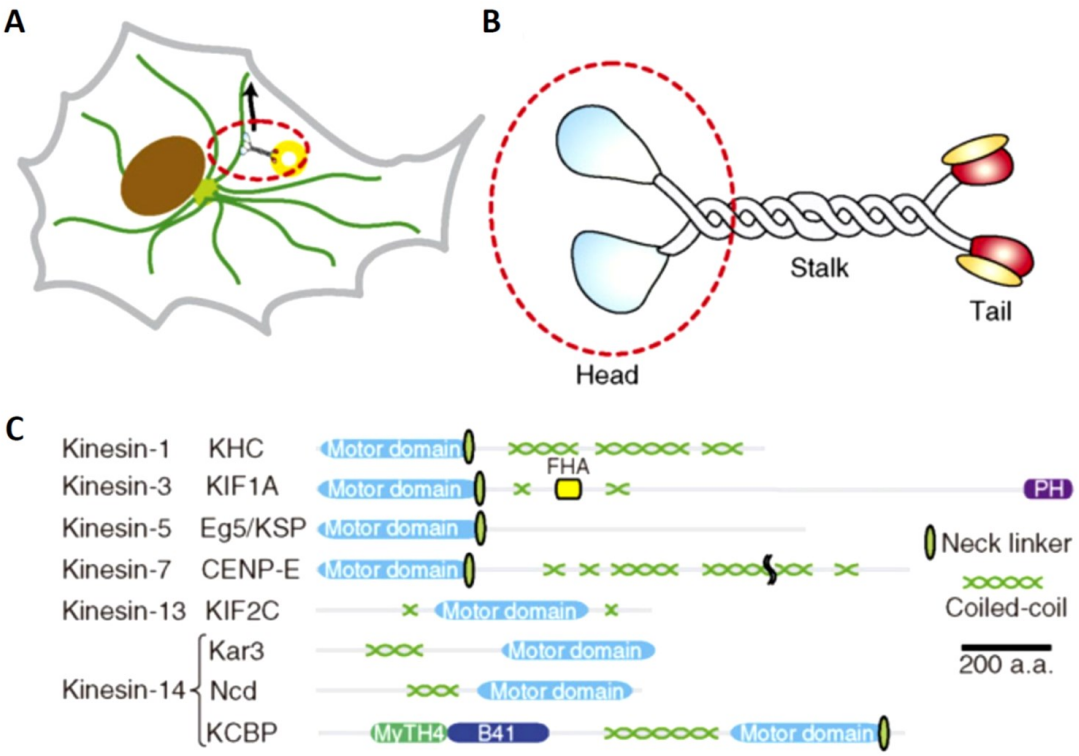

Figure 1.2 Architecture of kinesins.

(A) Kinesins are involved in various cargo transports in cells. (B) Schematics of the overall structure of conventional kinesin. (C) Some examples of the primary domain organization of kinesins. Adapted with permission from (Kikkawa, 2008).

Alterations in motor kinesins may lead to various human diseases such as cancer, multifactorial and monogenic disorders (Figure 1.3). Variants in human KIF genes have been shown to be involved in monogenic prenatal (birth defects) or postnatal (neurodevelopmental disorders and intellectual disability) (Kalantari & Filges, 2020).

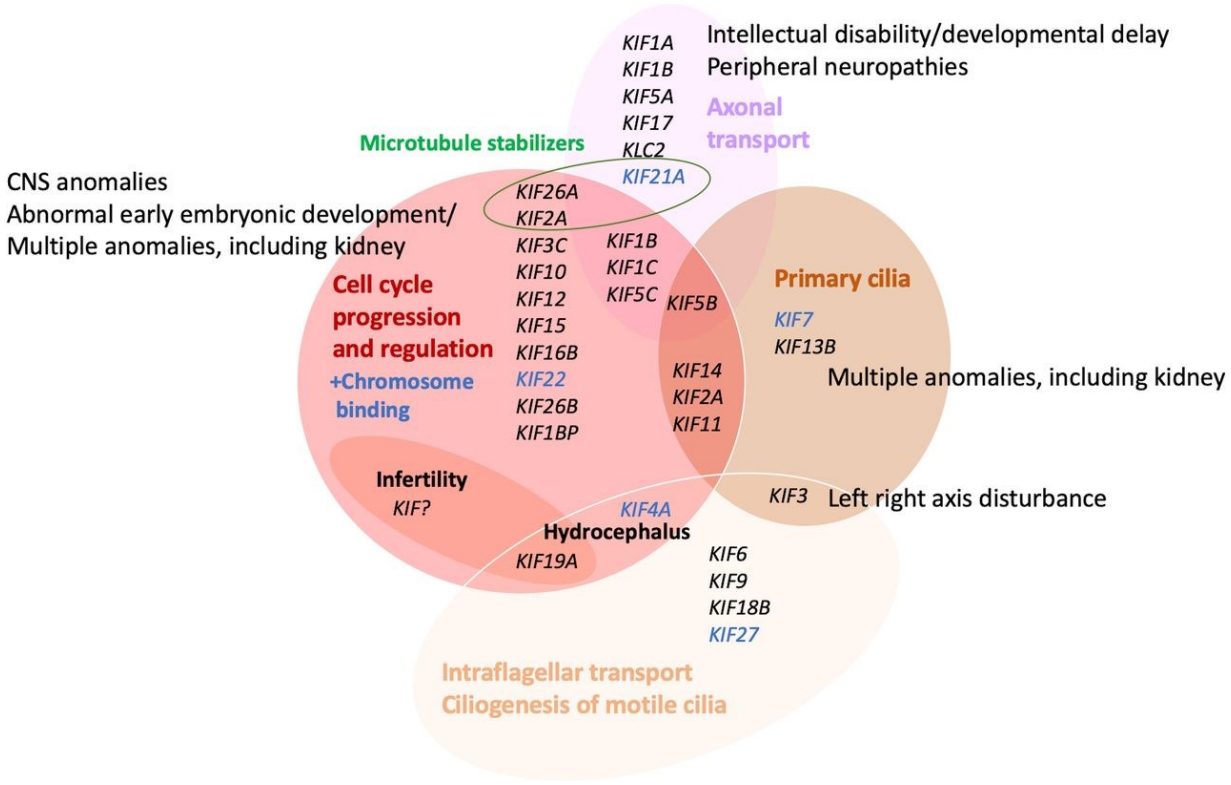

Figure 1.3 Association of KIF genes to different functions and relation to birth defect or monogenic phenotype groups. Adapted with permission from (Kalantari & Filges, 2020).

Kinesins are characterized by having a highly conserved motor domain (head) that is able to bind both ATP and the microtubule (Vale & Fletterick, 1997). This protein motor domain contains a catalytic core that is able to hydrolyze one ATP molecule per kinesin step and exchange the recently hydrolyzed-ADP for a new ATP (Schnitzer & Block, 1997). The binding of ATP and subsequent hydrolysis in the motor domains leads to conformational changes that allows them to walk along the microtubule (cargo-carrying kinesins) or to depolymerize microtubules (catastrophe-inducing kinesins) (Vale & Fletterick, 1997). The kinesin head is typically followed by an internal coiled-coil (stalk), which allows for homodimerization, heterodimerization, and tetramerization of at least two kinesin polypeptides. Kinesins that lack a coiled-coil domain generally function as monomers. Finally, kinesins have a highly phylogenetically-divergent (tail)

domain that is able to bind multiple types of cargo including organelles and other cytoskeletal components (Reddy A.S.N., 2011; Vale & Fletterick, 1997; Zhu & Dixit, 2012).

1.2.2 Kinesin-13 proteins and ATP-dependent catalytic depolymerization of MTs

Within the kinesin-13 family, there are two subfamilies: the ubiquitous KIF24 subfamily and the mammalian-specific KIF2 subfamily. There are three members in KIF2 subfamily: Kif2A, Kif2B, and Kif2C. Kinesin 13 motors are different from the other kinesins, and they do not move (walk) along microtubules, but promote tubulin dimer disassembly, playing a key role in microtubule dynamics (Desai et al., 1999; Noda et al., 1995; Walczak & Mitchison, 1996).

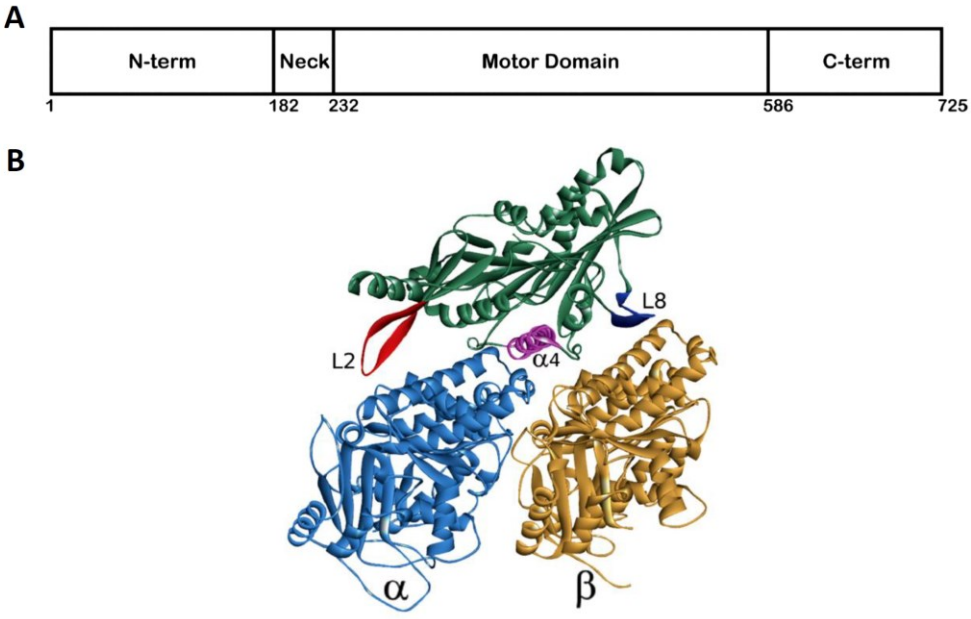

Figure 1.4 Domain composition and structure of kinesin-13 KIF2C.

(A) Domain composition of human KIF2C. (B) Structure of the human KIF2C, in complex with α/β-tubulin. Adapted with permission from (Wang et al., 2017). The major parts of the secondary structure which defines the microtubule-binding interface are highlighted. Adapted with permission from (Friel & Welburn, 2018).

Members of the kinesin-13 family have been implicated in vesicle transport (Noda et al., 1995) and, more importantly, in MT depolymerization (Desai & Mitchison, 1997; Manning et al., 2007; Mennella et al., 2005; Walczak, 2003). Upon binding to the MT end, they induce a conformational change in its structure that leads to disassembling tubulin subunits from the polymer end (Desai et al., 1999). The MT-destabilizing properties of kinesin-13 members are unique because they use ATP hydrolysis to induce depolymerization of MTs from both ends, instead of using it to walk along MTs (Desai et al., 1999; Helenius et al., 2006; Hunter et al., 2003).

1.2.3 Study of Kinesin-13 driven MT depolymerization: the use of ATP analogs

It has been indicated by electron microscope that in the presence of adenosine5′-([β,γ]-imido)triphosphate [AMPPNP], which is a nonhydrolyzable ATP analog, kinesins have a higher affinity for microtubules and they tend to form a uniform decoration pattern over tubulin, in which the motor domain binds with a well-defined configuration to each tubulin heterodimer (Cope et al., 2010; Hunter & Allingham, 2020; Tan et al., 2006).

The kinesin-13-induced catalytic depolymerization of microtubules occurs in an ATP-dependent process. Desai et al. found that AMPPNP-bound XKCM1, a microtubule-destabilizing enzyme, was enriched at MT ends, and also formed a stable complex with tubulin dimers (Desai et al., 1999). This observation opened the hypothesis that although ATP-bound is required for targeting microtubule ends, its hydrolysis may happen after depolymerization to release the enzyme from the dissociated tubulin dimers, recycling the enzyme for additional rounds of catalysis. Despite the efforts to verify the process, which is critical in terms of the mechanisms involved in kinesin-13-induced microtubule depolymerization, it is still unknown whether the ATP hydrolysis step is

required to dissociate tubulin dimers from microtubules ends (Desai et al., 1999; Helenius et al., 2006; Ogawa et al., 2004; Shipley et al., 2004; Michael Wagenbach et al., 2008).

1.2.4 Kinesin-13 class specific neck and MT depolymerization

Kinesin-13's conserved motor domains are located internally in their primary sequences, with an N-terminal localization domain and C-terminal domain that contributes, with the N-terminus, to motor dimerization. A highly conserved, positively charged, class-specific neck sequence of ~60 amino acids is located at the upstream of the motor core. The motor core itself has intrinsic MT depolymerization activity, demonstrating that the relatively few class-specific modifications in the kinesin-13 motor core are responsible for the class's unusual function. Nevertheless, the activity of this minimal motor core is very low compared to the full-length motor. On the other hand, monomeric constructs lacking both the N- and C-terminal domains but containing the neck and motor core have MT depolymerization activity comparable to the full-length motor. It has been shown that the kinesin-13 neck sequence makes a significant contribution to depolymerization efficiency and is essential to enable these motors to control cellular MT dynamics (Chatterjee et al., 2016; Miki et al., 2005; Carolyn A. Moores et al., 2006; Moores et al., 2002; Soppina et al., 2014; Talapatra et al., 2015).

1.2.5 KIF2C and its roles during cell cycle

KIF2C, also known as Mitotic centromere-associated kinesin (MCAK) is a member of Kinesin-13 protein family, which is found in the cytoplasm throughout the cell cycle, highly enriched at centrosomes, centromeres/kinetochores and the spindle midzone during mitosis. In line with this localization, KIF2C has characterized functions in many aspects of mitosis such as spindle

assembly, MT dynamics, correct kinetochore-microtubule attachments, and chromosome positioning and anaphase sister chromatid segregation. KIF2C has also been implicated in correcting misaligned chromosomes during their congression to the metaphase plate (Desai et al., 1999; Manning et al., 2007; Ogawa et al., 2004; Sanhaji et al., 2011).

The importance of KIF2C in ensuring the faithful segregation of chromosomes prior to cytokinesis is consistent with the observation that it is upregulated in various types of cancer and could be involved in causing the aneuploidy that is often associated with this disease. Depletion or inhibition of KIF2C results in improper spindle maintenance and misaligned chromosomes during metaphase and lagging chromosomes during anaphase by interfering with the poleward movement of chromosomes (Maney et al., 1998). This is consistent with KIF2C depolymerizing MTs because chromosome movement during anaphase is associated with the shortening of the MTs that connect the chromosome (via the kinetochore at which KIF2C is localized) to the pole. Altogether, both overexpression and depletion of KIF2C in cultured mammalian cells cause defects in mitotic spindle assembly and errors in chromosome segregation. Thus, it would appear that normal mitotic progression and maintaining genetic integrity during mitosis require relatively precise levels of KIF2C (Ganguly et al., 2008; Sanhaji et al., 2011).

But KIF2C is also present in the nuclei of interphase cells, where it has been shown that there are no microtubules (Ganguly et al., 2008). This localization of , and its possible roles in the nuclei during interphase remain a mystery.

1.3 MT, Kinesin-13, DNA damage response (DDR)

DNA molecules are constantly subjected to genotoxic stresses, including exogenous agents such as ultraviolet (UV) radiation, ionizing radiation (IR), X-rays, and chemicals, that can lead to DNA

damage (Chatterjee & Walker, 2017; Mah et al., 2010; Rastogi et al., 2010). Endogenous sources of DNA damage arise from normal cellular metabolism which generates reactive oxygen species that react with the DNA molecule (Maynard et al., 2009; Tubbs & Nussenzweig, 2017). Therefore, to preserve the integrity of genetic information during transformation from one generation to the next, robust and accurate mechanisms for both detection and repair of the damaged DNA are crucial to avoid mutations or cell death. An extensive cellular network called the DNA damage response (DDR) reacts to DNA damage, regulating DNA repair, cell cycle arrest, chromatin remodeling and apoptosis (Jackson & Bartek, 2009; Li et al., 2021; Rastogi et al., 2010).

Specialized nucleoprotein structures, called telomeres, protect chromosome ends. It has been shown that DNA damage response proteins are intimately involved in telomere metabolism (Viscardi et al., 2007). This feature allows researchers to use telomere-based systems to track DNA damage foci in living cells. One of these studies has indicated that 53BP1 and dynamic microtubules are required for DSB mobility and that the disruption of motor proteins or microtubules, disrupts the random mobility of damaged DNA (Lottersberger et al., 2015). It has also been shown that fission yeast with defective DNA repair functions displayed elongated morphology associated with microtubule stabilization (Graml et al., 2014). Another study demonstrated that microtubule stabilization is required for intracellular trafficking of DNA repair proteins in response to DNA damage (Poruchynsky et al., 2015), revealing a link between the DDR and microtubule networks.

Some studies in yeast have indicated the involvement of microtubule motor proteins in DNA damage response (Mekhail, 2018; Oshidari et al., 2018). DSB repair has been reported to be linked to Kinesin-14, a microtubule minus-end directed motor protein complex, which is composed of the catalytic subunit Kar3 and structural subunit Cik1 (Chung & Zhao, 2015; Mekhail, 2018). DSB

repair pathways appear to promote chromosome movement through a mechanism involving microtubules and kinesin-14/Kar3 motors, and this mechanism is required for efficient repair (Chung & Zhao, 2015; Oshidari et al., 2018). Also a bridging protein, Kar9, which is recruited to the plus ends of astral microtubules growing toward the new daughter cell has been reported as a target of ataxia telangiectasia mutated (ATM) in DNA DSB repair. It has been shown to affect the association of RAD52, a known DNA repair protein, to the DNA DSB foci (Malavazi et al., 2008; Malavazi et al., 2006). However, there is no data on the involvement of these motor proteins in mammalian cells.

Centromere release from the microtubule attachment has been reported as a driving mechanism for increased mobility in response to DNA damage (Lawrimore et al., 2017; Strecker et al., 2016). All these data and also the importance of microtubule cytoskeleton for the full extent of chromatin response to DNA DSB, suggest the involvement of microtubules in DDR. This function of microtubules in DDR requires a thorough mechanistic study, even though many studies have indicated that there are no microtubules in the nucleus during interphase (Lian et al., 2014; Lloyd & Chan, 2006; Prigozhina et al., 2004; Ren et al., 2003).

1.3.1 DNA double strand break (DSB) and different repair mechanisms

DSBs are produced following exposure to DNA-damaging agents, such as ionizing irradiation, and endogenously from the collapse of replication forks or during programmed genome rearrangements. DSBs are the most toxic DNA lesions, as a single DSB is lethal to a cell (Sandell & Zakian, 1993). DNA DSBs also contribute to the genomic instability which could lead to cancer development, and therefore DSB repair pathways serve as important mechanisms for tumor suppression. There are two primary evolutionarily conserved pathways that repair DSBs, the

choice of which is determined by cell cycle phase and chromatin context: non-homologous end-joining (NHEJ) and homologous recombination (HR).

NHEJ involves the direct ligation of two broken ends, a mode of repair that is considered imprecise, since any degradation of the DSB ends result in loss of genetic information after ligation. HR is the more faithful mode of DSB repair, as it involves the direct exchange of genetic information (Chapman et al., 2012). However, if recombination is not properly regulated, it can result in loss-of-heterozygosity, non-reciprocal translocations, large deletions or duplications all which are examples of chromosome rearrangements (Kolodner et al., 2002; Symington, 2002). HR requires the formation of ssDNA for homology search and the presence of a homologous donor sequence which acts as a template for DSB repair (Piazza et al., 2018; Piazza et al., 2019).

NHEJ and HR can be viewed as competing pathways of DNA damage repair. While inhibiting HR has no effect on NHEJ, abrogating NHEJ increases the frequency of HR indicating that NHEJ precedes HR in repair pathway choice (Frank-Vaillant & Marcand, 2002). Initiation of resection irreversibly commits the cell to HR repair (Paull & Gellert, 1998; Symington, 2002).

1.3.2 Models to study HR & NHEJ repair mechanisms in cells

Human cell lines have been generated with a chromosomally integrated copy of an individual reporter for either NHEJ or HR, for monitoring and interrogation of these repair mechanisms (Mao et al., 2008; Mao et al., 2009). Each reporter contains an inactive expression cassette for green fluorescent protein (GFP) that is interrupted by one or more recognition sites for the specific-cutting endonuclease I-SceI, which generates a defined DSB. The individual reporters are designed such that a defined DSB repair outcome leads to restoration of a GFP expression cassette.

Accordingly, the GFP-marked repair outcome is measured by transiently expressing I-SceI, culturing the cells to allow completion of repair, then determining the percentage of GFP+ cells (Gunn & Stark, 2012).

1.3.3 p53 & DDR

P53, which is known as the "Guardian of the Genome", plays a central role in DNA damage response (Strachan, 1999 ; Williams & Schumacher, 2016). DNA damage promotes Post-translational modifications (PTMs) on P53, causing P53 activation and in response, P53 can activate cell cycle arrest, repair the damaged DNA, activate specific cell death pathways, and metabolic changes in the cell via induction of an array of genes (Feroz & Sheikh, 2020; Kastenhuber & Lowe, 2017).

The role of the DNA damage response factor, p53-binding protein 1 (53BP1) in DSB repair and its contribution to cell-cycle appropriate execution of NHEJ and HR has been studied extensively (Escribano-Díaz et al., 2013; Panier & Boulton, 2014; Zimmermann & de Lange, 2014). 53BP1 accumulates at sites of DNA damage and marks sites of DNA damage. Many of the functions of 53BP1 are mediated by binding partners that associate with the 53BP1 N terminus upon phosphorylation by the ataxia telangiectasia mutated (ATM) and ataxia telangiectasia and Rad3 related (ATR) kinases (Figure 1.5). The contribution of 53BP1 to DSB repair pathway choice, which is a critical role of this protein, has received considerable attention in the context of the treatment of BRCA1-deficient cancers with poly (ADP-ribose) polymerase inhibitors (PARPi) (Banerjee et al., 2010). BRCA1 in known to promote HR while, 53BP1 inhibits DNA-end resection which is required for HR. This process is through phosphorylation of 53BP1 by ATM which leads to the recruitment of RIF1. Dephosphorylation of 53BP1 releases RIF1, a process that

is promoted by BRCA1 with participation of PP4C, directing repair toward HR (Figure 1.6) (Isono et al., 2017).

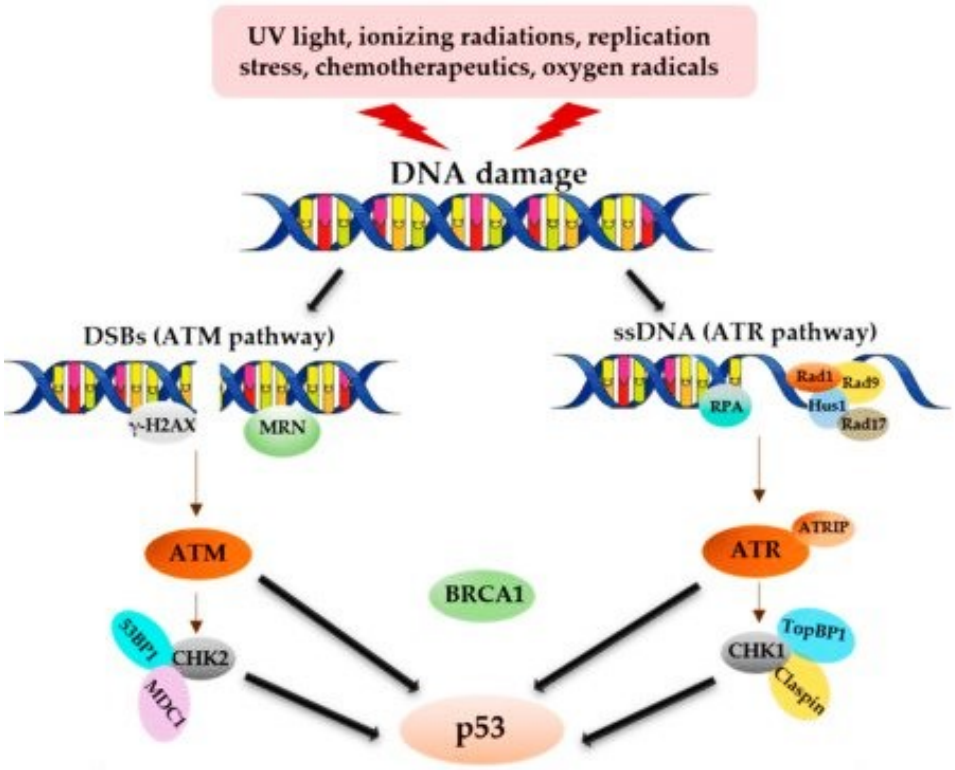

Figure 1.5 Overview of the DDR and p53 functional roles.

DNA damage sites are recognized by the damage sensor proteins, where they recruit the transducers cascade, and ultimately activate the DNA damage repair factors. Adapted with permission from (Vadivel Gnanasundram et al., 2021).

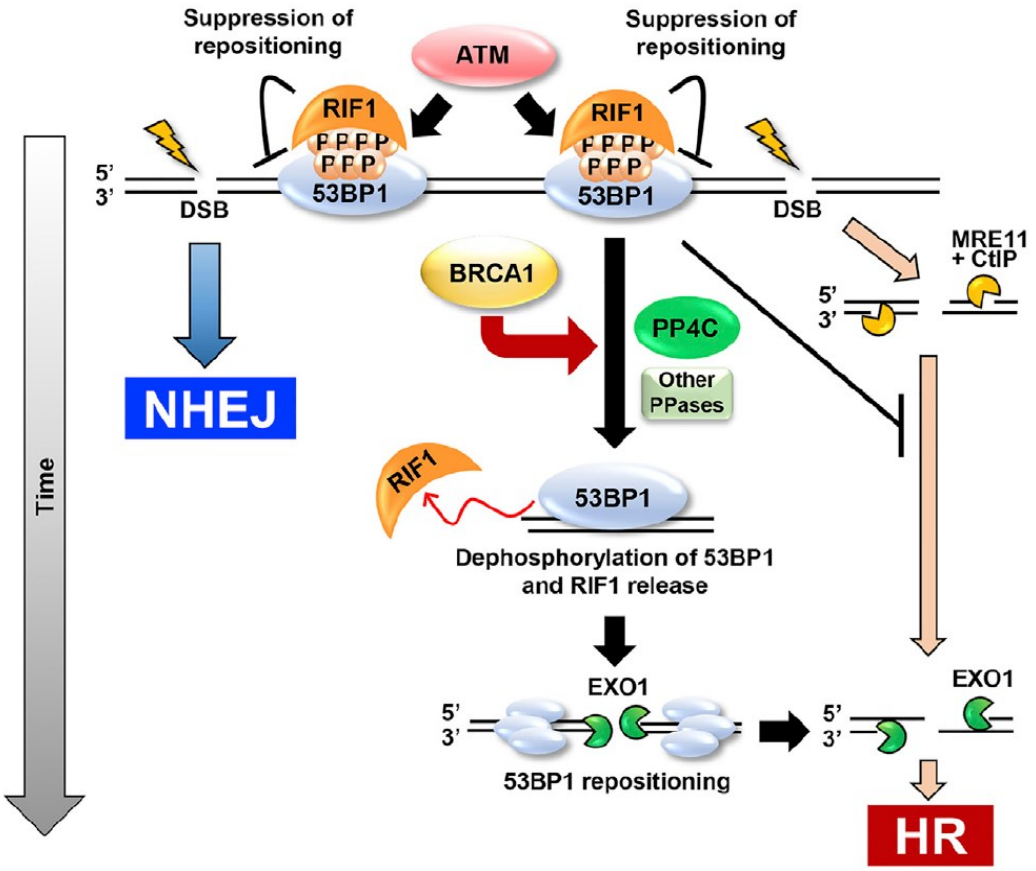

Figure 1.6 Interaction of 53BP1 and BRCA1 in repair pathway choice.

BRCA1 promotes 53BP1 dephosphorylation and RIF1 release, promoting repair by HR. Adapted with permission from (Isono et al., 2017).

A conserved phenomenon of the DNA damage response seen from yeast to mammals is the reorganization of checkpoint and repair proteins into punctate sub-nuclear foci that are detectable by fluorescence microscopy (Lisby et al., 2004). DNA damage foci are important for the proper execution of the DDR, as they allow a rapid and local increase in protein concentration around DNA damage (Giglia-Mari et al., 2011; Polo & Jackson, 2011). Furthermore, foci have been widely used as markers of DNA damage and the discovery of the genetic requirements for foci

assembly have greatly advanced our understanding of the DDR (Kolas et al., 2007; Lisby et al., 2004; Melo et al., 2001).

1.3.4 PARP1 and ATM in DNA repair mechanism

The association of poly (ADP-ribose) polymerase 1 (PARP1) to different types of DNA damage sites is one of the first events in the DNA repair process. PARP1 is an important player in DNA repair process which modifies itself and other proteins post translationally by adding poly (ADP-ribose) (PAR) units to them. This poly(ADP)ribosylation (PARylation) activity is indispensable for most of the known functions of PARP1 in DNA damage response (DDS), including repair of single-strand breaks (SSBs) and double-strand breaks (DSBs) (Lord et al., 2015; Montoni et al., 2013; Ray Chaudhuri & Nussenzweig, 2017). PARP1 distinguishes DNA break sites, and its activity plays an important role in the early recruitment of factors which contribute to the DSB repair process (Ali et al., 2012; Kim et al., 2005; Langelier & Pascal, 2013; Polo & Jackson, 2011; Sukhanova et al., 2016). PARP1 deficiency or inhibition of its activity leads to a delay in activation of DDR proteins. PARP1 is a crucial factor in the control and also the recruitment of important HR repair proteins (Haince et al., 2007). Breast cancer type 1 susceptibility protein (BRCA1) is one of the most important among these proteins, which modulate the initial steps of DSB resection and also the loading of RAD51 onto DNA, which is necessary for strand exchange during HR (Caron et al., 2019; Dziadkowiec et al., 2016). The human ALC1 (Amplified in Liver Cancer 1) protein is a chromatin remodeling enzyme from SNF2 family which functions together with PARP1 to catalyze ATP- and NAD+-dependent nucleosome remodeling. ALC1-dependant mobilization is another important factor in the recruitment of repair factors like RAD51 to DNA

damage site (Figure 1.7). Overexpression of the ALC1 protein leads to transformation of cultured cells and appearance of spontaneous tumors (Ma et al., 2008).

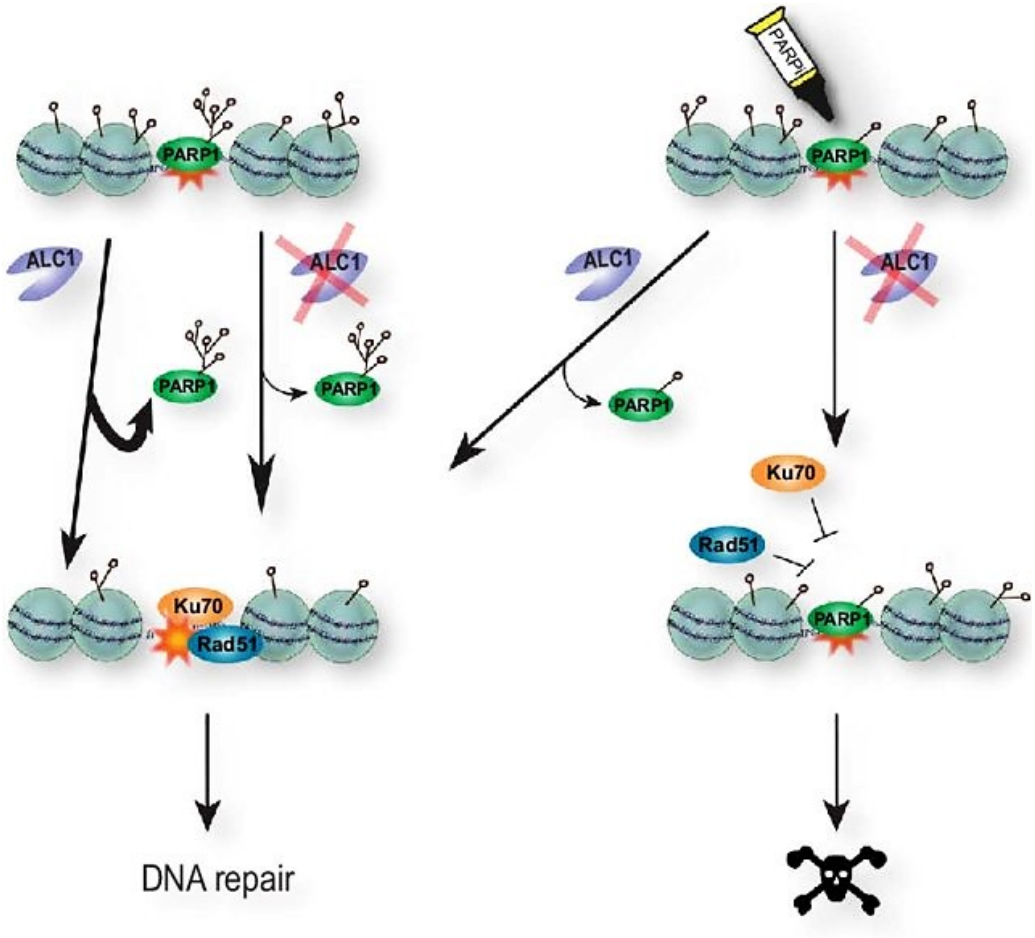

Figure 1.7 A model for the role of ALC1 in olaparib-mediated synthetic lethality.

PARP1 is recruited to sites of DNA damage and it PARylates itself and the proteins that are recruited to the break site. The removal of PARP1 from DNA damage sites involves a combination of auto-PARylation and ALC1-dependent mobilization. This allows the recruitment of essential factors such as Ku70 or Rad51. The impairment of auto-PARylation in ALC1-deficient cells inhibits the release of PARP1 from DNA damage sites, preventing the recruitment of substantial repair factors, leading to cell death. Adapted with permission from (Juhász et al., 2020).

ATM kinase, ATR kinase, and DNA-dependent protein kinase are the most upstream DNA repair kinases in mammalian cells (Lempiäinen & Halazonetis, 2009; Lovejoy & Cortez, 2009). DNA damage triggers the phosphorylation of a large number of proteins in an ATM- or ATR-dependent manner (Beli et al., 2012; Bensimon et al., 2010; Matsuoka et al., 2007; Smolka et al., 2007; Stokes et al., 2007). The distinction of DDR-related functions of ATM and ATR have been shown in numerous studies. ATM is activated primarily by only DSBs, while ATR responds to different types of DNA damage, including DSBs and a variety of DNA lesions that interfere with replication (Maréchal & Zou, 2013; Shiotani & Zou, 2009).

1.3.5 Possible involvements of microtubules and MAPs in DDR

Microtubules and kinesin motor proteins mediate the movement of cargos in certain directions. Unlike these movements, sub-telomeric DSB sites exhibit arbitrary mobility in random directions within the nucleus. These movements can be quantified by single particle motion analysis called mean square displacement (MSD) (Chung & Zhao, 2015). Therefore, despite the dependence of these DSBs on microtubules and motor proteins for repair, they exhibit random mobility.

When disruption of telomere capping happens, the telomeres start moving faster inside the nucleus, and behave like DSB ends (Dimitrova et al., 2008; Lottersberger et al., 2015). This mobility promotes telomere fusion repair of the uncapped telomeres through NHEJ pathway. The increased mobility and fusion repair of uncapped telomeres is disrupted by Kinesin-1 or Kinesin-2 knockdown, or via treatment with microtubule stabilizing agent, paclitaxel or microtubule destabilizing agent, nocodazole (Lottersberger et al., 2015).

Furthermore, in both yeast and murine cells, the increased random mobility was observed in damaged DNA outside of telomeres and their repair was depending on microtubules dynamics

and/or kinesin motor proteins (Chung & Zhao, 2015; Lottersberger et al., 2015). The model proposes that cytoplasmic microtubules and motor proteins might contribute to the mobilization of damaged chromatin within the nucleus through interactions with nuclear envelope-bridging protein complexes like the Linker of Nucleoskeleton and Cytoskeleton (LINC) complex (Tapley & Starr, 2013). Consistent with the described model, it has also been shown that the mobility and fusion repair of uncapped telomeres in mammalian cells depends on the LINC complex (Lottersberger et al., 2015). In this model they proposed that the microtubule dynamics affects the DNA DSB foci mobility by randomly poking the nuclear envelope. Based on this hypothesis, microtubule dynamics remotely affect the general movements of proteins inside the nuclear envelop, without direct interaction and biding to any component with the nucleus (Lottersberger et al., 2015).

Another possibility is if motor proteins and microtubule subunits operate like DNA repair proteins. This hypothesis is consistent with pull-down experiments showing that yeast Kinesin-14 is physically recruited to sub-telomeric DSB sites (Chan et al., 2011; Chung & Zhao, 2015; Poon & Mekhail, 2012). In addition, in human cells subjected to ionizing radiation, the kinesin KIF4A is associated with BRCA2 at DSB sites and KIF4A loss compromises the formation of Rad51 DNA repair foci (Wu et al., 2008). Moreover, ionizing radiation-induced damaged DNA foci exhibit increased mobility that is dependent on kinesins and microtubules (Lottersberger et al., 2015). Taken together, microtubules and motor proteins might play a role in DSB mobility and repair, although the directed transportation of cargo and the random movement of damaged DNA foci inside nuclei do not exactly match.

1.4 Hypothesis & objectives

The critical role of kinesin-13 proteins which is regulating spindle microtubule dynamics during cell mitosis is through their depolymerization activity. However, the exact mechanisms involved in their microtubule depolymerizing activity has remained a mystery for decades. The necessity of understanding their mechanism of action becomes even more crucial with the discovery of the new role of KIF2C in DNA damage response. To be able to figure out what KIF2C exactly do in the process of DNA DSB foci dynamics, we would need a better understanding of kinesin-13 induced microtubule depolymerzation. We hypothesize that the interaction of KIF2C with tubulin might be a key factor in the formation and mobility of DNA DSB foci, which would directly affect DNA repair efficiency and the integrity of genome. Hence, a thorough overview of tubulin biochemistry and kinesin-13 mechanism of action would substantially contribute to this apprehension. In this thesis we are trying to move the understanding of these mechanisms forward.

This thesis is based on the articles that either have been published or are in the process of being published. In Chapter 2 we present the X-ray crystal structure of a kinesin-13 construct (Kif2A-NM) bound to tubulin dimers to unravel the molecular mechanism of microtubule depolymerization by kinesin-13 proteins. Chapter 3 reports my work on the molecular relationship between structural change and nucleotide hydrolysis, where we provide experimental evidence indicating that tubulin conformational change leads to GTP hydrolysis. Chapter 4 attempt to determine the role of KIF2C in this process and in association with known players of DNA DSB response. The thesis concludes with a brief overview of the presented research findings and future directions of the work in Chapter 5.

CHAPTER 2: Ternary complex of Kif2A-bound tandem tubulin heterodimers represents a kinesin-13-mediated microtubule depolymerization reaction intermediate

Daria Trofimova[1], Mohammadjavad Paydar[2], Anthony Zara[1], Lama Talje[2], Benjamin H. Kwok[2†] and John S. Allingham[1†]

[1] Dept. of Biomedical and Molecular Sciences, Queen's University, Kingston, ON K7L 3N6, Canada.

[2] Institute for Research in Immunology and Cancer (IRIC), Département de médecine, Université de Montréal, P.O. Box 6128, Station Centre-Ville, Montréal, QC H3C 3J7, Canada.

[†]Correspondence and requests for materials should be addressed to B.H.K. (email: benjamin.kwok@umontreal.ca) or to J.S.A. (email: allinghj@queensu.ca)

2.1. AUTHOR CONTRIBUTION

Daria Trofimova: designed research, purified protein reagents, characterized the kinesin-tubulin interaction biochemically, crystallized the complex and determined its structure, analyzed the data and wrote the manuscript with input from all authors.

Mohammadjavad Paydar: purified protein reagents, characterized the kinesin-tubulin interaction biochemically and analyzed the data.

Anthony Zara: analyzed the data.

Lama Talje: purified protein reagents, characterized the kinesin-tubulin interaction biochemically.

Benjamin H. Kwok: designed research, purified protein reagents, characterized the kinesin-tubulin interaction biochemically, analyzed the data and wrote the manuscript with input from all authors.

John S. Allingham: designed research, purified protein reagents, crystallized the complex and determined its structure, analyzed the data and wrote the manuscript with input from all authors.

2.2 ABSTRACT

Kinesin-13 proteins are major microtubule regulatory factors that catalyze removal of tubulin subunits from microtubule ends. The class-specific "neck" and loop 2 regions of these motors are required for microtubule depolymerization, but their contributing roles are still unresolved because their interactions with microtubule ends have not been observed directly. Here we report the crystal structure of a catalytically active kinesin-13 monomer (Kif2A) in complex with two bent αβ-tubulin heterodimers in a head-to-tail array, providing a view of these interactions. The neck of Kif2A binds to one tubulin dimer and the motor core to the other, guiding insertion of the KVD motif of loop 2 in between them. AMPPNP-bound Kif2A can form stable complexes with tubulin in solution and trigger microtubule depolymerization. We also demonstrate the importance of the neck in modulating ATP turnover and catalytic depolymerization of microtubules. These results provide mechanistic insights into the catalytic cycles of kinesin-13.

2.3 INTRODUCTION

Microtubules are dynamic protein polymers that grow and shrink by addition and loss of αβ-tubulin subunits at their ends (Desai & Mitchison, 1997). A wide variety of regulatory factors control microtubule polymerization dynamics to allow rapid spatial remodeling of the microtubule cytoskeleton during the cell cycle(Desai & Mitchison, 1997; Heald & Nogales, 2002). This activity is essential for mitotic spindle assembly and chromosome segregation(Walczak et al., 2013), and enables directional transport of intracellular cargoes(Hirokawa et al., 2009). Kinesin-13 proteins are major microtubule-destabilizing factors in higher eukaryotes and a specialized class of motor proteins in the kinesin superfamily (Walczak et al., 2013). Rather than moving directionally along microtubules, kinesin-13s catalyze tubulin disassembly at microtubule ends (Desai et al., 1999). This activity is produced by a unique motor core found in the central region of the protein and is the basis for kinesin-13s' common designation as Kin-M (middle) or Kin-I (internal) kinesins (Desai et al., 1999; Lawrence et al., 2004).

Since the first seminal characterization of a kinesin-13 protein from *Xenopus* (XKCM1) as a microtubule depolymerase (Desai et al., 1999), we have gained substantial knowledge on kinesin-13 isoforms and their roles in microtubule dynamics regulation. We know that the four kinesin-13 members in humans, Kif2A, Kif2B, Kif2C (also known as MCAK), and Kif24, function in a wide range of biological processes, such as spindle assembly, chromosome segregation, microtubule-kinetochore attachment, and cilia formation (Walczak et al., 2013). Most, if not all, of these essential functions are associated with the ability of kinesin-13s to depolymerize microtubules and alter their polymerization dynamics. However, our understanding of how these enzymes catalyze the disassembly of microtubules is still limited.

In reconstituted *in vitro* systems, kinesin-13 proteins can rapidly target microtubule ends either directly or through one-dimensional diffusion (Helenius et al., 2006), and this targeting is enhanced by kinesin-13's positively charged neck (Cooper et al., 2010). Once at microtubule ends, these enzymes induce protofilament bending, as electron micrographs of depolymerizing microtubule ends show massive curled protofilament peels (Desai et al., 1999). It has been shown that each kinesin-13 motor core binds a single tubulin protofilament (Hunter et al., 2003), and forms contacts through the motor domain that stabilize intra-dimer curvature (Asenjo et al., 2013; Tan et al., 2008). Interestingly, the presence of the neck restricts motor domain binding to alternate tubulin dimers of curved tubulin protofilament rings (Mulder et al., 2009), but the molecular basis for this, and its implications on microtubule depolymerization, have not been determined.

The catalytic depolymerization of microtubules by kinesin-13 is an ATP-dependent process (Desai et al., 1999; Friel & Howard, 2011; Hunter et al., 2003; M. Wagenbach et al., 2008). In the landmark paper, Desai *et al*. found that AMPPNP-bound XKCM1 was enriched at microtubule ends, but also formed a high affinity stable complex with tubulin dimers; resolvable by size-exclusion chromatography (SEC) (Desai et al., 1999). This led to the hypothesis that although ATP is needed for targeting microtubule ends, its hydrolysis occurs later after depolymerization to release the enzyme from the dissociated tubulin dimers for additional rounds of catalysis (Wang et al., 2015). This idea is supported by the observation that ATP hydrolysis-defective mutants of human Kif2C are still capable of depolymerizing taxol-stabilized microtubules (M. Wagenbach et al., 2008; Wang et al., 2015). In contrast, an alternative model has also been proposed in which ATP hydrolysis occurs on the microtubule polymers prior to tubulin release (Friel & Howard, 2011; Hunter et al., 2003). This is based on a series of kinetics and microscopy-based experiments showing that microtubule ends strongly stimulate ATP

turnover (Hunter et al., 2003). Therefore, it remains an open question whether the ATP hydrolysis step is needed for dissociating tubulin dimers from microtubule polymers. Resolving this question is crucial in understanding the molecular basis of kinesin-13-catalyzed microtubule depolymerization.

Mechanism aside, another important fundamental question is: What constitutes a functional depolymerase? Full-length kinesin-13 proteins are dimeric (Noda et al., 1995; Wordeman & Mitchison, 1995), and yet monomeric kinesin-13 constructs composed of the conserved motor domain and the N-terminally located neck are fully capable of depolymerizing microtubules (Maney et al., 2001; Moore & Wordeman, 2004; Niederstrasser et al., 2002; Ogawa et al., 2004; Ovechkina et al., 2002). Accordingly, the neck plus the motor domain (denoted NM hereafter) is sometimes referred to as the minimal domain (i.e. kinesin-13-NM). Kinesin-13s from lower eukaryotes may be an exception of the neck requirement for microtubule depolymerization (Moores et al., 2002). Biochemical and mutagenesis studies of these functional units have shown that the key elements required for microtubule depolymerization are the conserved KVD motif within loop L2 of the motor core, which also contains the ATPase domain, and the positively charged kinesin-13 neck (Asenjo et al., 2013; C. A. Moores et al., 2006; Ogawa et al., 2004; Ovechkina et al., 2002). Although crystallization studies have given us a glimpse of the structure of the KVD motif of the motor domain (Ogawa et al., 2004; Wang et al., 2017; Wang et al., 2015), direct experimental data on how it may promote disassembly of adjacent tubulin dimers is lacking in these early publications. Moreover, the complete neck domain is either not present or not resolved in these structures.

To better understand the molecular mechanism by which these key structural elements of kinesin-13 proteins induce microtubule depolymerization, we present the X-ray crystal structure

of a microtubule-depolymerization competent kinesin-13 construct (Kif2A-NM) bound to a head-to-tail array of two tubulin dimers. We also define the role of ATP hydrolysis by kinesin-13 in the catalyzed depolymerization reaction. Our Kif2A-NM-tubulin complex structure reveals that an AMPPNP-bound Kif2A monomer can simultaneously bind to two tubulin dimers, and that this interaction is accompanied by severe bending of the longitudinally associated tubulin dimers, more so than any other αβ-tubulin structures reported to date. Our biochemical analysis suggests that this outward bending of tubulins, resembling the kinesin-13-catalyzed structural changes at microtubule ends, is sufficient to trigger depolymerization.

2.4 RESULTS

2.4.1 Structure of the Kif2A-NM−tubulin tetramer complex

Human Kif2A is a 706-amino-acid kinesin-13 that functions as a homodimer *in vivo* (Aizawa et al., 1992). Its motor domain is situated between residues 223 and 553, and is flanked by long N and C-terminal regions that mediate subcellular targeting and dimerization (Figure 2.1a) (Ems-McClung et al., 2007; Maney et al., 2001; Wordeman et al., 1999). A monomeric motor domain construct that includes the kinesin-13-specific neck (Kif2A-NM; amino acids 153-553) exhibits the ability to catalytically depolymerize microtubules *in vitro* (Figure 2.1b), similar to that of the full-length dimeric kinesin-13 as previously reported (Ems-McClung et al., 2007; Friel & Howard, 2011; Helenius et al., 2006; Hertzer et al., 2006; Maney et al., 2001). However, a motor domain construct lacking the majority of the neck (Kif2A-MD; amino acids 203-554) is incapable of depolymerizing microtubules *in vitro*, consistent with published literature (Hertzer et al., 2006; Ogawa et al., 2004; Ovechkina et al., 2002; W. Wang et al., 2012). A prediction is that the neck of kinesin-13 motors acts as an additional tether to the microtubule wall (Moores & Milligan, 2006), but its precise binding site and contribution to microtubule depolymerization proficiency is unknown.

To gain insight into the mechanism of microtubule depolymerization by kinesin-13, we set out to solve the crystal structure of a depolymerization-competent Kif2A construct (Kif2A-NM) in complex with tubulin. In the presence of the non-hydrolyzable ATP analog AMPPNP, a mixture of Kif2A-NM, tubulin, and the tubulin-capping protein DARPin (Cao et al., 2014; Pecqueur et al., 2012) (molar ratio of about 0.8:1:1) gave two species that eluted earlier than the tubulin:DARPin complex by SEC (**Figure 2.1c**). Their apparent molecular masses were estimated to be 270 and 150 kDa based on molecular weight standards and both contained Kif2A-NM, tubulin, and

DARPin according to SDS-PAGE analysis (**Figure 2.1d**). When we pooled and concentrated the 150 kDa peak fractions for crystallization, we observed that much of the smaller species converted into the larger species upon re-running SEC, indicating that the two are interchangeable (Supplementary Figure 2.1). Of the two peaks, higher quality crystals grew from the 150 kDa one and these were harvested for X-ray diffraction.

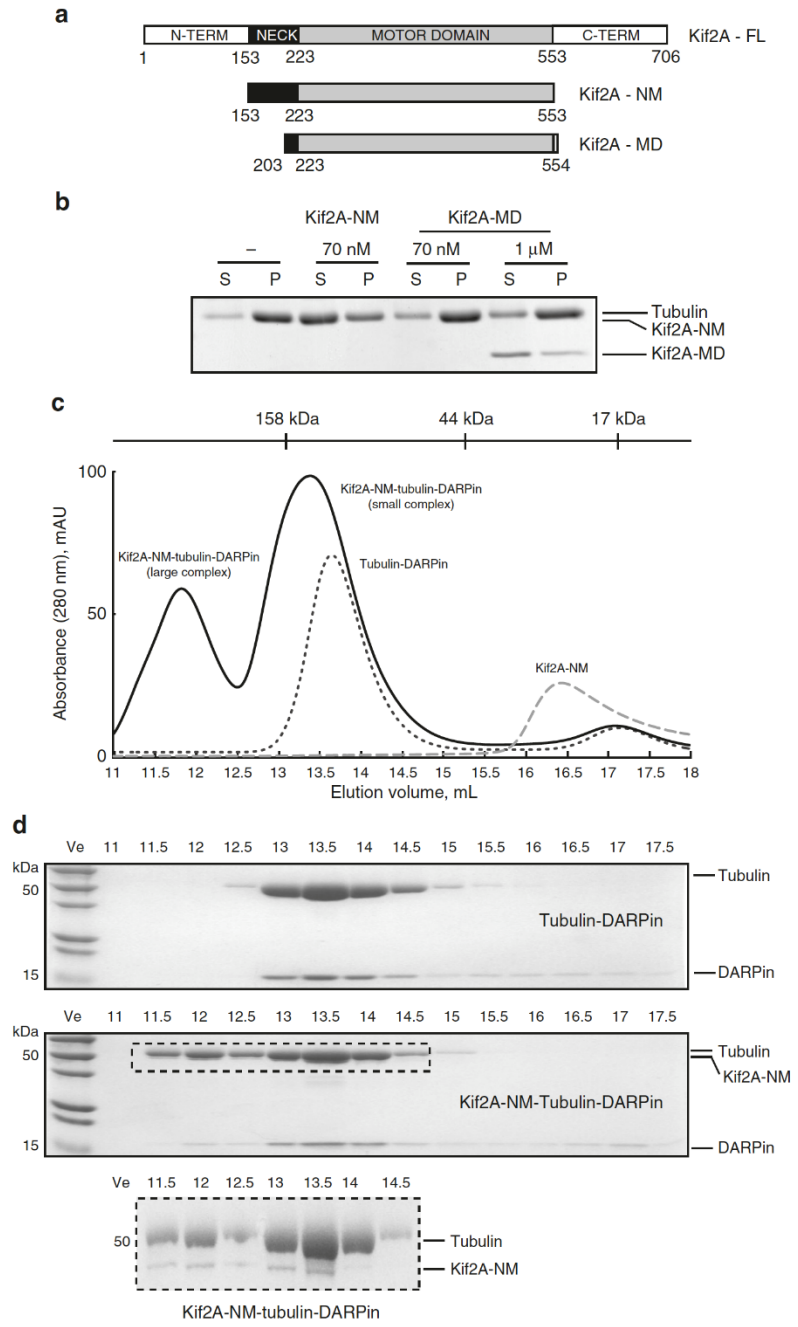

Figure 2.1 Functional analysis of Kif2A constructs

(**a**) Domain composition of human Kif2A and schematic of the Kif2A constructs used in this study. The length of the bar is proportional to the number of amino acids. (**b**) microtubule depolymerization activity of Kif2A constructs. Taxol-stabilized microtubules were incubated with

the indicated concentrations of Kif2A-NM and Kif2A-MD, or no kinesin for 10 min in BRB80 buffer. Free tubulin and microtubule polymers were separated into supernatant (S) and pellet (P) fractions by ultra-centrifugation-based sedimentation assay. Fractions were resuspended and boiled in Laemli buffer. Equal portions were loaded and analyzed on a SDS-PAGE gel. (**c**) SEC profiles of Kif2A-NM alone (grey dashed line), tubulin-DARPin complex (black dotted line), and Kif2A-NM-tubulin-DARPin complex in 0.8:1:1 molar ratio (black solid line). All samples were supplemented with 0.1 mM AMPPNP and applied to an S 200 10/300 GL column in HEPES buffer. (**d**) 12% SDS-PAGE gels of elution fractions from the above experiments. The molecular weight of Kif2A-NM = 48 kDa, tubulin = 50 kDa and DARPin = 18 kDa. The inset shows a 10% SDS-PAGE gel of fractions containing the Kif2A-NM-tubulin-DARPin complex in order to visualize the Kif2A and tubulin proteins.

The structure of the crystallized complex was determined by molecular replacement (MR) using the coordinates of the ADP-bound Kif2A motor domain (PDB ID: 2GRY), and the α-tubulin, β-tubulin, and DARPin subunits from the Kinesin-1-tubulin complex (PDB ID: 4LNU (Cao et al., 2014)) as separate rigid bodies. The MR solution comprised one Kif2A-NM monomer bound to the concave side of a curved assembly of two αβ-tubulin dimers arranged head-to-tail and capped at the plus end by DARPin (**Figure 2.2a**). The final structure was refined to a resolution of ~3.5 Å (**Table S2.1**), giving electron density maps that show well-connected main chain density for all subunits of the Kif2A-NM-tubulin-DARPin complex. Notably, the N-terminal section (residues 157 to 195) of the neck of Kif2A can be seen interacting with one of the tubulin dimers (labeled $\alpha_1\beta_1$; buried surface area = 915 Å^2). The other dimer (labeled $\alpha_2\beta_2$) is occupied by the Kif2A motor domain, which contains Mg AMPPNP in the active site. As predicted from molecular modeling

studies (Ogawa et al., 2004; Wang et al., 2015), the tip of the β-hairpin of loop 2 of the motor domain reaches into the interdimer interface to interact with both α_2 and β_1 tubulin.

To confirm that the subunit arrangement in the crystallographic complex is also formed in solution, we performed in-line SEC and small-angle X-ray scattering (SEC-SAXS) experiments on the contents of the 270 kDa peak. The SAXS data shows that the shape of the molecular envelope has nearly identical dimensions to the crystallized 1:2:1 Kif2A-NM-tubulin-DARPin complex (**Figure 2.2b**). It is elongated with a maximal dimension (D_{max}) of 195 Å, and is asymmetric, with a bulge on one end where Kif2A is located. The radius of gyration (Rg) was estimated to be 55.9 Å, and the modeling fit was validated by comparing the experimental and theoretical SAXS profiles. The theoretical scattering curve obtained for the crystallized complex fits the experimental SAXS profile with a χ^2-value of 1.09 (Supplementary Figure 2.2 and Table S 2.1). This result demonstrates that Kif2A-NM can bind to two αβ-tubulin dimers in solution.

To determine the relationship between the molecular assemblies in the SEC peaks, we varied the molar ratio of DARPin relative to Kif2A-NM and tubulin in the assembly mixture. We found that addition of excess DARPin favoured formation of the small complex over the large one (**Figure 2.2c**). This implies that excess DARPin is able to wedge apart the tubulin dimers held together by Kif2A-NM, thereby releasing the one associated with the neck domain. However, when DARPin is in lower abundance, such as in the experimental condition during SEC to isolate the ternary complex (**Figure 2.1c**), the head-to-tail array of tubulin dimers can form a stable complex with AMPPNP-bound Kif2A-NM. These findings suggest that excess DARPin can compete Kif2A-NM off the tethered double tubulin dimers. This discovery would prove useful for understanding how neck domain interaction with tubulin contributes to catalytic activity of Kif2A-NM, as described below.

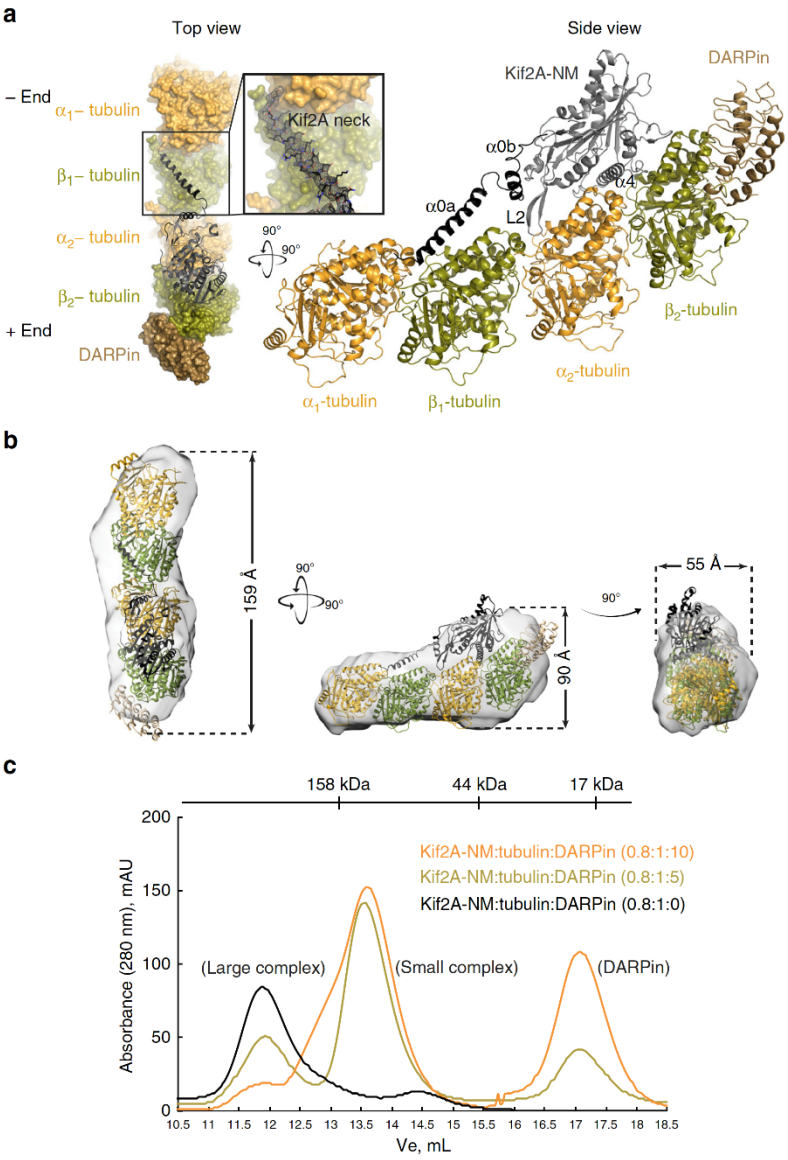

Figure 2.2 Structure of Kif2A-NM in complex with tubulin and DARPin.

(**a**) The X-ray crystal structure of a Kif2A-NM-tubulin-DARPin complex is shown in two views (from the top and side of the tubulin filament). The Kif2A is in black; α-tubulin is in orange; β-tubulin is in green; and DARPin is in light brown. The insert represents the F_{obs}-F_{calc} omit map (contoured at 3.0 σ) of the neck of Kif2A-NM calculated after deletion of the neck from final model. All figures of structural models were generated with PyMOL (Schrodinger, 2010). (**b**) SAXS envelopes for the Kif2A-NM-tubulin-DARPin complex. The crystal structure of the

complex shown in ribbons representation and superimposed onto envelopes (in grey) by Chimera (Pettersen et al., 2004). (**c**) SEC profiles of mixtures of Kif2A-NM, tubulin, and DARPin at the indicated molar ratios. All mixtures were supplemented with 0.1 mM AMPPNP and passed through a S200 10/300 GL column in HEPES buffer.

2.4.2 Interactions of the Kif2A neck with tubulin

Although the electron density map did not provide coverage of all the amino acid side-chains in the model, there was adequate density for many bulkier residues to permit unambiguous assignment of the helical register of the neck (**Figure 2.3a-b**). The neck contacts both subunits in the $\alpha_1\beta_1$-tubulin dimer (**Figure 2.3b**). Residues 157-159 form a random coil that interacts with the C-terminal end of helix H11 in α_1-tubulin and the C-terminus of β_1-tubulin. Interestingly, this surface of the tubulin dimer is not an interface for the motor domain of kinesins. Residues 160-185 form a well-defined helix (α0a) that runs antiparallel to helix H12 of β_1-tubulin. Many of the positively charged residues in α0a juxtapose the large patch of negatively charged residues on the surface of β_1-tubulin. This supports previous observations that point mutations that preserve the positive charge richness of the neck retain depolymerization function (Ovechkina et al., 2002). Additional neck-stabilizing interactions include the non-polar side chain of Val160 and several negatively charged (Glu164, Glu171, Glu182) and polar residues (Asn158, Gln167, Gln178) that contact the buried helix H12 of β_1-tubulin.

Helix α0a is brought into alignment with helix H12 of β_1-tubulin by a second, shorter helix (α0b; residues 195-208; **Figure 2.3a**) that forms alongside the β-hairpin of loop 2 **(Figure 2.3b)**. Helices α0a and α0b are connected by a short, kinked loop (formed by residues 188-194) that changes the direction of the neck. They also interact via a salt bridge between Arg181 and Glu196.

This conformation of α0b is almost identical to that of ADP-Kif2C (PDB ID: 2HEH) and the short loop 2 construct of Kif2C (PDB ID: 4Y05) (Ogawa et al., 2004; Wang et al., 2015), suggesting that α0a of Kif2C aligns along H12 of β-tubulin as well. The other reported conformations of α0b in the Kif2C-tubulin complex (PDB ID: 5MIO) (Wang et al., 2017) and the "activated conformation" of the mouse Kif2C core (PDB IDs: 5XJA and 5XJB) (Ogawa et al., 2017) indicate that the neck can dissociate from the distal tubulin binding site whilst the motor core is engaged with tubulin (Supplementary Figure 2.3). The purpose, if any, of these conformations within the kinesin-13 catalyzed microtubule depolymerization cycle is uncertain given the absence of proper context (e.g. an adjacent tubulin dimer), and will likely require alternate experimental settings to resolve.

2.4.3 Movement of the longitudinal tubulin interface

The Lys262, Val263, Asp264 triplet (KVD motif) of Kif2A interacts with both β_1-tubulin and α_2-tubulin at the inter-dimer interface (**Figure 2.3c**). Val263 inserts into a hydrophobic pocket formed by the non-polar atoms of Tyr262, Pro263, Arg264, Ile265, Asp431, Glu434, and Val435 of α_2-tubulin, while the C_α and C_β atoms of Asp264 of Kif2A are nearest to Tyr262 of α_2-tubulin and Lys402 of β_1-tubulin. Adjacent to the KVD triplet, Leu265 interacts with His406 (β_1) and Tyr262 (α_2), and Thr266 is in position to H-bond with the ε-amino group of Lys402 (β_1). Although Lys262 and Asp264 are close to acidic and basic resides of α_2 and β_1, respectively, H-bonds or salt bridges are not observed in the Kif2A-NM-tubulin-DARPin complex in the manner predicted previously by computational modeling (Wang et al., 2015). Rather, the side-chain of Lys262 appears to extend away from the tubulin surface, and Asp264's side-chain turns inward to form an intramolecular H-bond with Thr266. Interestingly, these interactions and the overall L2 loop conformation are

remarkably similar to those of the Kif2C-tubulin complex (PDB ID: 5MIO) (Wang et al., 2017). Given the recent observation that interchanging the lysine/glutamate residues of the Kif2C KVD motif compromised microtubule-depolymerization activity (Wang et al., 2015), it is possible that the importance of these residues play out at an earlier stage of microtubule binding than has been captured in the Kif2A-NM-tubulin-DARPin complex.

Directly next to the KVD insertion site, there is noticeable movement of the T7–H8 motif of α_2-tubulin away from its position in the Kif2C-tubulin complex (**Figure 2.3d;** the r.m.s.d. of the Cα positions of this motif is 3.0 Å and maximum Cα displacement is 6.1 Å). This finding is important because the T7–H8 motif forms a major longitudinal interface in protofilaments and is presumed to act as a cohesive structural unit with the T3 and T5 loops of the opposing β-tubulin subunit (Alushin et al., 2014). Curved tandem tubulin complexes formed by stathmin-like proteins do not exhibit this dramatic deformation either, unless they are complexed with microtubule-depolymerizing agents that lie close to the T7–H8 motif, such as vinblastine (**Figure 2.3d,** the r.m.s.d. of Cα positions is 0.8 Å relative to PDB ID: 4EB6) (Gigant et al., 2000; Panda et al., 1996; Ranaivoson et al., 2012; Ravelli et al., 2004). It is therefore possible that positioning the tip of loop 2 near this motif helps elicit a T7–H8 conformational change as part of the protofilament bending mechanism by kinesin-13. This change was not observed in the Kif2C-tubulin complex (Wang et al., 2017), presumably due to the lack of an adjoining tubulin dimer.

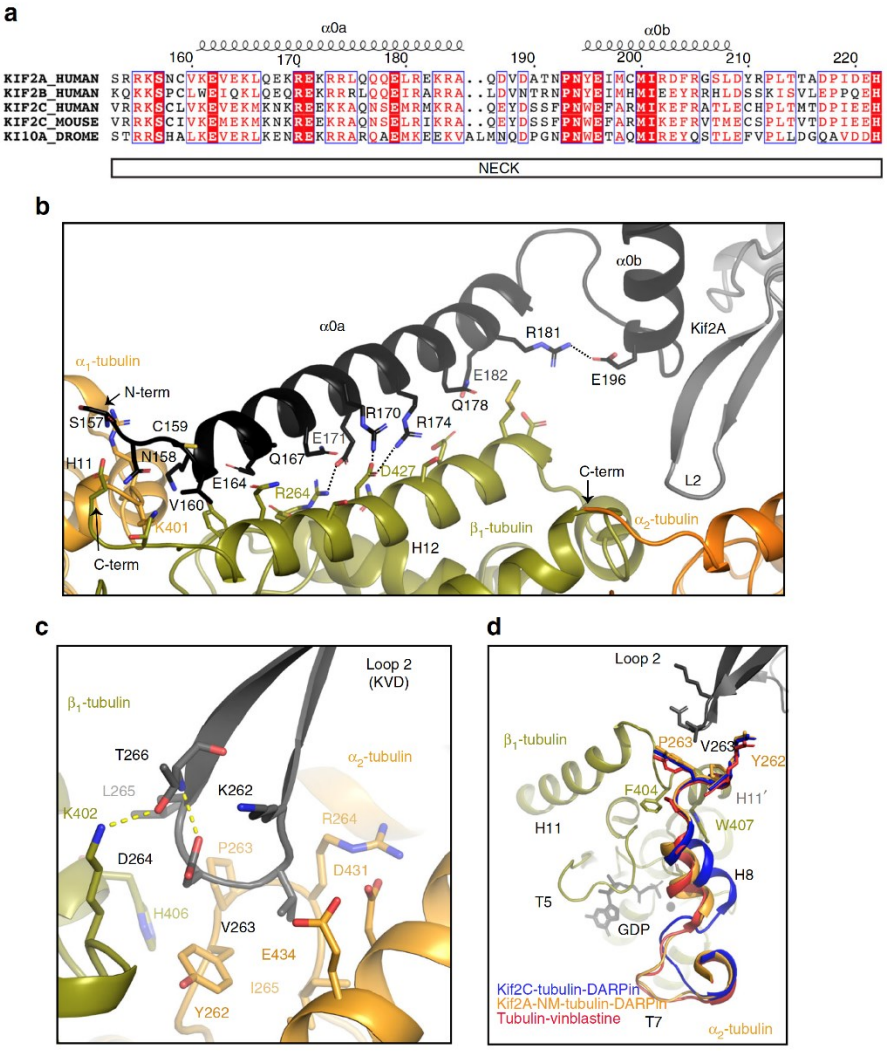

Figure 2.3 Kif2A neck and loop 2 interactions with tubulin.

(**a**) Sequence alignment of selected kinesin-13 motors was performed by Clustal Omega (Sievers et al., 2011), and the assignment of the secondary structure for the neck was performed using ESPript (Robert & Gouet, 2014) according to the tubulin-bound Kif2A crystal structure. (**b**) Regions in α_1-tubulin (orange) and β1-tubulin (green) that interact with the Kif2A neck helix (black) are shown in cartoon format, with selected side chain residues shown as sticks. (**c**) Interactions of loop 2 of Kif2A with β_1 (green) and α_2-tubulin (orange) at the interdimer interface.

(**d**) Conformation of the T7 – H8 motif of α_2-tubulin in the Kif2A-NM-tubulin-DARPin complex (orange) is shown as a view looking through α_2-tubulin, toward the nucleotide pocket of β1-tubulin (green). T7 – H8 of the Kif2C-tubulin-DARPin complex (PDB ID: 5MIO; blue) and stathmin-tubulin-vinblastine complex (PDB ID: 4EB6, red) are shown, along with the position of KVD motif of Kif2A, after superposition using PyMol.

2.4.4 Conformation of the tubulin-bound Kif2A motor domain

In the complex, Kif2A-NM is bound to the non-hydrolyzable ATP analog AMPPNP. Superimposing isolated (tubulin-free) ADP-Kif2A (PDB ID: 2GRY) via the P-loop shows a considerable reconfiguration of Switch 1 and 2 (**Figure 2.4a**), similar to AMPPNP-bound Kif2C-tubulin and many AMPPNP-bound motile kinesins (Chang et al., 2013; Gigant et al., 2013; Parke et al., 2010; Wang et al., 2017). The two universally conserved serine residues in Switch 1 (Ser431 and Ser433) are within distance to establish hydrogen bonds with the terminal nucleotide phosphate and bound Mg^{2+}, and loop L11 is now fully ordered in the Kif2A-NM-tubulin-DARPin complex. Loops L8 and L12 (and the β5a-β5b hairpin) also change position in the AMPPNP-Kif2A-NM motor core to interact with helices H8 and H12 of β_2-tubulin **(Figure 2.4b)**. The same is true for α4 and L11, which, along with α6, contact the H3, H11 and H12 helices of α_2-tubulin. The most striking change from isolated Kif2A involves a ~26° rotation of the α4 and α5 helices, allowing L12 to engage helix H12 of β_2-tubulin**.** A nearly identical rotation of α4 and α5 was observed in the Kif2C-tubulin complex, adding support to the proposal that the tubulin-bound conformation of kinesin-13s is similar to that of kinesin-1 in its tubulin-bound state (Cao et al., 2014; Gigant et al., 2013; Wang et al., 2017; Wang et al., 2015), as emphasized in **Figure 2.4c**. These findings argue against postulations that a more curved tubulin interface on the kinesin-13

motor domain explains their microtubule depolymerization capability (Mulder et al., 2009; Ogawa et al., 2004). Although the recent mouse Kif2Ccore:ADP-AlFx and Kif2Ccore:ADP-BeFx structures (PDB ID: 5XJA and 5XJB, respectively) were used to support this hypothesis and are presented as the "activated" conformation that sustains the KIF2-tubulin 1:2 complex (Ogawa et al., 2017), the tubulin binding elements of these structures (L8, β5a-β5b β-sheet, L11, L12, α4, α5 and α6) superimpose poorly with those of Kif2A-NM (Supplementary Figure 2.4).

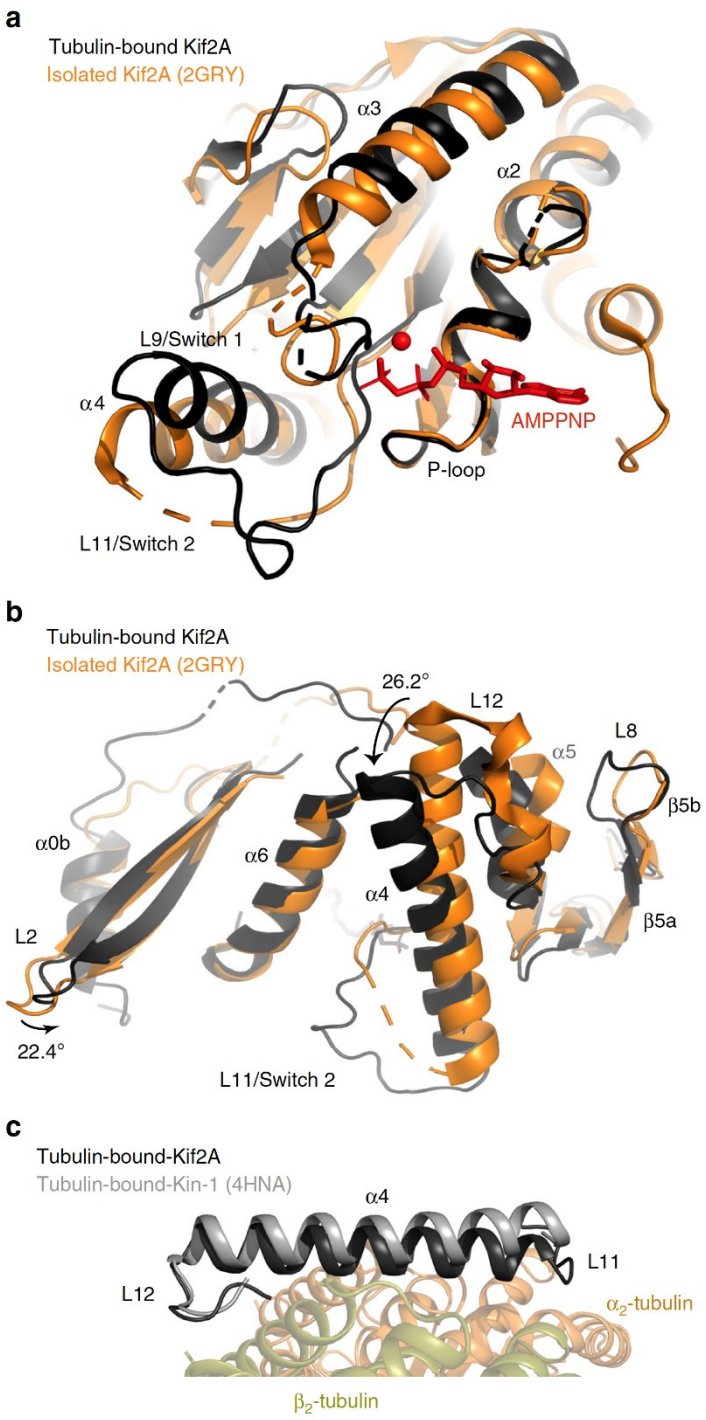

Figure 2.4 Conformation of the Kif2A motor domain.

(a) View of the nucleotide-binding pocket of tubulin-bound Kif2A (black) superimposed on isolated ADP-Kif2A (orange; PDB ID: 2GRY) via the P-loop. **(b)** View of the tubulin-binding

surface. **(c)** Comparison of the α4 helix orientation in the tubulin-bound Kif2A (black) and tubulin-bound Kin-1 (PDB ID: 4HNA, grey). Tubulin is represented in cartoon format.

2.4.5 Curvature of the Kif2A-NM-bound tubulin oligomer

A notable feature in our Kif2A-tubulin ternary structure is that each tubulin subunit is related by a distinct bend angle **(Figure 2.5, side view)**, indicating that the interactions of the neck, L2 loop, and motor domain of Kif2A each affect tubulin polymer curvature in different ways. The curvature of $\alpha_2\beta_2$-tubulin (12.1°) marginally exceeds the Apo and ADP–AlF_4-bound kinesin-1 complexes (11.6° and 9.2°, respectively) (Cao et al., 2014; Gigant et al., 2013), and is less curved than the Kif2C-DARPin fusion (14.7°) (Wang et al., 2017). In contrast, the tubulin dimer bound by Kif2A's neck is much more curved (15.3°), and there is an even larger bend at the inter-dimer interface (15.8°). This implies that the kinesin-13-specific neck and the extended L2 loop of Kif2A are the major contributors to longitudinal tubulin bending. Combined with the curvature at $\alpha_2\beta_2$-tubulin, the tethered tubulin complex formed by Kif2A-NM is more curved than any other tubulin structure (see examples in Supplementary Figure 2.5).

The Kif2A-NM-tubulin-DARPin complex also shows a rotational displacement of β-tubulin relative to α-tubulin in both dimers (**Figure 2.5, top view**). While this has been described for cryo-EM structures of tubulin rings formed by the *Drosophila* kinesin-13 Klp10A (Asenjo et al., 2013), and for stathmin-tubulin complexes containing vinca-domain ligands (Ranaivoson et al., 2012), the divergence from linearity is more pronounced for Kif2A-NM-bound tubulin (**Figure 2.5**). This, in combination with the substantial outward curvature of tubulin subunits, would be incompatible with the straight lateral contacts within the microtubule lattice.

By superimposing each Kif2A-NM-bound tubulin subunit onto the corresponding subunits

of the less-curved stathmin-tubulin-cholchicine complex (PDB ID: 1SA0), subtle structural differences emerge that could explain how additional curvature and rotation are accommodated in the Kif2A-NM-tubulin complex. One involves the shift in the T7-H8 helix of α_2-tubulin described earlier. Coincidental with this change are subtle adjustments of the side chain dihedral angles of Phe404, His406 and Trp407 in H11' of β_2-tubulin. These residues form a localized pocket of non-polar side chains of helix H8 at the inter-dimer interface. Similar changes are visible, albeit less pronounced, at the intra-dimer interface of $\alpha_1\beta_1$-tubulin. In β_1-tubulin, there is also a slight upward shift of the helix H12 toward Kif2A, along with movement of the H10-S9 loop ~ 0.6 Å closer to α_1-tubulin. At the $\alpha_2\beta_2$-tubulin, where curvature is the lowest, there is barely any change.

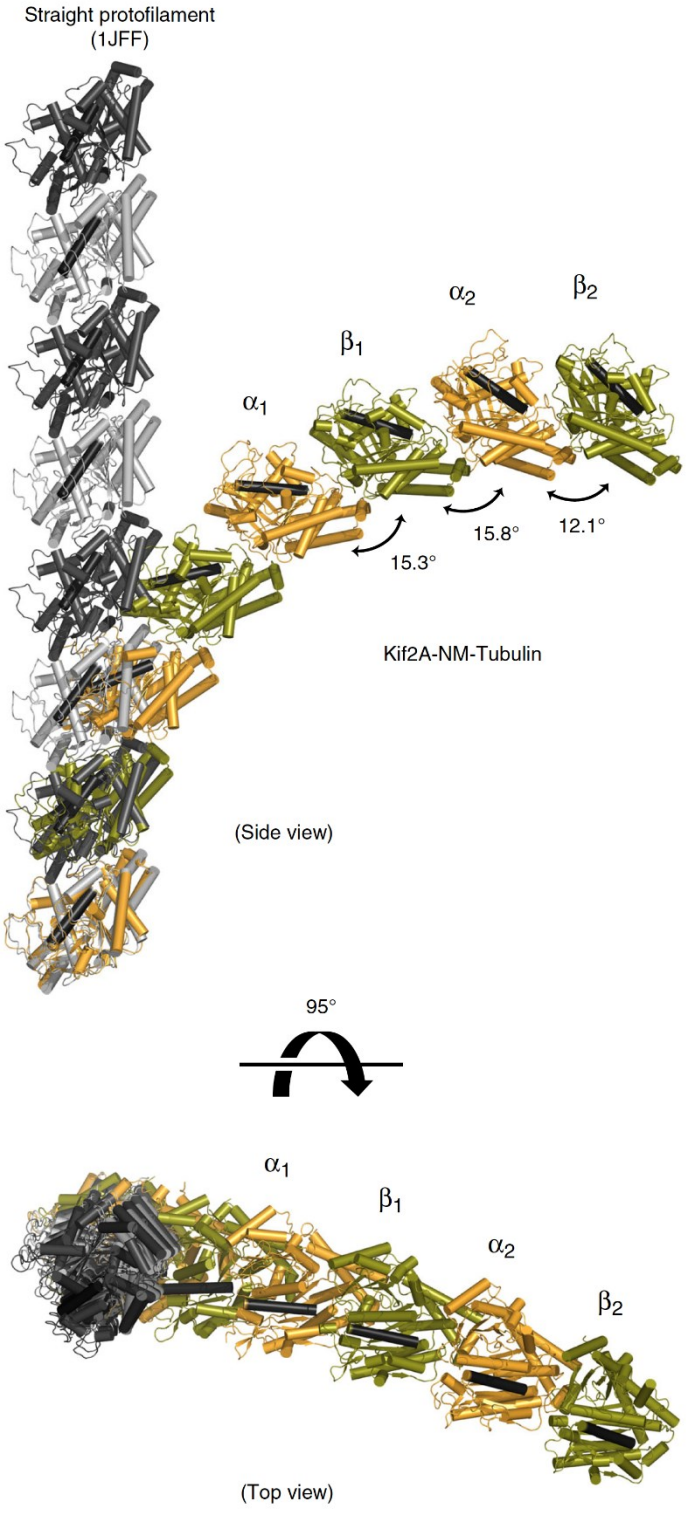
Straight protofilament
(1JFF)
α2
β2
β1
α1
15.8°
12.1°
15.3°
Kif2A-NM-Tubulin
(Side view)
95°
α1
β1
α2
β2
(Top view)

Figure 2.5 Curvature and rotational displacement of tubulin induced by Kif2A-NM.

Views are from the side and looking down the long axis of the straight protofilament model. Tubulin subunits of the Kif2A-NM-tubulin-DARPin complex (Kif2A and DARPin are not shown) are colored orange (α-tubulin) and green (β-tubulin), within which a single helix is colored black as a reference point. Straight protofilament structure (α-tubulin in light grey, β-tubulin in dark grey PDB ID: 1JFF) is shown for reference. Extended protofilaments were generated by aligning additional copies of each tubulin complex in an overlapping fashion. The degree of rotation between α and β-tubulin subunits in the Kif2A-NM-tubulin-DARPin complex was determined from the transformation required to superimpose each subunit within, or between, each heterodimer using the RotationAxis plugin in PyMOL (https://pymolwiki.org/index.php/RotationAxis).

2.4.6 ATP turnovers are modulated by neck binding to tubulin

To evaluate the relevance of the 1:2 Kif2A-tubulin complex in terms of Kif2A's function as an enzyme, we measured the tubulin-stimulated ATPase activity of the Kif2A-NM and Kif2A-MD constructs in the presence or absence of excess DARPin. We postulated that if binding of the Kif2A neck to a second αβ-tubulin subunit participates in the tubulin-stimulated turnover of ATP, Kif2A-NM activity should be affected by the presence of excess DARPin because DARPin and the neck cannot bind to the $\alpha_1\beta_1$-tubulin dimer simultaneously. Indeed, we observed that excess DARPin significantly suppressed tubulin-stimulated ATPase activity of Kif2A-NM (**Figure 2.6a**). In contrast, the Kif2A-MD construct, which only forms a 1:1 complex with tubulin (Supplementary Figure 2.6), was not affected by DARPin. To verify that our observation is true of other kinesin-13s, we performed this ATPase experiment with human Kif2C and observed an

identical result (**Figure 2.6b**). This suggests that formation of the 1:2 kinesin-tubulin complex is also true for Kif2C/MCAK.

2.4.7 microtubule-stimulated ATP turnover and tubulin disassembly

Given the competing nature of DARPin and kinesin-13-NM in binding to tubulin dimers as demonstrated by the dimer-stimulated ATPase activity **(Figure 2.6a-b**), we wondered if we could use DARPin to probe for the catalytic cycles of kinesin-13-mediated microtubule depolymerization, in particular, the relationship between ATP hydrolysis of kinesin-13 and tubulin disassembly. Since DARPin's binding site is masked when tubulins are incorporated into the polymer (except those at the ends) we anticipated that it would have no or limited effect on microtubule-stimulated activity of kinesin-13. To verify this, we measured the average microtubule-stimulated ATPase rates of Kif2A-NM and Kif2A-MD in the absence or presence of DARPin with excess microtubules (at [tubulin dimer] = 2 μM) over a 10-min reaction time. We chose the 10-min reaction time because of the relatively constant turnover rate over this time period when microtubules were still in excess (i.e. when [tubulin] > 1 μM). To our surprise, we found that DARPin significantly suppressed microtubule-stimulated ATPase activity of Kif2A-NM, but not that of Kif2A-MD (**Figure 2.6c**). Identical results were obtained for Kif2C-NM and Kif2C-MD (**Figure 2.6d**). Because of this unexpected result, we considered the possibility that DARPin might potentiate, instead of inhibit, Kif2A-NM- and Kif2C-NM-induced microtubule depolymerization resulting in microtubule concentration falling below 1 μM (at which microtubules became limiting in stimulating ATP turnover of Kif2A-NM, and would result in a decrease in ATPase rate). To address this, we ran time course experiments at 2.5-min intervals to monitor ATPase activity of Kif2A-NM over time. As we anticipated, the ATPase rates of our

control experiment without DARPin stayed unchanged over the 10-min time period. In contrast, the initial ATPase rate of Kif2A-NM in the presence of DARPin (both 2 μM and 20 μM) did not deviate much from that of the control, but the rate diminished over time (**Figure 2.6e**). To confirm that the time-dependent decrease in ATPase rate was due to the loss of polymers over time, we removed portions of the reactions in some of our experimental sets (n=3) and subjected them to ultracentrifugation to separate microtubules and the dissociated tubulin dimers. The results from these sedimentation experiments indeed confirmed our hypothesis (**Figure 2.6f**). We found that DARPin potentiated the effect of Kif2A-NM and that the excess loss of microtubules could account for the decrease in ATPase rates in the presence of DARPin at later time points.

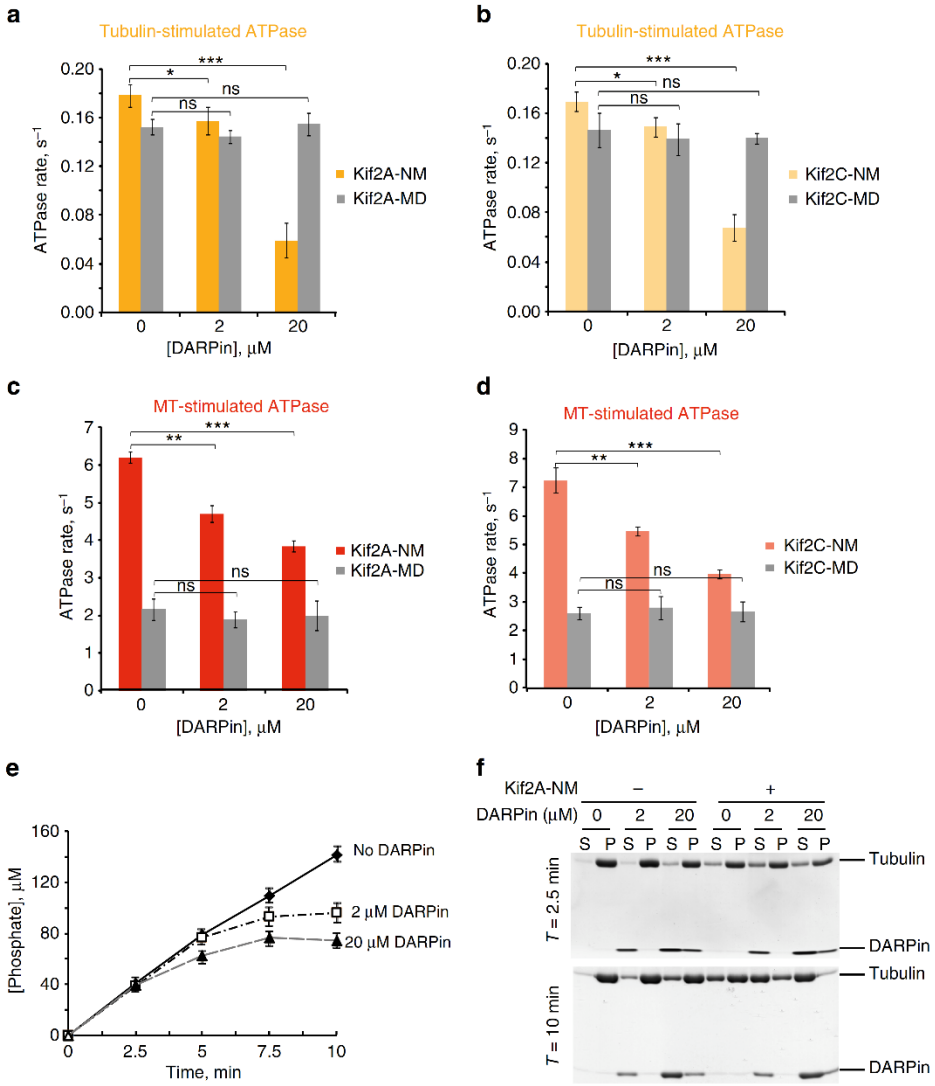

Figure 2.6 Microtubule-stimulated ATPase and microtubule-depolymerizing activities of kinesin-13s.

(**a-b**) Effect of DARPin on tubulin-stimulated ATPase activity of kinesin-13 proteins. ATP turnover rates of Kif2A-NM (orange) and Kif2A-MD (grey) in the presence of tubulin with the indicated concentrations of DARPin are shown in (**a**). Equivalent data for Kif2C-NM (light orange) and Kif2C-MD (grey) are shown in (**b**). (**c-d**) Effects of DARPin on microtubule-stimulated ATPase activities of kinesin-13 proteins: (**c**) ATP turnover rates by Kif2A-NM (red)

and Kif2A-MD (grey) in the presence of 2 μM of taxol-stabilized microtubules and the indicated concentrations of DARPin are shown. (**d**) Corresponding data sets of experiments for Kif2C-NM (light red) and Kif2C-MD (grey) as shown. Data from a-b represent averages from at least 4 independent experiments. Error bars, S.D.; ns: $p > 0.05$; * $p \leq 0.05$; ** $p \leq 0.01$; *** $p \leq 0.001$, by Student *t*-test. (**e**) Time course plots of inorganic phosphate release by Kif2A-NM under the same experimental conditions as in (**c**). Averages from N=3. Error bars, S.D. (**f**) Monitoring of microtubule polymers present at the 2.5-min and 10-min time points of the experiment shown in (**c**) (right 3 pairs) and the corresponding controls without Kif2A-NM (left 3 pairs) by a centrifugation-based sedimentation assay. S, supernatant fraction; P, pellet fraction. Samples were resolved by SDS-PAGE and gels were stained with Coomassie-blue. A representative gel is shown.

Our biochemical analyses of Kif2A-NM with DARPin presented an interesting scenario: DARPin interfered with Kif2A-NM binding to tubulin and inhibited its tubulin dimer-stimulated ATP turnover, but potentiated its effect on microtubule depolymerization. This brought back an important question: What is ATP hydrolysis actually needed for? Our Kif2A-NM-tubulin-DARPin structure suggests that Kif2A-NM binding induced curvature of adjacent tubulin dimers in the presence of AMPPNP that could be sufficient to trigger tubulin dissociation from microtubule polymers. However, published data from vertebrate kinesin-13s indicated that AMPPNP is insufficient to support catalytic depolymerization of microtubules (Wang et al., 2015). Therefore, ATP hydrolysis is likely needed either for depolymerization, or for releasing kinesin-13s from the dissociated tubulin dimers to ensure catalytic removal of tubulin dimers from microtubule ends. Our SEC data suggested excess DARPin could dissociate the 1:2 Kif2A-NM:tubulin complex into 1:1 complex instead. Deducing from this result, we postulated that excess DARPin might mimic ATP turnover-mediated Kif2A-NM dissociation from the 1:2

complex with adjacent tubulin dimers from microtubule ends. To test this, we performed Kif2A-NM-induced microtubule depolymerization assays in the presence of DARPin with AMPPNP or ADP (as a control). Consistent with published literature (Ogawa et al., 2017; Wang et al., 2015), Kif2A-NM was not able to induce substantial microtubule depolymerization with either AMPPNP or ADP (**Figure 2.7a**). Remarkably, in the presence of DARPin, Kif2A-NM was able to depolymerize microtubules with AMPPNP, but not with ADP. Similar result was obtained using Kif2C-NM (**Figure 2.7b**). Importantly, DARPin alone (from 0.25-2 μM) has negligible effect on microtubule depolymerization (Supplementary Figure 2.7). Given that AMPPNP is a non-hydrolyzable analog of ATP, our result indicated that ATP binding, rather than its hydrolysis, is needed to induce microtubule depolymerization. It also suggests that ATP hydrolysis is required for releasing the bound Kif2A-NM from the dissociated tubulin dimers, and that the presence of DARPin bypasses this requirement by releasing the enzyme from the bound tubulin dimers, likely via competition with its neck binding to β_1-tubulin (refers to illustration in **Figure 2.2a**). We reasoned that although DARPin does not bind to the same site as the Kif2A neck, its association with β_1-tubulin is incompatible with simultaneous binding of the neck helix and thereby displacing the $\alpha_1\beta_1$-tubulin dimer from the ternary complex. This interpretation is consistent with our observation in the SEC experiments that only AMPPNP, and not ATP or ADP, is able to produce stable 1:2:1 Kif2A-NM-tubulin-DARPin complexes (Supplementary Figure 2.8) and that excess DARPin suppresses this complex formation. Altogether, our structural and biochemical data provide a detailed molecular explanation on how kinesin-13 motors catalytically depolymerize microtubules.

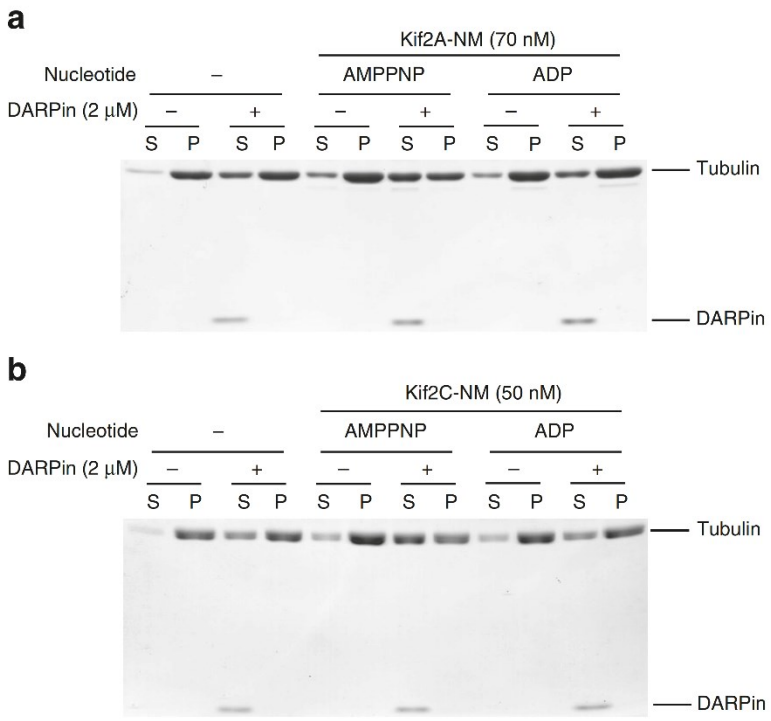

Figure 2.7 Nucleotide-dependent effect of DARPin on microtubule depolymerization by kinesin-13.

(**a-b**) Depolymerization of taxol-stabilized microtubules by Kif2A-NM (**a**) or Kif2C-NM (**b**) in the absence or presence of 2 μM DARPin and the indicated nucleotides (no nucleotide, AMPPNP, or ADP) was assessed by microtubule sedimentation assay. Samples were processed as described in **(6f)**. A representative gel from at least three independent experiments is shown.

2.5 DISCUSSION

The structural and biochemical studies presented here fill several major gaps in our understanding of the microtubule depolymerization mechanism of kinesin-13 motors. Our X-ray crystal structure of the Kif2A-NM-tubulin-DARPin complex reveals that ATP-bound Kif2A-NM binds two tubulin dimers and induces drastic bending of tubulin both intra-molecularly (within dimers) and inter-molecularly (between dimers). Here, the degree of tubulin curvature exceeds that of any tubulin oligomer reported to date (Asenjo et al., 2013; Ayaz et al., 2012; Cao et al., 2014; Gigant et al., 2013; Nawrotek et al., 2011; Pecqueur et al., 2012). Our biochemical and structural data provide evidence that this complex represents a trapped depolymerization intermediate of Kif2A-mediated microtubule depolymerization that is stable in solution prior to ATP hydrolysis. Importantly, this structure is distinct from the kinesin-13-tubulin complex structures reported in the two recently published studies (Ogawa et al., 2017; Wang et al., 2017) in two critical ways. First, it unambiguously shows the placement of the Kif2A neck against the second tubulin dimer. This interaction plays an indispensable role in forming the 1:2 Kif2A-tubulin complex by providing a critical anchor point for binding to the second tubulin dimer. Second, the crystal structure provides ample information to explain how Kif2A induces tubulin bending, especially at the interface between tubulin dimers. Guided and reinforced by neck and motor core interactions with the tubulin dimers on either side, the unique KVD motif of kinesin-13 inserts into the hydrophobic cavity at the inter-dimer interface and appears to displace the T7 loop and H8 helix of the α_2-tubulin subunit. This conformational change may generate sufficient strain to weaken longitudinal interfaces within the microtubule lattice, leading to tubulin dissociation.

The Kif2A-NM-tubulin-DARPin structure also indicates that the structural change of the α4 helix of kinesin-13 motors upon tubulin binding is unremarkable and unlikely to mediate a

direct effect for microtubule depolymerization. Moreover, our biochemical analysis of the Kif2A-MD construct clearly shows that the α4 helix and the class-specific KVD motif alone are insufficient to form the 1:2 complex and trigger microtubule depolymerization. In contrast, the kinein-13 neck peptide has been reported to induce lateral disintegration of microtubules (Shimizu et al., 2013). However, our Kif2A structure clearly shows that the neck forms a helical rather than a β-structure as reported (Shimizu et al., 2013). It is likely that the neck plays a more dominant role than the motor domain core to trigger drastic bending of two adjacent tubulin dimers, intra-molecularly and inter-molecularly. As microtubules assembled *in vitro* have straight or slightly tapered ends (Chrétien et al., 1995; Hyman, Salser, et al., 1992; Janosi et al., 2002), kinesin-13 motors likely first encounter a rather straighter protofilament, compared to those observed at depolymerizing ends (Mandelkow et al., 1991; C. A. Moores et al., 2006). This assessment is supported by the robust microtubule-stimulated ATPase activity of both kinesin-13-MD and –NM constructs. Upon binding to a microtubule end, neck binding may coordinate with the KVD motif to trigger the structural change needed for bending the adjacent tubulin dimers. While it is surprising that salt bridges are not observed between the charged residues of the KVD motif (Lys262 and Asp264) and the surface of tubulin in the Kif2A-NM-tubulin-DARPin complex, it is possible that they form upon initial binding of Kif2A to protofilaments at microtubule ends. These interactions could help guide the tip of loop 2 into the inter-dimer interface, and direct Val263 toward the full depth of its hydrophobic binding pocket on tubulin. At this point, additional bending of the tubulin protofilament would bring α_2 and β_1-tubulin too close to the sides of the KVD finger to maintain the initial salt bridges with the tubulin surface. It is thus only through the combined action of the neck, KVD motif and the motor domain core that kinesin-13 is able to induce extreme outward curvature of protofilament ends and trigger tubulin disassembly.

Combined with the rotational displacement of tubulin subunits, the extreme bending of adjacent tubulin dimers by Kif2A-NM may be sufficient to trigger dissociation of tubulin oligomers from the polymers because their curvature exceeds those typically observed at microtubule ends or within end-mimicking protofilament rings (Moores & Milligan, 2008). The fact that these drastically bent tubulins have not been directly observed by cryo-EM or in other crystallized structures suggests that they can no longer associate with the polymer or adjacent tubulins, and will rapidly revert back to the unconstrained curvature. In the Kif2A-NM-tubulin-DARPin structure presented here, this reversion is prevented by the presence of AMPPNP-trapped kinesin-13. Consistent with this assessment, our biochemical data show that Kif2A-NM is capable of depolymerizing microtubules in the presence of AMPPNP. On the other hand, the catalytic depolymerization (involving multiple cycles) requires ATP hydrolysis to release the kinesin-13 enzyme from the dissociated tubulin oligomers, as hinted by other studies (Ogawa et al., 2017; Wang et al., 2015). Motivated by our structural information and SEC data with DARPin, we showed that this requirement can be bypassed by the use of DARPin in our *in vitro* microtubule depolymerization assay. These data provide further evidence that ATP binding to kinesin-13 rather than its hydrolysis is needed to trigger depolymerization at microtubule ends, likely by inducing more outward bending and destabilization of the curved protofilaments.

During the revision of this manuscript, Benoit *et al*. reported high-resolution cryo-EM structures of *Drosophila* kinesin-13 KLP10A bound to curved or straight tubulin in different nucleotide states(Benoit et al., 2018). These complexes show how conformational changes of the nucleotide pocket are coupled with movement of loop 2 in accord with the straightness of the tubulin polymer. Analogous to AMPPNP-Kif2A-NM, the nucleotide pocket of AMPPNP-KLP10A closes when in contact with curved tubulin, but remains open when bound to straight

tubulin. Another similarity is that two-dimensional class average images of KLP10A-NM tubulin complexes show an elongated bar of density that emerges from the motor domain and extends to the next tubulin intra-dimer interface in virtually the same manner as helix α0a of the neck of Kif2A-NM. Although the authors suggest that the neck is not a major contributor to tubulin bending, our data on Kif2A-NM show otherwise. First, Kif2A-MD without the neck can neither form a 1:2 complex with tubulin nor depolymerize microtubule. Second, the degree of $\alpha_1\beta_1$-tubulin curvature induced by Kif2A-NM exceeds those observed for KLP10A-NM. Together, the structural and biochemical data presented here help further define the molecular and mechanistic interplay between kinesin-13 and tubulin at microtubule ends.

2.6 METHODS

2.6.1 Protein expression and purification

Tubulin was isolated from bovine brain and purified by two cycles of polymerization-depolymerization in a high-molarity PIPES buffer as described by Castoldi *et al.* (Castoldi & Popov, 2003). Purified tubulin was flash-frozen in liquid N_2 and stored at -80°C until use.

A plasmid coding Designed Ankyrin Repeat Protein, DARPin D1, was a kind gift from Dr. Jawdat Al-Bassam (University of California Davis). The gene was sub-cloned into the pET16b vector with *Nco*I and *Xho*I restriction enzymes, providing an N-terminal 6xHis-tag to DARPin. DARPin protein was expressed in Rosetta®GAMI B (DE3) *E. coli* (Stratagene) cells in LB medium after induction with 0.5 mM IPTG for 4 h at 37 °C. Cells were harvested by centrifugation, lysed by sonication and DARPin was purified by Ni-NTA chromatography. Eluted protein was subjected to SEC on a Superdex 200 26/60 column (GE Healthcare) equilibrated with HEPES buffer (20 mM HEPES, 150 mM NaCl, 1 mM $MgCl_2$, pH 7.2). Protein concentration was estimated by UV absorption using an extinction coefficient of 6990 M^{-1} cm^{-1}. DARPin was concentrated in an Amicon® Ultra filter (Millipore, cut off 10 kDa) to 20 mg mL^{-1}, flash frozen in liquid N_2 and stored at -80°C.

The human Kif2A (isoform 3, UniProtKB - O00139) construct containing the neck and the motor domain (Kif2A-NM; residues 153-553) was originally generated by the Structural Genomics Consortium in Toronto and was obtained from Dr. Hernando Sosa (Albert Einstein Medical College, NY). Kif2A-NM protein expression was induced in BL21(DE3) pLysS *E. coli* (Promega) cells cultured in LB medium with 0.5 mM IPTG at 30°C overnight. Cells were lysed in buffer A (50 mM Potassium phosphate, pH 8.0, 250 mM NaCl, 1 mM $MgCl_2$, 0.1% Triton X-100, 10 mM β-mercaptoethanol, 10 mM imidazole) supplemented with 0.5 mM ATP and protease

inhibitors. The lysate was then centrifuged, and the supernatant fraction was incubated with pre-equilibrated Ni-NTA resin (Qiagen) for 1-1.5 hours. Histidine-tagged Kif2A-NM bound resin was then washed with buffer A with 0.5 M NaCl and 0.1 mM MgATP before eluting with buffer E (50 mM Potassium phosphate, pH 7.0, 100 mM NaCl, 250 mM imidazole, 1 mM $MgCl_2$, 0.1 mM ATP, 5 mM β-mercaptoethanol). Eluted fractions containing Kif2A-NM protein were pooled, diluted 2-fold in 20 mM HEPES buffer, pH 6.8 and absorbed onto a SP Sepharose Fast Flow column (GE Healthcare). The column was washed with buffer C (20 mM HEPES, pH 6.8, 50 mM NaCl, 1 mM DTT, 1 mM $MgCl_2$, 0.2 mM ATP). After a quick final wash with buffer C without ATP, Kif2A-NM was eluted with buffer C with 0.5 M NaCl in the absence of ATP. The purified protein fractions were pooled and supplemented with at least molar equivalence of the desired nucleotide (e.g. AMPPNP) and concentrated to 50 mg mL^{-1} using a Amicon® Ultra-4 filter (Millipore) in the final storage buffer (20 mM HEPES, pH 6.8, 0.5 M NaCl, 5 mM $MgCl_2$, 5 mM DTT, and ~2x molar equivalence of the desired nucleotide) and then flash-frozen in liquid N_2.

Human Kif2A motor domain without the neck (denoted Kif2A-MD, residues 203-554) was amplified by PCR with the following primers (5'-GACTTAAGCTTGAATTCGACTTTAGAGGAAGTTTGGATTAT-3' and 5'-CTGATATCGCGGCCGCTTAAGTCAATTCTTTGACCCTATTTG-3') and cloned into a pGex-6P1 vector at the EcoRI and NotI sites. Protein expression and purification were performed essentially the same way as previously described for the KIF14MD_D772 construct (Arora et al., 2014) The PreScission Protease-cleaved Kif2A-MD protein was used for this study. Human Kif2C-NM (187-589) and Kif2C-MD (255-589) were cloned, expressed and prepared as previously described (Talje et al., 2014).

2.6.2 Kif2A-NM-tubulin-DARPin complex formation

Rapidly thawed tubulin solution (300 µL, 10 mg mL^{-1}) was mixed with 254.8 µL of HEPES buffer (20 mM HEPES, 150 mM NaCl, 1mM $MgCl_2$, pH 7.2) supplemented with 2.5 µL of 50 mM GDP and 42.7 µL of 20 mg/mL DARPin and incubated on ice for 10 min. Kif2A-NM (12.8 µL, 50 mg mL^{-1}) protein was diluted in 487 µL of HEPES buffer, and then slowly added to tubulin-DARPin solution in five small aliquots. The final Kif2A-NM-tubulin-DARPin mixture was then supplemented with AMPPNP to a final concentration of 0.1 mM and incubated on ice for 30 min. The molar ratio of Kif2A-NM:tubulin:DARPin was 0.8:1:1.05. This mixture was spun down for 10 min at 14,000×g at 4 °C and 1 mL of supernatant was loaded onto a HiLoad 26/60 Superdex 200 column (GE Healthcare) equilibrated with HEPES buffer. AMPPNP (final conc. = 0.05 mM) was added to protein-containing fractions immediately after eluting from the column. The fractions containing the small (150 kDa) complex were concentrated down to an A_{280} of ~10 using an Amicon® Ultra filter (Millipore, cut off 50 kDa), flash frozen in liquid N_2, and stored at -80°C.

2.6.3 Analytical size-exclusion chromatography

Kif2A (2.57 nmol), tubulin (5.15 nmol), and DARPin (5.4 nmol) were mixed with GDP (final conc. 0.1 mM), and either AMPPNP, ATP, or ADP (0.1 mM) in a 150 µL total volume of HEPES buffer (HEPES 20 mM, NaCl 150 mM, $MgCl_2$ 1mM, pH 7.2). The mixture was incubated for 30 min on ice and then 100 µL of the sample was injected onto the column. SEC was performed on a Superdex 200 10/300 GL chromatography column (GE Healthcare) equilibrated with HEPES buffer. The column was calibrated with molecular weight standards (GE Healthcare). Control experiments were performed with each protein alone. The collected fractions (500 µL) were

concentrated by Amicon® Ultra filters (cutoff 10 kDa), then mixed with Laemmli buffer and resolved by SDS-PAGE.

2.6.4 microtubule depolymerization assay

Microtubule preparation and sedimentation-based microtubule depolymerization assays were done essentially as described previously(Talje et al., 2014). Briefly, Kif2A-NM or Kif2A-MD at the indicated concentrations were mixed with taxol-stabilized microtubule in BRB80-based depolymerization buffer (80 mM PIPES pH 6.8, 1 mM $MgCl_2$, 1 mM EGTA, 20 μM taxol, 75 mM KCl, 0.25 mg/mL BSA, 1 mM DTT, 0.02% Tween), supplemented with 1 mM ATP or the indicated nucleotide, and when indicated, with DARPin at the specified concentrations. Reactions were incubated at room temperature for 10 min unless specified otherwise. Free tubulin in solution was separated from remaining microtubules pellet by centrifugation at 240,000 ×g for 5 min at 25°C. The supernatant fraction was retrieved from the sedimentation mixture and added to ¼ volume of 4×SDS loading buffer (Laemmli buffer). The remaining pellet was resuspended in an equal volume of 1×SDS loading buffer containing a similar buffer composition as the depolymerization buffer. Equal portions of the supernatant and pellet samples were resolved on SDS-PAGE. The gel was stained with Coomassie blue.

2.6.5 ATPase activity assay

A malachite green-based phosphate detection assay was used to measure kinesin-13-mediated ATPase activity, as previously described(Talje et al., 2014). Briefly, reactions were assembled in the same buffer condition as in the depolymerization assay, with the indicated concentrations of tubulin/microtubules, kinesin-13 protein constructs, DARPin, and nucleotides. Reactions were

allowed to proceed for the indicated length of time (usually 10-15 min, within the linear portion of the reaction curve), quenched with perchloric acid and malachite green reagent. The signal was quantified by the absorbance at 620 nm in a Genios Plus plate reader (Tecan).

2.6.6 Crystallization and X-ray structure determination

Crystals of the Kif2A-NM-tubulin-DARPin complex that were suitable for X-ray diffraction data collection grew in 3 days from 10-µL hanging drops containing the concentrated Kif2A-NM-tubulin-DARPin complex in a 1:1 ratio with a precipitant solution containing 8% PEG 8000, 6% ethylene glycol, 10 mM DTT, 100 mM HEPES, pH 7.5 at 277 K. Prior to diffraction data collection, crystals were transferred into a cryoprotectant composed of 15% PEG 8000, 22% EG, and 100 mM HEPES, pH 7.5, and were then frozen in liquid N_2.

Diffraction data were collected from a single crystal at beamline 08ID-1 of the Canadian Light Source (Saskatoon, Canada) at 100 K, and were indexed, integrated, and scaled with HKL2000 (Otwinowski & Minor, 1997). The structure was solved by molecular replacement with MolRep (Vagin & Teplyakov, 2000) using the structure of the tubulin subunits from the kinesin-1-tubulin complex (PDB ID: 4LNU) as a starting model. Once protein chains for one of the tubulin dimers were placed, interpretable density was visible for modeling a second set of tubulin chains and the DARPin molecule from the same structure (PDB ID: 4LNU). Next, the Kif2A molecule was found using PHASER (McCoy et al., 2007) with provision of the tandem tubulin-DARPin complex obtained from MolRep, and the Kif2A-ADP structure (PDB ID: 2GRY) as separate ensembles. The Kif1A-AMPPNP structure (PDB ID: 1VFV) and kinesin-1-tubulin structure (PDB ID: 4LNU) were used to place AMPPNP, GDP, GTP and Mg^{2+} ions into the complex. The structure was refined with Phenix.refine (Adams et al.) and manually optimized using COOT (Emsley &

Cowtan, 2004) to produce a final model with satisfactory R_{work}/R_{free}. The model quality was evaluated with MOLPROBITY (Davis et al., 2007), and by the wwPDB Validation Service.

2.6.7 SEC-SAXS Data Collection and Analysis

In-line size-exclusion chromatography and small-angle X-ray scattering (SEC-SAXS) measurements on the Kif2A-NM-tubulin-DARPin mixture were performed at the G1 Station of the Cornell High Energy Synchrotron Source (CHESS) (Acerbo et al., 2015) using 1.267 Å X-rays with a flux of 7.76 x 10^{11} photons per second at a beam size of 250 µm x 250 µm. For the SEC-SAXS analysis, a mixture of Kif2A, tubulin and DARPin was passed continuously through an X-ray sample cell via an in-line size-exclusion column (Superdex 200 10/300 GL, GE Healthcare) at a flow rate of 1 mL min^{-1}. The column was pre-equilibrated with running buffer consisting of 20 mM HEPES, 150 mM NaCl, 1 mM $MgCl_2$, pH 7.2. The protein sample was prepared at 25 µM tubulin, 27 µM DARPin, 20 µM Kif2A-NM and 0.1mM AMPPNP and injected into a 100-µL loop.

Approximately 1200 two-second exposures were collected per sample, and 100 buffer profiles preceding the elution peaks were averaged and used for background subtraction. SAXS images were collected on dual Pilatus 100K-S detector system at sample-to-detector distances of 1.47 m. Samples were oscillated in the flow cell at 22 °C during data collection. SAXS data were processed using the BioXTAS RAW software (Nielsen et al., 2009).The radius of gyration (Rg) and scattering intensity (I(0)) were calculated from the Guinier approximation, and the pair distribution function, P(r), was calculated by GNOM (Svergun, 1992). The dummy atom model of the Kif2A-NM-tubulin-DARPin complex was calculated using DAMMIF (Franke & Svergun, 2009). Ten independent dummy atom models were averaged and selected using DAMAVER

(Volkov & Svergun, 2003). The resulting experimental SAXS profile was then compared with simulated (theoretical) scattering curve of the Kif2A-NM-tubulin-DARPin complex crystal structure using the program CRYSOL (Svergun et al., 1995).

2.7 Data availability

Coordinates and structure factors have been deposited in the Protein Data Bank with accession code: 6BBN [http://www.rcsb.org/pdb/results/results.do?tabtoshow=Unreleased&qrid=76521118]. Small-angle X-ray scattering data and models have been deposited in the Small-Angle Scattering Biological Data Bank with accession code: SASDCR9 [https://www.sasbdb.org/search/?q=SASDCR9]. Other data are available from the corresponding authors upon reasonable request.

2.8 Acknowledgements

We thank Peter L. Davies, Rachel Trister, Jacqueline Hellinga, Byron Hunter, Tyler Vance, Irsa Shoukat, and Robert Campbell for technical assistance and help with preparation of the manuscript. We thank Dr. Jawdat Al-Bassam, (University of California Davis) for providing a plasmid with the DARPin D1 gene. Diffraction data were collected at the Canadian Light Source, Saskatoon, Canada (beamline 08ID-1), and we thank the beam line group for making these experiments possible. This work was supported by funding to J.S.A. and B.H.K. from CCSRI, CIHR and NSERC. J.S.A. holds a Canada Research Chair (Tier 2) in Structural Biology. B.H.K. is a recipient of the Fonds de recherche du Québec - Santé (FRQS) Chercheure-boursière Junior 1 and Junior 2 Awards and the Canadian Institutes of Health Research (CIHR) New Investigator Award. The Institute for Research in Immunology and Cancer (IRIC) is supported in part by the Canadian Center of Excellence in Commercialization and Research (CECR), the Canada Foundation for Innovation and FRQS.

2.9 Competing interests

The authors declare no competing interests.

2.10 Supplementary Information

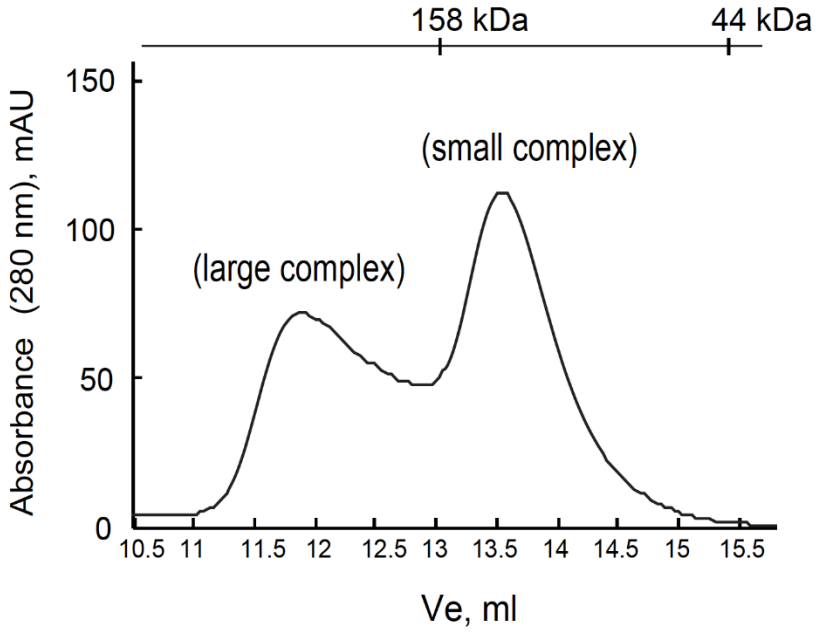

Supplementary Figure 2.1. Kif2A-NM-tubulin-DARPin small complex rearrenges to large complex upon concentration. Fractions corresponding to the small complex of Kif2A-NMtubulin-DARPin werr concentrated 10-fold, and incubated for 30 min, and then re-run on the S200 10/300 GL column in HEPES buffer.

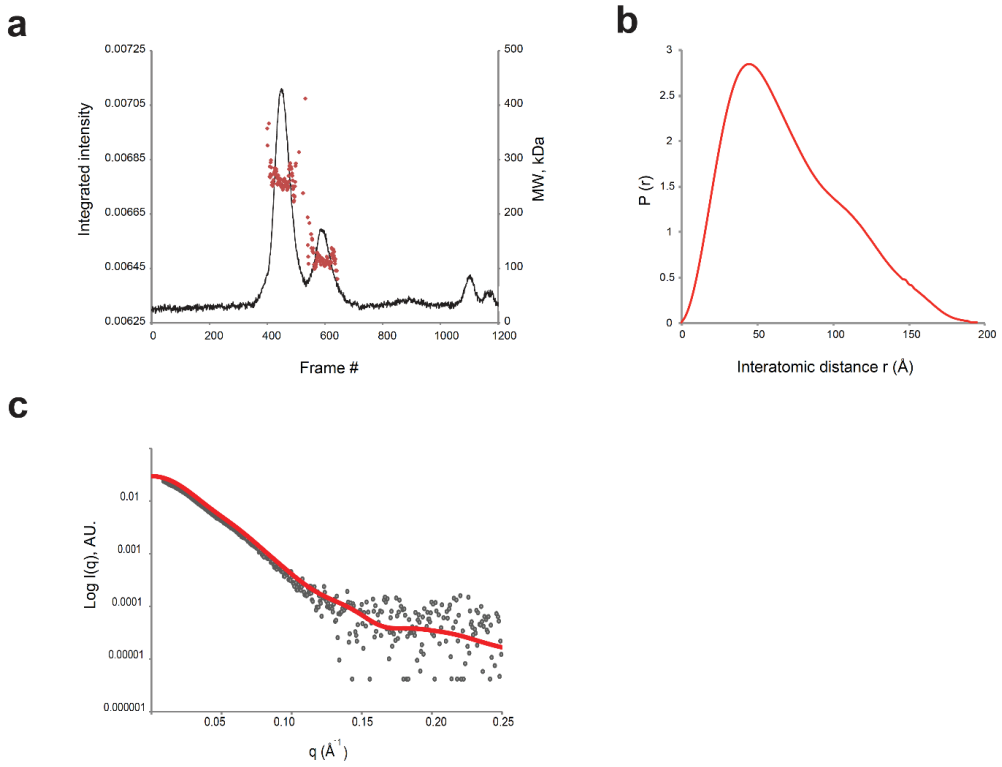

Supplementary Figure 2.2. SAXS analysis of the Kif2A-NM-tubulin-DARPin complex. (a) SEC-SAXS elution profile of Kif2A-NM-tubulin-DARPin mixture. Integrated intensity (black line) and the corresponding molecular weight correlations (red diamonds) were plotted across the elution peaks. (b) Pair-dis-tance (r) probability distribution computed from the experimental SAXS data for frames 433-473 by ATSAS. (c) CRYSOL comparison of the experimental scattering for the 1:2:1 Kif2A-NM-tubu-lin-DARPin complex (gray circles) with the simulated scattering profile from the Kif2A-NM-tubulin-DARPin crystal structure (red line).

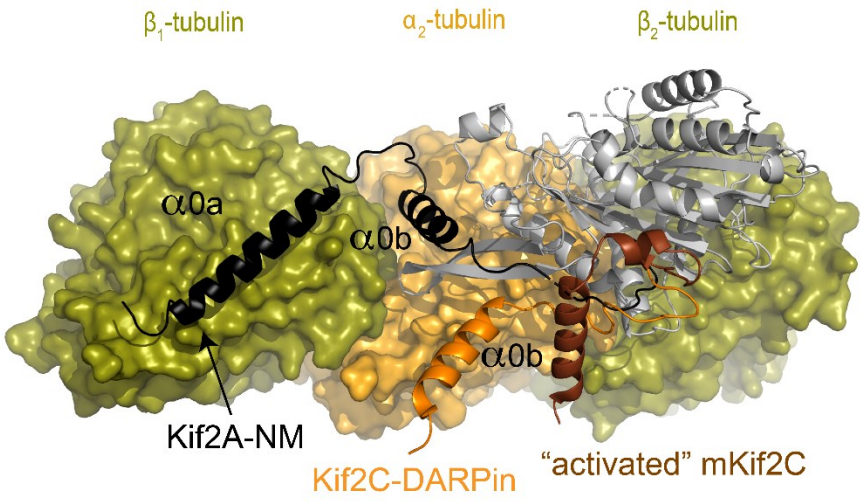

Supplementary Figure 2.3. Conformations of the neck helices of kinesin-13 proteins observed in crystal structures. Motor domain of Kif2A is represented in grey. The neck parts of Kif2A-NM-tubulin-DARPin complex, _0a and _0b, are in black. _0b of Kif2C-tubulin-DARPin complex (PDB ID: 5MIO) is in orange and _0b of the "activated conformation" of mKif2C (PDB ID: 5XJA) is in brown. Tubulin is shown as a surface representation.

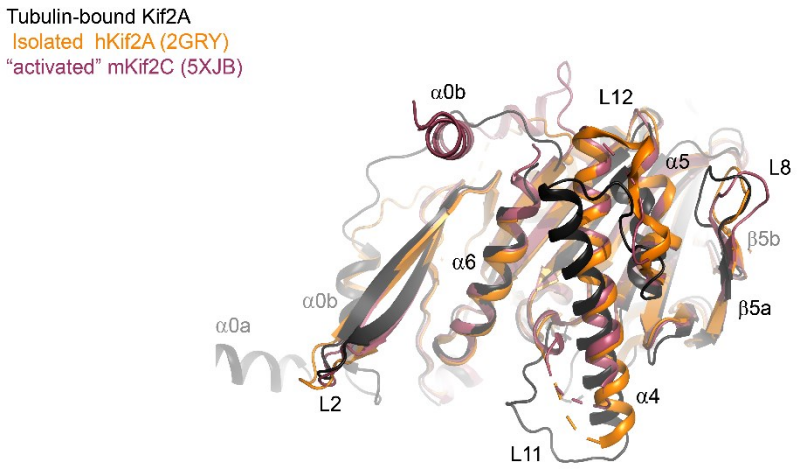

Supplementary Figure 2.4. Conformations of the Kif2A motor domain relative to "activated" Kif2C. The motor domain of tubulin-bound Kif2A-NM (black) is superimposed on isolated ADPKif2A (orange) and the mKif2Ccore:ADP-BeFx structure (maroon) via the P-loop. The r.m.s.d. for 94 equivalent Cα posi-tions in 5XJA is 3.63 Å, and the r.m.s.d. for 97 equivalent Cα positions in 5XJB is 3.59 Å). Proteins are viewed from tubulin surface.

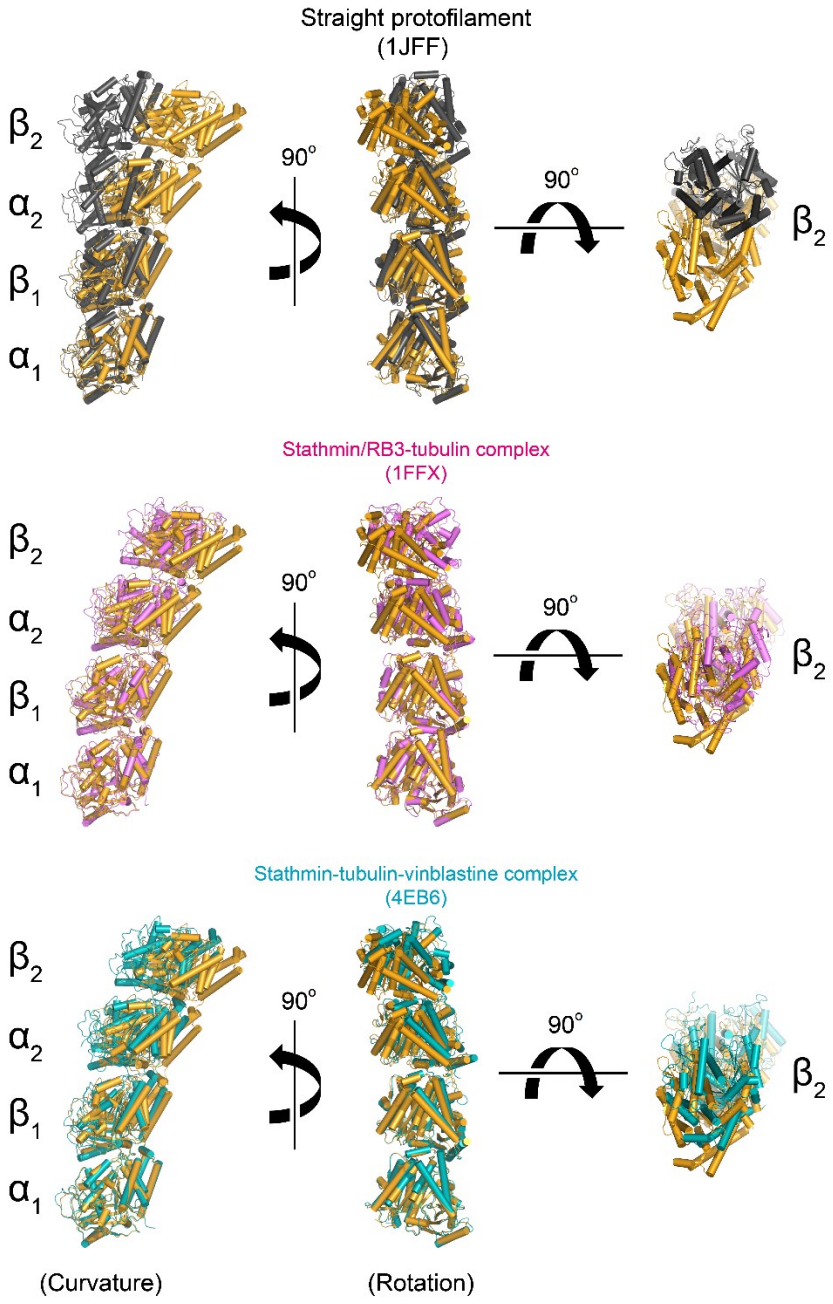

Supplementary Figure 2.5. Curvature and rotational displacement of tubulin complexes. Views are from the side (left), looking from the outer surface of the protofilament, into the Luminal space (middle), and looking into the long axis of the protofilament from the plus-end (right). Supoerposition was performed using the α1-tubulin subunit of each complex. Tubulin subunits of the Kif2A-NM-tubulin-DARPin complex are coloured orange.

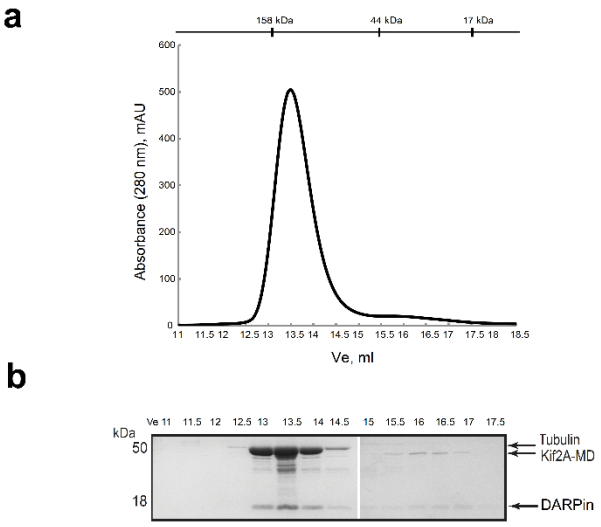

Supplementary Figure 2.6. Kif2A-MD forms a complex with tubulin in the presence of AMPPNP. (a) Size- exclution chromatography (SEC) profile of Kif2A-MD-tubulin-DARPin (1:1:1.05 molar ratio) supplemented with 1 mM AMPPNP in HEPES buffer. (b) 12% SDSPAGE gel of SEC fractions from the above experiment. Molecular weight of Kif2A-MD = 42 kDa, tubulin = 50 kDa, and DARPin = 18 kDa

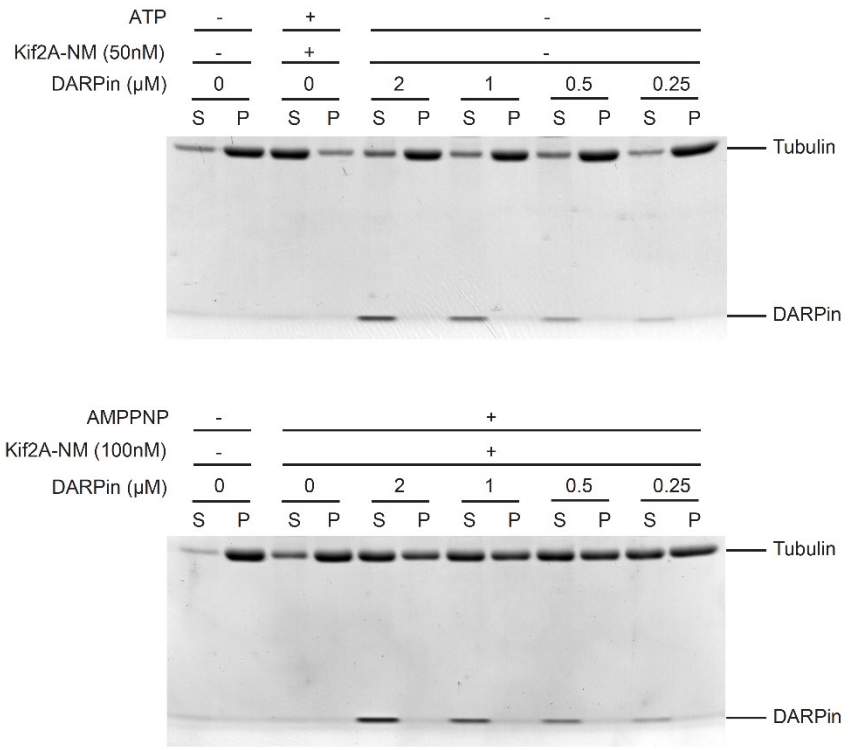

Supplementary Figure 2.7. Level of microtubule depolymerization in the presence of varying amounts of DARPin without (upper gel) or with Kif2A-NM (lower gel). The samples were processed as in Figure 2.7 and evaluated by microtubule sedimentation assay and coomassie blue stained gels.

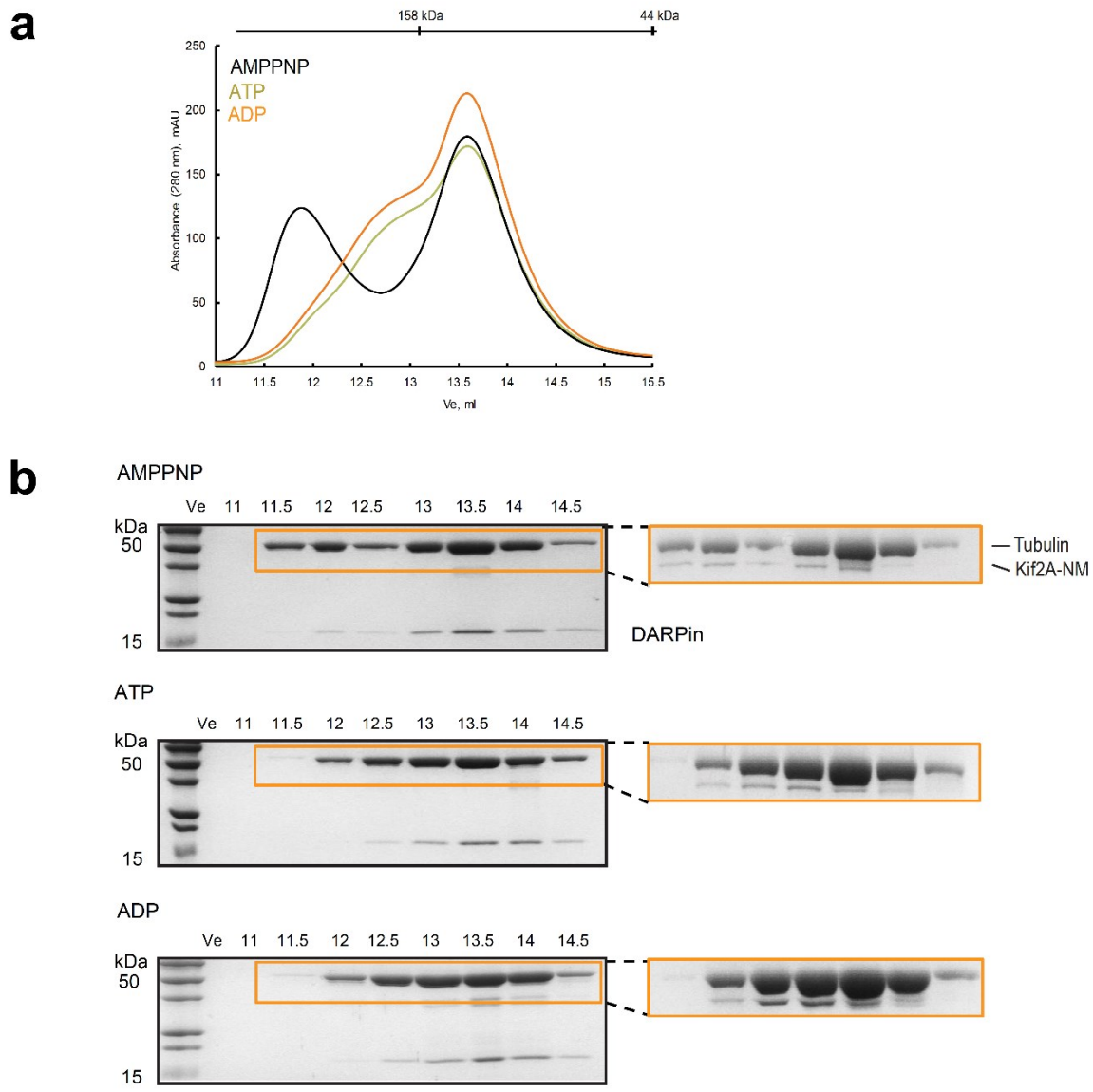

Supplementary Figure 2.8. Kif2A-NM-tubulin-DARPin complexes formed in the presence of different nucleotides. (a) Size-exclution chromatography (SEC) profiles of Kif2A-NMtubulin-DARPin complexes (0.5:1:1.05 molar ratio) supplemented with 0.1 mM ATP (green), ADP (orange), and AMPPNP (black) separated on a S 200 10/300 GL column in HEPES buffer. (b)12% SDS-PAGE gels of SEC fractions from the above experiments. Molecular weight of Kif2A-NM = 48 kDa, tubulin = 50 kDa and DARPin = 18 kDa. Insets show Kif2ANM- tubulin-DARPin fractions resolved on 10% SDS-PAGE gels.

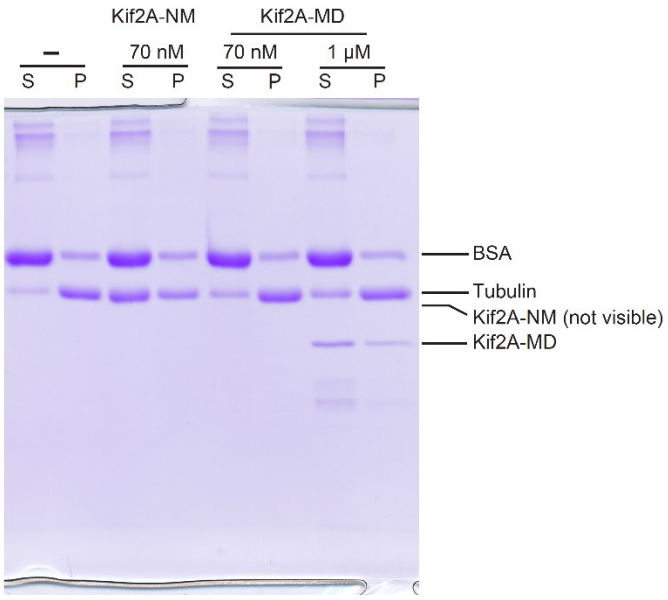

Supplementary Figure 2.9. Uncropped gel of Figure 2.1b

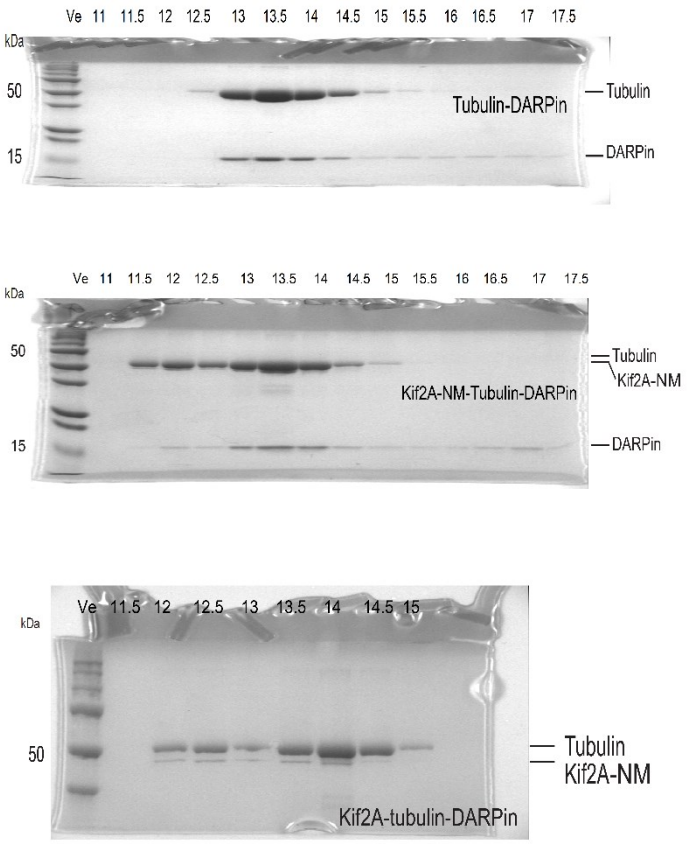

Supplementary Figure 2.10. Uncropped gels of Figure 2.1d

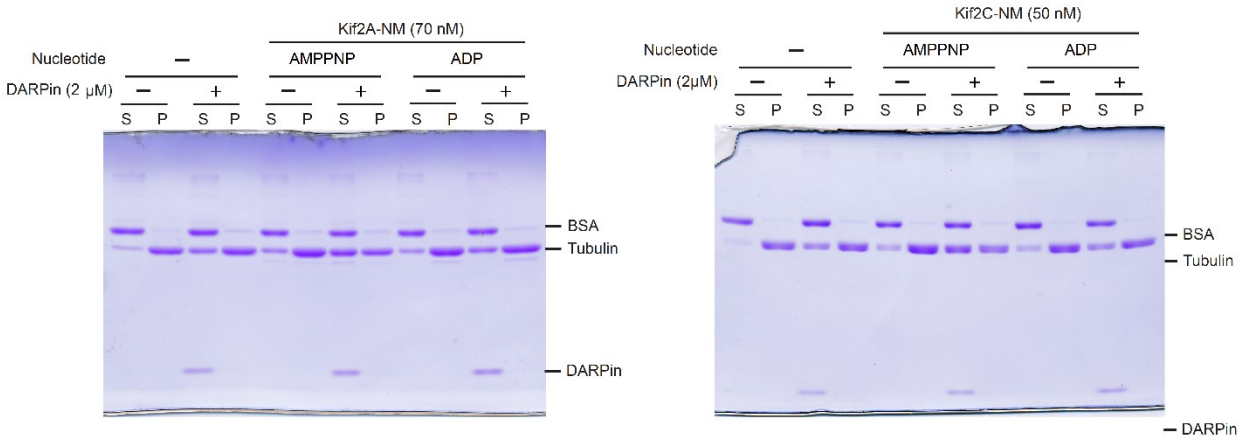

Supplementary Figure 2.11. Uncropped gels of Figure 2.7a and 7b

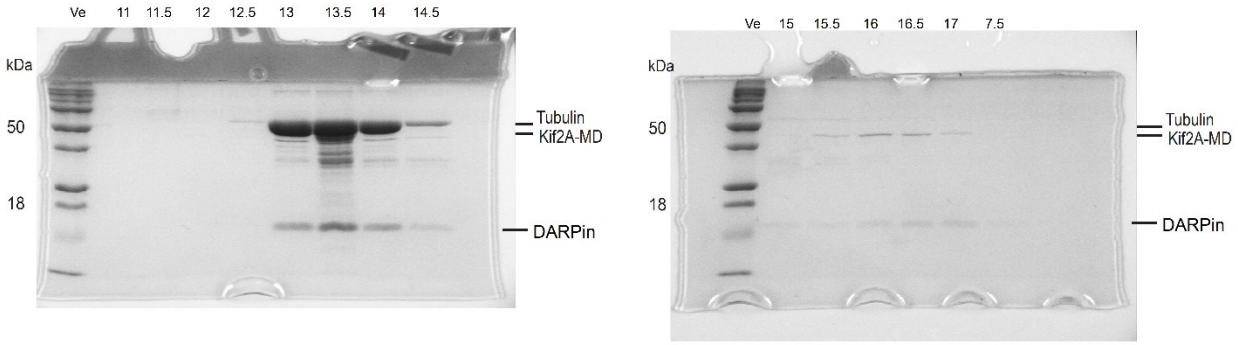

Supplementary Figure 2.12. Uncropped gels of Supplementary Figure 2.6

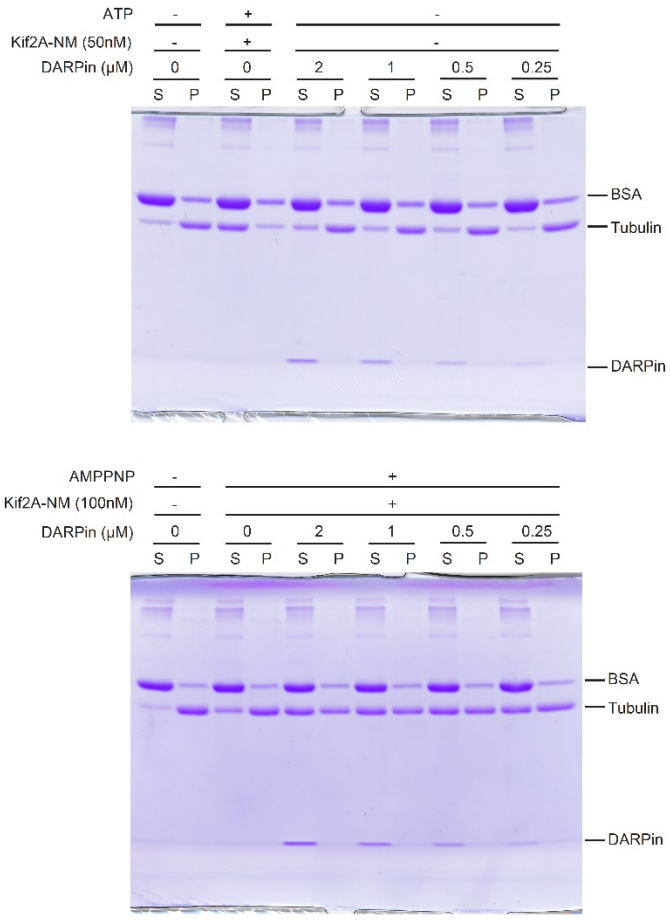

Supplementary Figure 2.13. Uncropped gels of Supplementary Figure 2.7

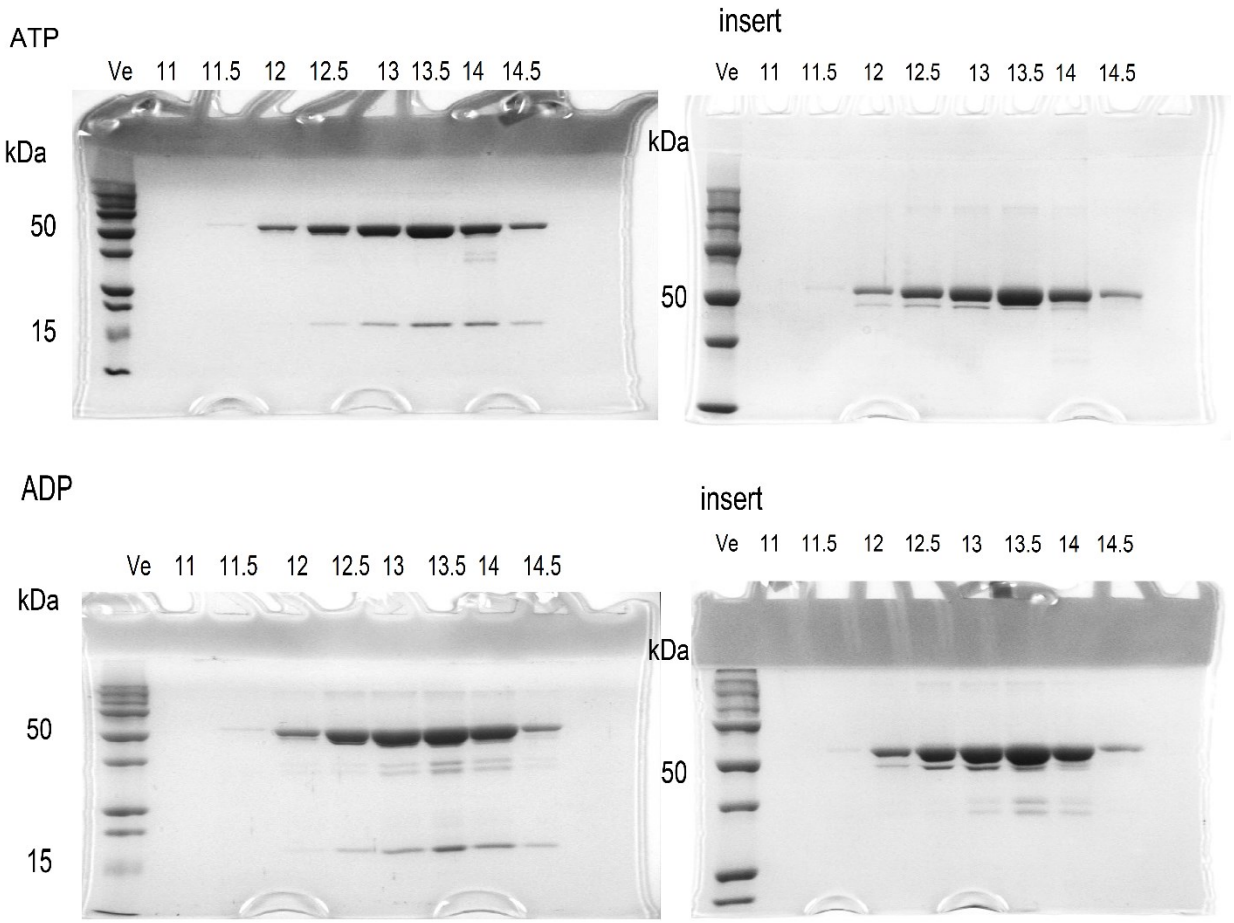

Supplementary Figure 2.14. Uncropped gels of Supplementary Figure 2.8b

Table S 2.1 BioSAXS data collection and scattering-derived parameters.

Data collection parameters	
Beam line	G1 Station of the Cornell High Energy Synchrotron Source
Beam geometry	Beam size: 250 μm x 250 μm
Wavelength (Å)	1.267
Camera distance (mm)	1470
Exposure time (s)	2
Temperature (K)	295
Structural parameters	
I0 (cm-1) (from Guinier)	0.0298
Rg (Å) (from Guinier)	54.9
I0 (cm-1) (from P(r))	0.0298
Rg (Å) (from P(r))	55.9
Dmax (Å)	195
Molecular mass determination	
Experimental Mw using a volume of correlation (kDa)	258.5
Calculated Mw from sequence (kDa)	266
Software employed	
Primary data processing	BioXTAS RAW
Ab initio analysis, validation and averaging	DAMMIF/DAMAVER

# of modeling iteration	10
$\chi 2$ of ab initio model	0.991
DAMAVER NSD	0.74± 0.083
Computation of model intensities	CRYSOL
Comparison of theoretical profile with experimental data $\chi 2$	1.093
Three dimensional graphics representations	Chimera

CHAPTER 3: Evidence for conformational change-induced hydrolysis of β-tubulin-GTP

Mohammadjavad Paydar[1] and Benjamin H. Kwok[1†]

[1] Institute for Research in Immunology and Cancer (IRIC), Département de médecine, Université de Montréal, P.O. Box 6128, Station Centre-Ville, Montréal, QC H3C 3J7, Canada.

[†] Corresponding author: B. H. Kwok: benjamin.kwok@umontreal.ca

3.1 AUTHOR CONTRIBUTION

Mohammadjavad Paydar: Designed and performed experiments, analyzed and interpreted data, prepared and completed the manuscript.

Benjamin H. Kwok: Conceived the project, designed and performed experiments, analyzed and interpreted data, wrote the first draft, prepared and completed the manuscript.

3.2 ABSTRACT

Microtubules, protein polymers of α/β-tubulin dimers, form the structural framework for many essential cellular processes including cell shape formation, intracellular transport, and segregation of chromosomes during cell division. It is known that tubulin-GTP hydrolysis is closely associated with microtubule polymerization dynamics. However, the precise roles of GTP hydrolysis in tubulin polymerization and microtubule depolymerization, and how it is initiated are still not clearly defined. We report here that tubulin-GTP hydrolysis can be triggered by conformational change induced by the depolymerizing kinesin-13 proteins or by the stabilizing chemical agent paclitaxel. We provide biochemical evidence that conformational change precedes tubulin-GTP hydrolysis, confirming this process is mechanically driven and structurally directional. Furthermore, we quantitatively measure the average size of the presumptive stabilizing "GTP cap" at growing microtubule ends. Together, our findings provide the molecular basis for tubulin-GTP hydrolysis and its role in microtubule polymerization and depolymerization.

3.3 INTRODUCTION

Microtubules, protein polymers of α/β-tubulin dimers, are a major component of the cell cytoskeleton. microtubules provide the framework for giving a cell its shape, for intracellular transport and for segregating the chromosomes during cell division. The formation of microtubule polymers and the regulation of their dynamics in space and time are crucial for their functions during different phases of the cell cycle. The fundamental questions of how these polymers are formed and their dynamics controlled at the molecular level are still not fully understood.

3.3.1 Microtubule polymerization and tubulin-Guanosine triphosphate (GTP) hydrolysis.

Microtubule polymerization occurs when α/β-tubulin subunits join together to form a polymer of hollow tubule (Desai & Mitchison, 1997). Polymerization is initiated by a process called nucleation - the assembly of two or more tubulin dimers. This can happen spontaneously or build on pre-existing templates such as the γ-tubulin ring complex (Erickson & Pantaloni, 1981; Moritz et al., 1995; Osawa & Asakura, 1975). Once the nucleus is formed, more subunits can be added to form filaments and are self-organized into a hollow tubular structure. It has been well established that microtubule polymerization is a stochastic process, with polymers cycling between periods of growing and shrinking. This phenomenon is known as dynamic instability (Mitchison & Kirschner, 1984a).

It was known early on that microtubule polymerization requires GTP (Arai & Kaziro, 1977; Caplow & Shanks, 1990; Stewart et al., 1990) and that α/β-tubulin dimers, subunits of microtubules are GTPases. In their nucleotide-binding pockets, α-tubulin contains a non-interchangeable GTP constitutively while β-tubulin has a hydrolysable and exchangeable GTP (David-Pfeuty et al., 1977; MacNeal & Purich, 1978; Spiegelman et al., 1977). GTPs in β-tubulin

subunits are hydrolyzed during microtubule polymerization and within the microtubule lattice in two steps: from GTP to guanosine diphosphate(GDP)-P_i and then to GDP (Carlier & Pantaloni, 1981; Weisenberg et al., 1976). GTP hydrolysis is presumed to contribute to microtubule polymerization dynamics and regulating the catastrophe switch (Bowne-Anderson et al., 2013), but the underlying molecular mechanism is still poorly understood.

Early EM study showed that polymerizing ends are often blunt and straight while the depolymerizing ends are curved or tapered (Mandelkow et al., 1991). This led to the pleasingly simple hypothesis that GTP-tubulins are straight, and the GDP tubulins are curved. The straight conformation of GTP-tubulin facilitates the incorporation of dimers into polymer ends forming the stabilizing GTP cap and the formation of lateral bond with adjacent protofilaments. As polymerization proceeds, GTP gets hydrolyzed and the GDP-tubulins in the microtubule middle are constrained to the straight conformation and are inherently unstable (Alushin et al., 2014; Grafmüller et al., 2013). Upon removal of the stabilizing GTP cap, the GDP-tubulin dimers are exposed and the constrains are released, leading to the outward curvature of the depolymerizing protofilaments. This model is appealing because it explains most of the biochemical and conformational events associated with microtubule polymerization and depolymerization. However, accumulating structural studies have found that both GTP- and GDP-tubulin dimers are curved (Buey et al., 2006; Nawrotek et al., 2011; Rice et al., 2008), and that curved or tapered filaments are also observed in polymerizing microtubule ends (Chrétien et al., 1995; McIntosh et al., 2018; Müller-Reichert et al., 1998). In light of these findings, it is conceivable that curved GTP-tubulins are added to the polymerizing ends. As polymerizing ends grow and filaments straighten through interaction with adjacent filaments, GTP hydrolysis ensues. Recent high resolution cryo-electron microscopy (cryo-EM) studies on microtubule polymers stabilized with

paclitaxel or hydrolysis-resistant GMPCPP have suggested that GTP-bound tubulin stabilized the polymers by strengthening the lateral and longitudinal interactions between neighboring tubulin subunits, and that hydrolysis leads to the destabilization GDP-tubulin in the lattice (Alushin et al., 2014; Grafmüller et al., 2013; Prota et al., 2013). Upon depolymerization, the previously constrained dimers return to their naturally curved state, and the energy stored in the constrained tubulin dimer is released to do mechanical work. While this revised model is logical and sound, it is still puzzling as to what triggers GTP hydrolysis and why since GTP hydrolysis per se is not needed for the addition of GTP-tubulin subunit at microtubule ends.

3.3.2 GTP cap and microtubule stability.

Being enriched in GTP-bound tubulin dimers, the growing end of microtubules is often referred to as the "GTP cap"; this structure is thought to stabilize microtubules (Caplow & Shanks, 1996; Drechsel & Kirschner, 1994). It has also been proposed that some GTP-bound tubulin dimers may exist in the middle of the microtubule (GTP islands), due to incomplete GTP hydrolysis during polymerization or defects (Carlier, 1982; Carlier & Pantaloni, 1981; Chrétien et al., 1992; Dimitrov et al., 2008). Evidence for this proposal has been obtained indirectly using a tubulin conformation-specific antibody (Dimitrov et al., 2008). The islands of GTP-bound tubulin have been speculated to be responsible for microtubule rescue, switching microtubules from shortening to growing (Cassimeris, 2009; Dimitrov et al., 2008). The length/size of the GTP cap has been a mystery and controversial for decades. Earlier studies suggested the GTP cap size could be as small as a single GTP-tubulin layer (Caplow, 1992; Desai & Mitchison, 1997; Erickson & O'Brien, 1992). This is, however, inconsistent with recent findings by indirect probing with microtubule end-binding (EB) proteins, which have been shown to bind preferentially to GTP- or GDP-P_i-bound tubulin (Maurer

et al., 2011; Maurer et al., 2012; Zanic et al., 2009; Zhang et al., 2015). There have been efforts using EB binding as an indirect method to determine the GTP cap size *in vivo*, and some have reported it to contain hundreds of tubulin dimers (~750 dimers spread over ~55 rows) (Brouhard & Sept, 2012; Dominique Seetapun et al., 2012). It has been proposed that the length of EB comet tail is closely linked to the growth rate and stability of microtubules (Bieling et al., 2007; Duellberg et al., 2016; Maurer et al., 2012), strengthening the idea that the GTP cap stabilizes the microtubule polymers. Curiously , in a more recent study, the length of outwardly curved microtubule ends was measured to be about ~40-80 nm *in vitro* and also in cells from different species, using EM tomography (McIntosh et al., 2018). On the other hand, it has been shown that EB1 binds to the outwardly curved growing microtubule ends, but also extends its binding to some parts of straight lattice (Guesdon et al., 2016). This suggests that GTP-bound tubulin dimers are enriched at the polymerizing curved ends but could also exist in some parts of the microtubule lattice.

3.3.3 Microtubule dynamics in cells.

In cells, microtubule dynamics are largely regulated by microtubule associated proteins (MAPs). Tubulin post-translational modifications have also been shown to regulate different microtubule features, including their dynamics, by altering their binding affinity to MAPs (Westermann & Weber, 2003; Wloga & Gaertig, 2010). Some of these proteins promote microtubule polymerization/stabilization, like Stu2/XMAP215/Dis1 family polymerases, which contain multiple TOG domains that bind αβ-tubulin dimers (Ayaz et al., 2012). Another member of polymerizing MAPs is TPX2, which is known as an microtubule catastrophe suppresser (Roostalu et al., 2015). On the other hand, microtubule depolymerizing MAPs are also important in controlling microtubule dynamics. Members of Kinesin-8 family are microtubule destabilizing

motors that move towards the plus-end of microtubules. The depolymerization mechanism of Kinesin-8 motor proteins, however, varies between different species (Gupta et al., 2006; Locke et al., 2017; Savoian & Glover, 2010). In contrast, kinesin-13 family members (KIF2A, KIF2B and KIF2C/MCAK) are major catastrophe factors that actively remove subunits from microtubule ends (Howard & Hyman, 2007; Walczak et al., 2013). These proteins hydrolyze adenosine triphosphate (ATP) when they encounter tubulin dimers, free or in the polymers. However, their depolymerizing function only happens at the ends of microtubules, where they use the energy derived from ATP hydrolysis to dissociate tubulin dimers (Friel & Howard, 2011; Hunter et al., 2003). Our structural study shows each kinesin-13 monomer can bind to two tubulin dimers in tandem and increase both the intra- and inter-dimer curvature (Trofimova et al., 2018). We postulate that this extreme bending of tubulin dimers by kinesin-13 ultimately leads to their dissociations from protofilament ends.

We report here that kinesin-13 proteins induce a conformational change in tubulin dimers that triggers the hydrolysis of the exchangeable GTP on β-tubulins. We provide experimental evidence to show that it is the conformational change of tubulin that leads to GTP hydrolysis and not the other way around. We further demonstrate that this structural change of the tubulin dimer has to be directional, from a more curved to a straighter conformation and not vice versa, to trigger GTP hydrolysis. Furthermore, the same mechanism also occurs during microtubule polymerization as tubulin dimers straighten to form a hollow tubule. Finally, we provide a molecular account for the occurrence of GTP-tubulin associated microtubule ends, often termed the “GTP cap”, and quantitatively measure its average length. In sum, our work presented here reveals the inner workings of tubulin biochemistry: the molecular relationship between structural change and nucleotide hydrolysis.

3.4 RESULTS

3.4.1 Tubulin-GTP hydrolysis can be triggered by binding and unbinding of kinesin-13 proteins.

The presence of GDP in β-tubulin, in our previous structural study of the KIF2A-tubulin ternary complex (Trofimova et al., 2018), prompted us to determine if the hydrolysis of tubulin GTP occurred spontaneously during the sample preparation and crystallization processes, or if it was induced by forming the complex with KIF2A-NM (neck+motor; amino acids 153–553). To address this directly, we first used a fluorescence-based assay to detect the presence of GDP over time when tubulin dimers either were incubated alone or with KIF2A-NM in the presence of AMP-PNP and DARPin (Designed Ankyrin Repeat Protein, a polypeptide that binds to β-tubulin and prevents microtubule polymerization). Our data showed that tubulin-GTP turns over very slowly on its own (with a rate of 0.0003 S^{-1}), but the hydrolysis rate increased significantly when incubated with KIF2A-NM in the presence of AMP-PNP and DARPin (with an initial rate of 0.16 S^{-1},**Figure 1A**). Note that tubulin dimers incubated with AMP-PNP-bound KIF2A alone or with DARPin alone did not promote GTP hydrolysis. From our previous study (Trofimova et al., 2018), we knew that DARPin could compete with the neck region of KIF2A-NM for binding to β-tubulin and thereby release KIF2a-NM from the complex. Therefore, excess DARPin should disrupt and prevent the tandem tubulin complex formation and suppress GTP hydrolysis. Indeed, DARPin titration in the same experimental setting yielded the result that is consistent with this prediction (**Figure 1B**).

Our results showed that GTP hydrolysis required the associated tubulin dimers to be released from AMP-PNP-bound KIF2A-NM by DARPin (i.e. disrupts the 1:2 KIF2A:tubulin dimer complex, as previously shown (Trofimova et al., 2018)). This suggests that the bending of

tubulin dimers by KIF2A-NM per se does not trigger GTP hydrolysis; instead it is the return of free tubulin dimers to their native conformation that promotes the activity. If this assertion is correct, ATP hydrolysis by KIF2A, stimulated by tubulin dimers, should also trigger GTP hydrolysis. As DARPin was used only to facilitate the crystallization of the KIF2A-NM tubulin complex, it should not be needed for KIF2A or other kinesin-13 proteins to interact with tubulin dimers at microtubule ends, where they induce microtubule depolymerization. To ensure that what we observed was not an artifact of DARPin-forced release of KIF2A-NM from tubulin, and to determine if kinesin-13-induced tubulin-GTP hydrolysis also occurs in the presence of ATP, we performed the same experiment in the presence of ATP. As anticipated, this was indeed the case (**Figure 1C**). GTP turnover occurred in the presence of ATP as robustly as robustly as it did with AMP-PNP and DARPin. Although the GDP detection reagent that we used has a lower sensitivity to adenosine diphosphate (ADP) (see calibration curve in **Supplementary Figure 3.1**), the signal is measurable and therefore should be subtracted from the total signal (**Figure 3.1C**, solid and dotted red lines represent before and after background subtraction, using the determined ATP turnover rate). To obtain further evidence on this point, we performed the same experiment using radio-labeled γ^{32}P-GTP as a tracer to unambiguously distinguish GTP hydrolysis from ATP hydrolysis. This experiment showed a time-dependent increase of GTP hydrolysis (**Figure 3.1D-E**), consistent with the result from the GDP detection assay (**Figure 3.1C**). As a control, we monitored the basal tubulin-GTP turnover over longer periods of time, using radio-labeled γ^{32}P-GTP, which showed slow basal GTP hydrolysis of 0.0002 (s^{-1}) **(Supplementary Figure 3.2),** also consistent with the rate measured by GDP detection assay. Monitoring tubulin-GTP hydrolysis in the presence of another kinesin-13 construct, MCAK-NM, yielded results almost identical to those with KIF2A-NM **(Supplementary Figure 3.3)**.

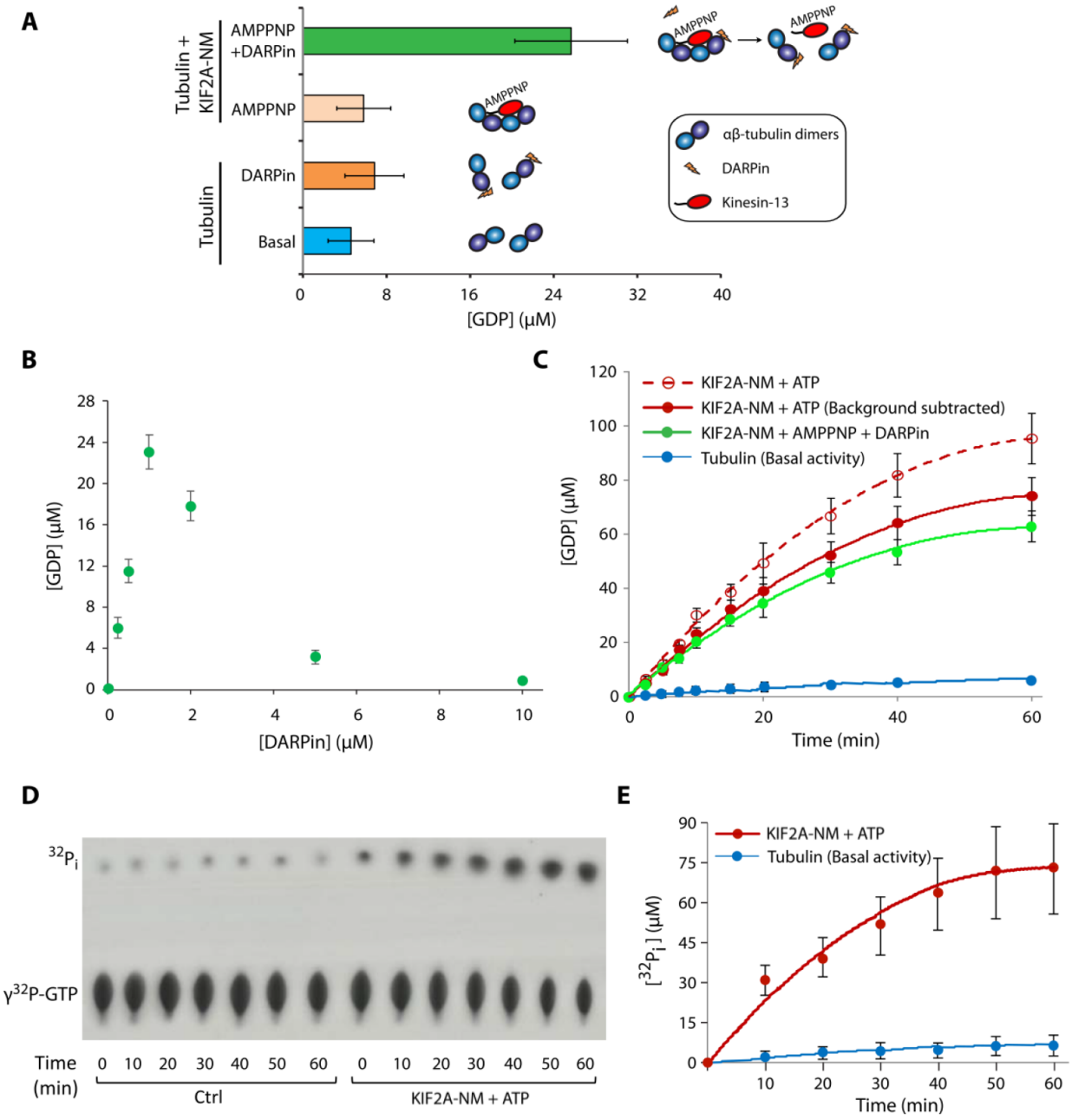

Figure 3.1 Binding dynamics of the Kinesin-13 KIF2A with tubulin dimers trigger β-tubulin-GTP hydrolysis.

(A) Tubulin-GTP hydrolysis measured by GDP production (ProFoldin GDP detection assay) when tubulin dimers (4 μM) and GTP (0.2 mM) were incubated alone, with DARPin (1 μM) or in the presence of KIF2A-NM (200 nM) with AMP-PNP (0.2 mM) or with AMP-PNP and DARPin for

15 minutes at room temperature. **(B)** To determine the effect of DARPin, tubulin-GTP hydrolysis measured by GDP production when tubulin-GTP dimers were incubated in the presence of KIF2A-NM and AMP-PNP with different concentrations of DARPin, under the same condition as in (A). **(C)** Time-course experiments comparing the tubulin-GTP turnovers between tubulin dimers that were incubated in the presence of KIF2A-NM with AMP-PNP and DARPin and those with KIF2A-NM with ATP (0.2 mM) under the same condition as in (A). For (A-C), the level of GDP was measured using a GDP detection assay (ProFoldin). **(D)** A time course experiment in which basal tubulin-GTP hydrolysis was measured and compared with in KIF2A-NM-induced GTP hydrolysis (in the presence of ATP) using a γ^{32}P-GTP radio-labeled GTPase assay under the same experimental setting as described as in (C). γ^{32}P-GTP and $^{32}P_i$ were resolved by thin layer chromatography and exposed to a film. A representative autoradiogram is shown. **(E)** Quantification of $^{32}P_i$ of each time point in the time course experiment shown in (D). The radioactive spots on the developed x-ray films or on the scanned phospho-imager screens were quantified using ImageJ software or Typhoon FLA 9500 laser scanner, respectively. The level of hydrolysis was calculated using the ratio of the hydrolyzed spot and the initial concentration of the nucleotides. All the data shown represent an average of at least three independent experimental runs. Error bars represent standard deviations. (ns (not significant): $p>0.05$; *$p\leq0.05$; **$p\leq0.01$; ***$p\leq0.001$, by Student's *t*-test)

3.4.2 Tubulin-GTP hydrolysis occurs via catalytic microtubule depolymerization by kinesin-13s, but not by non-catalytic means.

Kinesin-13 proteins, including KIF2A and MCAK, are known to depolymerize microtubules (Desai et al., 1999; Hunter et al., 2003). We wondered if the observed induction of GTP-tubulin

hydrolysis occurs during microtubule depolymerization when kinesin-13s encounter tubulin at microtubule ends. To address this, we performed kinesin-13 (KIF2A-NM and MCAK-NM)-induced depolymerization assay using microtubule polymers that retained their GTP-bound like state. Microtubules can be made with slowly hydrolyzable GTP analogs, guanosine 5-3-O-(thio)triphosphate (GTPγS) or guanylyl-(alpha, beta)-methylene-diphosphonate (GMPCPP). Hydrolysis of GTPγS produces GDP, just as GTP hydrolysis does. It has been shown that kinesin-13 proteins can depolymerize these microtubule polymers (Noda et al., 2011). To determine if kinesin-13 proteins can trigger GTPγS hydrolysis upon microtubule depolymerization, we first generated ^{35}S-labeled GTPγS microtubules. To reduce background radioactivity from unpolymerized tubulin and excess ^{35}S-GTPγS, we separated the ^{35}S-labeled GTPγS microtubule polymers from the rest of the reaction mixture by ultracentrifugation through a glycerol cushion. We resuspended the radio-labeled microtubules in stabilizing PIPES-based buffer and used it in a kinesin-13 mediated depolymerization reaction. We resolved the GTPγS hydrolysis via thin layer chromatography (TLC) and monitored the level of microtubule depolymerization by sedimentation assay. From this experiment, we could observe concomitant GTPγS hydrolysis and microtubule depolymerization with both KIF2A-NM and MCAK-NM (**Figure 3.2A-C & Supplementary Figure 3.4**). This result indicates that the depolymerization of these microtubules by kinesin-13s can trigger GTPγS hydrolysis. Analogous experiment with GMPCPP microtubules in kinesin-13-mediated depolymerization using a phosphate detection assay yielded similar result indicating that hydrolysis of GMPCPP also occurred upon microtubule depolymerization (**Supplementary Figure 3.5**). This observation is intriguing because kinesin-13-induced microtubule depolymerization is even strong enough to force the hydrolysis of GTPγS or GMPCPP, which normally does not occur during the polymerization process. This raises the possibility that this

unusual hydrolysis occurs either when microtubules undergo depolymerization, or only when a tubulin conformational change is specifically induced by kinesin-13 proteins. To distinguish these two possibilities, we sought to depolymerize microtubules by alternative means. Exposure to Ca^{2+} or cold temperature is known to cause microtubule depolymerization, including those microtubules formed with GTPγS or GMPCPP (Cassimeris et al., 1986; Müller-Reichert et al., 1998; O'Brien et al., 1997). For this, we set up depolymerization reactions using ^{35}S-labeled GTPγS microtubules. Interestingly, both Ca^{2+} and cold treatments did not trigger GTPγS hydrolysis (marked by the lack of ^{35}S-labeled P_i release, **Figure 3.2D top & Figure-2E**) despite their high efficiency in depolymerizing microtubules (indicated by tubulin dimer release in supernatant **Figure 3.2D bottom & Figure2F**). Together, these experiments indicate that microtubule depolymerization induced by kinesin-13 proteins, but not by calcium or cold treatment, causes a conformational change of tubulin dimers severe enough to trigger hydrolysis of GTPγS or GMPCPP, and by inference, GTP as well.

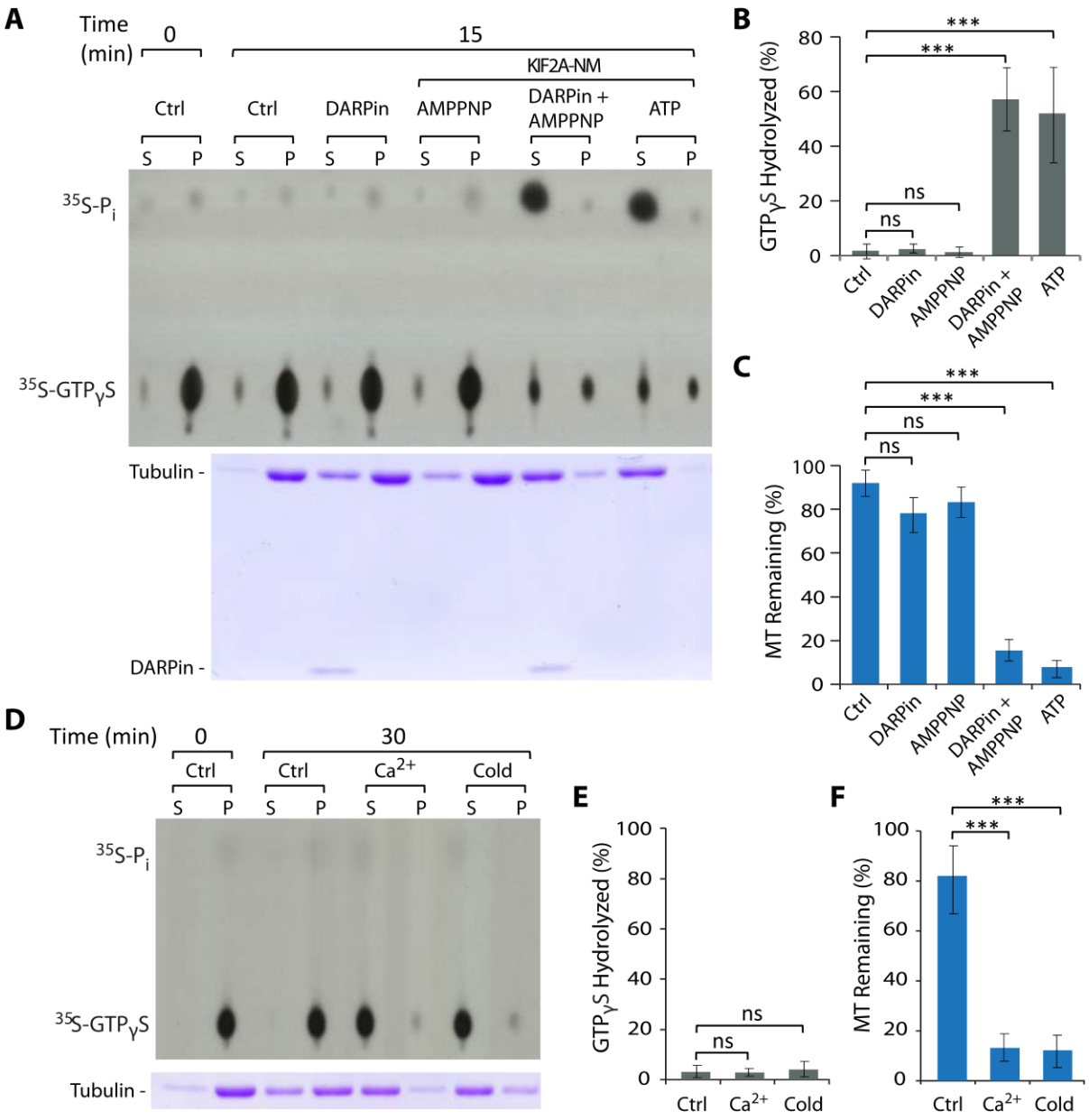

Figure 3.2 Kinesin-13 mediated microtubule depolymerization, unlike non-catalytically induced depolymerization, triggers tubulin-GTP hydrolysis.

(A) Microtubule depolymerization assay was set up using ^{35}S-GTPγS-labeled microtubules alone (Ctrl) or in the presence of DARPin alone, with KIF2A-NM and AMP-PNP, with KIF2A-NM, AMP-PNP and DARPin, or with KIF2A-NM and ATP. Reactions were carried out at room temperature for 15 minutes. Samples containing ^{35}S-GTPγS and ^{35}S-P$_i$ were resolved by thin layer

chromatography (TLC) and radioactivity was detected by exposure to a film. A representative autoradiogram was shown on the top panel. The level of microtubule polymers was monitored at the 15-minute time point using an ultracentrifugation-based sedimentation-based assay. Samples from the supernatant (S) and pellet (P) fractions were resolved by SDS-PAGE and the gel stained by Coomassie blue. A representative gel is shown on the bottom panel. Microtubules were used at 2 μM, KIF2A-NM at 50 nM and DARPin at 1μM. **(B-C)** Quantification of data from experiments shown in (A). B, data from autoradiograms; C, data from Coomassie blue stained gels. **(D-F)** Depolymerization of ^{35}S-GTPγS-labeled microtubules at room temperature (ctrl), or by treatment of cold temperature (4°C) or Ca^{2+} (1 mM) for 30 minutes. Samples were processed, quantified and analyzed in the way as those shown in (A-C). A representative autoradiogram and a Coomassie Blue stained gel were shown in (D), and their quantifications were shown in (E) and (F), respectively. All data represent the average of at least 3 independent experimental sets. Error Bars, S.D. (ns (not significant): $p>0.05$; *$p\leq0.05$; **$p\leq0.01$; ***$p\leq0.001$, by Student's *t*-test)

3.4.3 Interdependent relationship between kinesin-13 ATPase rate and tubulin-GTP turnovers

From our previous study (Trofimova et al., 2018), we know that each kinesin-13-NM motor molecule can form a complex with two tubulin dimers in tandem and changes their curvatures, but we do not know whether this interaction triggers hydrolysis of both GTP molecules or just one. Our crystal structure suggests one of the two dimers is more curved than the other when they bind to KIF2A-NM with AMP-PNP. However, we do not have information as to whether the degrees of curvature are the same in the presence of ATP and whether the change(s) in curvature of either or both dimer(s) is (are) sufficient to trigger tubulin-GTP hydrolysis upon release. To address this,

we first set up nucleotide hydrolysis experiments with KIF2A-NM or MCAK-NM and free tubulin dimers with radio-labeled α^{32}P-ATP and γ^{32}P-GTP tracers, and resolved samples by TLC (**Figure 3.3A**). From these experiments, we could quantitatively measure how much ATP and GTP hydrolyzed in the same reaction based on the amount of released radio-labeled α^{32}P-ADP and $^{32}P_i$, respectively (**Figure 3.3B**). We consistently observed that for each ATP hydrolyzed, there was approximately twice as much GTP hydrolyzed. In parallel experiments, we used the same set up and added both radio-labeled tracers in the same reaction mix, and we obtained the same result (**Supplementary Figure 3.6**). These data indicate that upon each encounter, for each ATP molecule hydrolyzed by KIF2A-NM, there is a corresponding hydrolysis of two GTP molecules from the two associated tubulin dimers. This also suggests that both tubulin dimers, within the ternary complex, undergo conformational changes that are severe enough to trigger tubulin-GTP hydrolysis upon their releases from the associated kinesin-13 protein.

It has also been shown that microtubule polymers stimulate kinesin-13 ATPase activity more than free tubulin dimers (Hunter et al., 2003). We hypothesized that straighter tubulin conformations stimulate kinesin-13 ATPase activity more than the more curved ones. To test this, we set up kinesin-13 ATPase assays in the presence of tubulin dimers with different guanine nucleotides (GTP, GTPγS, GDP or Apo-state). Consistent with this hypothesis, we observed that GTP- or GTPγS-tubulin dimers stimulated kinesin-13 ATPase turnovers significantly higher than those with GDP or the Apo-state using three independent detection assays (radioactivity, malachite green-based phosphate detection assay and ADP-Glo™ assay). These data are summarized in **Table 3.1** and **Supplementary Figure 3.7A-B**. This interpretation is based on the published structural data indicating that GTP-tubulin dimers (PDB code: 4DRX) are slightly straighter than GDP-tubulin (PDB code: 1SAO) (Brouhard & Rice, 2014; Pecqueur et al., 2012; Ravelli et al.,

2004). We postulated that these differences in ATPase rate might be due to differences in the binding affinity of kinesin-13 for tubulin dimers in different nucleotide states. To test this, we set up a binding assay using tubulin dimers in different nucleotide states with either His-tagged KIF2A-NM or MCAK-NM, which could be captured by Ni-charged magnetic beads. As expected, tubulin dimers associated with GTP- or GTPγS- showed significantly higher binding affinity to both KIF2A-NM or MCAK-NM, than those with GDP- or no nucleotide (Apo) **(Supplementary Figure 3.7C-E)**.

Table 3.1 Stoichiometric and Interdependent relationship between Kinesin-13 ATPase rates and β-tubulin-GTP turnover rates.

The rates of Kinesin-13 ATP hydrolysis and tubulin-GTP turnovers were determined using two independent methods: radio-labeled α^{32}P-ATP, γ^{32}P-GTP and ^{35}S-GTPγS in an enzymatic assay (as shown in Figure 3.3 and Supplementary Figure 3.6); and Malachite green-based phosphate detection assay (shown in Supplementary Figure 3.7). The levels of ATP hydrolysis of kinesin-13s (KIF2A-NM and MCAK-NM) were quantified for different nucleotide-bound tubulins. (* To calculate the rate of GTP hydrolysis, we had to use ATPγS instead of ATP.)

	Nucleotide state	Hydrolysis rate (s^{-1})			
		Hot assay		Malachite green	
		ATP	GTP	ATP	GTP
KIF2A-NM	Tub-GTP	0.13 ± 0.04	0.23 ± 0.06	0.16 ± 0.04	0.31 ± 0.09 *
	Tub-GTPγS	0.14 ± 0.04	0.26 ± 0.07	0.18 ± 0.05	-
	Tub-GDP	0.09 ± 0.03	-	0.12 ± 0.04	-
	Tub-APO	0.11 ± 0.02	-	0.11 ± 0.03	-
MCAK-NM	Tub-GTP	0.15 ± 0.04	0.29 ± 0.06	0.17 ± 0.05	0.33 ± 0.07
	Tub-GTPγS	0.16 ± 0.04	0.31 ± 0.06	0.18 ± 0.05	-
	Tub-GDP	0.11 ± 0.04	-	0.13 ± 0.03	-
	Tub-APO	0.10 ± 0.03	-	0.13 ± 0.04	-

Based on the ATPase rates of KIF2A-NM and the corresponding tubulin-GTPase rates summarized in Table 3.1, we could also observe the 1:2 ratio that we had determined earlier in Figure 3.3. Together, these results demonstrated the interdependent relationship between kinesin-13 ATPase activity and tubulin-GTP turnovers as well as the associated tubulin conformational states.

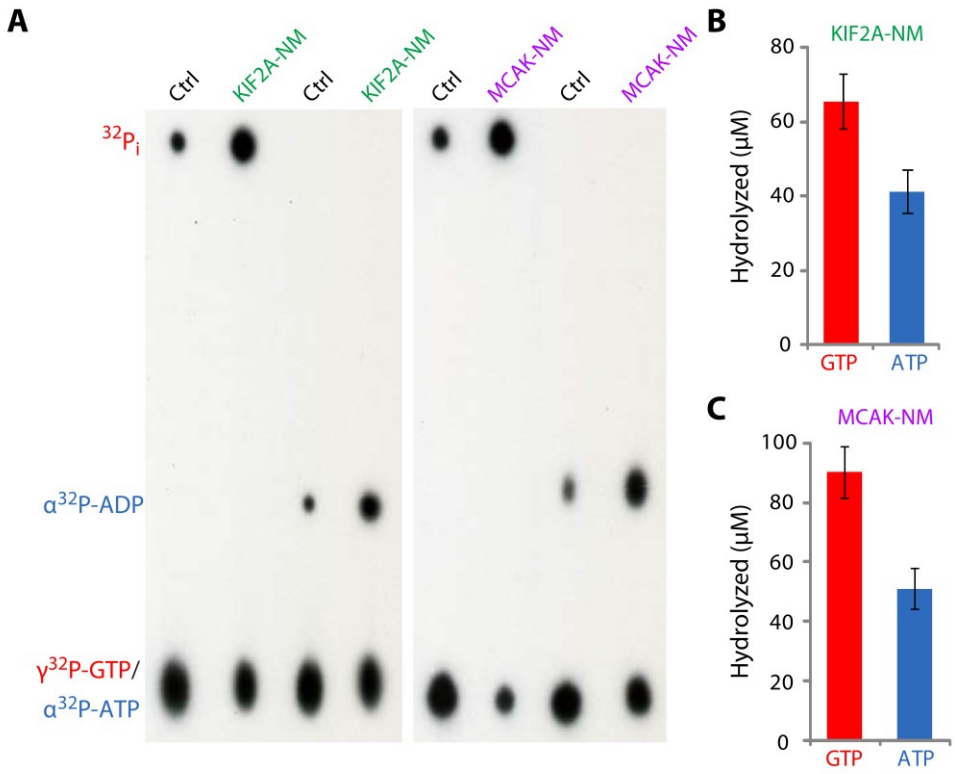

Figure 3.3 Stoichiometric relationship between kinesin-13 ATPase activity and the induced β-tubulin-GTP turnover.

(A) Kinesin-13-induced ATP hydrolysis and tubulin-GTP turnover were monitored using radio-labeled α^{32}P-ATP and γ^{32}P-GTP as tracers in an enzymatic assay as described in Figure 3.2. A representative autoradiogram of a TLC plate (out of 3 independent experimental runs) is shown. Tubulin dimers were used at 4 μM, KIF2A-NM and MCAK-NM at 500 nM, ATP and GTP at 200 μM. Reactions were carried out at room temperature for 10 minutes. **(B-C)** Quantification data for the experiments shown in (A). The levels of ATP and GTP hydrolysis were quantified based on the percentage of α^{32}P-ADP (from α^{32}P-ATP) and $^{32}P_i$ (from γ^{32}P-GTP) of the total amount of α^{32}P-ATP and γ^{32}P-GTP used in the corresponding reaction. Data represent averages of at least 3 independent experimental sets. Error Bars, S.D.

3.4.4 Conformational change-induced tubulin-GTP hydrolysis during microtubule polymerization.

Our finding, that conformational change in tubulin dimers can trigger GTP hydrolysis in our kinesin-13 induced experiments, prompted us to consider the possibility that conformation-induced tubulin-GTP turnover also occurs during microtubule polymerization. It is known that both GTP-tubulin and GDP-tubulin dimers are more curved compared to the straight conformation of tubulin subunits within the microtubule lattice except for those at polymer ends. We postulated that the reason GTPγS and GMP-CPP tubulins promote microtubule polymerization is because they are already in a straighter conformation, and thus the remaining change in conformation required for lattice formation is not big enough to trigger hydrolysis of these slowly hydrolyzable GTP analogs. Likewise, paclitaxel promotes tubulin polymerization in the presence of GTP by straightening the associated free tubulin dimers. If this assessment is true, we should be able to observe paclitaxel-induced tubulin-GTP hydrolysis prior to polymerization. To test this possibility directly, we set up experimental conditions where tubulin-GTP and paclitaxel were both present at low concentrations to disfavor spontaneous polymerization, at 2 μM and 0-2 μM respectively. To further ensure that polymerization did not occur readily, we ran the experiment at 4°C, using the GDP detection assay. As anticipated, we observed almost instantaneous conversion of GTP to GDP in the presence of paclitaxel but not at its absence (**Figure 3.4A**). We also noted that the plateau of GDP accumulation was reached quickly and never exceeded the concentrations of paclitaxel used. We verified that there was no detectable level of microtubule polymerization under these conditions by ultracentrifugation-based sedimentation assay (**Supplementary Figure 3.8**). Together, these data suggest that paclitaxel binding triggers a conformational change of free tubulin dimers from their native curvature to a straighter state in the absence of polymer formation

(although we cannot exclude the possibility that transient occurrence of tubulin oligomers). We postulated that if this assertion is correct, paclitaxel-stabilized tubulin-GDP might also be able to form polymer. This was observed when we attempted tubulin-GDP polymerization in the presence of paclitaxel (**Figure 3.4B**). The polymers that formed from tubulin-GDP are essentially the same as those formed form tubulin-GTP as assessed by their ability to sediment upon ultracentrifugation (**Figure 3.4B-C**), their ability to stimulate kinesin-13 ATPase activity (**Figure 3.4E**), and by their filamentous structure observed by negative stained EM (**Figure 3.4D**). Together, these results suggested the following: First, tubulin-GTP hydrolysis can result from paclitaxel binding and its effect on tubulin conformation (tubulin straightening). Second, tubulin-GTP hydrolysis is not an absolute requirement for microtubule polymerization. Third, paclitaxel-induced conformational change of tubulin dimers, likely straightening as supported by previously published data (Elie-Caille et al., 2007), can facilitate microtubule polymerization in the absence of tubulin-GTP (and therefore its hydrolysis as well).

3.4.5 Evidence for tubulin-GTP at microtubule ends – the "GTP Cap".

Our finding that conformational change of tubulin dimers, namely its straightening, leads to GTP hydrolysis, prompted us to hypothesize the following: During microtubule polymerization, as tubulin dimers straighten and incorporate into protofilaments, the conformational change activates the GTPase activity of β-tubulin. In this scenario, the only tubulin dimers that remain GTP-bound are those at the polymerizing microtubule ends. This model predicts that during microtubule polymerization once nucleation has been established, the level of GTP-tubulin at microtubule ends should remain at similar level as the number of polymerizing ends will stay relatively constant. To test this, we carried out a time course experiment with tubulin in the presence of GTP and γ^{32}P-GTP tracer, followed by ultracentrifugation-based sedimentation to separate the polymerizing

microtubules and unpolymerized tubulin dimers. Indeed, we observed that while the net hydrolysis of GTP increased with time as more and more polymers formed (**Figure 3.4F, left**), the amount of GTP in the polymers (i.e. pellets in sedimentation assay) was constant throughout the polymerization process (comparing 5, 10, 20 min time points in **Figure 3.4F, right**). For comparison, we also performed the same experiment with paclitaxel. As expected, paclitaxel eliminated GTP incorporation at microtubule ends (**Figure 3.4J**). We also observed that the overall GTP hydrolysis in the presence of paclitaxel was lower than that of polymerization enhanced by DMSO, where growing and shrinking of microtubules occurred more readily and continuously (**Figure 3.4G-I**). This result is consistent with the understanding that paclitaxel favors microtubule polymerization, but suppresses its dynamics (and hence lower overall GTP hydrolysis, marked by lower inorganic phosphate (P_i) release than the corresponding DMSO polymerization at all time points, **Figure 3.4I**).

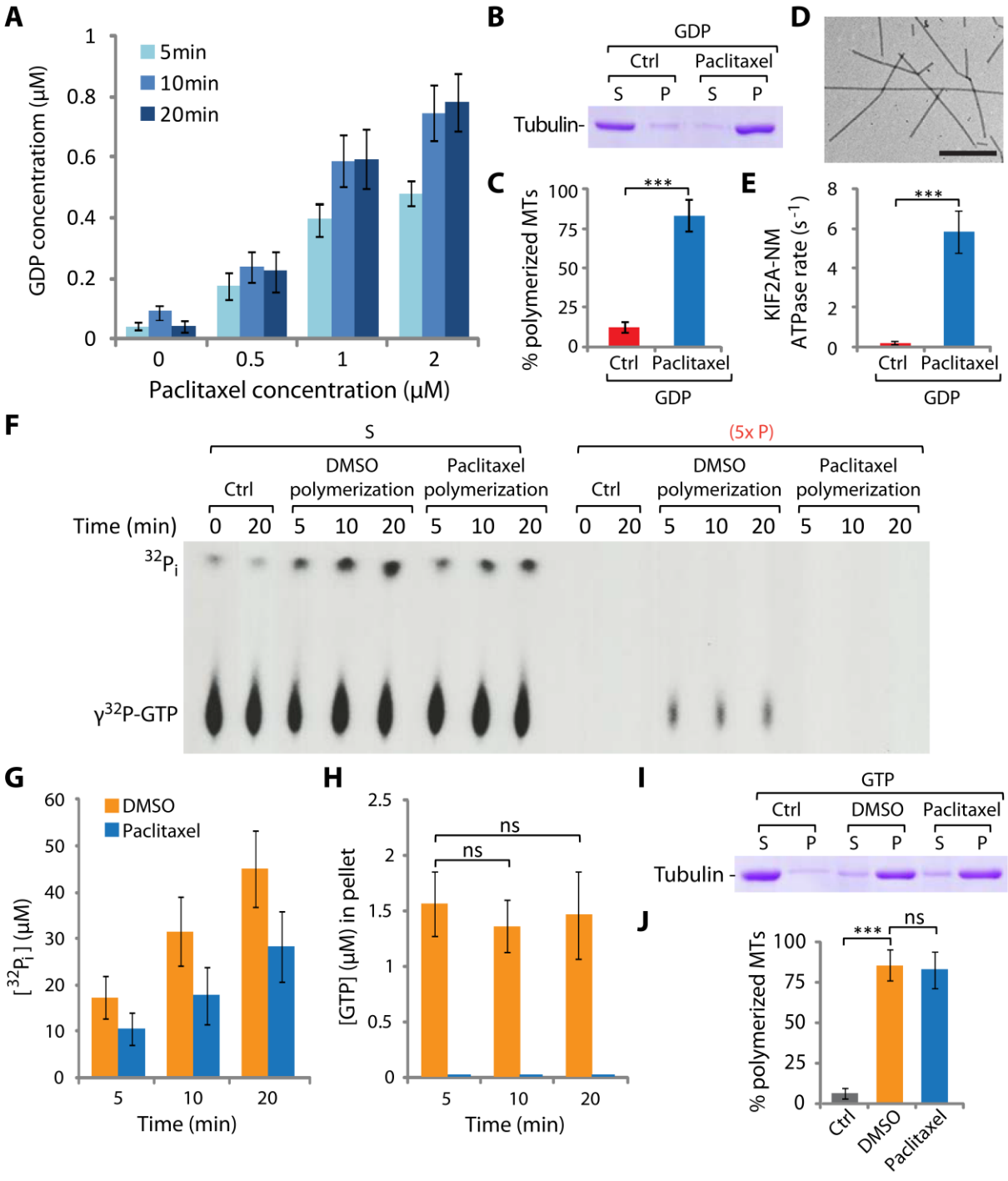

Figure 3.4 Conformational change of tubulin dimers precedes GTP hydrolysis as they incorporate into microtubule polymers.

(A) The amount of tubulin-GTP hydrolyzed induced by different concentrations of paclitaxel (from 0 – 2 μM, as indicated) was measured over time (at 5, 10, 20 min) at 4°C, using a GDP

detection assay. Tubulin dimers were used at 2 μM with 50 μM GTP. **(B)** Microtubules were polymerized using tubulin-GDP (5 μM tubulin dimers and 200 μM GDP) in the absence or presence of 20 μM paclitaxel. The polymerization reactions were carried out at 37°C for 30 min. The levels of microtubule polymerization were determined using an ultra-centrifugation-based sedimentation assay. Samples from the supernatant (S) and pellet (P) fractions were resolved by SDS-PAGE and the gel stained by Coomassie blue. A representative gel is shown. **(C)** The levels of polymerized MTs in (B) were quantified using ImageJ gel analysis. **(D)** Negative stained TEM images of MTs generated in (B). Scale bar, 1 μm. **(E)** The ATPase rate of KIF2A-NM in the presence of the MTs polymerized in (B) was determined using a Malachite green-based phosphate detection assay. **(F)** MTs were polymerized using 10 μM tubulin dimers in the presence of 10% DMSO or 20 μM paclitaxel (with 200 μM GTP and the presence of a radio-labeled γ^{32}P-GTP tracer). GTP hydrolysis was monitored during microtubule polymerization by quantifying the level of $\gamma^{32}P_i$ generated, as described in Figure 3.3. The unpolymerized tubulin dimers and polymerized MTs were separated into supernatant (S) and pellet (P) fractions through ultra-centrifugation. To detect the level of γ^{32}P-GTP more readily, the pellet fractions were loaded at 5x equivalence of the amount of the corresponding supernatant fractions. A representative autoradiogram from three independent experimental runs is shown. **(G-H)** Quantifications of $\gamma^{32}P_i$ in the supernatant fractions (indicative of overall GTP hydrolysis) and γ^{32}P-GTP in the pellet fractions (indicative of the amount of GTP on microtubule polymers) from the samples in F were shown in (G) and (H), respectively. **(I-J)** The levels of microtubule polymerization in reactions shown in (F) at 20 min were determined using a sedimentation assay. Samples were resolved by SDS-PAGE, stained and quantified in the same way as described above in (B-C). A representative Coomassie-blue stained

gel (I) and the corresponding quantification (J) from three independent experiments were shown. Error bars, S.D. (ns (not significant): $p>0.05$; *$p\leq0.05$; **$p\leq0.01$; ***$p\leq0.001$, by Student's *t*-test)

Results from our polymerization experiments predicted that if we started with more polymerization nuclei or smaller/shorter nuclei (and therefore more nuclei at the same concentration), we should observe more GTP incorporation at microtubule ends. To test this prediction, we prepared shorter and longer seeds by polymerizing GMPCPP-tubulin at two different concentrations. The experimental scheme is illustrated in **Figure 3.5A** (and in **Supplementary Figure 3.9A**). Higher tubulin concentration favored more numerous spontaneous nucleation and therefore produced shorter seeds (R1, Figure 3.5A). Conversely, lower concentration lead to longer microtubule seeds (R2, Figure 3.5A). Alternatively, if we took longer seeds and then sheered them into shorter and more numerous ones with a 25-gauge syringe needle, we would produce seeds of different lengths depending on the number of strokes applied to the seed sample (R2'5x & R2'10x in Figure 3.5A). Using these different seeds, we set up polymerization reactions in the presence of the same concentration of free tubulin-GTP dimers at 5 μM in the presence of a radioactive γ^{32}P-GTP tracer. While all reactions proceeded efficiently (as evidenced by almost complete polymerization shown in sedimentation assay, **Figure 3.5E-F** & **Supplementary Figure 3.9B-C**), we consistently observed more γ^{32}P-GTP incorporations into microtubule polymers (pellet) in reactions containing more numerous seeds (i.e. more microtubule ends) while overall GTP hydrolysis did not differ as much among all reactions (**Figure 3.5C-D** & **Supplementary Figure 3.9D-E**). This result indicated that overall polymerization did not vary much among reactions since the same concentration of free GTP-tubulin dimers were used in all reactions (**Figure 3.5C** & **S9C**). On the other hand, the number of polymerizing ends extending from the seeds varies greatly depending on what type of seeds were used in the reactions, and as a

result we observed more GTP incorporation into the polymers in reactions with more numerous polymerizing ends (R1 vs R1', R2 and R2' in **Figure 3.5B-F** & **Supplementary Figure 3.9D**).

To provide a quantitative account of the polymers that forms in these reactions, we determined the length of MTs by electron microscopy (EM) (**Figure 3.5G**), and from which we could then calculate the number of microtubule ends. We prepared the samples using two methods: one was to dilute the polymerized samples into paclitaxel-containing stabilizing buffer and the other was to fix it with formaldehyde, and then observed them by negative stained EM. These preparations were solely to preserve microtubule lengths, and not the integrity of their ends. The length measurements that we obtained were consistent with what we predicted and observed in the radioactive tubulin-GTP polymerization experiments: with shorter seeds produced shorter MTs and longer seeds produced longer MTs. From these measurements and the quantification of GTP incorporation at microtubule ends (**Figure 3.5D,F** & **Figure 3.5H**), we could extrapolate the average length of GTP-tubulin-bearing protofilaments at each microtubule ends (= average microtubule length *x* % GTP in pellet, corrected by % tubulin polymerized) . Based on these calculations, we determined the average length of microtubule ends containing GTP-tubulin to be 69.42 ± 25.53 nm (assuming 13 protofilaments/microtubule). This is in agreement with the length of curved protofilaments at microtubule ends (40-80 nm), as recently measured by McIntosh *et al.* (McIntosh et al., 2018) using cryo-EM images of microtubule polymerized *in vitro* and in various cell types. Together, these data are consistent with the idea that GTP-β-tubulin-containing microtubule ends reflect those dimers that have not undergone straightening and therefore still retain their conformational curvature as that of the free dimers.

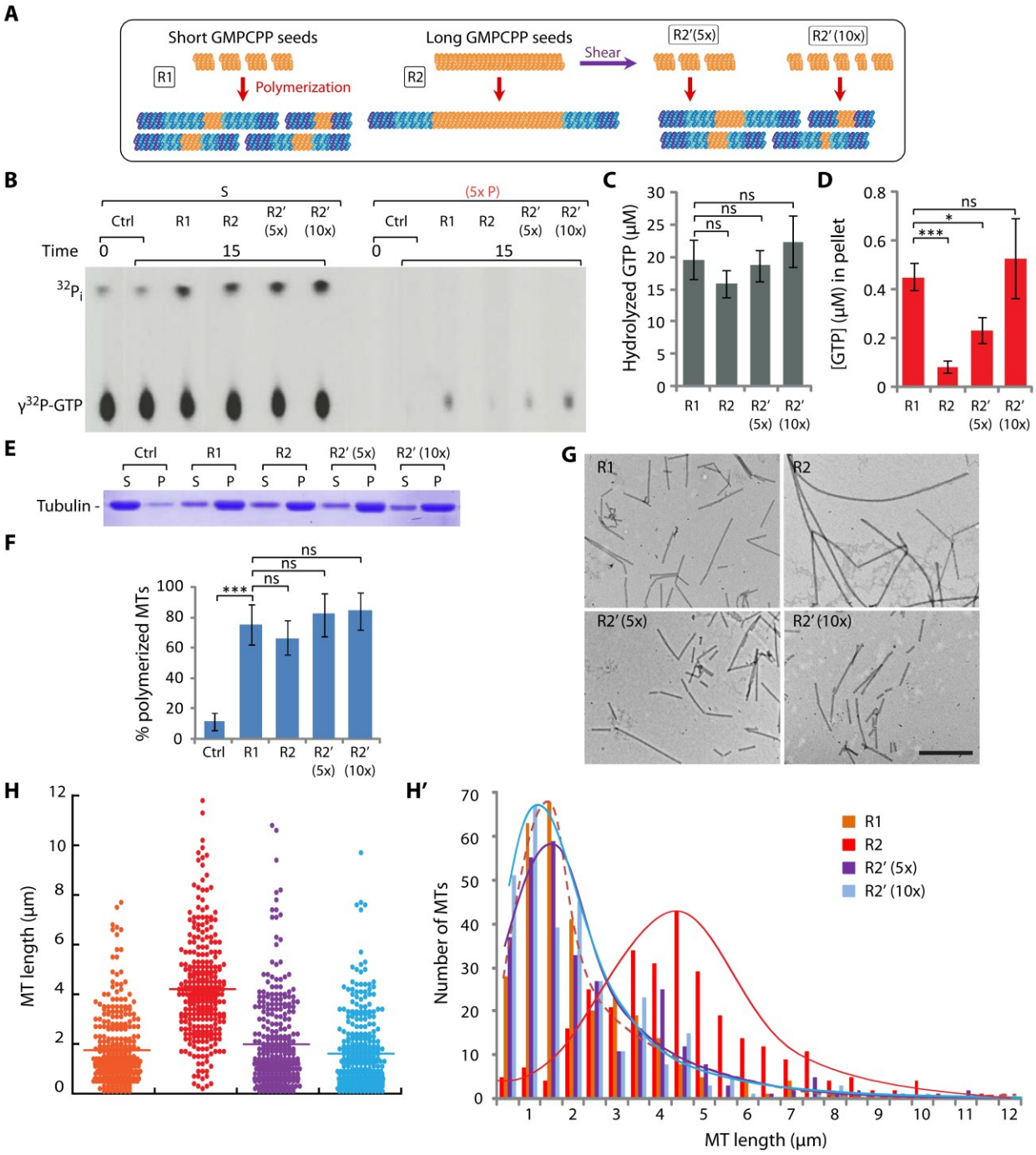

Figure 3.5 The level of GTP-bound tubulin dimers incorporation into microtubule polymers is directly proportional to the number of polymerizing microtubule ends.

(A) An illustration depicting MTs polymerized from different GMP-CPP seeds. Briefly, microtubule polymerization reactions were set up with 5 μM tubulin and 200 μM GTP alone (ctrl)

or in the presence of short (R1) and long (R2) GMP-CPP seeds (at 1 μM) or shorter seeds generated by shearing of long seeds through a 25-gauge needle 5 time (R2' 5x) or 10 times (R2' 5x). **(B-F)** GTP hydrolysis level was assessed using radio-labeled γ^{32}P-GTP as a tracer during the polymerization of MTs under the indicated reaction conditions as described in (A). Samples were processed the same way as described in Figure 3.4F-J. **(B)** A representative autoradiogram is shown. **(C-D)** The corresponding quantifications of overall GTP hydrolysis, as indicated by the amount of $\gamma^{32}P_i$ in the supernatant fractions (C), and of level of tubulin-GTP incorporation into microtubule polymers, as marked by γ^{32}P-GTP in the pellet fractions (D). **(E)** The levels of microtubule polymerization in the reactions shown in (B) were measured using a sedimentation-based assay. A representative Coomassie-blue stained gel is shown. **(F)** The corresponding quantification of microtubule polymerization reactions shown in (E). **(G)** Negative stained TEM images of MTs generated from the indicated reactions as depicted in (A) and as carried out in (B). Scale bar, 1 μm. **(H-H')** Length distributions of MTs polymerized under the indicated reaction conditions, represented by scattered plots (H) or binned histograms (H'). The lines in H indicates the mean length, while the peaks in H' marks the median length. Data represent averages of at least 3 independent experimental sets. Error Bars, S.D. (ns (not significant): $p>0.05$; *$p\leq0.05$; **$p\leq0.01$; ***$p\leq0.001$, by Student's *t*-test)

3.4.6 A model for conformational change driven tubulin-GTP hydrolysis.

Based on the experimental data that presented thus far, we propose the follow model for conformational change driven tubulin-GTP hydrolysis (as depicted in **Figure 3.6**). Free GTP-tubulin dimers exist in a native slightly curved state. When they undergo polymerization, tubulin dimers straighten up to incorporate into protofilaments within the microtubule lattice. The

straightening process triggers GTP hydrolysis (as evidenced in **Figure 3.4**). The polymer ends represent the transition state of this process and may retain the GTP-bound state prior to straightening (**Figure 3.4F & Figure 3.5**). This transition zone may represent the so-called "GTP cap" described in the literature. As tubulin dimers, free from or at microtubule ends, encounter kinesin-13 molecules, the complex formation further bends the tubulin dimers into an even more curved conformation, inferred from our published structural study (Trofimova et al., 2018). Our experimental data show that this bending per se does not trigger GTP hydrolysis, since no hydrolysis occurs in the presence of AMP-PNP-kinesin-13s (**Figure 3.1**). However, GTP hydrolysis occurs upon the release of tubulin dimers from the complex (**Figure 3.1-3.2**), indicating that the transition from the extremely curved state to the less curved native state triggers GTP hydrolysis, even for two less readily hydrolysable GTP analogs (GTPγS and GMP-CPP). On the other hand, kinesin-13-induced microtubule depolymerization differs from depolymerization mediated by Ca^{2+} or cold temperature (**Figure 3.2**). The later process causes the conformational transition of tubulin from straight to the native relaxed curve, which does not trigger the hydrolysis of GTPγS. Taken together, this model presents an intriguing scenario: GTP hydrolysis only occurs when tubulin dimer transitions from curved to straighter conformations (**Figure 3.6**, from right to left), but not from straight to curved (**Figure 3.6**, from left to right). In addition, tubulin-GTP hydrolysis does not occur because the tubulin dimer is in a specific conformation, but it is due to the directional structural transition/change between states.

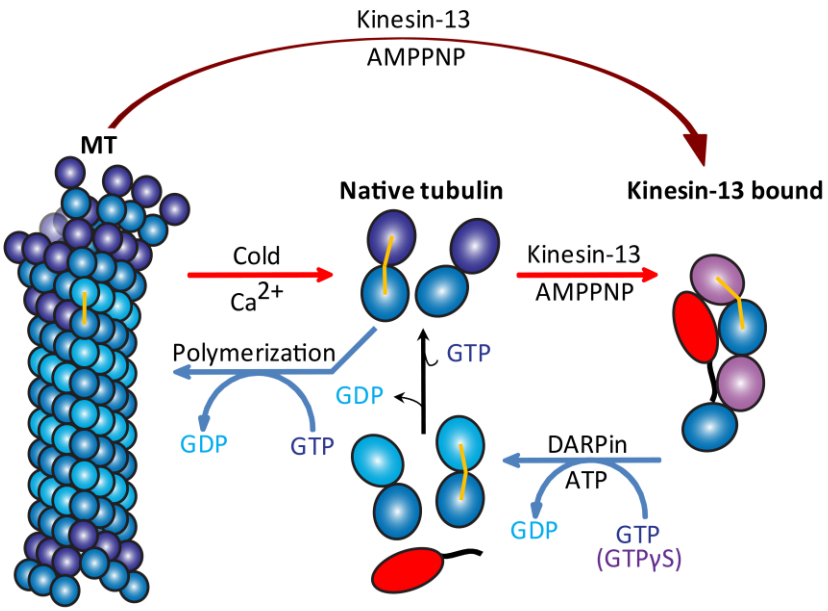

Figure 3.6 A model of conformational change-driven β-tubulin-GTP hydrolysis.

An illustration depicts MTs and tubulin dimers undergoing depolymerization and polymerization. This illustration also depicts the conformational changes of tubulin dimers from their native curved (GTP or GDP-bound) to a straighter state (within microtubule polymer) during polymerization or to an extreme curved structure (bound to kinesin-13) during depolymerization and back to their native curvature (upon released from kinesin-13). The curvature of αβ-tubulin dimers is marked by a yellow line going through the representative tubulin dimers. Note that GTP hydrolysis only occurs when αβ-tubulin dimers undergo conformational changes from a more curved conformation to a straighter one (from right to left), but not vice versa. (GTP-tubulin and GDP-tubulin dimers are shown in dark blue and light blue, respectively)

3.5 DISCUSSION

Following our previous structural study (Trofimova et al., 2018), we report here that Kinesin-13 proteins induced conformational transition of associated tubulin dimers can trigger β-tubulin GTP turnover. The observation that hydrolysis of one ATP molecule can lead to hydrolysis of two GTP molecules implies that the two tubulin dimers bound to the depolymerase are both in a conformation that is more curved than the native relaxed state of free αβ-tubulin dimers and can increase their GTPase activity upon release. On the other hand, different nucleotide-bound states of β-tubulin can stimulate kinesin-13 ATPase rate to a different degree (**Supplementary Figure 3.7A-B**), with GTP or its mimic GTPγS-bound being the highest, followed by GDP- and Apo-state (from straighter to more curved conformations, an assessment based on the available published structural information(Brouhard & Rice, 2014; Pecqueur et al., 2012; Ravelli et al., 2004). We also observed corresponding differences in binding affinity between kinesin-13 proteins and tubulin in different nucleotide states (**Supplementary Figure 3.7C-E**). By inference from this model, the kinesin-13 ATPase activity is highest when the depolymerase is interacting with tubulin in the shaft of a microtubule, as the tubulin dimers there are straightest of all and in tandem arrays. This interaction does not, however, lead to depolymerization. At microtubule ends, kinesin-13 proteins can interact with tubulin dimers on the exposed protofilament ends leading to the bending of tubulin dimers and splaying outward of protofilaments to facilitate its depolymerization. This is accompanied by the hydrolysis of tubulin-GTP dimers at microtubule ends upon their dissociation from kinesin-13 molecules, leading to the removal of GTP-tubulin-containing protofilament tips. Results form our experiments with the use of MTs formed by slowly hydrolyzable GTP analogs (GTPγS and GMPCPP, in **Figure 3.2A-C**, **Supplementary Figure 3.4A-C** & **Supplementary Figure 3.5A-C**), support this assertion.

What we did not expect in the beginning was that our investigation on kinesin-13 mediated microtubule depolymerization would reveal something more fundamental, namely the molecular basis of β-tubulin-GTP hydrolysis. It is generally thought that GTP hydrolysis leads to a conformational change of tubulin dimers as they incorporate into microtubule polymer (Alushin et al., 2014; Mitchison & Kirschner, 1984b; Müller-Reichert et al., 1998). Our data suggest otherwise. Our experiments with paclitaxel showed that it is the change of tubulin conformation that triggers GTP hydrolysis (**Figure 3.4**). In addition, our data on tubulin-GTP with AMP-PNP-bound kinesin-13s and DARPin also indicate that it is the change/transition of conformation, and not a particular nucleotide-bound state, that facilitates the GTP hydrolysis (**Figure 3.1-3.2**). Furthermore, this change needs to be directional (from a more curved to a less curved conformation, but not vice versa) to be productive, as we have shown the lack of GTP turnover with calcium or cold induced depolymerization (from a straight to a more curved conformation). It also appears that the degree of structural change matters too. For example, GTPγS- and GMPCPP-bound tubulins, unlike GTP-tubulins do not undergo hydrolysis during polymerization. There are at least two compatible explanations for that. One is that GTPγS and GMPCPP are less readily hydrolyzed than GTP. Another is that GTPγS- and GMPCPP-bound tubulins are in a straighter conformation than GTP-tubulin, as suggested by published structural data (Maurer et al., 2011; Maurer et al., 2012; Müller-Reichert et al., 1998; Wang & Nogales, 2005). As a result, their structural changes upon polymerization are not as great as that of GTP-tubulin and therefore not enough to trigger hydrolysis. We favor this explanation because structural change can indeed be severe enough to induce hydrolysis of GTPγS and GMPCPP, as we have seen this occurring in KIF2A-NM induced microtubule depolymerization (**Figure 3.2A-C** & **Supplementary Figure**

3.5A-C). Together, our data strongly support conformational change-induced tubulin-GTP hydrolysis.

A key question is how this conformational change-induced β-tubulin-GTP hydrolysis works at the molecular level in the context of available structural data. It has been shown that the β-tubulin-GTP binding pocket is completed with α-tubulin of the adjacent dimer (Zhang et al., 2015). The straightening of the two adjacent dimers with respect to each other can therefore trigger the hydrolysis of β-tubulin-GTP in between. This interpretation is consistent with the requirement of the formation of two tandem tubulin dimers by kinesin-13-NM for triggering β-tubulin-GTP hydrolysis (**Figure 3.1-3.2**) as well as the possibility of transient oligomer formation in our paclitaxel experiments (if it did indeed occurred, **Figure 3.4A-D**). Nevertheless, this interpretation cannot explain the observed 1:2 stoichiometric ratio of kinesin-13-ATP hydrolysis to tubulin-GTP hydrolysis for each encounter of the kinesin-13-tubulin ternary complex (**Figure 3.3**). An alternative or additional explanation to the observed 1:2 ratio may be that the "completion" of the β-tubulin-GTP binding pocket is not an absolute pre-requisite for hydrolysis and that GTP hydrolysis can occur on the β-tubulin exposed to solvent, with the tandem tubulin dimers or as free tubulin dimer in solution. Determining the molecular context of the triggering conformational change (from a "curved" conformation to a "straighter" one) will require additional structural and biochemical investigations in the future.

Our data from *in vitro* microtubule polymerization provide a quantitative measurement on the length of the elusive "GTP cap". Our conformational-based model suggests that this length is directly linked to the curvature of the tubulin dimers. It implies that this cap should reflect the outwardly tapering curvature of protofilament ends that has been commonly observed in previous EM studies (Chrétien et al., 1995; McIntosh et al., 2018; Müller-Reichert et al., 1998). Based on

our calculation, the length of the "GTP cap" is about 70 nm, at least for microtubule polymerized *in vitro*. This is consistent with a recent study by McIntosh et al. which determined the length of the curved protofilament ends to be about 40-80 nm, both *in vitro* and in multiple cell types, ranging from yeast to human (McIntosh et al., 2018). The agreement between these two measurements suggest that the curved tubulin-GTP dimers are added to the microtubule ends during polymerization and the subsequent straightening of the newly added subunits, in part by forming lateral bond with adjacent protofilaments, activates β-tubulin-GTPase activity to accelerate GTP turnover. Since nucleotide hydrolysis is a transitional process and not instantaneous, it is possible that there are still some tubulin dimers in their unhydrolyzed GTP or GDP-Pi states near the ends of the polymerizing ends of MTs, as have been visualized indirectly by the use of fluorescently labelled EB1 (Bieling et al., 2007; Rickman et al., 2017a).

The model that we put forth here is incompatible with the idea of GTP islands that exist deep in the middle of microtubule lattice as those tubulin dimers should be already in the straight conformation and therefore should be in the GDP-bound state. However, our model is not in conflict with the idea that damage can occur in the microtubule middle and that the transient existence of GTP-containing dimers during the repair of damaged protofilaments in the microtubule lattice (Aumeier et al., 2016). Besides this special scenario, tubulin-GTP dimers should be restricted to the extremities on microtubule polymers, at least *in vitro*. Taking this a step further, our model implies another provocative idea: the existence of the GTP cap may be merely a transition state of the tubulin polymerization process; the "GTP cap" simply marks the polymerizing ends, but itself per se does not offer active stabilizing role besides keeping the tubulin-GDP lattice from being exposed. In cells, however, microtubule end-binding proteins such as EB1 and its associated factors (e.g. the kinesin-13 KIF2C, KIF18B, and others) can modulate

microtubule polymerization dynamics spatially and temporally to regulate different cellular processes throughout the cell cycle. It is conceivable that these proteins may interact with tubulin dimers at microtubule ends and alter their conformations, and thereby modulating the extent of the GTP caps in cells. It is also conceivable that some MAPs (e.g. microtubule repair MAPs or tubulin modifying enzymes) could keep sections of microtubule middle in GTP-bound form, creating the apparent "GTP" islands observed in cells to serve specific cellular functions (Dimitrov et al., 2008). All in all, the intriguing ability for αβ-tubulin dimers to self-organize into polymers of hollow tubules, the underlying molecular mechanisms that drive this process, and how associated factors regulate microtubule dynamics in space and time throughout the cell cycle will continue to fascinate us for years to come.

3.6 MATERIALS AND METHODS

3.6.1 Materials

Tubulin, DARPin and Kinesin-13 protein constructs were prepared as previously described (Talje et al., 2014, Trofimova 2018). Most biochemicals were purchased from Bioshop Canada Inc. Nucleotides were obtained from Jena Bioscience via Cedarlane (Ontario, Canada). GDP detection kit was from ProFoldin (MA, USA) and ADP-Glo™ Kinase Assay kit from Promega Corporation. Radio-labeled nucleotides (α^{32}P-ATP, γ^{32}P-GTP, ^{35}S-GTPγS) were purchased from Perkin Elmer.

3.6.2 Microtubule Polymerization

DMSO polymerization: A premix was prepared with 2X BRB80, 2 mM DTT, 2 mM GTP or GTPγS and 20% DMSO. Recycled tubulin was thawed on ice and then an equal volume of the premix was added to it. Polymerization was done by incubating the reaction mixture in a circulating precision water bath at 37°C for 25-30 min.

We pelleted the ^{35}S-labeled GTPγS MTs through 1 ml of warm 40% glycerol in BRB80 cushion by spinning down at 90K RPM in a Sorvall TLA100 rotor for 5 min and then resuspended the MTs in BRB80 buffer containing paclitaxel.

Paclitaxel polymerization: Paclitaxel polymerization reaction mixture was prepared with 10 μM recycled tubulin in the presence of 200 μM GDP, 20 μM of paclitaxel and 1 mM DTT in 1X BRB80. Polymerization was done as described above.

Polymerization from GMPCPP seeds: GMPCPP seeds were prepared as follows: Recycled tubulin was thawed on ice and diluted to 30 μM in 1X BRB80 with 1 mM DTT and 0.2 mM GMPCPP. The mixture was incubated on ice for 10 min and then clarified by spinning down at 90K RPM in a Sorvall TLA100 rotor for 5 min at 2°C. The supernatant was recovered, aliquoted to 5 μl and

snap-frozen in liquid nitrogen and stored at -80°C for later usage. Short GMPCPP seeds were prepared by incubating the aliquoted 30 μM GMPCPP-bound tubulin mixture at 37°C in a precision circulating water bath for 15-20 min. The mix was then diluted to 100 μl using warm BRB80 + 1 mM DTT and spun down at 90K RPM for 5 min at 25°C using TLA100 rotor. The supernatant was discarded, and the pellet was re-suspended in 100 μl of warm BRB80 with 1 mM DTT. To prepare long GMPCPP seeds, the aliquoted 30 μM GMPCPP-bound tubulin mixture was diluted to 3 μM in warm 1X BRB80 + 1 mM DTT before incubating at 37°C for 15-20 min. After preparation, the long seeds could be sheared into shorter seeds by stroking the solution through a 25-gauge needle for 5 or 10 times. To polymerize microtubules from GMPCPP seeds, the prepared seeds (short/long/sheared) were added at either 1 or 0.25 μM to a polymerization mix containing 5 μM recycled tubulin and 200 μM GTP and incubated at 37°C for 25-30 min as described above.

3.6.3 Tubulin / Kinesin-13 mediated nucleotide hydrolysis assays

Kinesin-13 mediated microtubule depolymerization or tubulin-GTP hydrolysis assays were carried out as previously described (Talje, et al. 2014, Trofimova et al., 2018). Briefly, reactions were assembled in 30 μl volume in a BRB80-based buffer (80 mM PIPES, pH 6.8, 1 mM $MgCl_2$, 1 mM EGTA, 75 mM KCl, 0.25 mg/mL bovine serum albumin, 1 mM DTT, and 0.02% Tween), with the indicated concentrations of tubulin dimers, microtubules, kinesin-13 protein constructs, DARPin, and nucleotides. Reactions were carried out at room temperature for the specified lengths of time. Cold- and calcium-induced microtubule depolymerizations were performed in a similar manner in the absence of kinesin-13 protein constructs. After the reactions (in the case of microtubule polymerization and depolymerization assays), microtubule polymers remaining were separated from the free tubulin dimers by an ultracentrifugation-based sedimentation in a Sorvall

TLA100 rotor at 80K RPM for 5 min at 25°C. The supernatant fractions were retrieved from the sedimentation mixture and added to ¼ volume of 4× Laemmli buffer. The polymer-containing pellets were re-suspended in an equal volume of hot 1× Laemmli buffer (prepared by diluting the 4x buffer in depolymerization reaction buffer). Equal portions of the supernatant and pellet samples were resolved on SDS-PAGE. The gel was stained with Coomassie blue dye and scanned with either Epson Perfection 4990 Photo or CanoScan 5600F digital scanners. The bands were quantified using ImageJ (NIH).

3.6.4 Nucleotide hydrolysis detection methods

Malachite green phosphate detection assay: Malachite green-based phosphate detection assay was used to measure ATP and GTP hydrolysis rate, as previously described (Talje, et al. 2014). Briefly, reactions were assembled in 30 µl volume in the same BRB80-based buffer used for the nucleotide hydrolysis assay, with the indicated concentrations of tubulin/microtubules, kinesin-13 protein constructs, DARPin, and nucleotides. Reactions were allowed to proceed for the indicated lengths of time (10–15 min). The reactions were then quenched using equal volume (30 µl) of 90 mM perchloric acid. We then added 30 µl of the quenched mixture to 40 µl malachite green reagent in a 384-well transparent plate to develop the color. After 5-10 min of incubation at room temperature, the level of phosphate generated in each well was quantified by measuring the absorbance at 620 nm using a TECAN infinite M200 PRO plate reader. A standardized calibration curve was generated using a titration of monobasic potassium phosphate (KH_2PO_4) in the same reaction buffer (**Supplementary Figure 3.10A**).

$$Abs = a[P] + b$$

And the equation was used to calculate the concentration of phosphate generated in each well.

$$[P] = \frac{Abs - b}{a}$$

Verification of signal (or the lack thereof) from the presence of thiophosphate was done in similar manner with a titration of thiophosphate in the same reaction buffer (**Supplementary Figure 3.10B**). This level of background thiophosphate signal was used for background subtraction whenever applicable.

GDP detection assay: MicroMolar GDP assay kit (ProFoldin) was used to measure the level of GTP hydrolysis. A premix solution was prepared according to manufacturer instructions in a Tris-HCl based buffer (50 mM Tris-HCl, pH 8.0, 3 mM $MgCl_2$, 0.2 mM EDTA, 0.5 mM DTT, 50 mM NaCl, 0.003% Brij-35). Equal volumes (15 µl) of reaction samples and premix solution were mixed and incubated for 45 min at room temperature. Then 30 µl of 1X Fluorescent dye was added to the mixture and after 5 min the fluorescence intensity was read at 535 nm with excitation at 485 nm using TECAN infinite M200 PRO plate reader. GDP samples of known concentrations were used to obtain a linear standard curve of the fluorescent intensity (Fc) values and the GDP concentration [GDP] (**Supplementary Figure 3.1A**).

$$Fc = a[GDP] + b$$

GDP concentrations were calculated using the Fc values from the unknown samples and the a and b values from the standard curve.

$$[GDP] = \frac{Fc - b}{a}$$

To verify the level of signal interference from the presence of ADP in the mixture, another standard curve was plotted from a separate set of assays using a titration of known ADP concentrations (**Supplementary Figure 3.1B**).

ADP Glo assay: Reactions were assembled in 25 µl total volume, as described for the Malachite Green assay. Once the reactions were complete, the ADP-Glo™ Assay was performed in two steps. The reaction mixture was then added to 25 µl of ADP-Glo™ Reagent and incubated at room temperature for 40 minutes. Then the mixture was added to 50 µl of Kinase Detection reagent (to convert ADP to ATP and introduce luciferase and luciferin to detect ATP) and incubated at room temperature for 40-60 minutes (based on the concentration of ATP). The mixture was added to a 96-well white solid bottom plate in duplicates and luminescence was measured using TECAN infinite M200 PRO plate reader. Four ATP-to-ADP conversion standard curves were prepared at different ATP+ADP concentrations (1, 10, 100 or 1000 µM), in 25µl of 1X reaction buffer. ADP-Glo™ Kinase Assays were performed at room temperature as described for the samples and four standard curves were plotted from the luminescence values of the different concentrations of ATP/ADP (**Supplementary Figure 3.11**).

Radioactivity assay: Nucleotide hydrolysis or microtubule polymerization assays were performed in the same buffers as described, except that the reaction mixtures were supplemented with α^{32}P-ATP, γ^{32}P-GTP, ^{35}S-GTPγS tracers for the detection of hydrolysis. After the specified incubation time, reactions were quenched by the addition of equal volume of 1N formic acid. Small fractions of the samples were removed and spotted on a poly(ethyleneimine)-cellulose plate (EMD Millipore - TLC PEI Cellulose F - 1.05579.0001) and let air-dried for 5-10 min. Samples on the plate were resolved by thin-layer chromatography (TLC) in a glass chamber using 0.375 M KH_2PO4 (pH 3.5) as a resolving buffer. Afterwards, the TLC plate was air dried for at least 1 hour before exposure to an X-ray film or a phosphor-imager screen. The radioactive spots on the developed x-ray films or on the scanned phospho-imager screens were quantified using ImageJ

software or Typhoon FLA 9500 laser scanner, respectively. The level of hydrolysis was calculated using the ratio of the hydrolyzed spot and the initial concentration of the nucleotides ($ATP_{initial}$ or $GTP_{initial}$ in the solution).

$$[Pi] = [GTP_{initial}] \times (Pi/(Pi + GTP)$$

or

$$[ADP] = [ATP_{initial}] \times (ADP/(ADP + ATP)$$

3.6.5 Tubulin-Kinesin-13 Binding Assay

Tubulin-kinesin-13 binding assay was carried out via immunoprecipitation using Ni-charged MagBeads (GenScript, NJ), to pull down Histidine-tagged kinesin-13 proteins. Briefly, magnetic beads were washed with BRB80-based binding buffer (80 mM PIPES, pH 6.8, 1 mM $MgCl_2$, 1 mM EGTA, 75 mM KCl, 0.25 mg/mL bovine serum albumin, 1 mM DTT, and 0.02% Tween). The reactions were started by adding kinesin-13 proteins at the indicated concentrations to 2 µl of magnetic beads in BRB80-based binding buffer. The indicated concentrations of tubulin dimers and nucleotides were then added to the reaction mixtures that were assembled in a final volume of 30 µl. Reactions were carried out at room temperature for 5 minutes. The beads were then pulled down using a magnetic stand. The supernatant fractions were retrieved from the sedimentation mixture and added to ¼ volume of 4× Laemmli buffer. The beads were re-suspended in an equal volume of hot 1× Laemmli buffer (prepared by diluting the 4x buffer in the binding reaction buffer). Equal portions of the supernatant and pellet samples were resolved on SDS-PAGE. The gel was stained with Coomassie blue dye and scanned with either Epson Perfection 4990 Photo or CanoScan 5600F digital scanners. The bands were quantified using ImageJ (NIH).

3.6.6 Negative staining of MTs by Transmission Electron Microscopy (TEM)

Before sample application, the grids (Formvar Carbon Support Film on Square Grids - FCF200-Ni; Electron Microscopy Sciences) were glow discharged via a Pelco easy glow (Pelco, Fresno, USA) for 30 seconds. MTs were polymerized, as described above, and were either stabilized by diluting in BRB80 buffer containing paclitaxel (twice the tubulin concentration) or fixed using 4% formaldehyde, preparation and were diluted to 0.5 µM just before grid. 10 µl of the diluted sample was placed on a piece of parafilm and grid was placed on the top (with carbon side touching the sample) for ~1 min. Excess liquid was then removed by gently tilting the grid sideway on a Whatman blotting paper. The grid was then rinsed with a droplet of dH_2O and blotted again with a fresh Whatman paper. The rinse procedure was repeated two more times and the samples on the grid were then stained with 10 µl of 0.5% filtered EM-grade Uranyl Acetate (UA). After removing the excess UA by blotting, the grid was air dried for at least 1 hour. Grids were examined at the EM facility at the Université de Montréal in a FEI Tecnai 12 (Eindhoven, The Netherlands) transmission electron microscope operating at 80 kV. For each experimental condition, the lengths of 300 microtubules were quantified using ImageJ (NIH).

3.7 Acknowledgement

We thank the LSCTB platform at the Université de Montréal for the access to the Electron Microscopy facility. We thank members of the Kwok lab for their inputs and suggestions, and Drs. Richard J McIntosh and Nikita Gudimchuk for their critical reviews on the manuscript. We acknowledge the funding support from the Canadian Institutes of Health Research (to B.H.K: PJT 148982 & 152920). B.H.K. is a recipient of the Fonds de recherche du Québec - Santé (FRQS) Chercheure-boursière Junior 1 and Junior 2 Awards and the Canadian Institutes of Health Research (CIHR) New Investigator Award. M.P. is supported by a FRQS doctoral fellowship and by doctoral and financial programs at the Université de Montréal.

3.8 Declaration of Interests

The authors declare no competing financial interests.

3.9 SUPPLEMENTARY INFORMATION

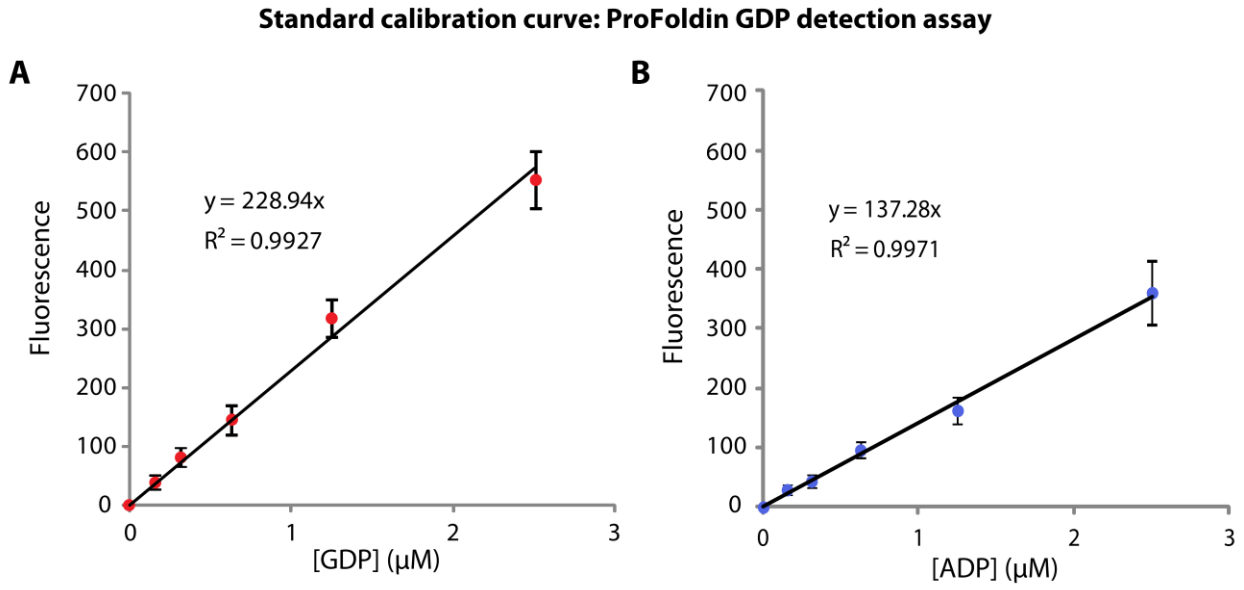

Supplementary Figure 3.1. Standard curves of ProFoldin MicroMolar GDP assay. (A) Standard curve of ProFoldin MicroMolar GDP assay, using different concentrations of GDP based on fluorescence measurements with emission at 535 nm and excitation at 485 nm. (B) Similar calibration curve was generated for the assay, using a series of concentration of ADP. Data represent averages of 3 independent experimental sets. Error Bars, S.D.

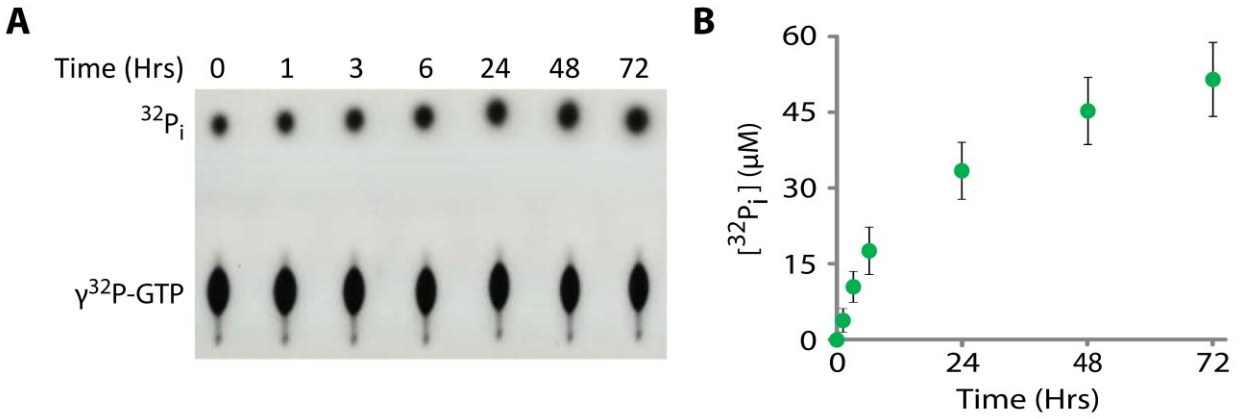

Supplementary Figure 3.2. Basal rate of tubulin-GTP hydrolysis. (A) A time course experiment in which basal tubulin-GTP hydrolysis was measured using a γ32P-GTP radio-labeled GTPase assay in the presence of 4 μM tubulin dimers and 0.2 mM of GTP. A representative autoradiogram is shown. (B) Quantification of 32Pi of each time point in the time course experiment shown in (A). Data represent the average of at least three independent experimental runs. Error bars, S.D.

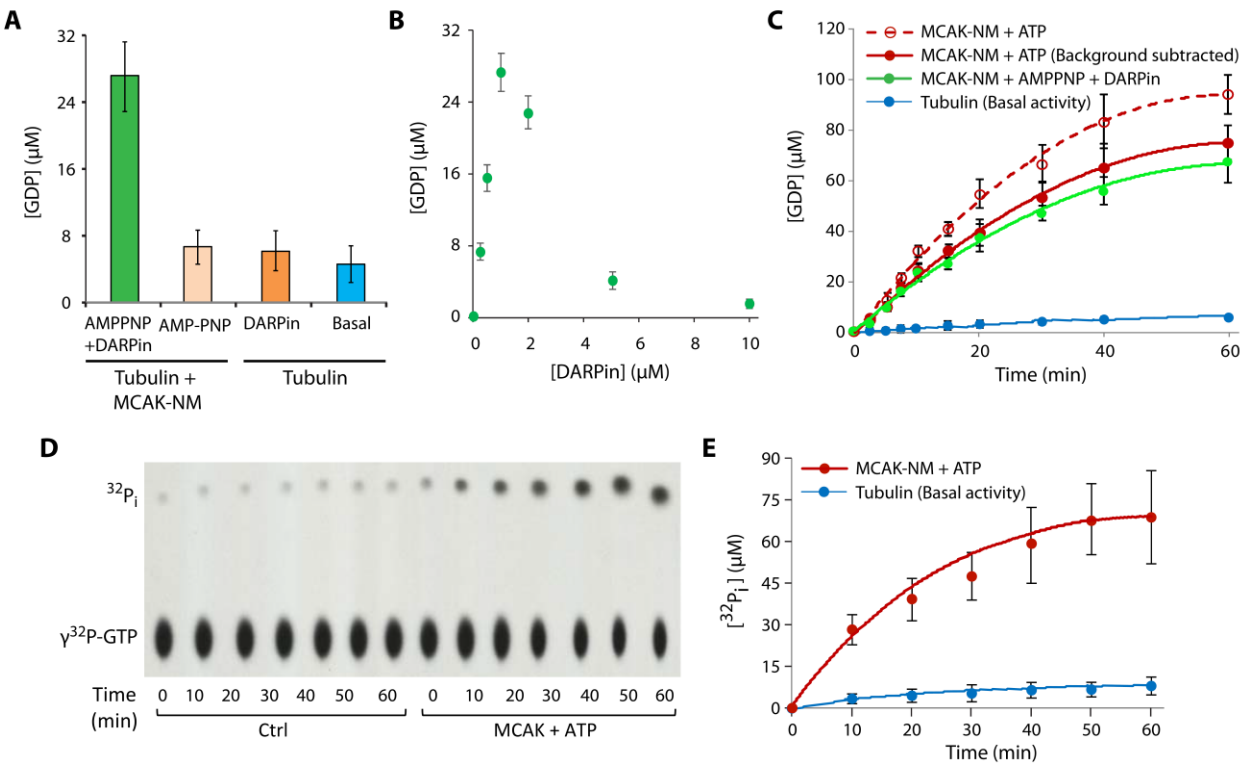

Supplementary Figure 3.3. The binding and unbinding of the Kinesin-13 protein MCAK to and from tubulin dimers induce β-tubulin-GTP hydrolysis. (A) Tubulin-GTP hydrolysis measured by GDP production (ProFoldin GDP detection assay) when tubulin dimers (4 μM) and GTP (0.2 mM) were incubated alone, with DARPin (1 μM) or in the presence of MCAK-NM (200 nM) with AMP-PNP (0.2 mM) or with AMP-PNP and DARPin for 15 minutes at room temperature. (B) To determine the effect of DARPin, tubulin-GTP hydrolysis measured by GDP production when tubulin-GTP dimers were incubated in the presence of MCAK-NM and AMP-PNP with different concentrations of DARPin, under the same condition as in (A). (C) Time-course experiments comparing the tubulin-GTP turnovers between tubulin dimers that were incubated in the presence of MCAK-NM with AMP-PNP and DARPin and those with MCAK-NM with ATP under the same condition as in (A). For (A-C), the level of GDP was measured using a GDP detection assay (ProFoldin). (D) A time course experiment in which basal and MCAK-NM-induced β-tubulin-

GTP hydrolysis (in the presence of ATP) using a γ32P-GTP radio-labeled GTPase assay under the same experimental setting as described as in (C). γ32P-GTP and 32Pi were resolved by thin layer chromatography and exposed to a film. A representative autoradiogram is shown. (E) Quantification of 32Pi of each time point in the time course experiment shown in (D). All the data shown represent averages of at least three independent experimental runs. Error bars, S.D. (ns (not significant): $p>0.05$; *$p\leq0.05$; **$p\leq0.01$; ***$p\leq0.001$, by Student's *t*-test)

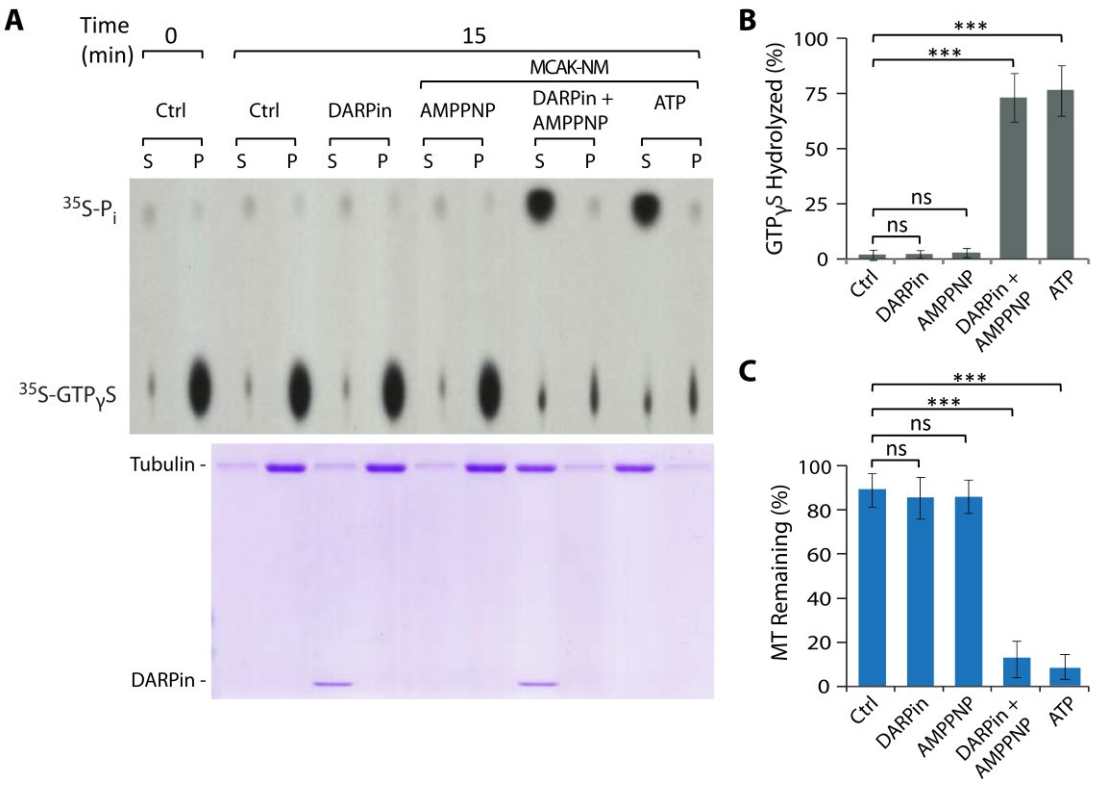

Supplementary Figure 3.4. MCAK-NM mediated microtubule depolymerization triggers tubulin-GTP hydrolysis. (A) Microtubule depolymerization assay was set up using 35S-GTPγS-labeled MTs alone (Ctrl) or in the presence of DARPin alone, with MCAK-NM and AMP-PNP, with MCAK-NM, AMP-PNP and DARPin, or with MCAK-NM and ATP. Reactions were carried out at room temperature for 15 minutes. Samples containing 35S-GTPγS and 35S-Pi were resolved by thin layer chromatography and radioactivity was detected by exposure to a film. A representative autoradiogram was shown on the top panel. The level of microtubule polymers was monitored at the 15-minute time point using an ultracentrifugation-based sedimentation-based assay. Samples from the supernatant (S) and pellet (P) fractions were resolved by SDSPAGE and the gel stained by Coomassie blue. A representative gel is shown on the bottom panel. MTs were used at 2 μM, MCAK-NM at 50 nM and DARPin at 1μM. (B,C) Quantification of data from experiments shown in (A).

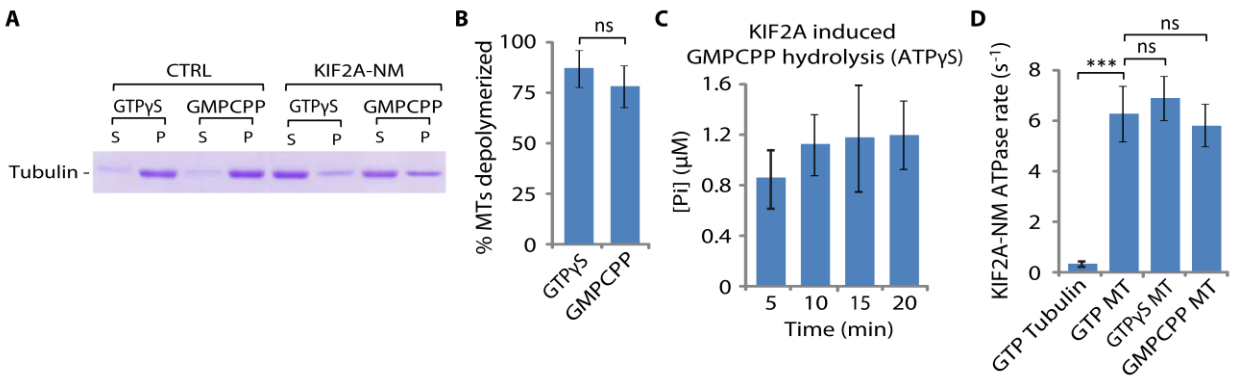

Supplementary Figure 3.5. Kinesin-13-mediated microtubule depolymerization triggers hydrolysis of β-tubulin-GMPCPP. (A) GTPγS and GMPCPP MTs were prepared using 10 μM tubulin and 200 μM of GTPγS or GMPCPP, respectively. Microtubule depolymerization reactions were set up using 2 μM GMPCPP MTs, without (Ctrl) or with 50 nM KIF2A-NM in the presence of 200 μM ATP. The level of depolymerization was monitored using a sedimentation-based assay. Reactions were carried out at room temperature for 15 minutes. A representative Coomassie-blue stained gel from 3 independent runs is shown. (B) The corresponding quantification of microtubule depolymerization reactions described in (A). (C) The occurrence of GMPCPP hydrolysis during KIF2A-NM-mediated microtubule depolymerization was detected by the presence inorganic phosphate (Pi) using Malachite Green-based phosphate detection assay. Depolymerization reaction was set up in a time course experiment using2 μM of pre-clarified GMPCPP MTs, 50 nM KIF2A-NM and 200 μM ATPγS. Pre-clarified GMPCPP MTs were prepared by pelleting in an ultracentrifugebased sedimentation and then re-suspending in a BRB-80-based buffer right before the experiment. The use of ATPγS, instead of ATP, here was to ensure that the signal detected was from GMPCPP hydrolysis since thiophosphate generates minimal background signal with malachite green reagent (see calibration curve in Supplementary Figure 10B). Reactions were carried out at room temperature for the indicated lengths of time. (D) Tubulin or MTstimulated

ATPase rates of KIF2A-NM were quantified using ADP Glo Kinase assay. Reactions were assembled, as described in the method section, with 50 nM KIF2A-NM and 200 μM ATP in the presence of 2 μM upolymerized tubulin, paclitaxel-stabilized GDP MTs, GTPγS MTs or GMPCPP MTs. Reactions were carried out at room temperature for 15 minutes. Data represent the average of at least 3 independent experimental sets. Error Bars, S.D. (ns (not significant): $p>0.05$; *$p\leq0.05$; **$p\leq0.01$; ***$p\leq0.001$, by Student's *t*-test)

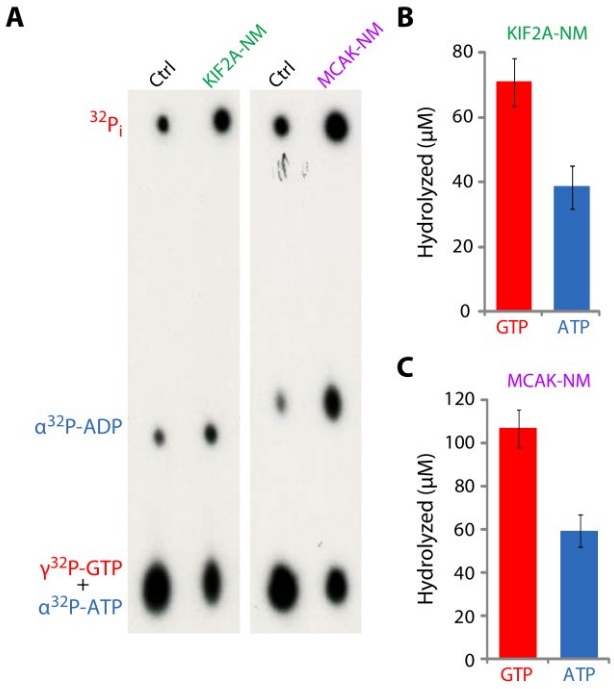

Supplementary Figure 3.6. Stoichiometric relationship between MCAK-NM ATPase activity and the induced tubulin-GTP turnover. (A) ATP hydrolysis of MCAK-NM and tubulin-GTP turnover were monitored using radio-labeled α32P-ATP and γ32P-GTP as tracers in an enzymatic assay, in a similar experiment as shown in Figure 3.3. However, in this experiment, both radio-labeled tracers were added to the same reaction mixtures. A representative autoradiogram of a TLC plate is shown. Tubulin dimers were used at 4 μM, KIF2A-NM and MCAK-NM at 500 nM, ATP and GTP at 200 μM. Reactions were carried out at room temperature for 10 minutes. (B-C) Quantification data for the experiments shown in (A). The levels of ATP and GTP hydrolysis were quantified based on the percentage of α32P-ADP (from α32PATP) and 32Pi (from γ32P-GTP) of the total amount of α32P-ATP and γ32P-GTP used in the corresponding reaction. Data represent the average of at least 3 independent experimental sets. Error Bars, S.D.

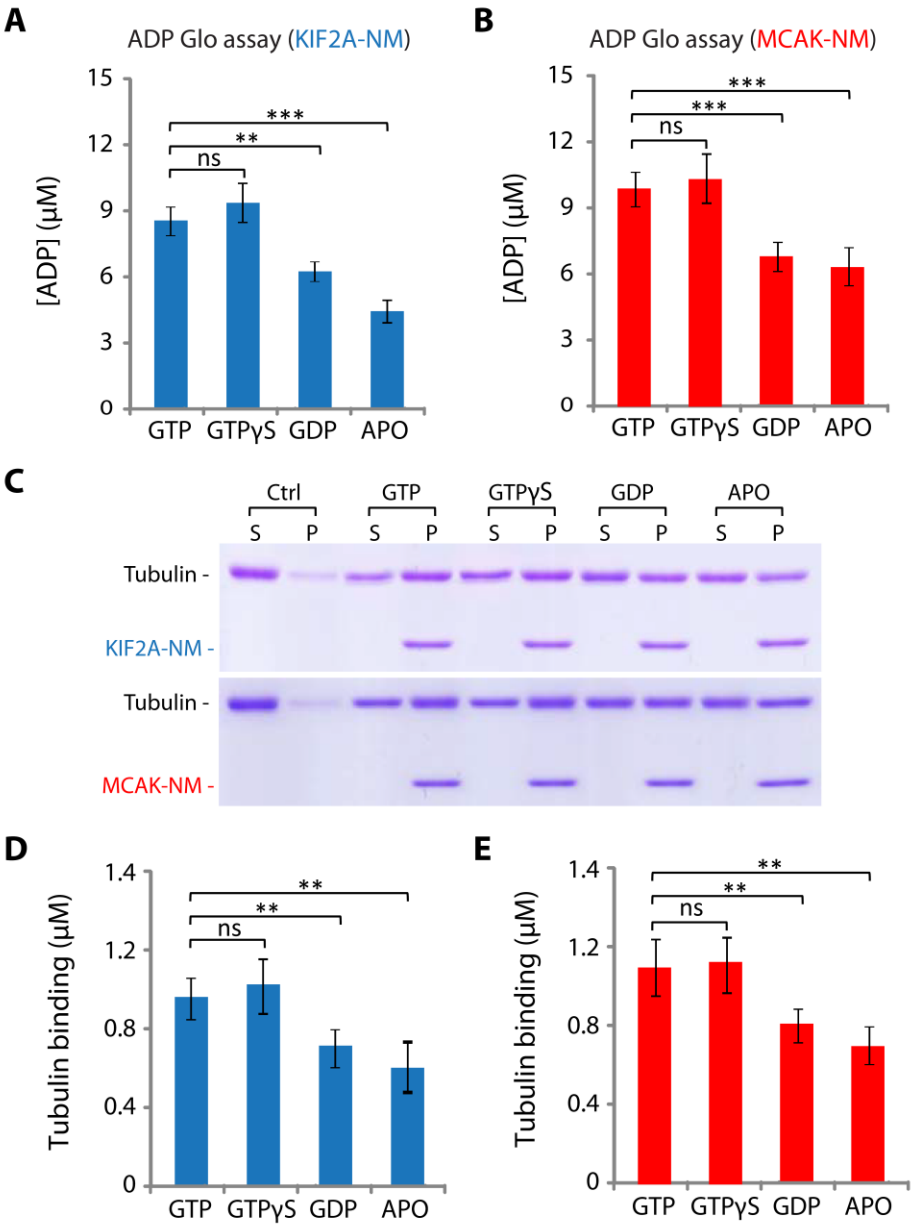

Supplementary Figure 3.7. Tubulin dimers in different nucleotide states differentially stimulate ATPase activity of kinesin-13 proteins and exhibit differential binding affinity to these kinesins. (A,B) ATP hydrolysis of KIF2A-NM (A) and MCAK-NM (B) in the presence of tubulin dimers with different nucleotides as indicated using ADP GloTM reagent which monitors the ADP level in the reactions. (C) Binding affinity Kinesin-13 proteins to different nucleotide-bound tubulin dimers was measured by His-tagged affinity pull down assay with Ni-coated magnetic beads. The

level of tubulin dimers associated with His-tagged KIF2A-NM or MCAK-NM, was assessed by SDS-PAGE and Coomassieblue staining. Representative gels are shown. (D-E) Corresponding quantifications of the binding data in (C) for KIF2A-NM (D) or MCAK-NM (E) are shown. Data represent averages of 3 independent experimental sets. Error bars, S.D. (ns (not significant): $p>0.05$; *$p\leq0.05$; **$p\leq0.01$; ***$p\leq0.001$, by Student's *t*-test)

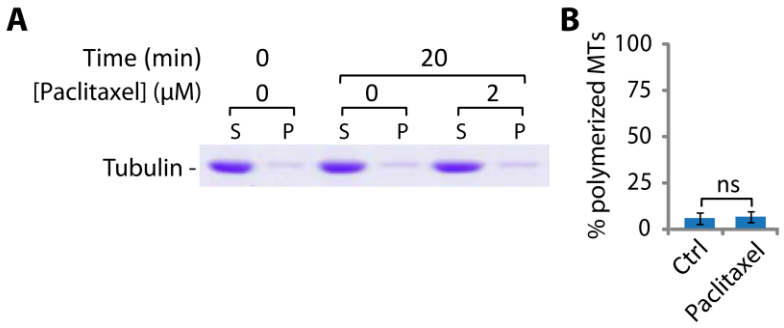

Supplementary Figure 3.8. Absence of microtubule polymerization in the presence of low tubulin and paclitaxel concentration at 4°C. (A) The levels of microtubule polymerization in the reactions shown in Figure 3.4A were assessed by ultracentrifugation-based sedimentation assay. A representative Coomassie-blue stained gel with negligible level of pelleted polymer is shown. (B) The corresponding quantification of microtubule polymerization reactions shown in (A). Data represent averages of at least 3 independent experimental sets. Error Bars, S.D.

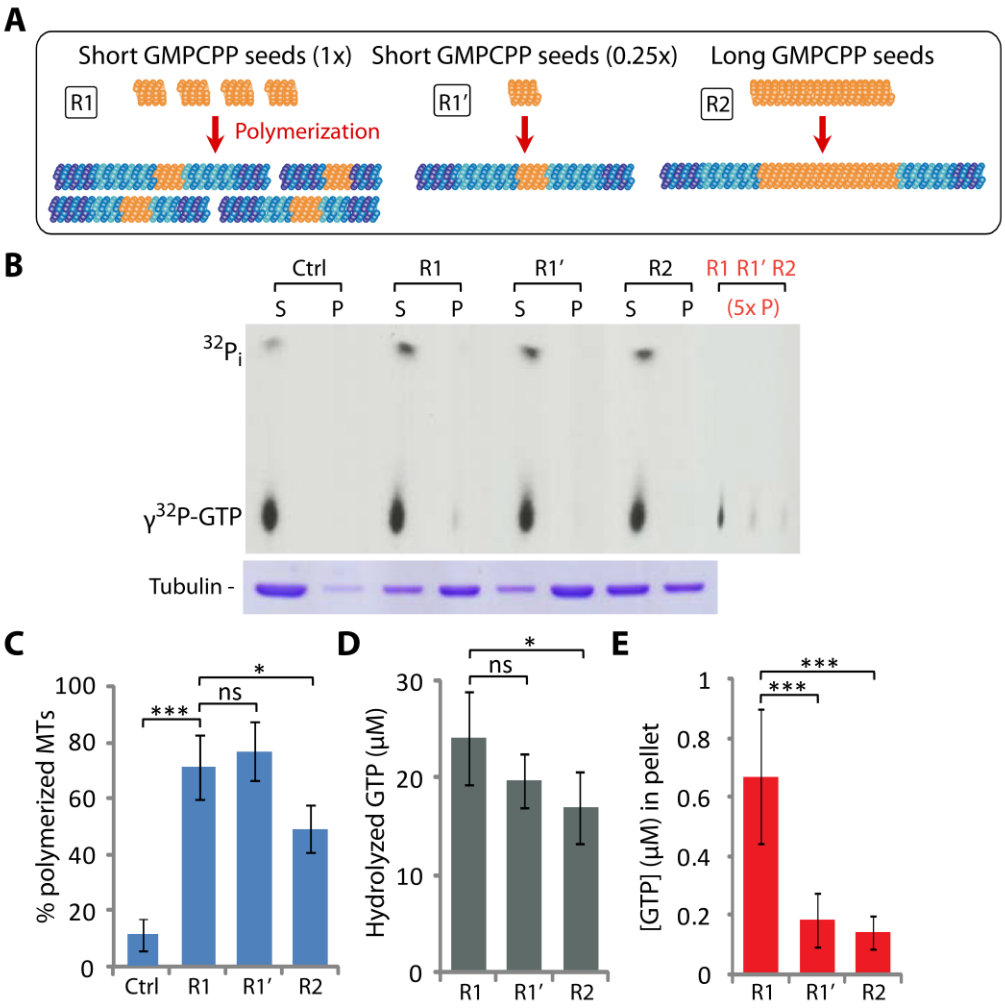

Supplementary Figure 3.9. The level of GTP-bound tubulin dimers incorporation into microtubule polymers is directly proportional to the number of polymerizing microtubule ends. (A) An illustration depicting MTs polymerized from different GMP-CPP seeds, as described in Figure 3.5. Briefly, microtubule polymerization reactions were set up with 5 μM tubulin and 200 μM GTP alone (ctrl) or in the presence of 1 μM short (R1), 0.25 μM short (R1'), or 1 μM long (R2) GMP-CPP seeds. (B-E) Level of GTP hydrolysis was assessed using radio-labeled γ32P-GTP as a tracer during the polymerization of MTs under the indicated reaction conditions as described in (A). Samples were processed the same way as described in Figure 3.4FJ. Note that the pellet (P) fractions were loaded at 5x equivalence of the amount of the corresponding supernatant (S)

fractions, in order to detect the level of γ32P-GTP more readily. (B) A representative autoradiogram is shown (top). The levels of microtubule polymerization were measured using a sedimentation-based assay. A representative Coomassieblue stained gel is shown (bottom). (C) The corresponding quantification of microtubule polymerization reactions shown in (B). (D-E) The corresponding quantifications of overall GTP hydrolysis, as indicated by the amount of γ32Pi in the supernatant (S) fractions (D), and of level of tubulin-GTP incorporation into microtubule polymers, as marked by γ32P-GTP in the pellet (P) fractions, corrected by the loaded amount (E). Data represent averages of at least 3 independent experimental sets. Error Bars, S.D. (ns (not significant): $p>0.05$; *$p\leq0.05$; **$p\leq0.01$; ***$p\leq0.001$, by Student's *t*-test).

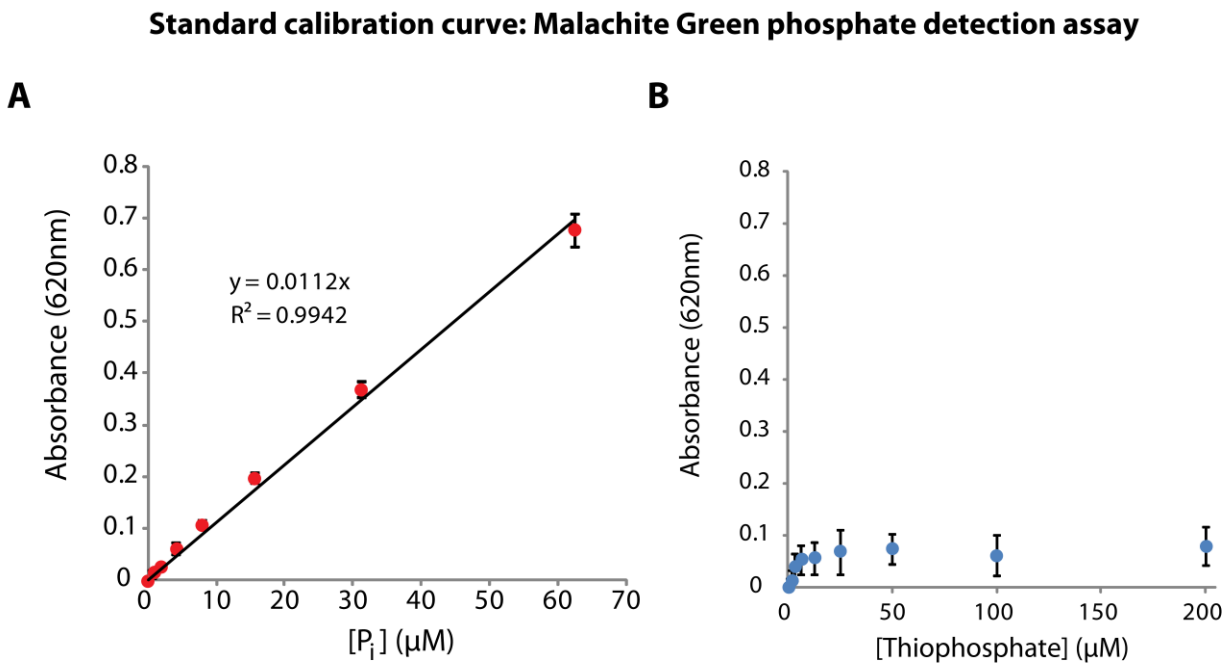

Supplementary Figure 3.10. Standard curves of Malachite Green-based phosphate detection assay. (A-B) Standard calibration curves of Malachite Green-based colorimetric phosphate detection assay, generated by measuring different concentrations of inorganic phosphate (A) or thiophosphate (B) at absorbance of 620nm. Data represent averages of 3 independent experimental sets. Error Bars, S.D.

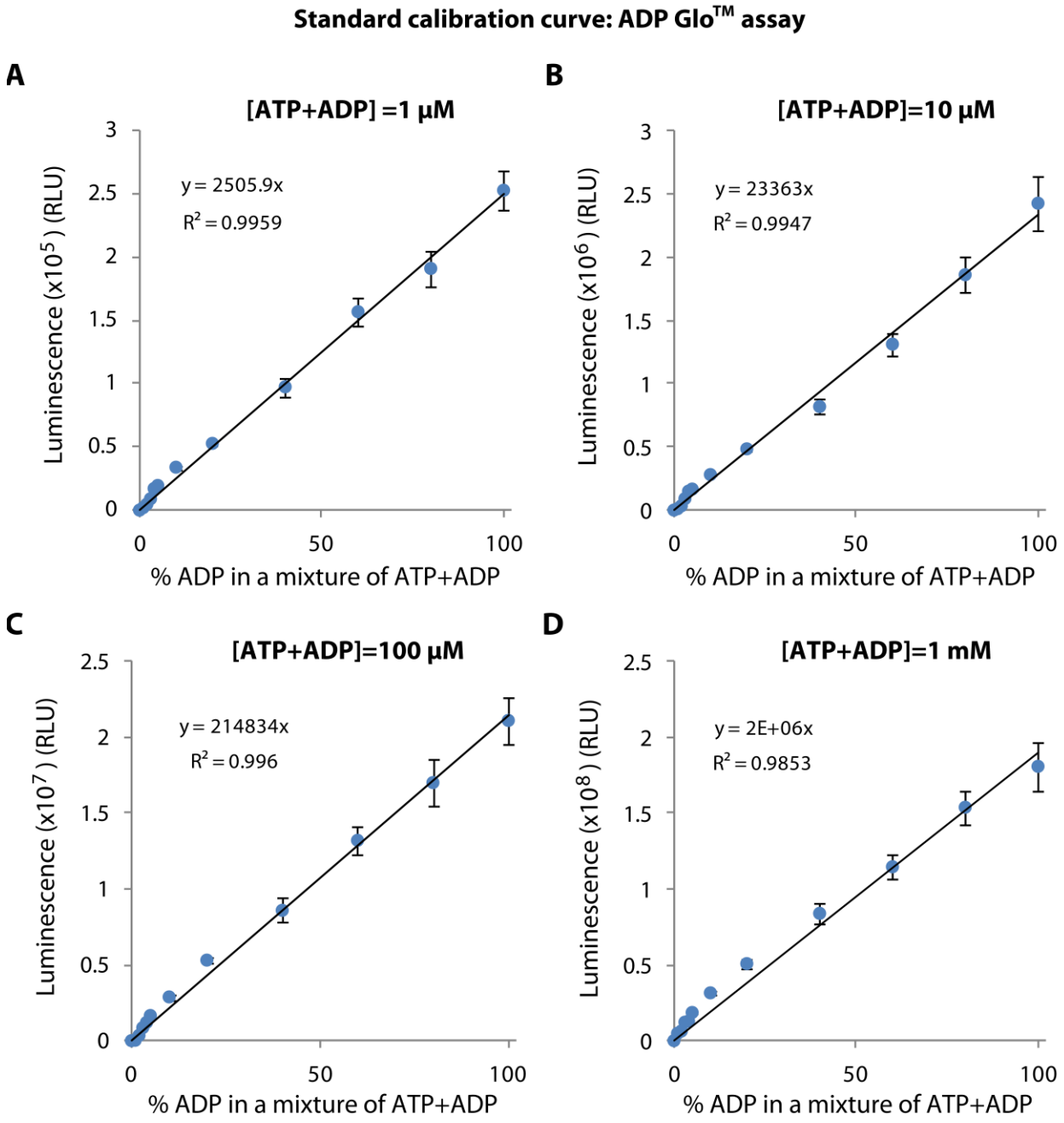

Supplementary Figure 3.11. Standard curves of ADP-Glo™ Kinase assay. (A-D) ATP-to-ADP conversion curves, using ADPGlo™ Kinase assay, at the indicated ATP+ADP concentrations, 1 µM (A), 10 µM (B), 100 µM (C) and 1 mM (D). Plots showlinear fits of luminescent signal and the amount of ADP in the reaction mixtures of ATP+ADP.

CHAPTER 4: Kinesin Kif2C in Regulation of DNA Double Strand Break Dynamics and Repair

Songli Zhu[1], Mohammadjavad Paydar[2], Feifei Wang[1,3], Yanqiu Li[1], Ling Wang[1], Benoit Barrette[2], Tadayoshi Bessho[4], Benjamin H. Kwok[2*] and Aimin Peng[1*]

1. Department of Oral Biology, College of Dentistry, University of Nebraska Medical Center, Lincoln, NE 68583.

2. Institute for Research in Immunology and Cancer (IRIC), Département de médecine, Université de Montréal, P.O. Box 6128, Station Centre-Ville, Montréal, QC H3C 3J7, Canada.

3. Institute of Physical Science and Information Technology, Anhui University, Hefei 230601, People's Republic of China

4. Eppley Institute for Research in Cancer and Allied Diseases, Fred & Pamela Buffett Cancer Center, University of Nebraska Medical Center, Omaha, NE 68198, USA.

* To whom correspondence should be addressed: Aimin Peng, Ph.D. Department of Oral Biology, College of Dentistry, University of Nebraska Medical Center, Lincoln, NE 68583. USA. Tel: 402-472-5903, Fax: 402-472-2551. Email: Aimin.Peng@UNMC.edu; Institute for Research in Immunology and Cancer (IRIC), Département de médecine, Université de Montréal. (514) 343-6111, ext. 0871. Email: benjamin.kwok@umontreal.ca.

4.1 AUTHOR CONTRIBUTION

(**Songli Zhu** and **Mohammadjavad Paydar** contributed **equally** to this work.)

Songli Zhu: Conceptualization, Data curation, Methodology, Writing - original draft

Mohammadjavad Paydar: Data curation, Methodology

Feifei Wang: Data curation, Methodology

Yanqiu Li: Data curation, Methodology

Ling Wang: Data curation, Methodology

Benoit Barrette: Resources, Data curation

Tadayoshi Bessho: Data curation, Methodology

Benjamin H Kwok: Conceptualization, Formal analysis, Funding acquisition, Writing - review and editing, Supervision

Aimin Peng: Conceptualization, Data curation, Formal analysis, Supervision, Writing - original draft, Writing - review and editing

4.2 ABSTRACT

DNA double strand breaks (DSBs) have detrimental effects on cell survival and genomic stability, and are related to cancer and other human diseases. In this study, we identified microtubule kinesin Kif2C as a protein associated with DSB-mimicking DNA templates and established DSB repair proteins in *Xenopus* egg extracts and mammalian cells. The recruitment of Kif2C to DNA damage sites was dependent on both PARP and ATM activities. Kif2C knockdown or knockout led to accumulation of endogenous DNA damage, DNA damage hypersensitivity, and reduced DSB repair via both NHEJ and HR. Interestingly, Kif2C depletion, or inhibition of its microtubule depolymerase activity, reduced the mobility of DSBs, impaired the formation of DNA damage foci, and decreased the occurrence of foci fusion and resolution. Taken together, our study identified Kif2C as a new player of the DNA damage response, and characterized a new mechanism that governs DSB dynamics and repair.

4.3 eLife Digest

DNA can be damaged in many ways, and a double strand break is one of the most dangerous. This occurs when both strands of the double helix snap at the same time, leaving two broken ends. When cells detect this kind of damage, they race to get it fixed as quickly as possible. Fixing these double strand breaks is thought to involve the broken ends being moved to 'repair centers' in the nucleus of the cell, but it was unclear how the broken ends were moved.

One possibility was that the cells transport the broken ends along protein filaments called microtubules. Cells can assemble these track-like filaments on-demand to carry cargo attached to molecular motors called kinesins. However, this type of transport happens outside of the cell's nucleus, and while there are different kinesin proteins localized inside the nucleus, their roles are largely unknown.

In an effort to understand how broken DNA ends are repaired, Zhu, Paydar et al. conducted experiments that simulated double strand breaks and examined the proteins that responded. The first set of experiments involved mixing cut pieces of DNA with extracts taken from frog eggs or human cells. Zhu, Paydar et al. found that one kinesin called Kif2C stuck to the DNA fragments, and attached to many proteins known to play a role in DNA damage repair. Kif2C had previously been shown to help separate the chromosomes during cell division. To find out more about its potential role in DNA repair, Zhu, Paydar et al. then used a laser to create breaks in the DNA of living human cells and tracked Kif2C movement. The kinesin arrived within 60 seconds of the DNA damage and appeared to transport the cut DNA ends to 'repair centers'. Getting rid of Kif2C, or blocking its activity, had dire effects on the cells' abilities to mobilize and repair breaks to its DNA. Without the molecular motor, fewer double strand breaks were repaired, and so DNA damage started to build up.

Defects in double strand break repair happen in many human diseases, including cancer. Many cancer treatments damage the DNA of cancer cells, sometimes in combination with drugs that stop cells from building and using their microtubule transport systems. Understanding the new role of Kif2C in DNA damage repair could therefore help optimize these treatment combinations.

4.4 INTRODUCTION

DNA damage is frequently induced by both endogenous metabolic products and exogenous genotoxic agents. Upon DNA damage, the cell promptly activates the cellular DNA damage response (DDR), a surveillance mechanism that leads to DNA repair, cell cycle arrest (checkpoint), and apoptosis (Li & Zou, 2005; Lou & Chen, 2005; Zhou & Elledge, 2000). Among all types of DNA damage, DNA double strand break (DSB) is of great toxicity and deleterious consequences. It is therefore crucial for cells to efficiently repair DSBs, whereas defects in DSB repair have been linked to cancer, immunodeficiency, neurological diseases, and aging (Jalal et al., 2011; Liang et al., 2009; Sancar et al., 2004).

The cell employs two major evolutionarily-conserved mechanisms, non-homologous end joining (NHEJ) and homologous recombination (HR) to repair DNA DSBs (Goodarzi & Jeggo, 2013; Sancar et al., 2004). HR restores the broken DNA strands using an intact strand as template, and is available in S and G2 phases after replication of chromatin DNA (Jasin & Rothstein, 2013). By comparison, NHEJ directly religates the two broken ends of a DSB, and is accessible throughout the entire interphase (Davis & Chen, 2013; Lieber, 2010). In addition to these core pathways of DSB repair, the spatiotemporal regulation of DSBs has emerged as a new aspect of DNA repair (Amitai et al., 2017; Chuang et al., 2006; Chung et al., 2015; Hauer & Gasser, 2017; Krawczyk et al., 2012; Lemaitre & Soutoglou, 2015; Levi et al., 2005; Lottersberger et al., 2015; Marcomini et al., 2018; Marnef & Legube, 2017; Mine-Hattab & Rothstein, 2013; Neumaier et al., 2012; Schrank et al., 2018). Potentially, the physical mobility of DSBs mediates the subnuclear organization and positioning of DSBs to facilitate DNA repair. However, the precise mechanisms which propel and navigate DSB mobility remain largely obscure.

Microtubules (MTs) are composed of α/β tubulin dimers, and responsible for a variety of cell movements, including the intracellular transport of various vesicles and organelles, and separation of chromosomes in mitosis (Dogterom et al., 2005; Forth & Kapoor, 2017; Maizels & Gerlitz, 2015). For example, cargos, including proteins, nucleic acids and organelles, can be moved along MTs by the action of motor proteins which utilize ATP hydrolysis to produce force and movement (Dogterom et al., 2005; Forth & Kapoor, 2017; Maizels & Gerlitz, 2015). A major group of molecular motors involved in intracellular transport are kinesins named Kif (kinesin superfamily protein). There are several dozen Kifs in mammalian cells to constitute at least 14 kinesin families (Hirokawa et al., 2009; Lawrence et al., 2004). Unlike most kinesins, Kif2C, also known as Mitotic Centromere Associated Kinesin or MCAK, and other members of the kinesin-13 family do not utilize their ATPase activities to transport cargos, but rather to depolymerize MTs by disassembling tubulin subunits at polymer ends (Desai et al., 1999; Hunter et al., 2003; Walczak et al., 2013; Wordeman & Mitchison, 1995). During cell division, Kif2C regulates microtubule dynamics and ensures the proper attachment of MTs to kinetochores, and thereby directing the positioning and movement of chromosomes (Ganem et al., 2005; Kline-Smith et al., 2004; Manning et al., 2007). In this study we identify and characterize Kif2C as a new factor involved in DSB repair; Kif2C is required for efficient DSB repair via both HR and NHEJ; and interestingly, Kif2C facilitates DSB mobility and modulates the formation, fusion, and resolution of DNA damage foci.

4.5 RESULTS

4.5.1 Kif2C associates with DSB-mimicking substrates and DNA repair proteins.

As described in our previous study (Zhu et al., 2017), we utilized DNA DSB-mimicking dA-dT oligonucleotides to isolate potential DNA damage-associated proteins in *Xenopus* egg extract, a cell-free system well-defined for studying DNA damage repair and signaling (Guo et al., 1999; Lupardus et al., 2007). Along with Ku70, PARP1, RPA, and many other factors known to be involved in DSB repair, Kif2C was proteomically identified as a co-precipitated protein of dA-dT. We confirmed, in both *Xenopus* egg extracts and human cell lysates, that Kif2C bound another, and longer, DSB-mimicking template (Figure 4.1A & 1B). We then supplemented in the extract either uncut, circular plasmid DNA, or linearized plasmid DNA with free DSB ends. Interestingly, Kif2C associated specifically with the cut plasmid DNA (Figure 4.1C), further indicating that Kif2C is a DSB-associated protein.

Next, we carried out proteomic analysis to identify proteins that were associated with Kif2C. This effort recovered a number of well-established DNA damage response proteins, including Ku70/Ku80, a DSB end binding complex, H2AX, a histone variant that is phosphorylated in chromatin regions flanking DSBs, and PARP1, an early responder of various DNA lesions (Figure 4.1D). The association of Kif2C with these DNA damage factors was subsequently confirmed using both pull-down and immunoprecipitation (Figure 4.1E, S1A & S1B). Treatment with DNase did not disrupt the protein association (Supplementary Figure 4.1C), suggesting that it was not mediated by DNA. It has been revealed that the catalytic function of Kif2C is mediated through a motor domain located in the middle region of the protein (Ems-McClung et al., 2007; Maney et al., 2001). Interestingly, both this middle region and the N-terminus of Kif2C exhibited appreciable

levels of associations with DNA repair proteins (Supplementary Figure 4.1D & 4.11E), suggesting the involvement of these motifs in DNA repair.

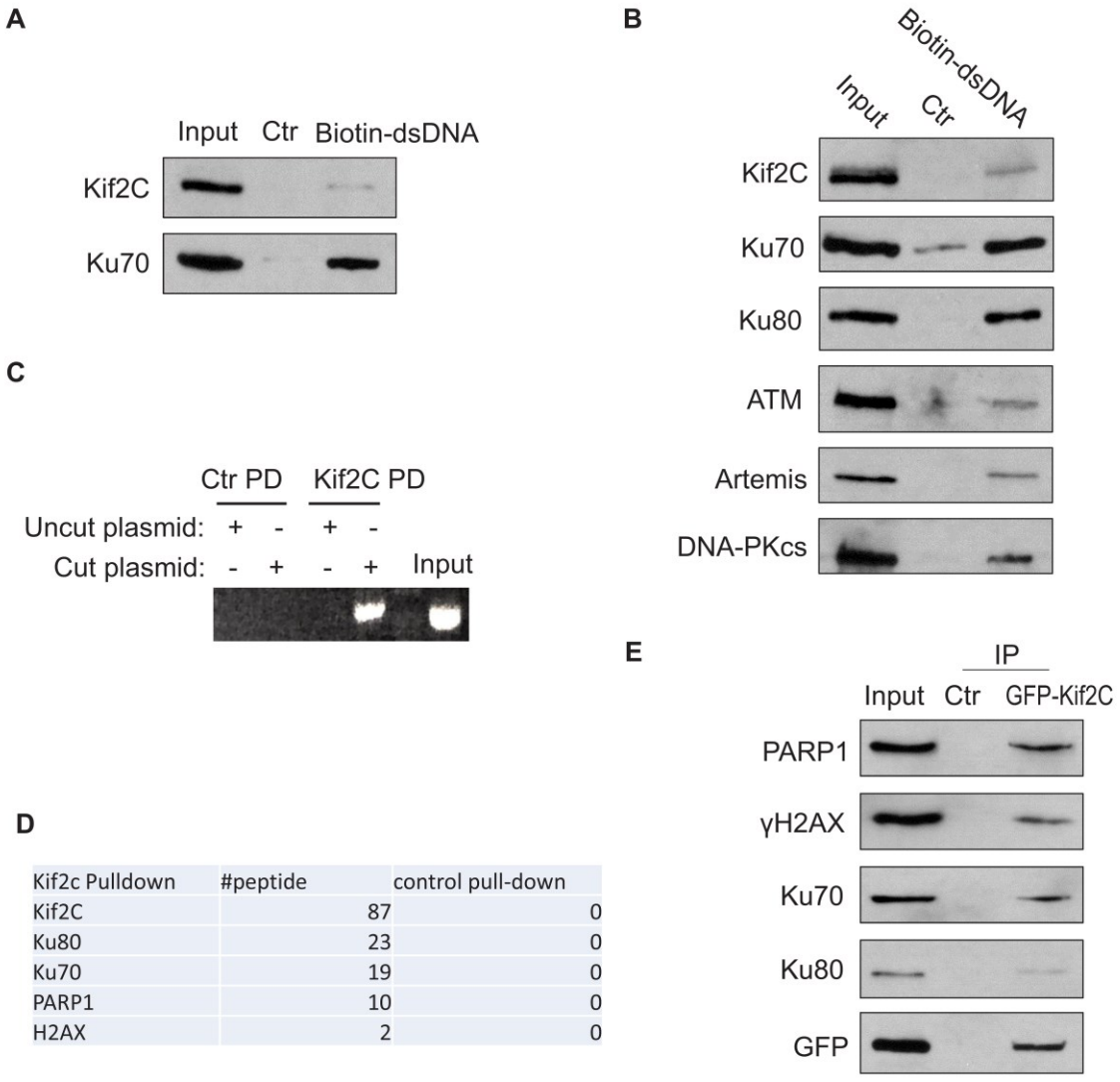

Kif2c Pulldown	#peptide	control pull-down
Kif2C	87	0
Ku80	23	0
Ku70	19	0
PARP1	10	0
H2AX	2	0

Figure 4.1 Kif2C associates with DNA double strands breaks and DNA repair proteins.

(A) Beads conjugated with a biotin-double stranded DNA fragment (dsDNA, 500 bp, as described in Materials and methods—DNA binding assay) were incubated in Xenopus egg extracts for 30 min, re-isolated, and resolved by SDS-PAGE. The input, control pull-down (with blank beads), and biotin-dsDNA pull-down were analyzed by immunoblotting. (B) Beads conjugated with

biotin-dsDNA (as in panel A) were incubated in HeLa cell lysates for 30 min, re-isolated, and resolved by SDS-PAGE. The input, control pull-down (with blank beads), and biotin-dsDNA pull-down were analyzed by immunoblotting. (C) Xenopus Kif2C was expressed with MBP-tag, and purified on amylose beads. As described in Materials and methods—pull-down assay, MBP-Kif2C or control (blank) beads were incubated in Xenopus egg extracts supplemented with cut or uncut plasmid, re-isolated, and analyzed by PCR and agarose gel electrophoresis/ ethidium bromide staining. (D) As described in Materials and methods—pull-down assay, human Kif2C was expressed with MBP-tag and purified on amylose beads. MBP-Kif2C or control (blank) beads were incubated in the lysates of doxorubicin-treated HeLa cells. Pull-down samples were analyzed by mass spectrometry. The identified DNA repair proteins and numbers of peptides are shown. (E) GFP-Kif2C was expressed in HeLa cells with doxorubicin-treatment. Immunoprecipitation (IP) was performed using anti-GFP or control (blank) beads. 10% input, control and GFP IP samples were analyzed by immunoblotting.

4.5.2 Kif2C undergoes two-stage recruitment to DNA damage sites.

The identification of Kif2C as a potential DSB-associated protein was largely unexpected, given that microtubule assembly is viewed as a cytoplasmic event, except in mitosis after nuclear envelop breakdown. On the other hand, Kif2C is primarily localized to the nucleus in interphase, but the function of Kif2C in intra-nuclear events is unknown. We showed in HeLa cells that Kif2C was recruited to DNA damage sites induced by laser microirradiation (Figure 4.2A & movie S1). Kif2C was enriched at laser-irradiated sites within 1 min, indicating it as an early responder to DNA damage (Figure 4.2A & 2B). We confirmed subsequently that Kif2C co-localized with γ-H2AX foci induced by ionized radiation (IR, Figure 4.2C); Kif2C foci co-localized and co-migrated with

53BP1 foci in cells treated with etoposide (Supplementary Figure 4.2 & movie S2). Immunofluorescent analysis of endogenous Kif2C revealed consistent pattern of co-localization with IR-induced γ-H2AX foci (Supplementary Figure 4.3A & S3B).

The fast recruitment of Kif2C to DNA damage sites prompted us to examine its dependence on PARP1-mediated PARylation, which undergoes rapid induction (<1 min) and removal (5-10 min). Interestingly, PARP inhibition disrupted the initial recruitment of Kif2C to laser-induced DNA damage sites; in the presence of a PARP inhibitor (PARPi), Kif2C slowly accumulated at DNA damage sites at about 10 min (Figure 4.2D & 2E). By contrast, the sustained, but not the initial, recruitment of Kif2C was dependent on ATM (Figure 4.2D & 2E).

To reveal additional molecular insights into the DNA damage recruitment of Kif2C, we generated multiple truncated segments of Kif2C, and examined their localization in laser-irradiated cells. Interestingly, the N-terminus of Kif2C exhibits efficient recruitment to DNA damage sites; the middle region of Kif2C containing the catalytic motif was very weakly enriched at DNA damage sites; and the C-terminus of Kif2C did not accumulate at DNA damage sites (Figure 4.2F & 2G). Consistent with the strong recruitment of Kif2C N-terminus to DNA damage sites, A Kif2C mutant deleted of the N-terminus was deficient in the DNA damage recruitment (Supplementary Figure 4.3C & S3D). To identify minimal elements within the N-terminus that mediate DNA damage recruitment, we generated a series of truncation mutants within the N-terminus (Figure 4.2H). Interestingly, the efficient recruitment of Kif2C N-terminus depended on both a short 5 amino acid (aa 86-90) and the neck domain (Figure 4.2H). The neck domain of Kif2C was shown to play a role in microtubule depolymerization (Maney et al., 2001), hence, our study indicates an additional function of this domain in the DNA damage recruitment of Kif2C. By comparison, the aa 86-90 region lies outside of the minimal functional domain of Kif2C's microtubule-

depolymerizing activity and is not associated with any known mitotic functions of Kif2C. Interestingly, both of these motifs are important for Kif2C recruitment to DNA damage sites as full-length Kif2C deleted of either one exhibited reduced recruitment to the sites of laser cut (Figure 4.2I). Consistent with the recruitment deficiency, these mutants also exhibited reduced association with DNA repair proteins (Supplementary Figure 4.4).

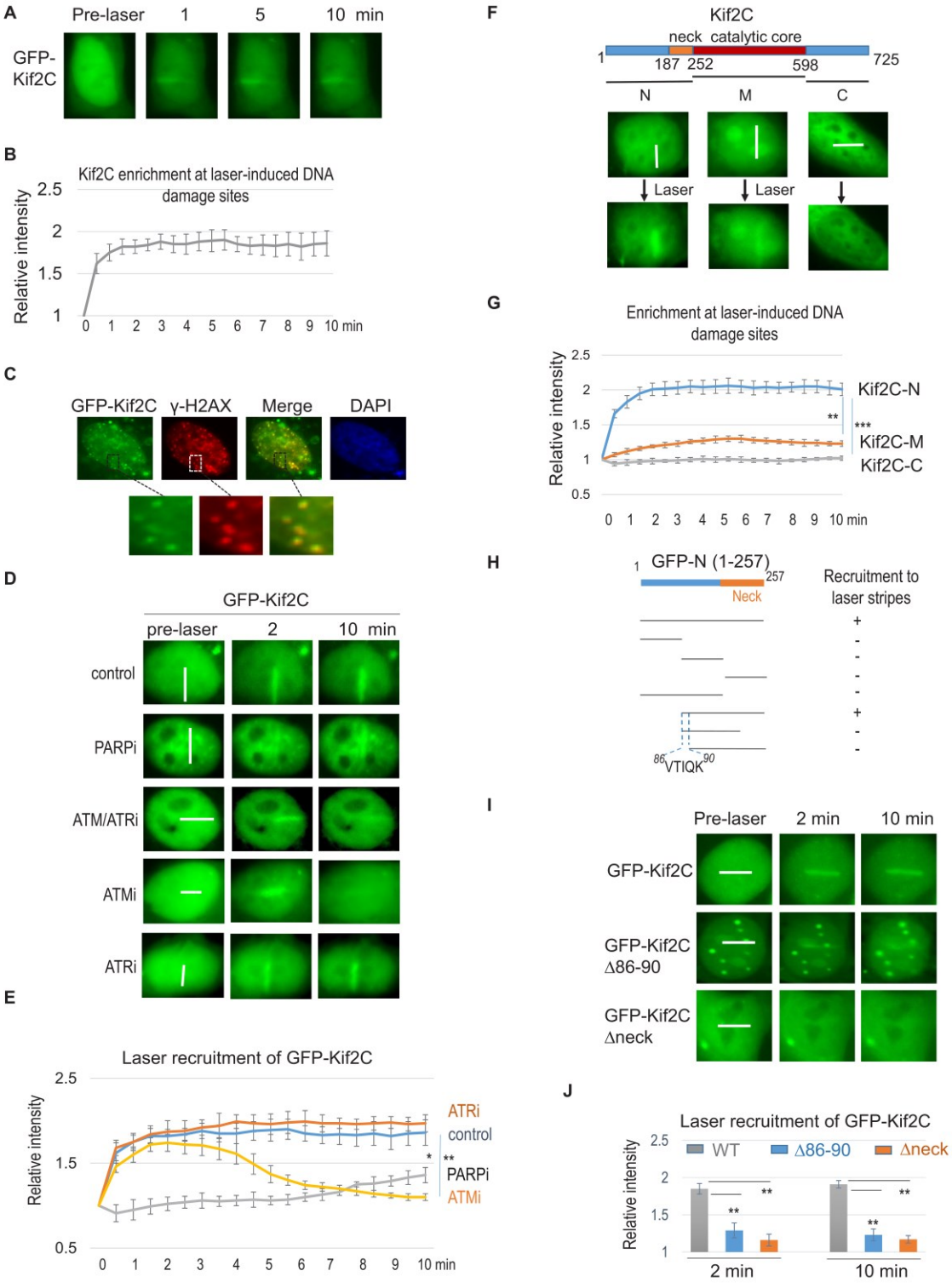

Figure 4.2 Kif2C is recruited to DNA damage sites in a two-stage manner.

(A) HeLa cells expressing GFP-Kif2C were subjected to laser micro-irradiation as described in Materials and methods—immunofluorescence and imaging. The fluorescent signal of GFP is shown at the indicated time points. (B) The intensity of the GFP signal at laser-cut sites was normalized to that outside of the laser-cut sites for the relative enrichment of GFP-Kif2C. The mean values and standard deviations are shown (quantification shown in 5 cells, consistent pattern observed in >10 cells and >3 independent experiments). (C) HeLa cells expressing GFP-Kif2C were treated with 10 Gy IR, the fluorescent signal of GFP and immunofluorescent signal of γ-H2AX are shown. Pre-extraction was performed by placing the dish on ice for 5 min with 0.1% Triton X-100 in 10 mM HEPES (pH 7.4), 2 mM MgCl2, 100 mM KCl, and 1 mM EDTA. (D) GFP-Kif2C was expressed in HeLa cells. Prior to laser-micro-irradiation, these cells were pre-treated with PARPi (olaparib, 10 μM), ATM/ATRi (caffeine, 2 μM), ATMi (Ku55933, 5 μM), or ATRi (Ve-821, 10 μM), as indicated. The localization of GFP-Kif2C at the indicated time points is shown. The white lines mark the regions of laser micro-irradiation. Consistent results were observed in >10 cells for each treatment. (E) The DNA damage recruitment of Kif2C was examined as in panel D. The intensity of the GFP signal at laser-cut sites was normalized to that outside of the laser-cut sites for the relative enrichment of GFP-Kif2C. The mean values and standard deviations are shown (N = 5). ATM/ATRi showed similar kinetics as ATMi. P values were determined by two-tailed Student's t-test (*<0.05, **<0.01, ***<0.001). (F) The N-terminus, middle segment (M), and C-terminus of MCAK was expressed with a GFP tag to examine their localization in laser-treated HeLa cells. The white lines mark the regions of laser micro-irradiation. Consistent results were observed in >10 cells for each segment. (G) The DNA damage recruitment of Kif2C-N, M, and C was examined as in panel F. The intensity of the GFP signal at laser-cut sites was normalized to that outside of the laser-cut sites for the relative enrichment. The mean

values and standard deviations are shown (N = 5). (H) A series of truncation mutants were generated from the N-terminus of Kif2C. These mutants, tagged with GFP, were analyzed for recruitment to laser-stripes 10 min after the treatment. The result of positive or negative recruitment was determined by consistent results in >10 cells. (I) GFP-Kif2C deleted of aa 86–90 or neck-motif was expressed in HeLa cells which were micro-irradiated by laser (as marked by white lines). Both the aa 86–90 and neck-motif of Kif2C are required for the efficient recruitment of Kif2C to laser stripes. The white line marks the path of laser. (J) The recruitment to laser stripes, as in panel I, was quantified for Kif2C (WT, or deleted of the aa 86–90 or neck-motif). The intensity of the GFP signal at laser-cut sites was normalized to that outside of the laser-cut sites for the relative enrichment. The mean values and standard deviations are shown (N = 5, **$p<0.01$).

4.5.3 Kif2C depletion or inhibition leads to accumulation of endogenous DNA damage.

As we revealed the recruitment of Kif2C to DNA damage, and the association of Kif2C with DSB templates and repair factors, we set out to investigate the function of Kif2C in the DDR. Interestingly, Kif2C knockdown in HeLa cells led to γ-H2AX induction (Figure 4.3A). The induction of γ-H2AX was also detected in U2OS cells deleted of Kif2C using CRISPR-Cas9-mediated gene editing (Figure 4.3B). Moreover, cells depleted of Kif2C exhibited increased foci formation of γ-H2AX and 53BP1 (Supplementary Figure 4.5). These lines of evidence suggested that Kif2C plays a role in DNA repair, and its removal caused accumulation of endogenous DNA damage. Consistent with this hypothesis, accumulation of DNA breaks in Kif2C knockout cells was shown using a single cell electrophoresis (comet) assay (Figure 4.3C). As expected, the re-expression of RNAi-resistant Kif2C rescued γ-H2AX induction (Figure 4.3D). By comparison, a G495A Kif2C mutant defective in ATP hydrolysis and microtubule depolymerization, as

characterized previously (W. Wang et al., 2012), was ineffective in suppressing endogenous DNA damage caused by Kif2C knockdown (Figure 4.3D & S5), indicating that the ATPase activity of Kif2C is required for its function in DNA repair. Previously reported structural insights into the enzymatic action of Kif2C revealed that tubulin-binding, in addition to ATPase, is required for microtubule depolymerization. For example, a β5 motif within the motor domain of Kif2C recognizes the distal end of β-tubulin, and R420S, a specific mutation in this motif disrupted tubulin-binding and microtubule depolymerization (Ritter et al., 2015; Wang et al., 2017). Like G495A, R420S mutant failed to rescue the accumulation of γ-H2AX in Kif2C knockout cells (Figure 4.3E), despite that these mutants were expressed at similar levels as WT (Figure 4.3D & 3E), and exhibited nuclear localization and DNA damage recruitment (Supplementary Figure 4.6A). Kif2C depletion or mutation did not cause significant disruption of cell cycle progression (Supplementary Figure 4.6B). Interestingly, Kif2C depletion did not additively enhance the induction of γ-H2AX in cells pre-treated with nocodazole, an inhibitor of microtubule assembly, suggesting that Kif2C functions in DNA repair in the context of microtubule assembly (Supplementary Figure 4.7A). Moreover, the Δ86-90 Kif2C mutant deficient in DNA damage recruitment was incapable of suppressing endogenous DNA damage in Kif2C KO cells (Figure 4.3F), indicating that the DNA damage recruitment of Kif2C is required for the prevention of DSB accumulation. Together, these findings indicate that both the DNA damage recruitment of Kif2C and its catalytic activity are involved in the DDR.

The Kwok laboratory previously identified DHTP (((Z)-2-(4-((5-(4-chlorophenyl)-6-(isopropoxycarbonyl)-7-methyl-3-oxo-3,5-dihydro-2H-thiazolo[3,2-a]pyrimidin-2-ylidene)methyl)phenoxy)acetic acid)) as an allosteric inhibitor of Kif2C (Talje et al., 2014). Interestingly, DHTP treatment in HeLa cells phenocopied Kif2C depletion and caused γ-H2AX

accumulation (Figure 4.3G). Although Kif2C also plays a role in mitosis (Manning et al., 2007), DHTP induced γ-H2AX accumulation efficiently in thymidine-arrested interphase cells (Figure 4.3H), indicating that mitotic defects are not the primary cause of DNA damage.

In line with the involvement of Kif2C in the DDR, Kif2C depletion significantly enhanced the response of HeLa cells to DNA damage treatment, as judged by both reduced cell viability and increased cell death (Figure 4.3I & 3J). A similar effect was confirmed also in SCC38 cells (Supplementary Figure 4.7B & S7C), or in HeLa cells with DHTP treatment (Supplementary Figure 4.7D). WT, but not Δ86-90, Kif2C rescued etoposide sensitivity in Kif2C knockout cells (Figure 4.3K), confirming the direct involvement of Kif2C in the DDR.

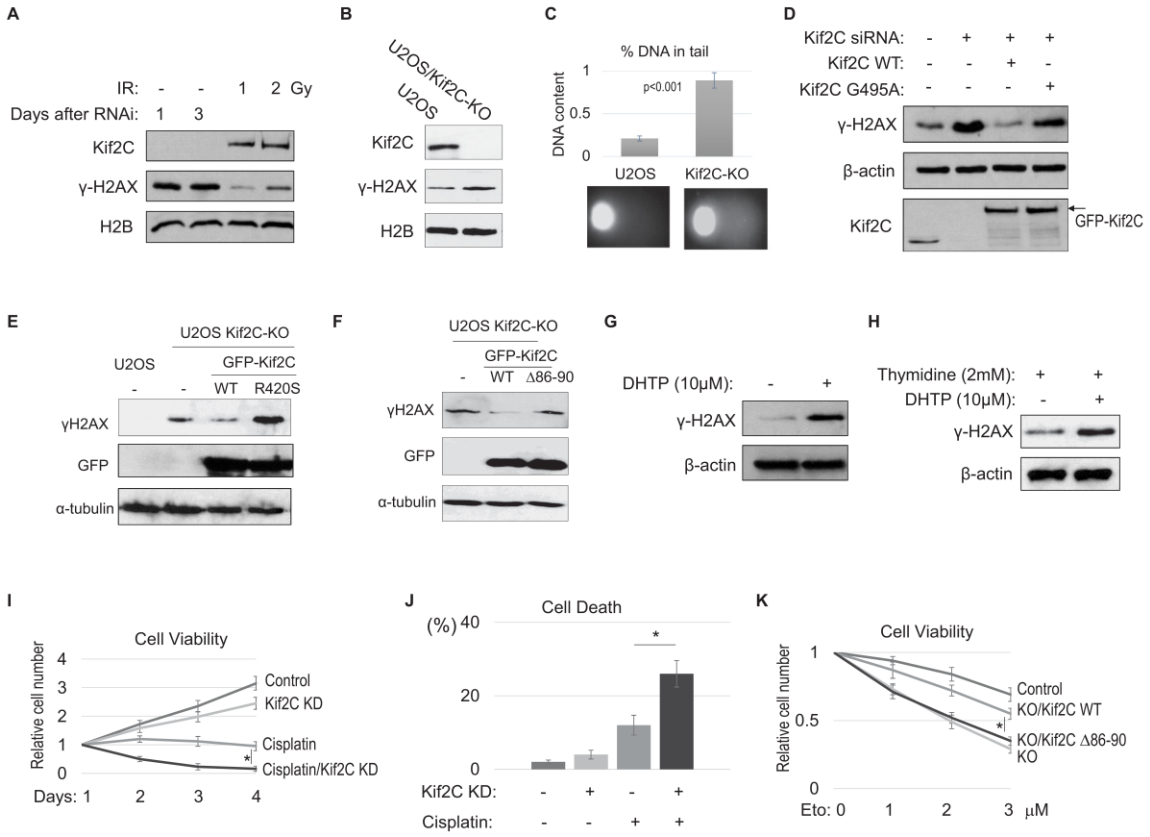

Figure 4.3 Kif2C suppression leads to accumulation of endogenous DNA damage and DNA damage hypersensitivity.

(A) HeLa cells were treated with Kif2C siRNA for 1 and 3 days, or with IR at 1 or 2 Gy (followed by 30 min incubation), as indicated. These cells were then harvested and analyzed by immunoblotting. (B) Kif2C gene deletion was carried out using the CRISPR-Cas9 technique in U2OS cells. Cell lysates were collected and analyzed by immunoblotting. (C) The comet assay was performed in control or Kif2C knockout (KO) U2OS cells, as described in Materials and methods. The percentage of DNA in the tail section was quantified, the mean values and standard derivations are shown (N > 20). Representative images are shown below. (D) HeLa cells were treated with control siRNA or Kif2C siRNA and reconstituted with siRNA resistant GFP-Kif2C (WT or G495A), as indicated. Cell lysates were harvested and analyzed by immunoblotting. (E) Control or Kif2C knockout (KO) U2OS cells were transfected with WT or R420S Kif2C tagged with GFP, as indicated. One day after transfection, the samples were analyzed by immunoblotting. (F) U2OS Kif2C knockout (KO) cells were transfected with WT or D86–90 Kif2C tagged with GFP, as indicated. One day after transfection, the samples were analyzed by immunoblotting. (G) Asynchronized HeLa cells were treated with 20 μM DHTP for 3 hr, as indicated. The cell lysates were analyzed by immunoblotting. (H) HeLa cells were first synchronized at G1/S by thymidine-arrest, and then treated with 10 μM DHTP for 3 hr. The cell lysates were analyzed by immunoblotting. (I) HeLa cells were incubated in cisplatin (6.7 μM) and Kif2C siRNA, as indicated. The relative cell viability was determined by normalizing the cell number to that of the first day. The mean values and standard deviations, calculated from three independent experiments, are shown. *$p<0.05$. (J) HeLa cells were treated as in panel I for 2 days and measured by the trypan blue exclusion assay for cell death. The mean values and standard deviations, calculated from three independent experiments, are shown. (K) WT or D86–90 Kif2C was expressed in Kif2C KO cells as in panel F. 1 day after transfection, these cells, along with control

U2OS, were treated with various doses of etoposide for 2 days. The relative cell viability was determined by first calculating the ratio of cell number in day 3 to that in day 1, and then normalizing the ratio of etoposide treated cells to that of the untreated. The mean values and standard deviations, calculated from three independent experiments, are shown.

4.5.4 Kif2C is required for efficient DSB repair via both HR and NHEJ.

To assess further the impact of Kif2C on DNA repair, the kinetics of □-H2AX post-IR treatment was probed in control and Kif2C depleted cells. Compared to the control HeLa cells, those treated with Kif2C siRNA exhibited more sustained γ-H2AX (Figure 4.4A-4C). A similar effect was observed when comparing Kif2C knockout U2OS cells to control U2OS cells (Figure 4.4D-4F). The DNA repair deficiency caused by Kif2C depletion was also confirmed using single cell electrophoresis (Supplementary Figure 4.8). Next, we sought to evaluate the impact of Kif2C on specific DSB repair pathways. The repair activity of NHEJ and HR was measured using an intrachromosomal, I-SceI-induced NHEJ assay and an intrachromosomal I-SceI-induced HR reporter system, respectively (Gunn & Stark, 2012) (Figure 4.4G & 4H). Interestingly, Kif2C depletion reduced both NHEJ and HR by 3-5 fold (Figure 4.4G & 4H).

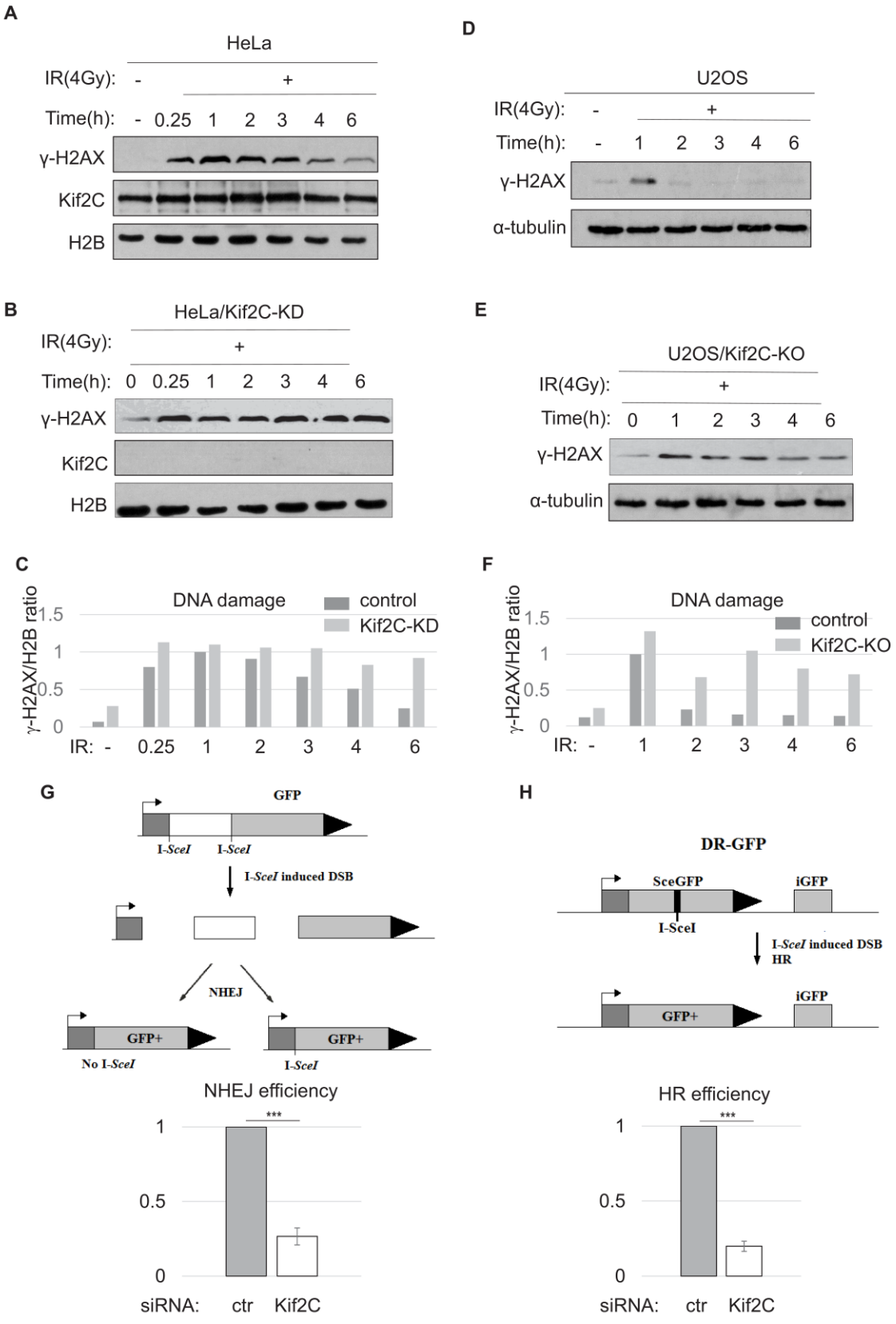
A
HeLa
IR(4Gy): - +
Time(h): - 0.25 1 2 3 4 6
γ-H2AX
Kif2C
H2B
B
HeLa/Kif2C-KD
IR(4Gy): +
Time(h): 0 0.25 1 2 3 4 6
γ-H2AX
Kif2C
H2B
C
DNA damage
control
Kif2C-KD
γ-H2AX/H2B ratio
1.5
1
0.5
0
IR: - 0.25 1 2 3 4 6
D
U2OS
IR(4Gy): - +
Time(h): - 1 2 3 4 6
γ-H2AX
α-tubulin
E
U2OS/Kif2C-KO
IR(4Gy): +
Time(h): 0 1 2 3 4 6
γ-H2AX
α-tubulin
F
DNA damage
control
Kif2C-KO
γ-H2AX/H2B ratio
1.5
1
0.5
0
IR: - 1 2 3 4 6
G
GFP
I-SceI
I-SceI
I-SceI induced DSB
NHEJ
GFP+
No I-SceI
GFP+
I-SceI
NHEJ efficiency
***
1
0.5
0
siRNA: ctr Kif2C
H
DR-GFP
SceGFP
iGFP
I-SceI
I-SceI induced DSB
HR
iGFP
GFP+
HR efficiency
***
1
0.5
0
siRNA: ctr Kif2C

Figure 4.4 Kif2C is required for DNA double strand break repair.

(A, B, C) HeLa cells treated with control (A) or Kif2C siRNA (B) were irradiated with 4 Gy IR and incubated as indicated. The cell lysates were analyzed by immunoblotting. Quantification is shown in panel C. (D, E, F) U2OS cells, control (D) or Kif2C knockout (KO, (E), were irradiated with 4 Gy IR, and incubated as indicated. The cell lysates were analyzed by immunoblotting. Quantification is shown in panel F (as relative to 1 hr time point in control HeLa cells). (G, H) Chromosome-integrated, I-SceI-induced NHEJ (G) or HR (H) reporter systems are illustrated in the upper panels. These reporter cells were transfected with control or Kif2C siRNA. DNA repair was measured by immunoblotting of GFP expression in relative to b-actin expression. The GFP/b-actin ratio in Kif2C-depleted cells was normalized to that in control cells for relative repair efficiency. The mean values and standard deviations, calculated from three independent experiments, are shown. Statistical significance was analyzed using an unpaired 2-tailed Student's t-test (***$p<0.001$). Kif2C depletion did not impact the expression of I-SceI (Supplementary Figure 4.9).

4.5.5 Kif2C mediates the movement of DSBs, and the formation, fusion, and resolution of DNA damage foci.

It is very intriguing how Kif2C promotes DSB repair, given that Kif2C is unlikely to function as a core factor for both NHEJ and HR. We speculated that Kif2C might function in regulation of DSB movement and dynamics in light of several existing findings. First, emerging evidence in both yeast and mammalian cells indicated increased chromatin mobility at sites of DNA DSBs (Chuang et al., 2006; Krawczyk et al., 2012; Lemaitre & Soutoglou, 2015; Levi et al., 2005; Lottersberger et al., 2015; Marnef & Legube, 2017), but the underlying mechanism is largely

unclear. Second, MTs are well known to support intracellular trafficking of proteins, chromosomes, and other materials, and kinesins are known to produce mechanical work from ATP hydrolysis (Dogterom et al., 2005; Forth & Kapoor, 2017; Maizels & Gerlitz, 2015). Recent studies showed that microtubule dynamics enhanced the motion of chromatin, especially telomeres, in response to DNA damage (Lawrimore et al., 2017; Lottersberger et al., 2015). Third, we showed that the microtubule depolymerase activity of Kif2C, mediated by ATP hydrolysis and tubulin-binding, is required for the prevention of γ-H2AX accumulation. To investigate this potential role of Kif2C, we quantified the mobility of etoposide-induced DSBs, as marked by GFP-53BP1 foci. The 3D trajectories of unbiasedly selected foci were tracked to determine the distance traveled by these foci (Figure 4.5A). We observed that Kif2C depletion, or inhibition of its microtubule depolymerase activity by DHTP, impaired the mobility of DSBs (Figure 4.5B-5D). This effect of Kif2C suppression was comparable to that of Taxol treatment which inhibits microtubule dynamics and was previously shown to retard DSB movement (Figure 4.5C & 5D) (Lottersberger et al., 2015). To clarify if Kif2C specifically regulates the mobility of damaged chromatin, we analyzed the movement of Centromere Protein B (CENP-B) and Pre-MRNA Processing Factor 6 (PRPF6), as controls. ((for undamaged, and general chromatin dynamics) for general intranuclear dynamics). Both CENPB and PRPF6 form distinct punctate foci in the nucleus that are not DNA damage-related, and these motilities can indicate undamaged, general chromatin dynamics, and general intra-nuclear dynamics, respectively. Intra-nuclear CENP-B and PRPF6 foci are relatively less dynamics than 53BP1 foci, and there was no significant difference between WT and Kif2C KO or DHTP treatment (Supplementary Figure 4.10A & S10B). On the other hand, Taxol treatment reduced foci dynamics of CENP-B and PRPF6 (Supplementary Figure 4.11). These data

demonstrated that Kif2C mediates DNA damage mobility without affecting other cellular dynamics in general.

Formation of DNA damage foci is a signature feature of the DDR, but the precise mechanism of this process is still unknown (Huen & Chen, 2010). Previous studies analyzing these foci as potential repair centers suggested the clustering of multiple DSB ends and the subsequent formation of macro-domains (Asaithamby & Chen, 2011; Aten et al., 2004; Aymard et al., 2017; Neumaier et al., 2012; Roukos et al., 2013). In yeast cells, persistent DSBs roam within the nucleus to form these repair centers (Lisby et al., 2003; Marnef & Legube, 2017). Mammalian DSBs were shown to travel for a similar distance (1-2 μM) as yeast DSBs. However, due to a much larger volume of the mammalian nucleus, mammalian DSBs do not roam within the nucleus, but join each other in close proximity (Marnef & Legube, 2017; Neumaier et al., 2012; Roukos et al., 2013). We analyzed the dynamics of DNA damage foci using high-resolution, live-cell imaging (Figure 4.5E). Interestingly, Kif2C depletion or pre-treatment with DHTP or Taxol reduced the formation of DNA damage foci (Figure 4.5F), despite that the level of DNA damage is rather elevated under Kif2C suppression (Supplementary Figure 4.9C). To further assess the impact of Kif2C on the dynamics of DNA damage foci, we first allowed the establishment of DNA damage foci (Figure 4.5G), and then challenged cells with DHTP or Taxol. Interestingly, we observed that the occurrence of foci fusion events was decreased by Kif2C depletion or inhibition (Figure 4.5H, movie S3); furthermore, foci resolution (disappearance) was also markedly influenced by these treatments (Figure 4.5I, 5J & movie S4). Presumably, foci fusion represents the movement of DSBs to form larger repair centers/foci, and foci disappearance reflects DNA repair or reassembly of foci. Together, we showed that Kif2C mediates the formation and dynamics of DNA damage foci.

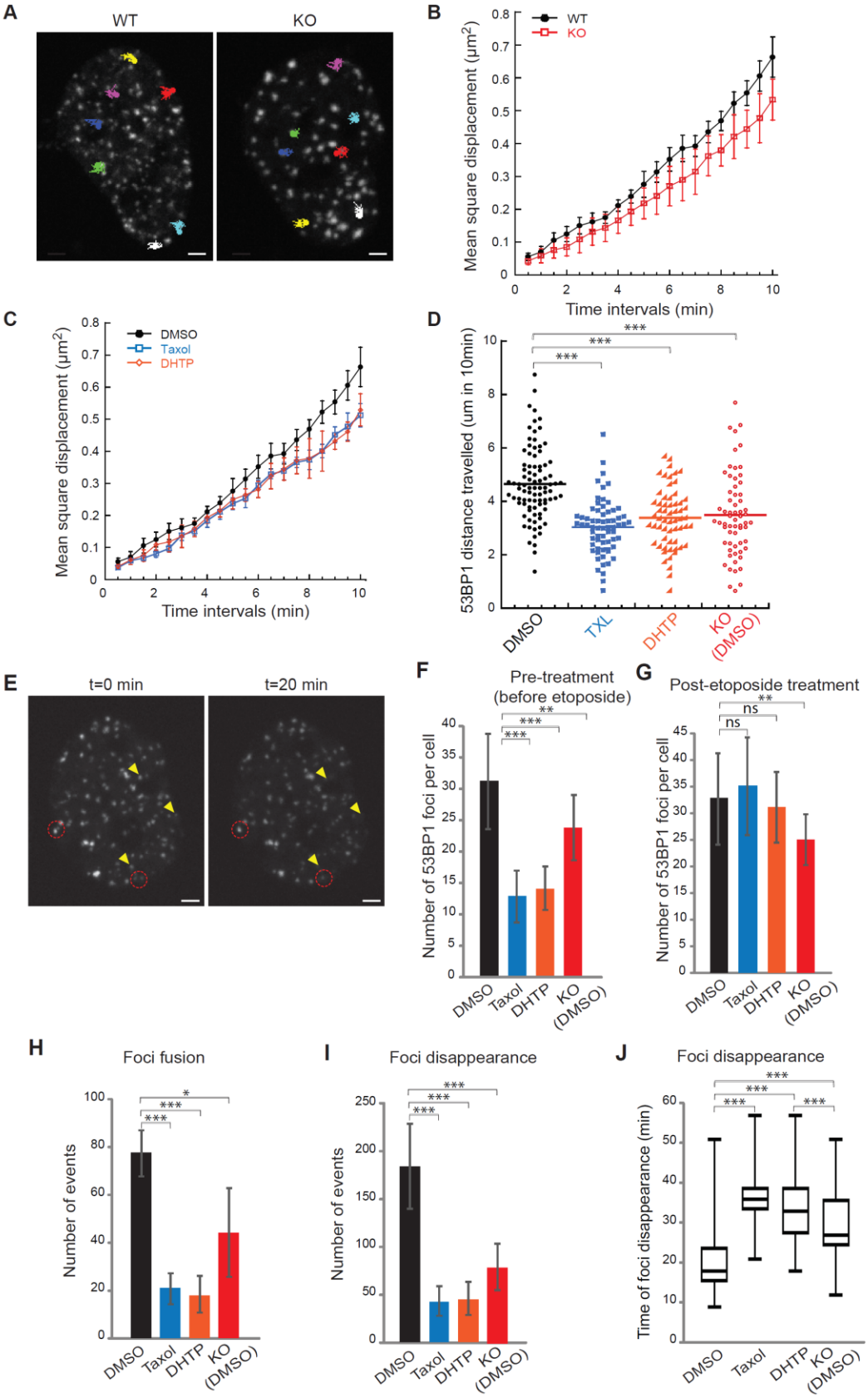
A
WT
KO
B
WT
KO
Mean square displacement (μm²)
Time intervals (min)
C
DMSO
Taxol
DHTP
Mean square displacement (μm²)
Time intervals (min)
D
53BP1 distance travelled (um in 10min)
***
***
***
DMSO
TXL
DHTP
KO (DMSO)
E
t=0 min
t=20 min
F
Pre-treatment (before etoposide)
Number of 53BP1 foci per cell
**
***
***
DMSO
Taxol
DHTP
KO (DMSO)
G
Post-etoposide treatment
Number of 53BP1 foci per cell
**
ns
ns
DMSO
Taxol
DHTP
KO (DMSO)
H
Foci fusion
Number of events
*
***
***
DMSO
Taxol
DHTP
KO (DMSO)
I
Foci disappearance
Number of events
***
***
***
DMSO
Taxol
DHTP
KO (DMSO)
J
Foci disappearance
Time of foci disappearance (min)
***
***
***
***
DMSO
Taxol
DHTP
KO (DMSO)

Figure 4.5 Kif2C mediates DNA double strand break mobility and foci dynamics.

(A) Examples of 10 min mobility traces of EGFP-53BP1 foci in WT and Kif2c knockout (KO) U2OS cells after etoposide (20 μM) treatment. Kif2C depletion did not impact 53BP1 expression (Supplementary Figure 4.10A). (B) Mean-square displacement measurements of EGFP-53BP1 foci in WT and Kif2C KO U2OS cells, shown in black in red, respectively. (C) Mean-square displacement measurements of EGFP-53BP1 foci in WT U2OS cells treated with the vehicle control (DMSO), Taxol (5 μM), or DHTP (20 μM), as indicated. (D) Quantification of the distance travelled by EGFP-53BP1 foci over 10 min in the corresponding cells described in B-C. (E) Examples of disappearance (yellow arrowheads) and fusion (red circle) events of EGFP-53BP1 foci induced by etoposide in U2OS cells. (F, G) Number of EGFP-53BP1 foci in WT or Kif2C KO U2OS cells, treated with the vehicle control (DMSO), Taxol, or DHTP. These inhibitors were added either 5 min before (F) or 5 min after (G) etoposide treatment. (H–J) Numbers of fusion (H) and disappearance (I–J) events of EGFP-53BP1 foci in the corresponding cells in panel G are shown. A total of 15 randomly selected cells were analyzed over three independent experimental runs. For disappearance events, number of occurrence in the first 30 min under each treatment condition is shown in (I) and the time required for foci disappearance (min) over the entire hour of recording is shown in (J) (>150 events quantified per condition). The box represents 50% of the foci disappearance events and the line shows the median of the data set. All microscopy image acquisitions began five minutes after final compound treatment, either every 30 s for 10 min (A–D) or every 3 min for one hour (H–J). All data were collected from at least three independent experimental sets. Error bars, S.D.; ns: p>0.05; *p_0.05; **p_0.01; ***p_0.001, by Student's t-test.

4.5.6 PARP1 and ATM regulate DSB dynamics largely via Kif2C.

As we showed that both PARP1 and ATM act upstream to mediate the recruitment of Kif2C to DNA damage sites, we speculated that PARP1 and ATM play a role in regulation of DSB movement and DNA damage foci formation. Indeed, inhibition of PARP and ATM both significantly reduced the mobility of GFP-53BP1 foci (Figure 4.6A & 6C). Interestingly, PARP or ATM inhibition only moderately retarded GFP-53BP1 foci movement in Kif2C depleted cells (Figure 4.6C), indicating that PARP and ATM govern DSB mobility largely, although not exclusively, through Kif2C. On the other hand, Kif2C depletion did not further suppress the mobility of GFP-53BP1 in cells with PARP or ATM inhibition (Supplementary Figure 4.12), suggesting that the function of Kif2C in this process is dependent on both PARP1 and ATM, which act upstream to mediate the DNA damage recruitment of Kif2C.

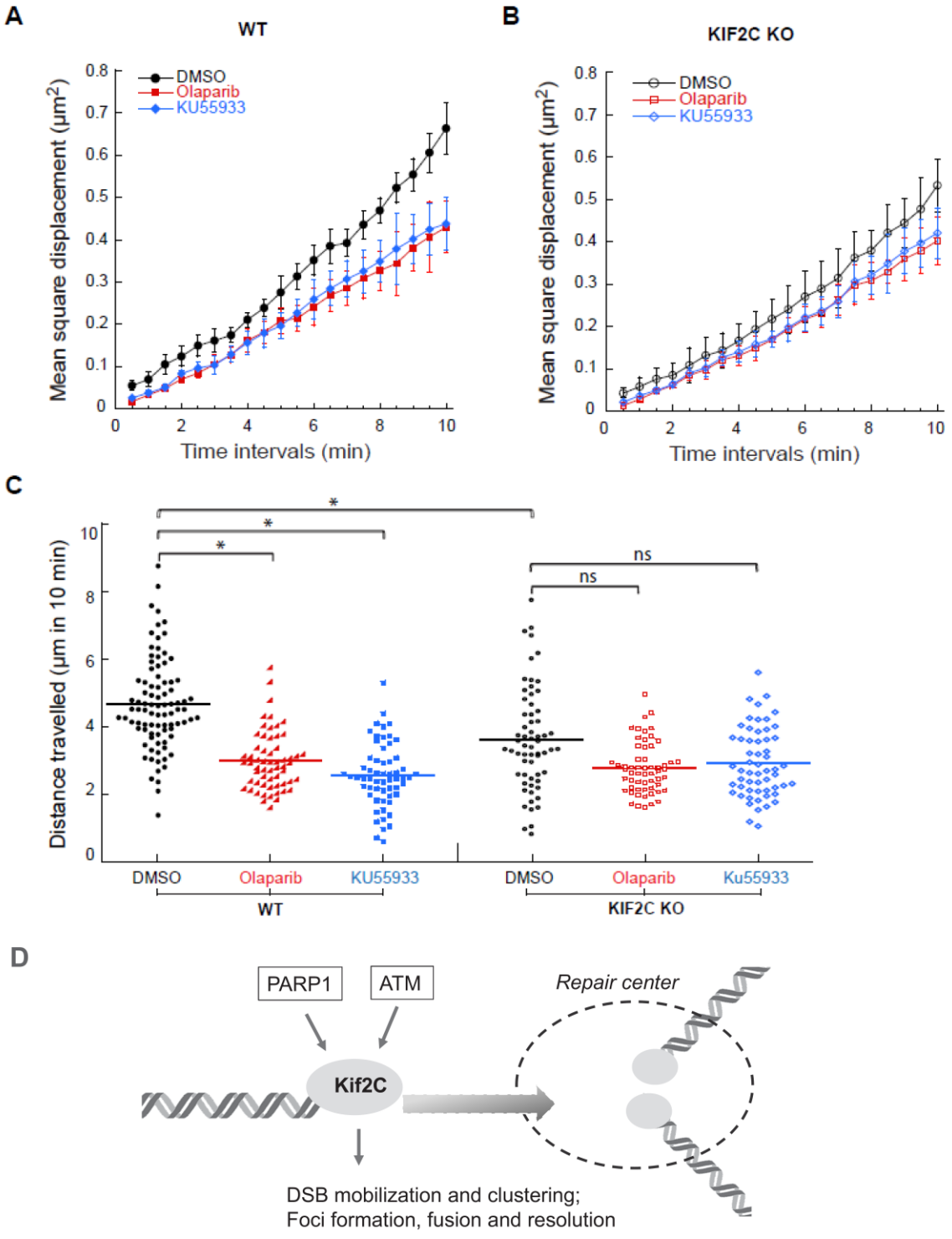
A
WT
DMSO
Olaparib
KU55933
Mean square displacement (μm²)
Time intervals (min)
B
KIF2C KO
DMSO
Olaparib
KU55933
Mean square displacement (μm²)
Time intervals (min)
C
Distance travelled (μm in 10 min)
*
*
*
ns
ns
DMSO
Olaparib
KU55933
DMSO
Olaparib
Ku55933
WT
KIF2C KO
D
PARP1
ATM
Repair center
Kif2C
DSB mobilization and clustering;
Foci formation, fusion and resolution

Figure 4.6 ATM and PARP inhibition impairs Kif2C-dependent foci mobility.

(A–B) Mean-square displacement measurements of EGFP-53BP1 foci in WT (A) and Kif2C KO (B) U2OS cells treated with the vehicle control (DMSO), the PARP1 inhibitor Olaparib (10 μM), or the ATM inhibitor KU55933 (20 μM), as indicated. More than 50 foci were analyzed in three independent experiments. (C) Quantification of the distance travelled by EGFP-53BP1 foci over 10 min in the corresponding cells described in A-B. Experimental set up and image acquisition were the same as described in Figure 4.5. (D) Kif2C mediates DSB end mobilization and the formation of DNA damage foci (model). Kif2C is recruited to DSB ends in a manner that depends on both ATM and PARP activities. Mediated by its microtubule depolymerase activity, Kif2C promotes the movement, and the subsequent clustering, of DSB ends. Therefore, Kif2C is an important downstream factor of the PARP and ATM-mediated DNA damage response that governs the mobility and dynamics of DSB ends.

4.6 DISCUSSION

4.6.1 Kif2C is a new player of the DNA damage response.

As a member of the microtubule depolymerase family, Kif2C was shown to govern several aspects of cell division in mitosis, including spindle assembly, chromosome congression, and kinetochore-microtubule attachment (Manning et al., 2007; Sanhaji et al., 2011). The role of Kif2C in interphase cells is less characterized, despite that its dominant localization in the nucleus suggests possible functions of Kif2C in intranuclear processes. Interestingly, we reported here a direct involvement of Kif2C in DNA repair, as a previously undefined interphase function of Kif2C. First, we showed that Kif2C associated with DSB-mimicking structures in *Xenopus* egg extracts and human cell lysates. Consistently, Kif2C bound several established DNA repair factors, including PARP1, H2AX, and Ku70/80. Second, Kif2C was recruited to DNA damage sites in interphase cells via two distinct mechanisms. The initial recruitment of Kif2C occurred within seconds in a PAR-dependent manner, whereas the sustained localization of Kif2C at DNA damage sites was disrupted by ATM inhibition. Thus, we characterized Kif2C as a downstream factor of the PARP1 and ATM-mediated DNA damage responses. Third, Kif2C was required for efficient DNA DSB repair via both NHEJ and HR; consequently, depletion or inhibition of Kif2C leads to both accumulation of endogenous DSB and DNA damage hypersensitivity. Interestingly, a Kif2C mutant (Δ86-90) specifically deficient in DNA damage recruitment was unable to rescue DSB accumulation or etoposide-sensitivity in Kif2C depleted cells. Furthermore, Kif2C inhibition led to DSB accumulation in cells synchronized at G1/S. Together, our studies revealed a new role of Kif2C in facilitating DNA DSB repair that is distinct from its known functions in mitotic progression.

4.6.2 Kif2C mediates the mobility of DSBs, and the formation of DNA damage foci.

While the core pathways of NHEJ and HR have been well studied, an emerging topic of DNA repair lies in the spatiotemporal dynamics of DSBs (Hauer & Gasser, 2017; Lemaitre & Soutoglou, 2015; Marnef & Legube, 2017; Mine-Hattab & Rothstein, 2013). In particular, clustering of DSB ends into "repair centers" has been observed for longer than a decade; and the increased mobility of DSB ends within the nucleus has been reported in yeast and mammalian cells (Chuang et al., 2006; Chung et al., 2015; Krawczyk et al., 2012; Lemaitre & Soutoglou, 2015; Levi et al., 2005; Lottersberger et al., 2015; Marnef & Legube, 2017; Neumaier et al., 2012). However, mechanistic understandings of these phenomena are largely absent within the context of current DDR regulators. We revealed in this study that a specific kinesin motor protein, Kif2C, directly promotes DSB mobility and mediates the formation and fusion of DNA damage foci. Our findings indicate that, upon recruitment to DSBs, Kif2C utilizes its ATPase and microtubule depolymerases activities to propel the physical movement to promote DNA repair; Kif2C facilitates the formation of DNA damage foci, which potentially involves the mobility and clustering of DSBs, as shown previously (Asaithamby & Chen, 2011; Aten et al., 2004; Aymard et al., 2017; Neumaier et al., 2012; Roukos et al., 2013). In addition to foci formation, we observed also the occurrence of DSB foci fusion and resolution, indicating that DSBs may undergo dynamic organization and reorganization during DNA repair. These events are reduced by Kif2C depletion or inhibition, thus reflecting a role of Kif2C in these processes.

In addition to the underlying mechanism, the functional impact of DSB mobility and foci formation also remains to be better clarified. It has been generally hypothesized that this pattern of DSB dynamics facilitates DSB repair, e.g., by keeping DSB ends in close proximity, and increasing the local concentration of repair proteins (Lottersberger et al., 2015; Mine-Hattab &

Rothstein, 2012, 2013). Furthermore, mounting evidence suggested that DSB mobility may enable homology search during HR (Marnef & Legube, 2017; Mine-Hattab & Rothstein, 2012; Schrank et al., 2018). On the other hand, microtubule and the linker of the nucleoskeleton and cytoskeleton (LINC)-mediated DSB mobility was shown to promote NHEJ of dysfunctional telomeres (Lottersberger et al., 2015). By characterizing Kif2C as specific regulator of DSB mobility, our study provided an opportunity to assess the functional involvement of DSB dynamics in repair. Interestingly, we demonstrated that Kif2C is required for the efficient DSB repair via both HR and NHEJ. Future studies shall be directed to determine more precisely how Kif2C mediates DSB dynamics, and how this process may interact with the core repair machinery of HR and NHEJ.

We showed that the initial or sustained recruitment of Kif2C to DNA damage sites is dependent on PARP1 or ATM activation, respectively. Thus, we set out to investigate if either PARP1 or ATM governs DNA damage dynamics via Kif2C. Of note, ATM was shown to govern DSB mobility in previous studies (Becker et al., 2014; Dimitrova et al., 2008). PARP1 is known to play a crucial role in sensing DNA damage, recruiting repair factors, and modulate chromatin structure, but its involvement in DSB movement was not reported. We clarified in our study that PARP1 and ATM inhibition markedly retarded DSB mobility. Inhibition of PARP1 or ATM in Kif2C-depleted cells less significantly affected DSB mobility, validating that Kif2C is a major downstream of PARP1 and ATM in regulation of DSB mobility, but at the same time, suggesting the existence of redundant pathways.

4.6.3 The emerging role of microtubule dynamics in DNA repair.

Since the first report of nuclear actin in *Xenopus*, the existence of the actin network in the nucleus, and its function in nuclear architecture and genomic regulation, have been well recognized

(Belin et al., 2015; Caridi et al., 2018; Grosse & Vartiainen, 2013; Misu et al., 2017; Schrank et al., 2018). By comparison, microtubule assembly is viewed as a cytoplasmic event, except in mitosis after nuclear envelop breakdown. Thus, the function of Kif2C, a microtubule depolymerase, in DNA repair is largely unexpected. In particular, our studies using established Kif2C mutants and inhibitor suggested the involvement of the ATPase and tubulin-binding activities of Kif2C in DNA repair. Potentially in line with our findings, previous studies showed that microtubule poisons caused endogenous DNA damage and reduced DNA repair (Branham et al., 2004; Lottersberger et al., 2015; Poruchynsky et al., 2015; Rogalska & Marczak, 2015).

While cytoplasmic MTs can indirectly influence the DDR, for example, via the nuclear import of repair factors (Poruchynsky et al., 2015), or via the nucleoskeleton and cytoskeleton (LINC) complex (Lottersberger et al., 2015), our study suggested a rather direct involvement of nuclear microtubule components in the DDR. This is particularly relevant as many kinesins, as well as low levels of tubulins, are present in the nucleus (Akoumianaki et al., 2009; Kirli et al., 2015; Kumeta et al., 2013). Interestingly, Kif4A and γ-tubulin were shown to associate with Rad51 and possibly other repair proteins (C. Lesca et al., 2005; Wu et al., 2008). Yeast kinesin-14 and nuclear pore proteins mediate the perinuclear tethering of telomeric DSBs in yeast cells (Chung et al., 2015). Moreover, recent evidence demonstrated that inhibitors of microtubule assembly reduced the mobility of DSBs (Lawrimore et al., 2017; Lottersberger et al., 2015), further suggesting a nuclear function of MTs.

To account for the potential role of microtubule dynamics in DNA repair, a provocative possibility is that microtubule assembly occurs in the nucleus after DNA damage, presumably at a low and transient level. Along this line, a previous study visualized increased tubulin nucleation and microtubule rearrangement after DNA damage, although it was not defined if this event occurs

at least partially in the nucleus (Porter & Lee, 2001). A study in yeast cells detected the assembly of long and stable MTs in the interphase nuclei when cell enters quiescence (Laporte et al., 2013); a more recent study visualized DNA damage-inducible intranuclear microtubule filaments (DIMs) in yeast cells using GFP-tagged tubulin (Oshidari et al., 2018). However, the formation of detectable DIMs in mammalian cells remains to be demonstrated. On the other hand, as an alternative hypothesis to be considered, microtubule filament assembly via tubulin nucleation may not occur in the nucleus of damaged mammalian cells, but rather, certain regulators and mechanisms of microtubule assembly/disassembly are employed by the DDR machinery to govern the dynamic movement and repair of broken DNA ends. In all cases, the characterization of Kif2C as a new DDR factor that mediates DNA damage movement and foci formation, in a manner involving its microtubule depolymerase activity, sheds new light on the spatiotemporal regulation of DNA damage dynamics. Future studies building on these findings shall further delineate the involvement of microtubule regulators in the DNA damage response.

4.7 MATERIALS AND METHODS

4.7.1 Cell Culture, transfection and treatment

Human cervix carcinoma (HeLa) and bone osteosarcoma epithelial (U2OS) lines, authenticated by ATCC, were maintained in Dulbecco's modified Eagle medium (DMEM, Hyclone) with 10% fetal bovine serum (FBS, Hyclone). Human head and neck squamous cell carcinoma UM-SCC-38 cells were authenticated and maintained as in previous studies (Brenner et al., 2010; L. Wang et al., 2012). Cell viability and death assays were performed as in our previous study (Wang et al., 2014). Briefly, cells were incubated for 1-4 days. The numbers of viable cells were counted using a hemocytometer. To measure cell death, trypan blue staining was performed by mixing 0.4% trypan blue in PBS with cell suspension at a 1:10 ratio. Ionized radiation was performed using an X-ray cabinet (RS-2000 Biological irradiator). Transfection of expression vectors was carried out using lipofectamine 2000 (Invitrogen) following the protocol recommended by the manufacturer. SiRNA targeting Kif2C (5-AUCUGGAGAACCAA GCAU-3', Integrated DNA Technologies) was transfected into cells using Lipofectamine RNAi MAX (Invitrogen). A non-targeting control siRNA was used as a control

.

4.7.2 Cloning and mutagenesis

Xenopus Kif2C gene was cloned from a *Xenopus* oocyte cDNA library and inserted into a pMBP vector with an N-terminal MBP-tag. Kif2C G495A, R420S, Δ86-90, Δneck, and siRNA-resistant mutants were generated using site-directed mutagenesis (Agilent) following the protocol recommended by the manufacturer. The human Kif2C expression vector was obtained from Addgene (mEmerald-MCAK-C-7, a gift from Michael Davidson via Addgene, plasmid # 54161).

4.7.3 DNA binding assay

Biotin labeled double strand DNA fragment (dsDNA, 500 bp) was generated using biotin-11-ddUTP (Thermo Scientific, #R0081) incorporation, and PCR amplification using Taq polymerase and a pMBP vector (as template). Biotin-labeled DNA (produced as above) or biotin dA-dT (70 mer) was conjugated on streptavidin magnetic beads (New England Biolabs, #S1420S) and incubated in *Xenopus* egg extracts and HeLa cell lysates. The beads were re-isolated using a magnet, washed five times, and then resolved by SDS-PAGE.

4.7.4 HR and NHEJ assays

Homologous recombination assay was performed in a HeLa-derived cell line stably integrated with a DR-GFP reporter cassette (a gift from Dr. Jeffrey Parvin at the Ohio State University). The reporter consisted of direct repeats of two differentially mutated green fluorescent proteins (GFP), Sce GFP and iGFP. SceGFP contains an I-SceI recognition site and in-frame termination codons. An 812-bp internal GFP fragment (iGFP) was used by HR to repair the DSB. Briefly, cells were seeded at 3 x 105 cells per well in a 6-well plate one day before siRNA treatment. After removing the siRNA, the cells were grown for 48 hr in fresh medium and transfected with an expression vector of I-SceI endonuclease (a gift from Dr. Maria Jasin at Memorial Sloan Kettering Cancer Center). In this assay, a full-length GFP is expressed only after DSBs introduced by I-SceI endonuclease are repaired by HR, and the level of full-length GFP expression was quantified by immunoblotting and NIH ImageJ.

The NHEJ assay was performed in U2OS-EJ5 cells (a gift from Dr. Jeremy Stark at the Beckman Research Institute of the City of Hope). Briefly, cells were seeded at 3 x 105 cells per well in a 6-well plate 24hr before siRNA treatment. After removing the siRNA, the cells were grown for 48

hr in fresh medium and transfected with an expression vector of I-SceI endonuclease. In this assay, GFP is expressed only after DSBs introduced by I-SceI endonuclease are repaired by NHEJ, and the level of GFP expression was quantified by immunoblotting and NIH ImageJ.

4.7.5 Immunoblotting

Sodium dodecyl sulfate-polyacrylamide gel electrophoresis (SDS-PAGE) and immunoblotting were carried out as previously described (Ren et al., 2017), using the following antibodies: γ-H2AX (A300-081A-M), and Ku80 (A302-627A-T) from Bethyl Laboratories (Montgomery, TX); ATM (sc-377293), DNA-PKcs (sc-390849), GFP (sc-9996), γ-H2AX (sc-517348), Kif2C (sc-81305), and Ku70 (sc-56129), from Santa Cruz Biotechnology (Dallas, TX); H2B (ab1790-100) and α-tubulin (ab7291) from Abcam (Cambridge, MA); β-actin (#4970T) from Cell Signaling Technology (Beverly, MA); and Artemis (GTX100128) from Genetex (Irvine, CA).

4.7.6 Immunofluorescence and imaging

Cells were grown on cover glasses, washed with PBS twice, and fixed with 3% formaldehyde with 0.1% Triton X-100 for 30min. 0.05% Saponin containing PBS was used to permeabilize the fixed cells followed by blocking with 5% goat serum for 30 min. Primary antibodies were diluted in blocking buffer and incubated with the cells for 2 hr. The cells were then incubated with Alexa Fluor secondary antibodies (Invitrogen, 1: 2,000) for 1 hr at room temperature. The nuclei of cells were stained with 4',6-diamidino-2-phenylindole (DAPI), and the stained cells were imaged using a Zeiss Axiovert 200M inverted fluorescence microscope at the UNMC Advanced Microscopy Core Facility. Laser microirradiation was performed using 405nm laser under the Zeiss Axiovert 200M Microscope with Marianas Software (Intelligent Imaging Innovations, Inc. Denver, CO).

4.7.7 Microscopic analysis of DNA damage foci mobility and dynamics

EGFP-53BP1 (or mApple-53BP1, or Control foci constructs: EGFP-PRPF6 or Cenp-B-mCherry)-transfected cells were seeded in ibidi µ-Dish 35 mm Quad dish the day prior to imaging. Formation of 53BP1 foci was induced by the addition of 20 µM etoposide. Other compounds such as taxol or DHTP were added to the cells either prior to (pre-treatment) or after (post-treatment) etoposide treatment. Image acquisition was carried out using a Zeiss spinning disk confocal microscopy system equipped with a 63× PlanAprochromat oil objective. After cells expressing those constructs were located and the imaging positions were selected, microscopy recordings were then started (usually 5 min after the last treatment, for consistency reason). Imaging of the control foci, that is CENP-B-mCherry and EGFP-PRPF6, was done in a similar manner except that their formation does not require etoposide addition. For foci mobility, time-lapse recordings were done every 30 seconds for 10 min. For foci disappearance or fusion, recordings were done every 3 min for one hours. Z-stack images were acquired at 0.5 µm intervals covering a range from 6 to 8 µm. Foci tracking was done using all the acquired stacks for positional information using ImageJ (NIH), and the foci number was quantified using the automatic particle counting option. For image presentation in figure panels, 2D-maximum intensity projection images were generated using the ZEN blue software. Data analysis and graph presentations were performed using Excel (Microsoft) and KaleidaGraph (Synergy). Student's t-test was used for statistical analysis. Mean-square displacement was calculated as previously described (Lottersberger et al., 2015) using the following equation

$$MSD(\Delta t) = \frac{1}{n}\sum_{i=1}^{n} Di(\Delta t)^2$$

Where

$$Di(\Delta t) = \sqrt{((x_t^i - x_t^{GC}) - (x_{t-\Delta t}^i - x_{t-\Delta t}^{GC}))^2 + ((y_t^i - y_t^{GC}) - (y_{t-\Delta t}^i - y_{t-\Delta t}^{GC}))^2}$$

4.7.8 Pull-down assay

For protein association studies, MBP Kif2C WT and mutants were expressed in BL21 bacteria cell, purified on amylose beads, and then incubated in HeLa cell lysates for 1hr at room temperature. The beads were re-isolated using low speed centrifugation, washed five times, and then resolved by SDS-PAGE. For the plasmid DNA pull-down assay in Figure 4.1C, pMBP plasmid was either uncut or linearized by EcoRV endonuclease (New England Biolabs, #R3195). MBP-Kif2C was conjugated on amylose beads and incubated in *Xenopus* egg extracts supplemented with either uncut or linearized pMBP plasmid for 1hr at room temperature. The beads were re-isolated using low speed centrifugation, washed five times, and then boiled in distilled water. The samples were used as templates for PCR with Taq Polymerase.

4.7.9 Single cell gel electrophoresis (comet assay)

Cells were washed with PBS, trypsinized, and plated in 0.65% low melting agarose. After solidification, slides were incubated in lysis solution (1 M NaCl, 3.5 mM N-laurylsarcosine, 50 mM NaOH) for 2 hr. Slides were then washed, and incubated in alkaline electrophoresis buffer (50 mM NaOH, 2 mM EDTA) for 30 min. After electrophoresis for 10 min at 20 V, slides were stained with propidum iodide (25 μg/mL).

4.7.10 Xenopus egg extracts

Eggs were rinsed in distilled water and de-jellied with 2% cysteine in 1x XB (1 M KCl,10 mM $MgCl_2$, 100 mM HEPES pH 7.7, and 500 mM sucrose). Eggs were washed in 0.2x MMR buffer

(100 mM NaCl, 2 mM KCl, 1 mM $MgCl_2$, 2 mM $CaCl_2$, 0.1 mM EDTA, 10 mM HEPES), and activated with Ca^{2+} ionophore. Eggs were then washed and crushed by centrifugation at 10,000 g. The cytoplasmic layer was transferred to new tubes, supplemented with an energy mix (7.5 mM creatine phosphate, 1 mM ATP, 1 $MgCl_2$), and then further separated by centrifugation at 10,000 g for 15 min.

4.8 ACKNOWLEDGEMENT

We thank Dr. Jay Reddy (University of Nebraska-Lincoln) for technical support with X-ray irradiation, and Christian Charbonneau of the Bioimaging facility of the Institute for Research in Immunology and Cancer (IRIC, Université de Montréal) for technical support with high-resolution microscopy. The UNMC Advanced Microscopy Core Facility was supported by the Nebraska Research Initiative, the Fred and Pamela Buffett Cancer Center Support Grant (P30CA036727), and an Institutional Development Award (IDeA) from the NIGMS of the NIH (P30GM106397). The IRIC is supported in part by the Canadian Center of Excellence in Commercialization and Research (CECR), the Canada Foundation for Innovation and Fonds de recherche du Québec – Santé (FRQS). This work was partially supported by NIH grant CA172574 to A.P., and funding to B.H.K. from the Canadian Institutes of Health Research (CIHR), Cancer Research Society (CRS) and FRQS.

Author contributions: S.Z., B.H.K., and A.P. conceived and designed experiments. S.Z., M.P., F.W., L.W., B.B., and T.B. performed experiments. S.Z., T.B., B.H.K., and A.P. analyzed and interpreted results. S.Z. and F.W. wrote the manuscript.

4.9 DECLARATION OF INTERESTS

The authors declare no competing interests.

4.10 SUPPLEMENTARY INFORMATION

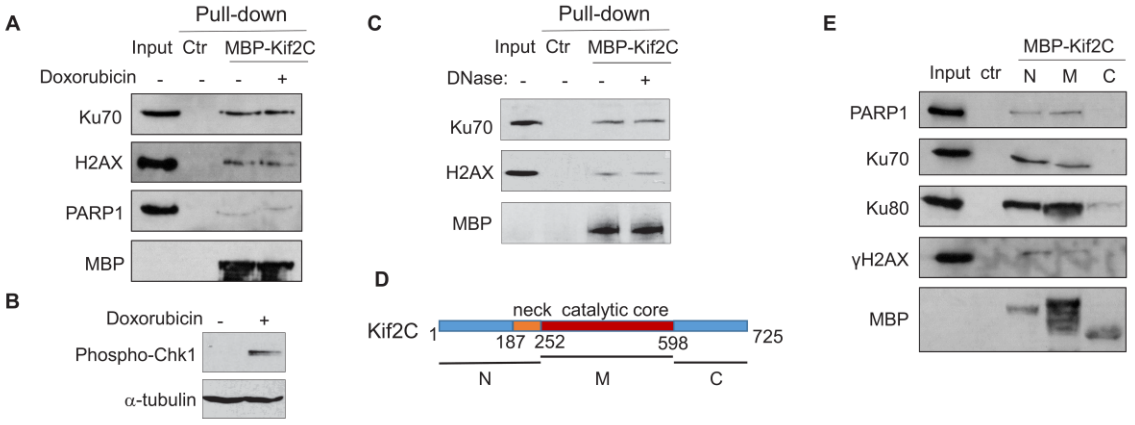

Supplementary Figure 4.1. Kif2C associates with DNA repair proteins. (A) MBP-Kif2C pull down was performed in HeLa cells with or without doxorubicin (2 mg/mL) treatment. Input, control pulldown with blank beads, and MBP pulldown samples were analyzed by immunoblotting. (B) Doxorubicin treatment, as in panel A, activated DNA damage signaling, as indicated by Chk1 phosphorylation at Ser-317. (C) MBP-Kif2C pull down was performed in HeLa cells as in panel A. Cell lysates were incubated with DNase I (100 units/mL) as indicated. Input, control pulldown with blank beads, and MBP pulldown samples were analyzed by immunoblotting. (D,E) The N, M, C segments of Kif2C, as shown in panel D, were used for pull-down in the lysates of HeLa cells treated with doxorubicin. Control (ctr) pull-down was performed using blank beads. Immunoblots are shown in panel E.

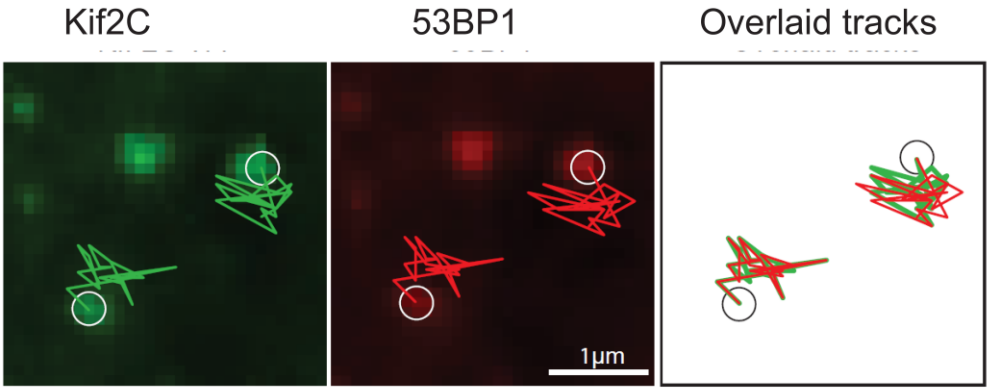

Supplementary Figure 4.2. The co-localization and co-migration of Kif2C and 53BP1 foci. Two representative examples of Kif2C and 53BP1 foci were tracked in U2OS cells. The coordinated movements of WT-KIF2C and 53BP1 foci are shown.

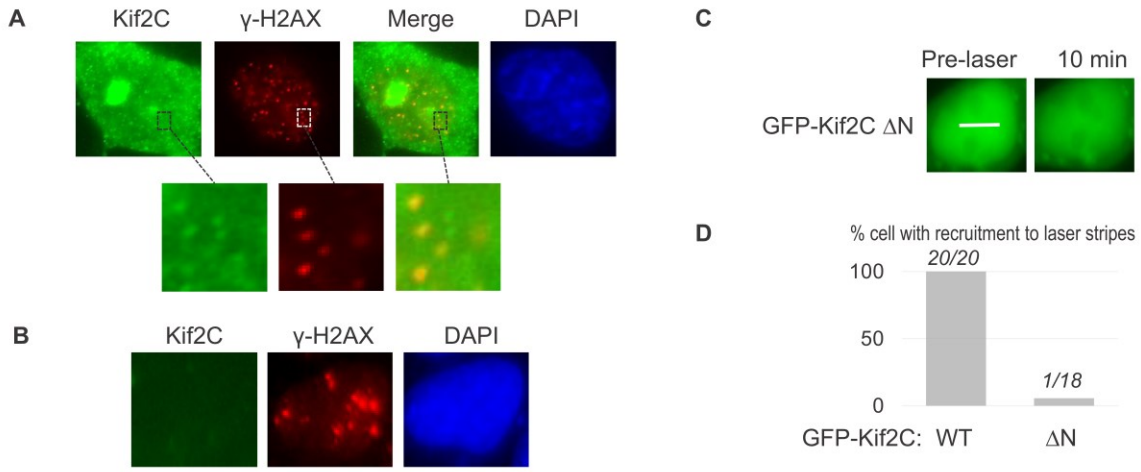

Supplementary Figure 4.3. Kif2C recruitment to DNA damage sites. (A) HeLa cells were treated with 10 Gy IR, the immunofluorescent (IF) signals of Kif2C and γ-H2AX are shown. Pre-extraction was performed by placing the dish on ice for 5 min with 0.1% Triton X-100 in 10 mM HEPES (pH 7.4), 2 mM MgCl2, 100 mM KCl, and 1 mM EDTA. (B) Kif2C and γ-H2AX IF was performed as in panel A, in Kif2C knockout (KO) cells. (C) The localization of GFP-Kif2C deleted of N-terminus before or after laser treatment is shown. The white line marks the path of laser. (D) Quantification of cells showing recruitment to laser stripes.

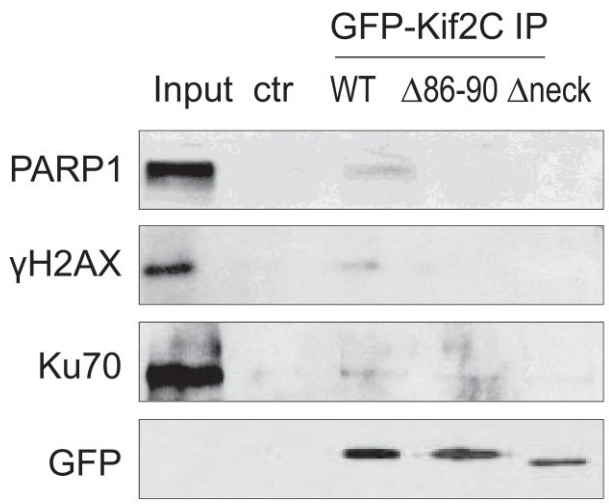

Supplementary Figure 4.4. Kif2C associations with repair proteins were disrupted by mutations. GFP-Kif2C (WT or deletion mutants) IP was performed using anti-GFP or control (blank) beads, as in Figure 4.1E. 10% input, control and GFP IP samples were analyzed by immunoblotting.

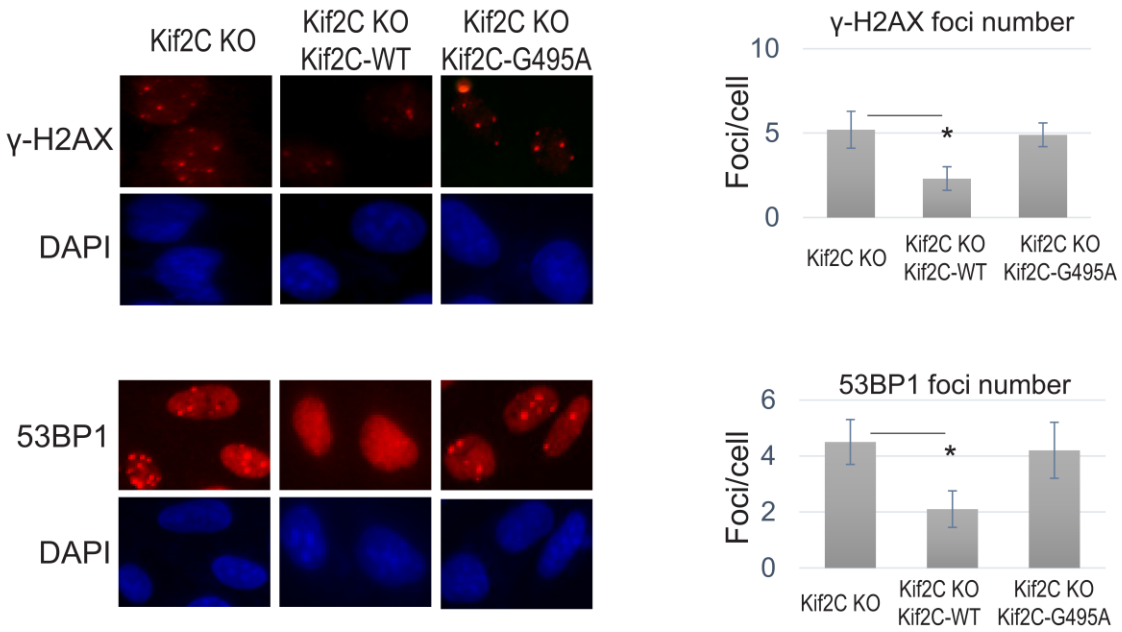

Supplementary Figure 4.5. Foci formation of γ-H2AX and 53BP1 in undamaged Kif2C knockout (KO) cells. Representative foci formation is shown in Kif2C KO cells with or without expression of WT or G495A Kif2C, as in Figure 4.3D. Quantifications of foci number are shown on the right panels (N > 20).

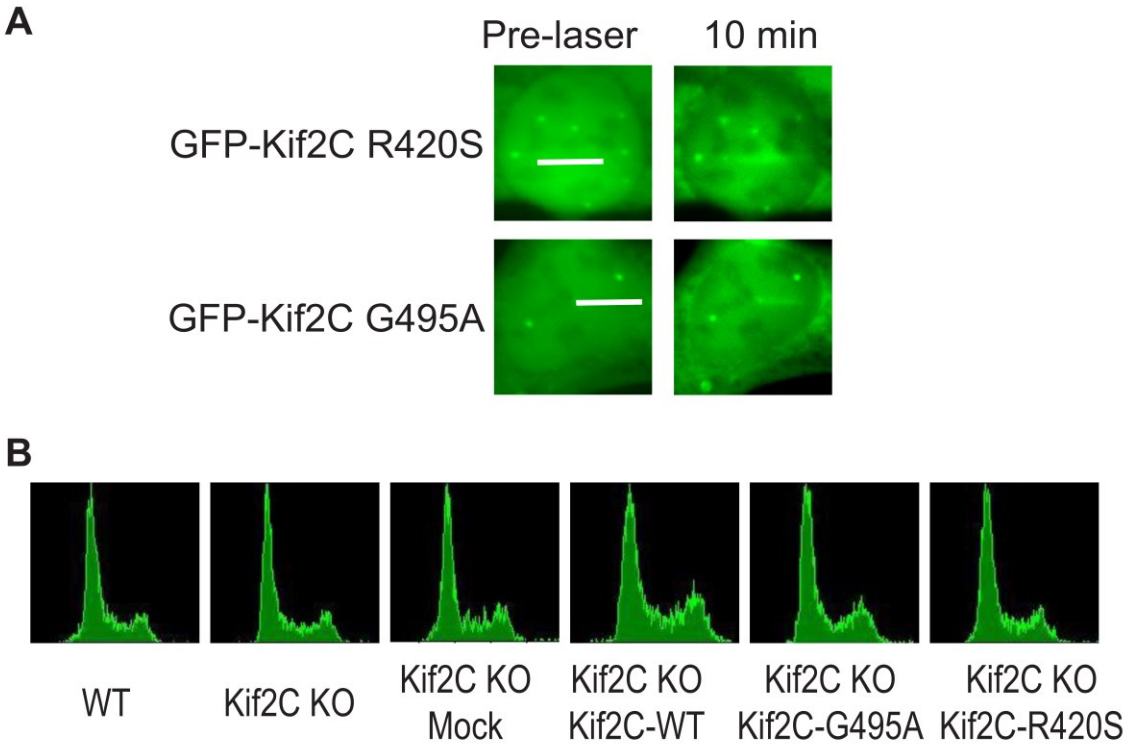

Supplementary Figure 4.6. Kif2C recruitment and cell cycle effect. (A) The recruitment of GFP-Kif2C R420S and G495A to laser-induced DNA damage sites. The GFP localization before or after laser treatment is shown. The white line marks the path of laser. (B) WT or Kif2C KO U2OS cells were analyzed by FACS for cell cycle distribution. Cells were mock transfected or transfected with WT, G495A or R420S Kif2C, as in Figure 4.3.

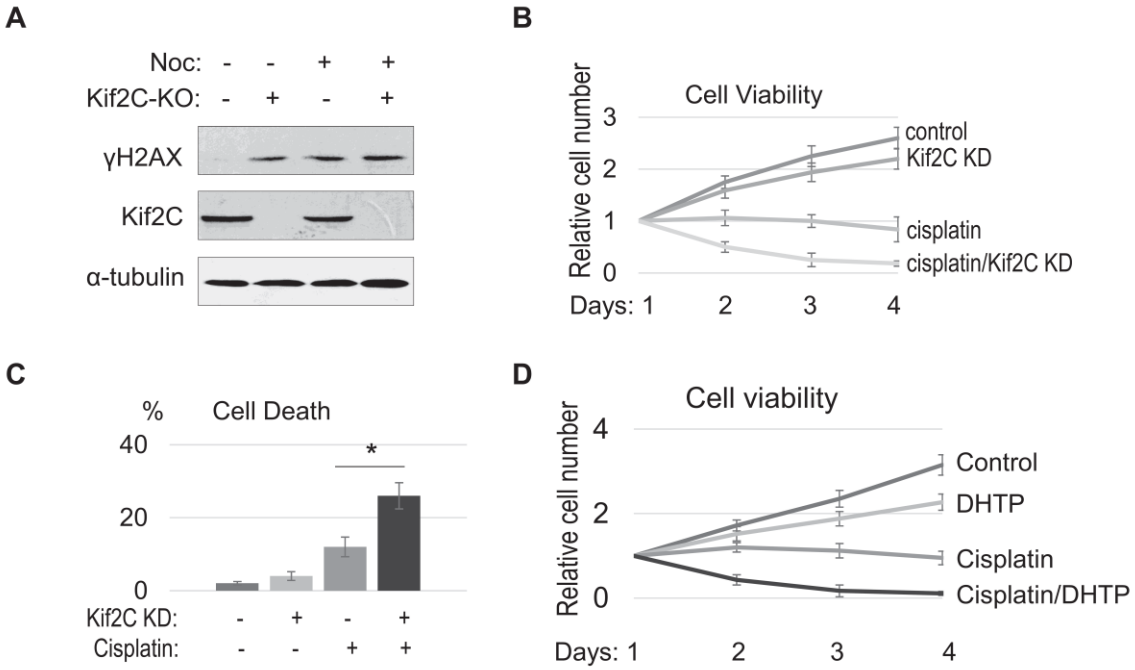

Supplementary Figure 4.7. The microtubule depolymerase activity of Kif2C is involved in the DNA damage response. (A) Kif2C depletion does not further induce DNA damage in cells treated with nocodazole (100 ng/ml). Control or Kif2C knockout (KO) U2OS cells were treated with nocodazole for 8 hr, as indicated. The samples were analyzed by immunoblotting. (B) Human head and neck cancer SCC38 cells were incubated in cisplatin (6.7 μM) and Kif2C siRNA, as indicated. The relative cell viability was determined by normalizing the cell number to that of the first day. The mean values and standard deviations, calculated from three independent experiments, are shown. (C) SCC38 cells were treated as in panel B for 2 days and measured by the trypan blue exclusion assay for cell death. The mean values and standard deviations, calculated from three independent experiments, are shown. (D) HeLa cells were incubated in cisplatin (6.7 μM) and DHTP (10 μM), as indicated. The relative cell viability was determined by normalizing the cell number to that of the first day. The mean values and standard deviations, calculated from three independent experiments, are shown.

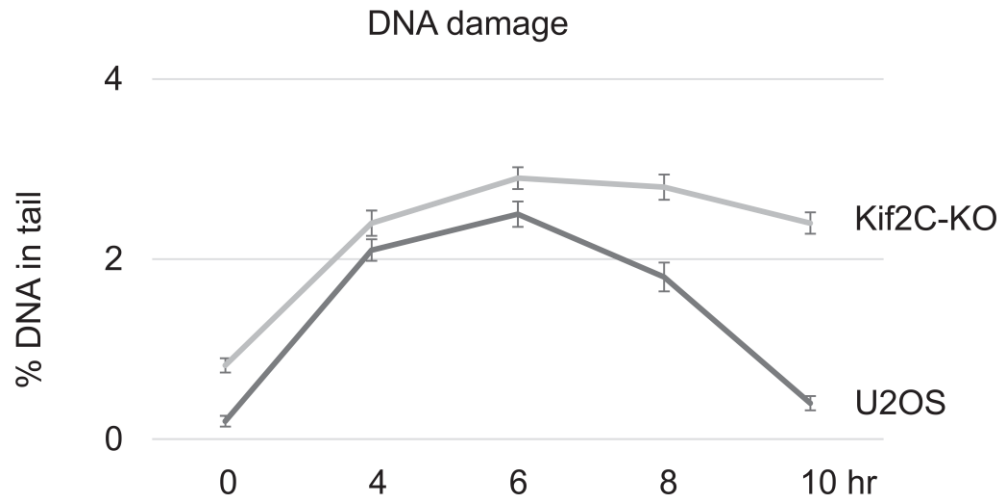

Supplementary Figure 4.8. Kif2C depletion impairs DNA repair. Comet assay was performed in U2OS cells with or without Kif2C knockout. The cells were treated with doxorubicin at time 0 for 1 hr. The percentage of DNA in the tail section was quantified, the mean values and standard derivations are shown (N > 10).

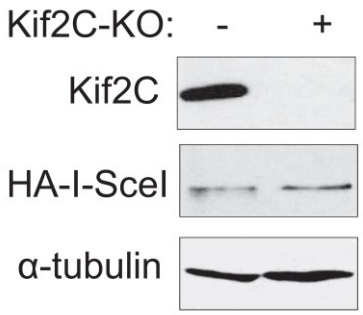

Supplementary Figure 4.9. Kif2C depletion did not affect the expression of I-SceI.

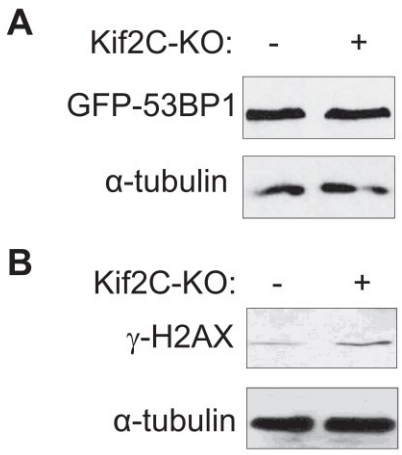

Supplementary Figure 4.10. Kif2C depletion did not affect the expression of GFP-53BP1 (A). Kif2C depletion increased γ-H2AX induced by etoposide (B).

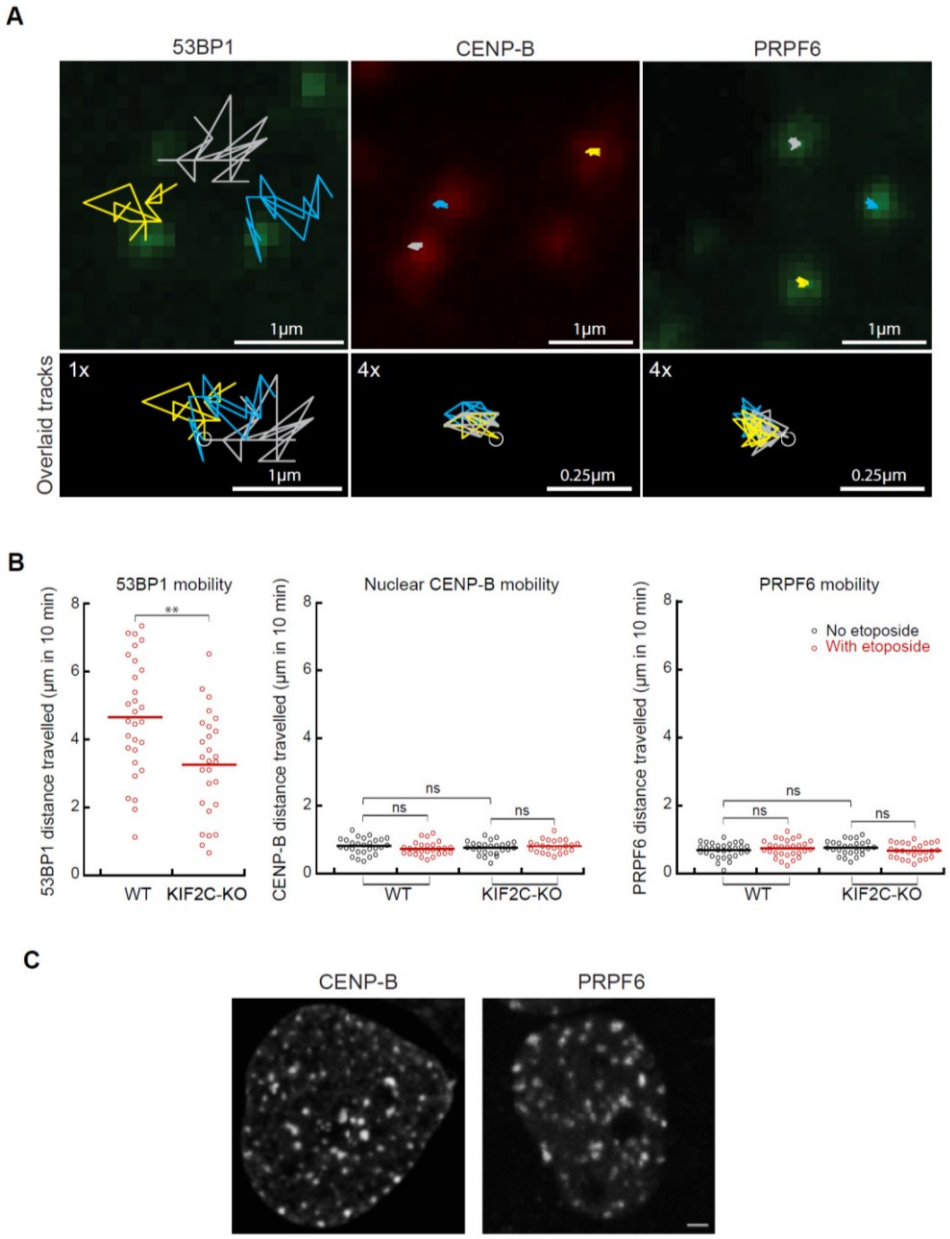

Supplementary Figure 4.11. Kif2C depletion did not influence the general nuclear dynamics. (A) Representative examples of 10 min mobility traces of EGFP-53BP1, mCherry-CENP-B and EGFP-PRPF6 in U2OS cells. The tracked traces were overlaid over the corresponding images (upper panel). The lower panel shows the same traces aligned with a common starting point (indicated by circles). Note that the randomness of 53BP1 traces and the coordinated movement of the CENP-B and PRPF6 foci, representing general nuclear dynamics. (B) Quantification of the

distance travelled by EGFP-53BP1, mCherry-CENP-B and EGFP-PRPF6 foci over 10 min in WT-U2OS and KIF2C-KO-U2OS cells. 53BP1 mobility was tracked 5 min after etoposide treatment, while the mobility of nuclear CENP-B and PRPF6 was tracked either with or without the addition of etoposide. (C) Examples of the intranuclear foci localization of CENP-B and PRPF6.

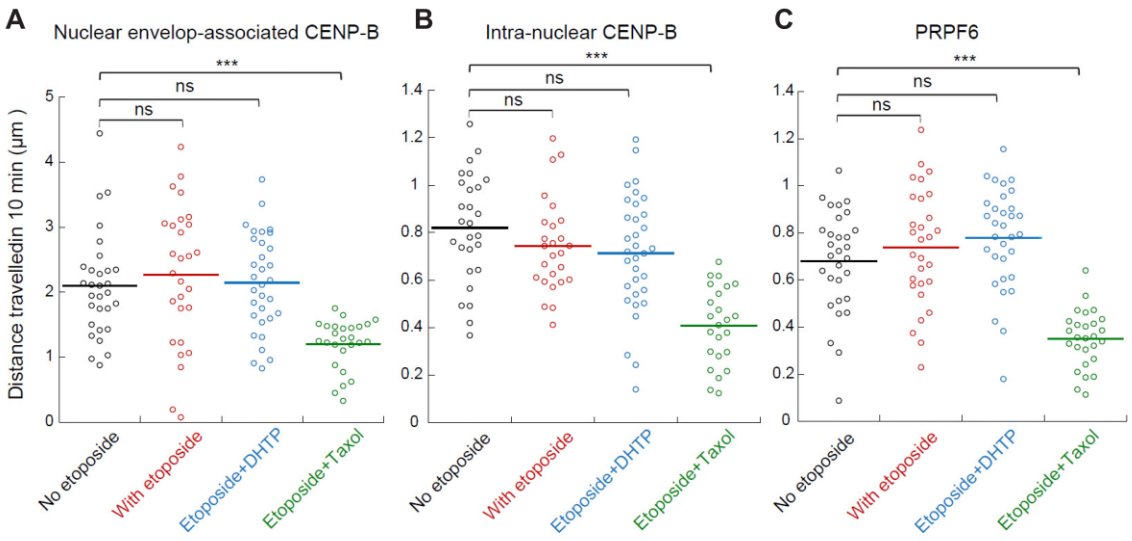

Supplementary Figure 4.12. Taxol, but not DHTP, reduced the general mobility of CENP-B and PRPF6. Quantification of the distance travelled by nuclear envelop-associated mCherry-CENP-B foci (A), intra-nuclear mCherry-CENP-B foci (B), or intra-nuclear PRPF6 foci (C) over 10 min in U2OS cells without or with etoposide treatment, in the presence or absence of DHTP (20 μM) or taxol (5 μM).

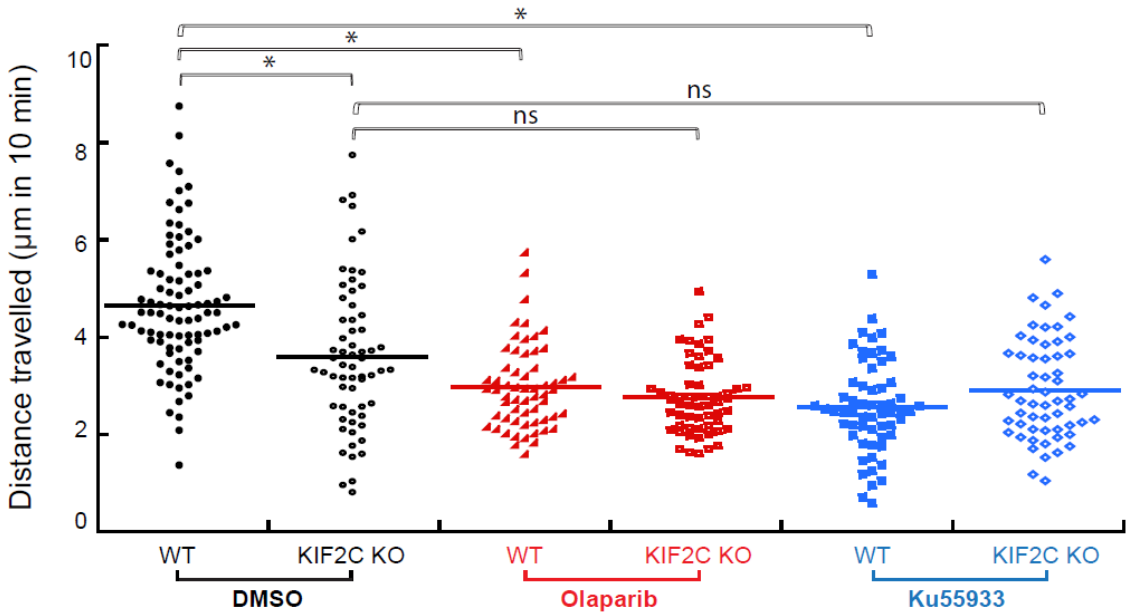

Supplementary Figure 4.13. ATM and PARP inhibition impairs Kif2C-dependent foci mobility. As shown in Figure 4.6A and B, Mean-square displacement measurements of EGFP-53BP1 foci were measured in WT and Kif2C KO U2OS cells treated with the vehicle control (DMSO), the PARP1 inhibitor Olaparib (10 µM), or the ATM inhibitor KU55933 (20 µM). Quantification of the distance travelled by EGFP-53BP1 foci over 10 min in the corresponding cells, as in Figure 4.6, is presented here in three groups (DMSO, Olaparib, and Ku55933).

CHAPTER 5. Discussion

5.1 Relationship between tubulin conformational change and GTP hydrolysis.

It is known that both GTP- and GDP-bound tubulin dimers adopt a curved conformation. It has also been shown that the growing end of microtubules are tapered and GTP-tubulin dimers are incorporated to the end of microtubule lattice in a curved conformation. However, the level of their curvature might change, as a cryo-EM study showed that GMPCPP-bound tubulin adopts a conformation between the straight and curved conformations (5°) (Wang & Nogales, 2005). Our paclitaxel experiment suggests that the GTP hydrolysis is a result of conformational change of GTP-bound tubulin dimers from curved or semi-curved to a straight conformation which can possibly occur during microtubule polymerization, when tubulin dimers are incorporated to the lattice. However, this model should be further investigated structurally and biochemically. With the advances in cryo-EM, it is feasible to acquire a high-resolution single molecule view of the tubulin conformational changes when GTP hydrolysis happens.

In our paclitaxel experiment, despite the low concentration of tubulin and low temperature, there are still possibilities that tubulin oligomers or tandem dimers form, which are not detectable, by the sedimentation assay we used. To confirm that the active catalytic site (β-tubulin binding pocket) between two tandem dimers is not a pre-requirement for GTP hydrolysis, we need to verify that there are no oligomers forming in the solution. For this, we propose dynamic light scattering (DSL) assay, a method which involves applying a laser beam to samples and monitoring fluctuations in the scattering intensity which results from the Brownian motion of the particles. By applying a scattering autocorrelation function, the average hydrodynamic diameter of particles in the sample can be calculated. DSL is able to detect the minor size differences of complexes and molecules even in very small quantities (Kalra et al., 2019). By this method we could distinguish

if tubulin dimers in the solution form oligomers or even tandem dimers in the presence of paclitaxel. An alternative option might be using recombinant tubulin to do the experiment, which enables us to use tubulins with specific mutations. There are some point mutations identified in β-tubulin that prevent tubulins from polymerization (Johnson et al., 2011). Recombinant tubulins carrying these mutations could be perfect candidates to do the paclitaxel GTP hydrolysis experiment to verify if GTP hydrolysis can still occur when there are no tubulin tandem dimers or oligomers forming in the solution.

High-resolution reconstruction of microtubules has shown that binding of the two interacting dimers is required to build a fully active catalytic site (β-tubulin-GTP binding pocket) between the β-tubulin-GTP with α-tubulin of the adjacent dimer (Zhang et al., 2015). In this scenario, the β-tubulin-GTP in between the two dimers gets hydrolyzed as a result of the curvature change of the two adjacent dimers with respect to each other to a straight conformation. This is compatible with the tandem tubulin dimers complex formed by Kinesin-13 binding, which triggers GTP turnover. The necessity of the active catalytic site for GTP hydrolysis induction in the presence of paclitaxel is also a possibility, if tubulin oligomers are formed transiently in the presence of paclitaxel. However, our observation on the 1:2 stoichiometric ratio of kinesin-13-ATP hydrolysis to tubulin-GTP hydrolysis for each encounter of the kinesin-13-tubulin ternary complex proposes an alternative hypothesis that the active catalytic site for GTP hydrolysis does not necessarily require the completion of the β-tubulin-GTP binding pocket between two tandem tubulin dimers. This hypothesis could provide insights into the understanding of how GTP hydrolysis occurs and what it actually does in terms of tubulin biochemistry and microtubule dynamics.

The idea that GTP binding straightened tubulin into a microtubule-compatible conformation before polymerization (Melki et al., 1989) was appealing as it was able to structurally explain why

microtubule assembly required GTP and how GTP hydrolysis could lead to depolymerization of microtubules. However, it is known now that GTP-tubulin is also curved, so how does GTP hydrolysis destabilize the microtubule lattice and trigger catastrophe? By comparison of the cryo-EM reconstructions of GMPCPP microtubules and GDP microtubules in a structural study, which indicated that GTP hydrolysis induces a strain into the microtubule lattice, just next to the exchangeable nucleotide-binding site, causing a conformational change in tubulin dimers (Alushin et al., 2014). This conformational change could trigger the hydrolysis of GTP, resulting in GDP-tubulin in a straight conformation incorporated to the microtubule lattice. Another possibility is that GTP-bound tubulin dimers in the lattice are distinguished from GDP dimers by specific MAPs and that is the source of microtubule dynamic instability.

5.2 Conformational change-driven tubulin-GTP hydrolysis also occurs during MT polymerization

Tubulin conformational changes and its subsequent GTP turnover could also explain tubulin curvature and nucleotide state during MT polymerization. It has been shown that free GTP-tubulin dimers exist in a native slightly curved state. When they undergo polymerization, GTP-bound tubulin dimers are incorporated into microtubule polymers in a curved or semi-curved (5° rotation) conformation (Brouhard & Rice, 2018; Wang & Nogales, 2005), compacted and forced to straighten up. Based on the model we are proposing, the tubulin dimers straightening process then triggers GTP hydrolysis, resulting in GDP-bound tubulin dimers incorporated into the microtubule lattice in a straight conformation. The polymer ends represent the transition state of this process and may retain the GTP-bound state prior to straightening (GTP cap).

We suggest that the tubulin curvature change from a curved to a straight conformation, could also happen the same way during microtubule polymerization following the incorporation of GTP-bound tubulin dimers to the microtubule lattice. This model could actually explain the outwardly tapered end of growing microtubules, which we think could match the GTP cap area. This is due to the fact that the length of the GTP cap we calculated using EM images and radioactive experiments (~70 nm), falls into the same range of the curved protofilament ends length as calculated by McIntosh et al. (40-80 nm) (McIntosh et al. 2018). The method we used measured the length of GTP cap has some advantages compared to the previous reports, as we are measuring the GTP-bound tubulin directly in our method instead of using a probe like EB1, which could also bind to GDP-Pi-bound tubulin dimers near the end of microtubules (Bieling et al., 2007; Rickman et al., 2017b). However, our method had some drawbacks as well. Due to the harsh preparation process of samples for EM, we had to stabilize microtubules using paclitaxel, which might affect the length and the structure of microtubules ends. Also, there might be some GTP hydrolysis during the sample preparation time for the radioactivity experiments, which would have affected the accuracy of our calculations.

However, does GTP cap actually stabilize microtubule growing ends, as it is widely believed in the literature? Based on what we are suggesting on the GTP hydrolysis during microtubule polymerization process, the GTP cap at the growing end of microtubules might be a transition state, where GTP has not been hydrolyzed yet, without any active stabilizing role. GTP cap could mask GDP-bound tubulin dimers from being exposed though and the end-binding MAPs could actually be the factors that modulate MT polymerization dynamics by binding to these sites, possibly via tubulin conformational changes and subsequent alterations of GTP hydrolysis speed, controlling the extent of GTP cap. Another challenge with our model is the GTP islands theory,

which suggests that GTP-bound tubulins exist in the middle of microtubule lattice and in straight conformation. Although our model does not reject the transient existence of GTP-containing dimers, in case of any damage in the lattice (Aumeier et al., 2016; Dimitrova et al., 2008), it does not comply with the suggested straight curvature of GTP islands, as we are proposing that straightening of the dimers is supposed to induce GTP hydrolysis.

5.3 Implications of the newly discovered role of KIF2C inside the cell nucleus.

The involvement of KIF2C or other MAPs in DNA DSB repair mechanism triggers further curiosity, owing to the presumption that there are no MTs in the nucleus. However, it has been shown that tubulin could enter the nucleus in certain conditions (Akoumianaki et al., 2009; Schwarzerová et al., 2019). To investigate the definitive role of KIF2C in DNA DSB repair mechanisms, we need to identify the binding partners and the proteins that are closely associated with KIF2C at DNA DSB foci. The first candidate would be tubulin, due to the fact that KIF2C is a microtubule associated protein. Although it has been shown that there are no microtubules inside the nuclei, it is possible that tubulins exist in the nuclei in a non-polymerized form. Studies using GFP-tagged proteins have shown that there are no traces of α- and β-tubulin in the nucleus (Schwarzerová et al., 2019). It has been shown that in the presence of leptomycin B (a nuclear export inhibitor) and nocodazole (a microtubule destabilizing agent), fluorescent-labeled tubulins accumulate in the nucleus (Akoumianaki et al., 2009). This can be used to investigate the possible association of tubulin to the DNA DSB foci and more specifically with KIF2C. Also another member of the tubulin family, γ-Tubulin has been shown to exist in the nuclei during the G1/S and G2/M phases of the cell cycle (Chumová et al., 2019). This tubulin subunit could associate with

KIF2C at DNA DSB foci, as it has been shown that γ-Tubulin colocalizes with RAD-51 in DNA repair foci in the nucleus (Claire Lesca et al., 2005).

An interesting and yet confusing point in our observations was that KIF2C affect both HR and NHEJ repair mechanisms. Our study also indicated that the new role of KIF2C in DNA DSB repair is closely related to the action of PARP1 and ATM, which seem to act upstream of KIF2C. PARP1, as a first responder that detects DNA damage, is implicated in the regulation of NHEJ and HR repair mechanisms. PARP1 has been shown to interact directly with p53, DNA polymerase alpha, Aprataxin (APTX) and DNA repair protein XRCC1 (Fischbach et al., 2018; Hanssen-Bauer et al., 2012; Harris et al., 2009; Ray Chaudhuri & Nussenzweig, 2017; Süsse et al., 2004). Another important DNA damage response protein indicating close interaction with KIF2C was ATM, which is a serine/threonine protein kinase, recruited and activated by DNA double-strand breaks. It phosphorylates several key tumor suppressors including p53, CHK2, BRCA1, NBS1 and H2AX that initiate activation of the DNA damage checkpoint, leading to cell cycle arrest, DNA repair or apoptosis(Ahmed & Li, 2007; Dahl & Aird, 2017; Deng, 2006; Lavin et al., 2015). Surprisingly, KIF2C depletion or inhibition of its microtubule depolymerization activity affected both NHEJ and HR repair mechanisms. This shows its possible involvement in both of these repair pathways. The actions of many proteins have been well defined in both NHEJ (such as Ku70, Ku80, BRCA1 and BRCA2) and HR (such as RecA, RAD51, RAD52 and XRCC2). Further investigations on the physical and functional interactions of KIF2C with these key proteins in NHEJ and HR repair mechanisms, especially those closely related to PARP1- or ATM- associated pathways could help unravel the precise roles of KIF2C in DDR.

5.4 Possible roles of KIF2C in DNA DSB foci mobility and DNA damage repair

Based on the effects of microtubule poisons, KIF2C and other MAPs on the DNA DSB foci mobility and dynamics, this idea that the mobility of DNA DSB foci might be microtubule-driven could emerge. The physical mobility of DNA DSB foci, which is an important factor for an efficient repair, is believed to mediate the sub-nuclear organization and positioning of DSBs and in turn to facilitate DNA repair. It has been shown that dynamic microtubules are required for DSB mobility (Lottersberger et al., 2015), where the cells, incubated with the microtubule poisons Taxol or nocodazole, which stabilize and depolymerize microtubules, respectively, indicated striking reduction in the mobility of the dysfunctional telomeres (Lottersberger et al., 2015). In their model, LINC complex (composed of SUN1/2) is proposed to transduce microtubule forces onto the chromatin. LINC complex associates with both inner and outer nuclear membranes and is known to span the inner and outer membranes of the nuclear envelope. This complex connects microtubules and other components of the cytoskeleton with the inside of the nucleus transferring the cytoskeletal forces to the content of nucleus (Starr & Fridolfsson, 2010; Wilson & Foisner, 2010; Chang et al., 2015). In this model they propose that random and untargeted poking of the nucleus by cytoskeleton components including microtubules in response to DNA DSBs might increase the motility of chromatins (Lottersberger et al., 2015). This model links the microtubule dynamics to the DNA DSB foci mobility, but if, as it is proposing, the microtubules affect the mobility of these foci by poking the nuclear envelope, they might also affect the general motility of other (non-DNA repair proteins) as well. However, we showed that, unlike 53BP1, the movement of CENP-B and PRPF6 was not affected by targeting microtubule dynamics. Also, we indicated via various assays that KIF2C, a microtubule depolymerizing kinesin, associates to the DNA DSB foci and affects the mobility of these foci. This finding proposes the possibilities of

direct and specific, rather that remote and random, interactions of microtubules/tubulins with DNA DSB repair foci. The motor proteins including KIF2C might be the key factors to find the way microtubule dynamics affects the mobility DNA DSB foci, where they might be recruited in the repair centers by tubulin subunits, which now play a role as DNA repair proteins. One possible model to explain what actually drives the mobility of DSB foci might involve tubulin dimers conformational changes and their subsequent GTP hydrolysis, which could directly affect the recruitment of MAPs including KIF2C. These changes could also affect the association of other components of the DNA repair foci which are recruited through the affected MAPs and therefore cause a constant mobility in these sites.

To better understand the role of KIF2C in DNA DSB foci mobility, it is crucial to identify the components that are associated with KIF2C in terms of DNA DSB foci dynamics. A number of various factors seem to play roles in the mechanism by which the DNA DSB foci mobility is driven. The importance of 53BP1 and microtubule dynamics has been previously shown and our study indicated that KIF2C, PARP1 and ATM also have distinct functions in DSB foci dynamics. We showed that PARP1 and ATM affect the mobility of DSB foci through KIF2C, as they both act upstream of KIF2C in this process. Besides tubulins, other MAPs like KIF4A might function as the driving motor of these random movements. There are also numerous non-microtubule associated proteins that might play a central role in the DNA DSB dynamics, such as DNA ligase IV, DNA polymerases λ and μ that are specifically involved in DNA DSB repair. In an alternative scenario, the mobility DNA DSB foci might happen without any specific driving agent, simply as a result of recruitment, activity and interactions of different protein factors to these sites.

5.5 Concluding Remarks

Microtubules are unique cytoskeletal polymers due to their structural complexity in their growing and shrinking ends. The mechanism and the molecular basis by which Kinesin-13 members dissociate tubulin subunits from the microtubule end, and as a matter of fact, depolymerize microtubules has been a mystery for decades. Our structural and biochemical analysis indicates the placement of the Kif2A class-specific neck against the adjacent tubulin dimer, which contributes to the formation of the 1:2 Kif2A–tandem tubulin dimer complex. Our model proposes that the bending of tubulins which is induced by a depolymerizing domain of KIF2A resembles the structural changes at MT ends imposed by Kinesin-13s, which triggers depolymerization. This model could help our understanding of the mechanisms involved in Kinesin-13 catalyzed microtubule depolymerization.

Another mystery regarding microtubule dynamics is the biochemical cycle of tubulin, which involves the incorporation of GTP-bound tubulin to the microtubule end, GTP turnover, and dissociation of GDP-tubulin from the end of microtubule. In another perspective, the conformational changes associated with the biochemical cycle of GTP hydrolysis could establish a solid understanding of the links between mechanical and biochemical processes in microtubule dynamics. Our model, proposing that tubulin curvature changes from a curved to a straighter conformation trigger GTP hydrolysis, opens a new perspective in tubulin's biochemical cycles. It also offers an explanation for the biochemical processes and conformational changes during both polymerization and Kinesin-13's catalytic depolymerization of microtubules. MCKA (KIF2C), a member of this protein family, requires tubulin binding for its activities. We found a new role for this mysterious member of kinesin-13 family: The recruitment of KIF2C to the DNA DSB foci, and its involvement in the dynamics of these repair sites, while there are no detectable microtubule

population within the nucleus. However, there are possibilities that tubulin subunits in the form of dimers, tandem dimers or small oligomers exist in the nucleus and interact with Kif2C and DNA DSB foci. As our data suggested, Kinesin-13 proteins are able to induce tubulin-GTP hydrolysis by binding to tubulin dimers, forming a tandem dimer complex, and inducing tubulin conformational changes, a process that might be the key to their functions in DDR, without involvement of microtubule polymers.

DNA DSB foci mobility in random directions, an important hallmark of these repair centers, has remained a mystery despite all efforts in the last few decades. There have been some hypotheses regarding involvement of microtubules as the drivers of this random movements. Hence, discovering the association of a microtubule associated protein, KIF2C, to these sites could be the key which could help us solve this puzzle. In another perspective, the new role of KIF2C we are reporting gives the answer to the previous uncertain hypotheses regarding the nuclear translocation of this microtubule associated protein during interphase. We also indicated that KIF2C and microtubule dynamics are important for intact mobility of the DNA DSB foci and also DNA repair efficiency.

The question remains if tubulins, KIF2C or other MAPs drive the mobility of DSB foci. And if they do, what mechanisms are involved? Formation of kinesin-13-bound tubulin tandem dimer even in the absence of microtubule polymers in our crystal model might also happen at the DNA DSB repair foci in the nuclei of cells during interphase. We indicated that KIF2C is associated to these foci. We still do not know if KIF2C is directly involved in DSB foci mobility. However, as KIF2C requires tubulin for its activity, there is the possibility that KIF2C is recruited to the DNA DSB foci by tubulin. We showed that KIF2C can trigger tubulin GTP hydrolysis by inducing conformational changes. Tubulin GTP hydrolysis may affect the association of other MAPs and

subsequently, other DNA repair factors at DSB foci, which might be a key factor, driving the mobility of these foci. These conformational changes of tubulin heterodimers at DNA DSB sites might happen frequently, triggering GTP hydrolysis, recharging with GTP-tubulin and repeating the same process. Tubulin in this model might play a key role in recruiting essential MAPs like KIF2C to the foci. Our finding on the new role of KIF2C in DDR could be a precious guide to the factors involved in the DNA DSB foci mobility, a phenomenon that is crucial for an efficient repair process and has remained a mystery for decades. Understanding the mechanism of Kinesin-13 proteins' action on tubulin on the one hand and the biochemical and mechanical processes involved in their actions could provide a better understanding of the mechanisms through which they act in DNA DSB repair.

REFERENCES

Acerbo, A. S., Cook, M. J., & Gillilan, R. E. (2015, Jan). Upgrade of MacCHESS facility for X-ray scattering of biological macromolecules in solution. *J Synchrotron Radiat, 22*(1), 180-186. https://doi.org/10.1107/S1600577514020360

Adames, N. R., & Cooper, J. A. (2000, May 15). Microtubule interactions with the cell cortex causing nuclear movements in Saccharomyces cerevisiae. *J Cell Biol, 149*(4), 863-874. https://doi.org/10.1083/jcb.149.4.863

Adams, P. D., Afonine, P. V., Bunkoczi, G., Chen, V. B., Davis, I. W., Echols, N., Headd, J. J., Hung, L. W., Kapral, G. J., Grosse-Kunstleve, R. W., McCoy, A. J., Moriarty, N. W., Oeffner, R., Read, R. J., Richardson, D. C., Richardson, J. S., Terwilliger, T. C., & Zwart, P. H. (Feb). PHENIX: a comprehensive Python-based system for macromolecular structure solution. *Acta Crystallogr D Biol Crystallogr, 66*(Pt 2), 213-221. https://doi.org/S0907444909052925 [pii]
10.1107/S0907444909052925

Ahmed, K. M., & Li, J. J. (2007). ATM-NF-kappaB connection as a target for tumor radiosensitization. *Current cancer drug targets, 7*(4), 335-342. https://doi.org/10.2174/156800907780809769

Aizawa, H., Sekine, Y., Takemura, R., Zhang, Z., Nangaku, M., & Hirokawa, N. (1992, Dec). Kinesin family in murine central nervous system. *J Cell Biol, 119*(5), 1287-1296. http://www.ncbi.nlm.nih.gov/pubmed/1447303

Akhmanova, A., & Hoogenraad, C. C. (2005, Feb). Microtubule plus-end-tracking proteins: mechanisms and functions. *Curr Opin Cell Biol, 17*(1), 47-54. https://doi.org/10.1016/j.ceb.2004.11.001

Akhmanova, A., & Steinmetz, M. O. (2015, 2015/12/01). Control of microtubule organization and dynamics: two ends in the limelight. *Nature Reviews Molecular Cell Biology, 16*(12), 711-726. https://doi.org/10.1038/nrm4084

Akoumianaki, T., Kardassis, D., Polioudaki, C., Georgatos, S., & Theodoropoulos, P. (2009, 05/01). Nucleocytoplasmic shuttling of soluble tubulin in mammalian cells. *Journal of cell science, 122*, 1111-1118. https://doi.org/10.1242/jcs.043034

Ali, A. A. E., Timinszky, G., Arribas-Bosacoma, R., Kozlowski, M., Hassa, P. O., Hassler, M., Ladurner, A. G., Pearl, L. H., & Oliver, A. W. (2012, Jun 10). The zinc-finger domains of PARP1 cooperate to recognize DNA strand breaks. *Nat Struct Mol Biol, 19*(7), 685-692. https://doi.org/10.1038/nsmb.2335

Alushin, G. M., Lander, G. C., Kellogg, E. H., Zhang, R., Baker, D., & Nogales, E. (2014). High-resolution microtubule structures reveal the structural transitions in αβ-tubulin upon GTP hydrolysis. *Cell, 157*(5), 1117-1129. https://doi.org/10.1016/j.cell.2014.03.053

Amitai, A., Seeber, A., Gasser, S. M., & Holcman, D. (2017, Jan 31). Visualization of Chromatin Decompaction and Break Site Extrusion as Predicted by Statistical Polymer Modeling of Single-Locus Trajectories. *Cell Rep, 18*(5), 1200-1214. https://doi.org/10.1016/j.celrep.2017.01.018

Arai, T., & Kaziro, Y. (1977). Role of GTP in the Assembly of Microtubules. *The Journal of Biochemistry, 82*(4), 1063-1071. https://doi.org/10.1093/oxfordjournals.jbchem.a131777

Arora, K., Talje, L., Asenjo, A. B., Andersen, P., Atchia, K., Joshi, M., Sosa, H., Allingham, J. S., & Kwok, B. H. (2014, Aug 26). KIF14 binds tightly to microtubules and adopts a rigor-like conformation [Research Support, N.I.H., Extramural
Research Support, Non-U.S. Gov't]. *J Mol Biol, 426*(17), 2997-3015. https://doi.org/10.1016/j.jmb.2014.05.030

Asaithamby, A., & Chen, D. J. (2011, Jun 3). Mechanism of cluster DNA damage repair in response to high-atomic number and energy particles radiation. *Mutat Res, 711*(1-2), 87-99. https://doi.org/10.1016/j.mrfmmm.2010.11.002

Asenjo, A. B., Chatterjee, C., Tan, D., DePaoli, V., Rice, W. J., Diaz-Avalos, R., Silvestry, M., & Sosa, H. (2013, Mar 28). Structural model for tubulin recognition and deformation by kinesin-13 microtubule depolymerases [Research Support, N.I.H., Extramural]. *Cell Rep, 3*(3), 759-768. https://doi.org/10.1016/j.celrep.2013.01.030

Aten, J. A., Stap, J., Krawczyk, P. M., van Oven, C. H., Hoebe, R. A., Essers, J., & Kanaar, R. (2004, Jan 2). Dynamics of DNA double-strand breaks revealed by clustering of damaged chromosome domains. *Science, 303*(5654), 92-95. https://doi.org/10.1126/science.1088845

Aumeier, C., Schaedel, L., Gaillard, J., John, K., Blanchoin, L., & Théry, M. (2016). Self-repair promotes microtubule rescue. *Nature cell biology, 18*(10), 1054-1064. https://doi.org/10.1038/ncb3406

Avendaño, C., & Menéndez, J. C. (2015). Chapter 9 - Anticancer Drugs Targeting Tubulin and Microtubules. In C. Avendaño & J. C. Menéndez (Eds.), *Medicinal Chemistry of Anticancer Drugs (Second Edition)* (pp. 359-390). Elsevier. https://doi.org/https://doi.org/10.1016/B978-0-444-62649-3.00009-0

Ayaz, P., Ye, X., Huddleston, P., Brautigam, C. A., & Rice, L. M. (2012, Aug 17). A TOG:αβ-tubulin complex structure reveals conformation-based mechanisms for a microtubule polymerase. *Science, 337*(6096), 857-860. https://doi.org/10.1126/science.1221698

Aymard, F., Aguirrebengoa, M., Guillou, E., Javierre, B. M., Bugler, B., Arnould, C., Rocher, V., Iacovoni, J. S., Biernacka, A., Skrzypczak, M., Ginalski, K., Rowicka, M., Fraser, P., & Legube, G. (2017, Apr). Genome-wide mapping of long-range contacts unveils clustering of DNA double-strand breaks at damaged active genes. *Nat Struct Mol Biol, 24*(4), 353-361. https://doi.org/10.1038/nsmb.3387

Bahmanyar, S., Nelson, W. J., & Barth, A. I. (2009). Role of APC and its binding partners in regulating microtubules in mitosis. *Adv Exp Med Biol, 656*, 65-74. https://doi.org/10.1007/978-1-4419-1145-2_6

Bai, H., Lester, G. M. S., Petishnok, L. C., & Dean, D. A. (2017). Cytoplasmic transport and nuclear import of plasmid DNA. *Bioscience reports, 37*(6), BSR20160616. https://doi.org/10.1042/BSR20160616

Banerjee, S., Kaye, S. B., & Ashworth, A. (2010, Sep). Making the best of PARP inhibitors in ovarian cancer. *Nat Rev Clin Oncol, 7*(9), 508-519. https://doi.org/10.1038/nrclinonc.2010.116

Barth, A. I., Caro-Gonzalez, H. Y., & Nelson, W. J. (2008, Jun). Role of adenomatous polyposis coli (APC) and microtubules in directional cell migration and neuronal polarization. *Semin Cell Dev Biol, 19*(3), 245-251. https://doi.org/10.1016/j.semcdb.2008.02.003

Bates, D., & Eastman, A. (2017). Microtubule destabilising agents: far more than just antimitotic anticancer drugs. *British journal of clinical pharmacology, 83*(2), 255-268. https://doi.org/10.1111/bcp.13126

Bates, D., Feris, E. J., Danilov, A. V., & Eastman, A. (2016). Rapid induction of apoptosis in chronic lymphocytic leukemia cells by the microtubule disrupting agent BNC105. *Cancer Biol Ther, 17*(3), 291-299. https://doi.org/10.1080/15384047.2016.1139245

Becker, A., Durante, M., Taucher-Scholz, G., & Jakob, B. (2014). ATM alters the otherwise robust chromatin mobility at sites of DNA double-strand breaks (DSBs) in human cells [Research Support, Non-U.S. Gov't]. *Plos One, 9*(3), e92640. https://doi.org/10.1371/journal.pone.0092640

Beli, P., Lukashchuk, N., Wagner, Sebastian A., Weinert, Brian T., Olsen, Jesper V., Baskcomb, L., Mann, M., Jackson, Stephen P., & Choudhary, C. (2012, 2012/04/27/). Proteomic Investigations Reveal a Role for RNA Processing Factor THRAP3 in the DNA Damage Response. *Molecular Cell, 46*(2), 212-225. https://doi.org/https://doi.org/10.1016/j.molcel.2012.01.026

Belin, B. J., Lee, T., & Mullins, R. D. (2015, Aug 19). DNA damage induces nuclear actin filament assembly by Formin -2 and Spire-(1/2) that promotes efficient DNA repair. [corrected]. *Elife, 4*, e07735. https://doi.org/10.7554/eLife.07735

Benoit, M., Asenjo, A. B., & Sosa, H. (2018, Apr 25). Cryo-EM reveals the structural basis of microtubule depolymerization by kinesin-13s. *Nat Commun, 9*(1), 1662. https://doi.org/10.1038/s41467-018-04044-8

Bensimon, A., Schmidt, A., Ziv, Y., Elkon, R., Wang, S. Y., Chen, D. J., Aebersold, R., & Shiloh, Y. (2010, Dec 7). ATM-dependent and -independent dynamics of the nuclear phosphoproteome after DNA damage. *Sci Signal, 3*(151), rs3. https://doi.org/10.1126/scisignal.2001034

Berlin, V., Styles, C. A., & Fink, G. R. (1990, Dec). BIK1, a protein required for microtubule function during mating and mitosis in Saccharomyces cerevisiae, colocalizes with tubulin. *J Cell Biol, 111*(6 Pt 1), 2573-2586. https://doi.org/10.1083/jcb.111.6.2573

Bieling, P., Laan, L., Schek, H., Munteanu, E. L., Sandblad, L., Dogterom, M., Brunner, D., & Surrey, T. (2007, Dec 13). Reconstitution of a microtubule plus-end tracking system in vitro. *Nature, 450*(7172), 1100-1105. https://doi.org/10.1038/nature06386

Bowne-Anderson, H., Zanic, M., Kauer, M., & Howard, J. (2013, May). Microtubule dynamic instability: a new model with coupled GTP hydrolysis and multistep catastrophe. *Bioessays, 35*(5), 452-461. https://doi.org/10.1002/bies.201200131

Brady, S. T. (1985, 1985/09/01). A novel brain ATPase with properties expected for the fast axonal transport motor. *Nature, 317*(6032), 73-75. https://doi.org/10.1038/317073a0

Branham, M. T., Nadin, S. B., Vargas-Roig, L. M., & Ciocca, D. R. (2004, May 9). DNA damage induced by paclitaxel and DNA repair capability of peripheral blood lymphocytes as evaluated by the alkaline comet assay [Research Support, Non-U.S. Gov't]. *Mutat Res, 560*(1), 11-17. https://doi.org/10.1016/j.mrgentox.2004.01.013

Brenner, J. C., Graham, M. P., Kumar, B., Saunders, L. M., Kupfer, R., Lyons, R. H., Bradford, C. R., & Carey, T. E. (2010, Apr). Genotyping of 73 UM-SCC head and neck squamous cell carcinoma cell lines [Research Support, N.I.H., Extramural]. *Head Neck, 32*(4), 417-426. https://doi.org/10.1002/hed.21198

Brouhard, G., & Sept, D. (2012, Sep 25). Microtubules: sizing up the GTP cap. *Curr Biol, 22*(18), R802-803. https://doi.org/10.1016/j.cub.2012.07.050

Brouhard, G. J., & Rice, L. M. (2014, Nov 10). The contribution of αβ-tubulin curvature to microtubule dynamics. *J Cell Biol, 207*(3), 323-334. https://doi.org/10.1083/jcb.201407095

Brouhard, G. J., & Rice, L. M. (2018, Jul). Microtubule dynamics: an interplay of biochemistry and mechanics. *Nat Rev Mol Cell Biol, 19*(7), 451-463. https://doi.org/10.1038/s41580-018-0009-y

Bryantseva, S. A., & Zhapparova, O. N. J. C. B. I. (2012). Bidirectional transport of organelles: unity and struggle of opposing motors. *36*.

Buey, R. M., Diaz, J. F., & Andreu, J. M. (2006). The Nucleotide Switch of Tubulin and Microtubule Assembly: A Polymerization-Driven Structural Change. *Biochemistry, 45*(19), 5933-5938. https://doi.org/10.1021/bi060334m

Cao, L., Wang, W., Jiang, Q., Wang, C., Knossow, M., & Gigant, B. (2014). The structure of apo-kinesin bound to tubulin links the nucleotide cycle to movement [Research Support, Non-U.S. Gov't]. *Nat Commun, 5*, 5364. https://doi.org/10.1038/ncomms6364

Caplow, M. (1992). Microtubule dynamics. *Current Opinion in Cell Biology, 4*(1), 58-65. https://doi.org/https://doi.org/10.1016/0955-0674(92)90059-L

Caplow, M., & Shanks, J. (1990, May 25, 1990). Mechanism of the microtubule GTPase reaction. *Journal of Biological Chemistry, 265*(15), 8935-8941. http://www.jbc.org/content/265/15/8935.abstract

Caplow, M., & Shanks, J. (1996). Evidence that a single monolayer tubulin-GTP cap is both necessary and sufficient to stabilize microtubules. *Molecular Biology of the Cell, 7*(4), 663-675. https://doi.org/10.1091/mbc.7.4.663

Caridi, C. P., D'Agostino, C., Ryu, T., Zapotoczny, G., Delabaere, L., Li, X., Khodaverdian, V. Y., Amaral, N., Lin, E., Rau, A. R., & Chiolo, I. (2018, Jul). Nuclear F-actin and myosins drive relocalization of heterochromatic breaks. *Nature, 559*(7712), 54-60. https://doi.org/10.1038/s41586-018-0242-8

Carlier, M.-F. (1982). Guanosine-5'-triphosphate hydrolysis and tubulin polymerization. *Molecular and Cellular Biochemistry, 47*(2), 97-113. https://doi.org/10.1007/bf00234410

Carlier, M. F., & Pantaloni, D. (1981). Kinetic analysis of guanosine 5'-triphosphate hydrolysis associated with tubulin polymerization. *Biochemistry, 20*(7), 1918-1924. https://doi.org/10.1021/bi00510a030

Caron, M.-C., Sharma, A. K., O'Sullivan, J., Myler, L. R., Ferreira, M. T., Rodrigue, A., Coulombe, Y., Ethier, C., Gagné, J.-P., Langelier, M.-F., Pascal, J. M., Finkelstein, I. J., Hendzel, M. J., Poirier, G. G., & Masson, J.-Y. (2019, 2019/07/04). Poly(ADP-ribose) polymerase-1 antagonizes DNA resection at double-strand breaks. *Nature Communications, 10*(1), 2954. https://doi.org/10.1038/s41467-019-10741-9

Carvalho, P., Gupta, M. L., Jr., Hoyt, M. A., & Pellman, D. (2004, Jun). Cell cycle control of kinesin-mediated transport of Bik1 (CLIP-170) regulates microtubule stability and dynein activation. *Dev Cell, 6*(6), 815-829. https://doi.org/10.1016/j.devcel.2004.05.001

Cassimeris, L. (2009). Stathmin regulates centrosomal nucleation of microtubules and tubulin dimer/polymer partitioning. . *Molecular Biolology of the Cell, 20*(15).

Cassimeris, L. U., Wadsworth, P., & Salmon, E. D. (1986). Dynamics of microtubule depolymerization in monocytes. *J Cell Biol, 102*(6), 2023-2032.

Castoldi, M., & Popov, A. V. (2003, Nov). Purification of brain tubulin through two cycles of polymerization-depolymerization in a high-molarity buffer. *Protein Expr Purif, 32*(1), 83-88. https://doi.org/10.1016/S1046-5928(03)00218-3

Chaaban, S., & Brouhard, G. J. (2017, Nov 1). A microtubule bestiary: structural diversity in tubulin polymers. *Mol Biol Cell, 28*(22), 2924-2931. https://doi.org/10.1091/mbc.E16-05-0271

Chan, J. N., Poon, B. P., Salvi, J., Olsen, J. B., Emili, A., & Mekhail, K. (2011, Jun 14). Perinuclear cohibin complexes maintain replicative life span via roles at distinct silent chromatin domains. *Dev Cell, 20*(6), 867-879. https://doi.org/10.1016/j.devcel.2011.05.014

Chang, Q., Nitta, R., Inoue, S., & Hirokawa, N. (2013, Jun 12). Structural basis for the ATP-induced isomerization of kinesin. *J Mol Biol, 425*(11), 1869-1880. https://doi.org/10.1016/j.jmb.2013.03.004

Chapman, J. R., Sossick, A. J., Boulton, S. J., & Jackson, S. P. (2012, Aug 1). BRCA1-associated exclusion of 53BP1 from DNA damage sites underlies temporal control of DNA repair. *J Cell Sci, 125*(Pt 15), 3529-3534. https://doi.org/10.1242/jcs.105353

Chatterjee, C., Benoit, Matthieu P. M. H., DePaoli, V., Diaz-Valencia, Juan D., Asenjo, Ana B., Gerfen, Gary J., Sharp, David J., & Sosa, H. (2016). Distinct Interaction Modes of the Kinesin-13 Motor Domain with the Microtubule. *Biophysical Journal, 110*(7), 1593-1604. https://doi.org/10.1016/j.bpj.2016.02.029

Chatterjee, N., & Walker, G. C. (2017, Jun). Mechanisms of DNA damage, repair, and mutagenesis. *Environ Mol Mutagen, 58*(5), 235-263. https://doi.org/10.1002/em.22087

Chatterji, P., Alegria, M., & Takeuchi, D. (2011, Sep). Psychiatric disorders and labor market outcomes: evidence from the National Comorbidity Survey-Replication. *J Health Econ, 30*(5), 858-868. https://doi.org/10.1016/j.jhealeco.2011.06.006

Chrétien, D., Fuller, S. D., & Karsenti, E. (1995, Jun). Structure of growing microtubule ends: two-dimensional sheets close into tubes at variable rates. *J Cell Biol, 129*(5), 1311-1328. https://doi.org/10.1083/jcb.129.5.1311

Chrétien, D., Metoz, F., Verde, F., Karsenti, E., & Wade, R. (1992). Lattice defects in microtubules: protofilament numbers vary within individual microtubules. *Journal of Cell Biology, 117*(5), 1031-1040. https://doi.org/10.1083/jcb.117.5.1031

Chuang, C. H., Carpenter, A. E., Fuchsova, B., Johnson, T., de Lanerolle, P., & Belmont, A. S. (2006, Apr 18). Long-range directional movement of an interphase chromosome site [Research Support, N.I.H., Extramural
Research Support, Non-U.S. Gov't
Research Support, U.S. Gov't, Non-P.H.S.]. *Curr Biol, 16*(8), 825-831. https://doi.org/10.1016/j.cub.2006.03.059

Chumová, J., Kourová, H., Trögelová, L., Halada, P., & Binarová, P. (2019). Microtubular and Nuclear Functions of γ-Tubulin: Are They LINCed? *Cells, 8*(3), 259. https://doi.org/10.3390/cells8030259

Chung, D. K., Chan, J. N., Strecker, J., Zhang, W., Ebrahimi-Ardebili, S., Lu, T., Abraham, K. J., Durocher, D., & Mekhail, K. (2015, Jul 24). Perinuclear tethers license telomeric DSBs for a broad kinesin- and NPC-dependent DNA repair process [Research Support, Non-U.S. Gov't]. *Nat Commun, 6*, 7742. https://doi.org/10.1038/ncomms8742

Chung, I., & Zhao, X. (2015). DNA break-induced sumoylation is enabled by collaboration between a SUMO ligase and the ssDNA-binding complex RPA. *Genes & development, 29*(15), 1593-1598. https://doi.org/10.1101/gad.265058.115

Cooper, J. R., Wagenbach, M., Asbury, C. L., & Wordeman, L. (2010, Jan). Catalysis of the microtubule on-rate is the major parameter regulating the depolymerase activity of MCAK. *Nat Struct Mol Biol, 17*(1), 77-82. https://doi.org/10.1038/nsmb.1728

Cope, J., Gilbert, S., Rayment, I., Mastronarde, D., & Hoenger, A. (2010, 2010/05/01/). Cryo-electron tomography of microtubule–kinesin motor complexes. *Journal of Structural Biology, 170*(2), 257-265. https://doi.org/https://doi.org/10.1016/j.jsb.2009.12.004

Dahl, E. S., & Aird, K. M. (2017, 2017-November-29). Ataxia-Telangiectasia Mutated Modulation of Carbon Metabolism in Cancer [Mini Review]. *7*(291). https://doi.org/10.3389/fonc.2017.00291

David-Pfeuty, T., Erickson, H. P., & Pantaloni, D. (1977). Guanosinetriphosphatase activity of tubulin associated with microtubule assembly. *74*(12), 5372-5376. https://doi.org/10.1073/pnas.74.12.5372 %J Proceedings of the National Academy of Sciences

Davis, A. J., & Chen, D. J. (2013, Jun). DNA double strand break repair via non-homologous end-joining. *Transl Cancer Res, 2*(3), 130-143. https://doi.org/10.3978/j.issn.2218-676X.2013.04.02

Davis, I. W., Leaver-Fay, A., Chen, V. B., Block, J. N., Kapral, G. J., Wang, X., Murray, L. W., Arendall, W. B., Snoeyink, J., Richardson, J. S., & Richardson, D. C. (2007, Jul). MolProbity: all-atom contacts and structure validation for proteins and nucleic acids. *Nucleic Acids Research, 35*, W375-W383. https://doi.org/10.1093/nar/gkm216

De Brabander, M., Geuens, G., Nuydens, R., Willebrords, R., & De Mey, J. (1981). Taxol Induces the Assembly of Free Microtubules in Living Cells and Blocks the Organizing Capacity of the Centrosomes and Kinetochores. *Proceedings of the National Academy of Sciences of the United States of America, 78*(9), 5608-5612. http://www.jstor.org/stable/11514

Demidenko, Z. N., Kalurupalle, S., Hanko, C., Lim, C. u., Broude, E., & Blagosklonny, M. V. (2008, 2008/07/01). Mechanism of G1-like arrest by low concentrations of paclitaxel: next cell cycle p53-dependent arrest with sub G1 DNA content mediated by prolonged mitosis. *Oncogene, 27*(32), 4402-4410. https://doi.org/10.1038/onc.2008.82

Deng, C.-X. (2006). BRCA1: cell cycle checkpoint, genetic instability, DNA damage response and cancer evolution. *Nucleic Acids Research, 34*(5), 1416-1426. https://doi.org/10.1093/nar/gkl010

Desai, A., & Mitchison, T. J. (1997). Microtubule polymerization dynamics. *Annu Rev Cell Dev Biol, 13*, 83-117. https://doi.org/10.1146/annurev.cellbio.13.1.83

Desai, A., Verma, S., Mitchison, T. J., & Walczak, C. E. (1999, Jan 8). Kin I kinesins are microtubule-destabilizing enzymes. *Cell, 96*(1), 69-78. https://doi.org/10.1016/s0092-8674(00)80960-5

Dimitrov, A., Quesnoit, M. l., Moutel, S., Cantaloube, I., Poüs, C., & Perez, F. (2008). Detection of GTP-Tubulin Conformation in Vivo Reveals a Role for GTP Remnants in Microtubule Rescues. *Science, 322*(5906), 1353-1356. https://doi.org/10.1126/science.1165401

Dimitrova, N., Chen, Y. C., Spector, D. L., & de Lange, T. (2008, Nov 27). 53BP1 promotes non-homologous end joining of telomeres by increasing chromatin mobility. *Nature, 456*(7221), 524-528. https://doi.org/10.1038/nature07433

Dogterom, M., Kerssemakers, J. W., Romet-Lemonne, G., & Janson, M. E. (2005, Feb). Force generation by dynamic microtubules [Research Support, Non-U.S. Gov't
Review]. *Curr Opin Cell Biol, 17*(1), 67-74. https://doi.org/10.1016/j.ceb.2004.12.011

Donhauser, Z. J., Appadoo, V., Kliman, E. J., Jobs, W. B., & Sheffield, E. C. (2018). Structural Changes in Tubulin Sheets Caused by Immobilization on Solid Supports. *ACS omega, 3*(12), 18196-18202. https://doi.org/10.1021/acsomega.8b02475

Drechsel, D. N., & Kirschner, M. W. (1994, Dec 1). The minimum GTP cap required to stabilize microtubules. *Curr Biol, 4*(12), 1053-1061. https://doi.org/10.1016/s0960-9822(00)00243-8

Duellberg, C., Cade, N. I., Holmes, D., & Surrey, T. (2016). The size of the EB cap determines instantaneous microtubule stability. *eLife, 5*, e13470
C13471 - eLife 12016;13475:e13470. https://doi.org/10.7554/eLife.13470

Dumontet, C., & Jordan, M. A. (2010, Oct). Microtubule-binding agents: a dynamic field of cancer therapeutics. *Nat Rev Drug Discov, 9*(10), 790-803. https://doi.org/10.1038/nrd3253

Dziadkowiec, K. N., Gąsiorowska, E., Nowak-Markwitz, E., & Jankowska, A. (2016, Dec). PARP inhibitors: review of mechanisms of action and BRCA1/2 mutation targeting. *Prz Menopauzalny, 15*(4), 215-219. https://doi.org/10.5114/pm.2016.65667

Elie-Caille, C., Severin, F., Helenius, J., Howard, J., Muller, D. J., & Hyman, A. A. (2007, Oct 23). Straight GDP-tubulin protofilaments form in the presence of taxol. *Curr Biol, 17*(20), 1765-1770. https://doi.org/10.1016/j.cub.2007.08.063

Ems-McClung, S. C., Hertzer, K. M., Zhang, X., Miller, M. W., & Walczak, C. E. (2007, Jan). The interplay of the N- and C-terminal domains of MCAK control microtubule depolymerization activity and spindle assembly. *Mol Biol Cell, 18*(1), 282-294. https://doi.org/10.1091/mbc.E06-08-0724

Emsley, P., & Cowtan, K. (2004, Dec). Coot: model-building tools for molecular graphics. *Acta Crystallogr D Biol Crystallogr, 60*(Pt 12 Pt 1), 2126-2132. http://www.ncbi.nlm.nih.gov/entrez/query.fcgi?cmd=Retrieve&db=PubMed&dopt=Citation&list_uids=15572765

Erickson, H. P., & O'Brien, E. T. (1992). Microtubule Dynamic Instability and GTP Hydrolysis. *Annual Review of Biophysics and Biomolecular Structure, 21*(1), 145-166. https://doi.org/10.1146/annurev.bb.21.060192.001045

Erickson, H. P., & Pantaloni, D. (1981). The role of subunit entropy in cooperative assembly. Nucleation of microtubules and other two-dimensional polymers. *Biophysical Journal, 34*(2), 293-309. https://doi.org/10.1016/s0006-3495(81)84850-3

Escribano-Díaz, C., Orthwein, A., Fradet-Turcotte, A., Xing, M., Young, J. T., Tkáč, J., Cook, M. A., Rosebrock, A. P., Munro, M., Canny, M. D., Xu, D., & Durocher, D. (2013, Mar 7). A cell cycle-dependent regulatory circuit composed of 53BP1-RIF1 and BRCA1-CtIP controls DNA repair pathway choice. *Mol Cell, 49*(5), 872-883. https://doi.org/10.1016/j.molcel.2013.01.001

Evans, L., Mitchison, T., & Kirschner, M. (1985, Apr). Influence of the centrosome on the structure of nucleated microtubules. *J Cell Biol, 100*(4), 1185-1191. https://doi.org/10.1083/jcb.100.4.1185

Fanale, D., Bronte, G., Passiglia, F., Calò, V., Castiglia, M., Di Piazza, F., Barraco, N., Cangemi, A., Catarella, M. T., Insalaco, L., Listì, A., Maragliano, R., Massihnia, D., Perez, A., Toia, F., Cicero, G., & Bazan, V. (2015). Stabilizing versus destabilizing the microtubules: a double-edge sword for an effective cancer treatment option? *Analytical cellular pathology (Amsterdam), 2015*, 690916-690916. https://doi.org/10.1155/2015/690916

Feroz, W., & Sheikh, A. M. A. (2020, 2020/11/16). Exploring the multiple roles of guardian of the genome: P53. *Egyptian Journal of Medical Human Genetics, 21*(1), 49. https://doi.org/10.1186/s43042-020-00089-x

Fischbach, A., Krüger, A., Hampp, S., Assmann, G., Rank, L., Hufnagel, M., Stöckl, M. T., Fischer, J. M. F., Veith, S., Rossatti, P., Ganz, M., Ferrando-May, E., Hartwig, A., Hauser, K., Wiesmüller, L., Bürkle, A., & Mangerich, A. (2018). The C-terminal domain of p53 orchestrates the interplay between non-covalent and covalent poly(ADP-ribosyl)ation of p53 by PARP1. *Nucleic Acids Research, 46*(2), 804-822. https://doi.org/10.1093/nar/gkx1205

Forth, S., & Kapoor, T. M. (2017, Jun 5). The mechanics of microtubule networks in cell division. *J Cell Biol, 216*(6), 1525-1531. https://doi.org/10.1083/jcb.201612064

Francis, R., Xu, X., Park, H., Wei, C.-J., Chang, S., Chatterjee, B., & Lo, C. (2011). Connexin43 Modulates Cell Polarity and Directional Cell Migration by Regulating Microtubule Dynamics. *PLOS ONE, 6*(10), e26379. https://doi.org/10.1371/journal.pone.0026379

Frank-Vaillant, M., & Marcand, S. (2002, Nov). Transient stability of DNA ends allows nonhomologous end joining to precede homologous recombination. *Mol Cell, 10*(5), 1189-1199. https://doi.org/10.1016/s1097-2765(02)00705-0

Franke, D., & Svergun, D. I. (2009, Apr). DAMMIF, a program for rapid ab-initio shape determination in small-angle scattering. *Journal of Applied Crystallography, 42*, 342-346. https://doi.org/10.1107/S0021889809000338

Friel, C. T., & Howard, J. (2011, Aug 26). The kinesin-13 MCAK has an unconventional ATPase cycle adapted for microtubule depolymerization. *EMBO J, 30*(19), 3928-3939. https://doi.org/10.1038/emboj.2011.290

Friel, C. T., & Welburn, J. P. (2018, Dec 17). Parts list for a microtubule depolymerising kinesin. *Biochem Soc Trans, 46*(6), 1665-1672. https://doi.org/10.1042/bst20180350

Fukushige, T., Siddiqui, Z. K., Chou, M., Culotti, J. G., Gogonea, C. B., Siddiqui, S. S., & Hamelin, M. (1999, Feb). MEC-12, an alpha-tubulin required for touch sensitivity in C. elegans. *J Cell Sci, 112 (Pt 3)*, 395-403.

Ganem, N. J., Upton, K., & Compton, D. A. (2005, Oct 25). Efficient mitosis in human cells lacking poleward microtubule flux. *Curr Biol, 15*(20), 1827-1832. https://doi.org/10.1016/j.cub.2005.08.065

Ganguly, A., Bhattacharya, R., & Cabral, F. (2008). Cell cycle dependent degradation of MCAK: evidence against a role in anaphase chromosome movement. *Cell cycle (Georgetown, Tex.), 7*(20), 3187-3193. https://doi.org/10.4161/cc.7.20.6814

Gatlin, J. C., & Bloom, K. (2010). Microtubule motors in eukaryotic spindle assembly and maintenance. *Seminars in cell & developmental biology, 21*(3), 248-254. https://doi.org/10.1016/j.semcdb.2010.01.015

Gigant, B., Cormier, A., Dorléans, A., Ravelli, R. B., & Knossow, M. (2009). Microtubule-destabilizing agents: structural and mechanistic insights from the interaction of colchicine and vinblastine with tubulin. *Top Curr Chem, 286*, 259-278. https://doi.org/10.1007/128_2008_11

Gigant, B., Curmi, P. A., Martin-Barbey, C., Charbaut, E., Lachkar, S., Lebeau, L., Siavoshian, S., Sobel, A., & Knossow, M. (2000, Sep 15). The 4 A X-ray structure of a tubulin:stathmin-like domain complex. *Cell, 102*(6), 809-816. http://www.ncbi.nlm.nih.gov/pubmed/11030624

Gigant, B., Wang, W., Dreier, B., Jiang, Q., Pecqueur, L., Pluckthun, A., Wang, C., & Knossow, M. (2013, Aug). Structure of a kinesin-tubulin complex and implications for kinesin motility [Research Support, Non-U.S. Gov't]. *Nat Struct Mol Biol, 20*(8), 1001-1007. https://doi.org/10.1038/nsmb.2624

Giglia-Mari, G., Zotter, A., & Vermeulen, W. (2011, Jan 1). DNA damage response. *Cold Spring Harb Perspect Biol, 3*(1), a000745. https://doi.org/10.1101/cshperspect.a000745

Goodarzi, A. A., & Jeggo, P. A. (2013). The repair and signaling responses to DNA double-strand breaks. *Adv Genet, 82*, 1-45. https://doi.org/10.1016/B978-0-12-407676-1.00001-9

Grafmüller, A., Noya, E. G., & Voth, G. A. (2013). Nucleotide-dependent lateral and longitudinal interactions in microtubules. *J Mol Biol, 425*(12), 2232-2246.

Graml, V., Studera, X., Lawson, J. L. D., Chessel, A., Geymonat, M., Bortfeld-Miller, M., Walter, T., Wagstaff, L., Piddini, E., & Carazo Salas, R. E. (2014, Oct 27). A genomic Multiprocess survey of machineries that control and link cell shape, microtubule organization, and cell-cycle progression. *Dev Cell, 31*(2), 227-239. https://doi.org/10.1016/j.devcel.2014.09.005

Grosse, R., & Vartiainen, M. K. (2013, Nov). To be or not to be assembled: progressing into nuclear actin filaments [Research Support, Non-U.S. Gov't
Review]. *Nat Rev Mol Cell Biol, 14*(11), 693-697. https://doi.org/10.1038/nrm3681

Grove, T. L., Lee, K. H., St Clair, J., Krebs, C., & Booker, S. J. (2008, Jul 15). In vitro characterization of AtsB, a radical SAM formylglycine-generating enzyme that contains three [4Fe-4S] clusters. *Biochemistry, 47*(28), 7523-7538. https://doi.org/10.1021/bi8004297

Guesdon, A., Bazile, F., Buey, R. M., Mohan, R., Monier, S., García, R. R., Angevin, M., Heichette, C., Wieneke, R., Tampé, R., Duchesne, L., Akhmanova, A., Steinmetz, M. O., & Chrétien, D. (2016, Oct). EB1 interacts with outwardly curved and straight regions of

the microtubule lattice. *Nat Cell Biol, 18*(10), 1102-1108. https://doi.org/10.1038/ncb3412

Gunn, A., & Stark, J. M. (2012). I-SceI-based assays to examine distinct repair outcomes of mammalian chromosomal double strand breaks. *Methods Mol Biol, 920*, 379-391. https://doi.org/10.1007/978-1-61779-998-3_27

Guo, Z., Sheng, Y., Kumagai, A., & Dunphy, W. G. (1999, NOV). Response of Xenopus egg extracts to damaged DNA. *Molecular Biology of the Cell, 10*, 3A-3A. <Go to ISI>://000083673500014

Gupta, M. L., Carvalho, P., Roof, D. M., & Pellman, D. (2006). Plus end-specific depolymerase activity of Kip3, a kinesin-8 protein, explains its role in positioning the yeast mitotic spindle. *Nature Cell Biology, 8*(9), 913-923. https://doi.org/10.1038/ncb1457

Haince, J. F., Kozlov, S., Dawson, V. L., Dawson, T. M., Hendzel, M. J., Lavin, M. F., & Poirier, G. G. (2007, Jun 1). Ataxia telangiectasia mutated (ATM) signaling network is modulated by a novel poly(ADP-ribose)-dependent pathway in the early response to DNA-damaging agents. *J Biol Chem, 282*(22), 16441-16453. https://doi.org/10.1074/jbc.M608406200

Hanssen-Bauer, A., Solvang-Garten, K., Akbari, M., & Otterlei, M. (2012). X-ray repair cross complementing protein 1 in base excision repair. *International journal of molecular sciences, 13*(12), 17210-17229. https://doi.org/10.3390/ijms131217210

Harkcom, W. T., Ghosh, A. K., Sung, M. S., Matov, A., Brown, K. D., Giannakakou, P., & Jaffrey, S. R. (2014). NAD⁺ and SIRT3 control microtubule dynamics and reduce susceptibility to antimicrotubule agents. *111*(24), E2443-E2452. https://doi.org/doi:10.1073/pnas.1404269111

Harris, J. L., Jakob, B., Taucher-Scholz, G., Dianov, G. L., Becherel, O. J., & Lavin, M. F. (2009). Aprataxin, poly-ADP ribose polymerase 1 (PARP-1) and apurinic endonuclease 1 (APE1) function together to protect the genome against oxidative damage. *Human Molecular Genetics, 18*(21), 4102-4117. https://doi.org/10.1093/hmg/ddp359

Hauer, M. H., & Gasser, S. M. (2017, Nov 15). Chromatin and nucleosome dynamics in DNA damage and repair [Research Support, Non-U.S. Gov't
Review]. *Genes Dev, 31*(22), 2204-2221. https://doi.org/10.1101/gad.307702.117

Hayden, J. H., Bowser, S. S., & Rieder, C. L. (1990, Sep). Kinetochores capture astral microtubules during chromosome attachment to the mitotic spindle: direct visualization in live newt lung cells. *J Cell Biol, 111*(3), 1039-1045. https://doi.org/10.1083/jcb.111.3.1039

Heald, R., & Nogales, E. (2002, Jan 01). Microtubule dynamics. *J Cell Sci, 115*(Pt 1), 3-4. http://www.ncbi.nlm.nih.gov/pubmed/11801717

Helenius, J., Brouhard, G., Kalaidzidis, Y., Diez, S., & Howard, J. (2006, 2006/05/01). The depolymerizing kinesin MCAK uses lattice diffusion to rapidly target microtubule ends. *Nature, 441*(7089), 115-119. https://doi.org/10.1038/nature04736

Hertzer, K. M., Ems-McClung, S. C., Kline-Smith, S. L., Lipkin, T. G., Gilbert, S. P., & Walczak, C. E. (2006, Feb). Full-length dimeric MCAK is a more efficient microtubule depolymerase than minimal domain monomeric MCAK. *Mol Biol Cell, 17*(2), 700-710. https://doi.org/10.1091/mbc.E05-08-0821

Hirokawa, N., Noda, Y., Tanaka, Y., & Niwa, S. (2009, Oct). Kinesin superfamily motor proteins and intracellular transport. *Nat Rev Mol Cell Biol, 10*(10), 682-696. https://doi.org/nrm2774 [pii]
10.1038/nrm2774

Holy, T. E., & Leibler, S. (1994, Jun 7). Dynamic instability of microtubules as an efficient way to search in space. *Proc Natl Acad Sci U S A, 91*(12), 5682-5685. https://doi.org/10.1073/pnas.91.12.5682

Horio, T., & Murata, T. (2014). The role of dynamic instability in microtubule organization. *Front Plant Sci, 5*, 511. https://doi.org/10.3389/fpls.2014.00511

Howard, J., & Hyman, A. A. (2003, 2003/04/01). Dynamics and mechanics of the microtubule plus end. *Nature, 422*(6933), 753-758. https://doi.org/10.1038/nature01600

Howard, J., & Hyman, A. A. (2007). Microtubule polymerases and depolymerases. *Curr Opin Cell Biol, 19*(1), 31-35.

Howard, W. D., & Timasheff, S. N. (1986, Dec 16). GDP state of tubulin: stabilization of double rings. *Biochemistry, 25*(25), 8292-8300. https://doi.org/10.1021/bi00373a025

Huen, M. S., & Chen, J. (2010, Feb). Assembly of checkpoint and repair machineries at DNA damage sites [Review]. *Trends Biochem Sci, 35*(2), 101-108. https://doi.org/10.1016/j.tibs.2009.09.001

Hume, A. N., & Seabra, M. C. (2011, Oct). Melanosomes on the move: a model to understand organelle dynamics. *Biochem Soc Trans, 39*(5), 1191-1196. https://doi.org/10.1042/bst0391191

Hunter, A. W., Caplow, M., Coy, D. L., Hancock, W. O., Diez, S., Wordeman, L., & Howard, J. (2003, Feb). The kinesin-related protein MCAK is a microtubule depolymerase that forms an ATP-hydrolyzing complex at microtubule ends. *Mol Cell, 11*(2), 445-457. https://doi.org/10.1016/s1097-2765(03)00049-2

Hunter, B., & Allingham, J. S. (2020, 2020/08/01). These motors were made for walking [https://doi.org/10.1002/pro.3895]. *Protein Science, 29*(8), 1707-1723. https://doi.org/https://doi.org/10.1002/pro.3895

Hyman, A. A., Middleton, K., Centola, M., Mitchison, T. J., & Carbon, J. (1992, 1992/10/01). Microtubule-motor activity of a yeast centromere-binding protein complex. *Nature, 359*(6395), 533-536. https://doi.org/10.1038/359533a0

Hyman, A. A., Salser, S., Drechsel, D. N., Unwin, N., & Mitchison, T. J. (1992, Oct). Role of GTP hydrolysis in microtubule dynamics: information from a slowly hydrolyzable analogue, GMPCPP [Research Support, Non-U.S. Gov't
Research Support, U.S. Gov't, P.H.S.]. *Mol Biol Cell, 3*(10), 1155-1167. http://www.ncbi.nlm.nih.gov/pubmed/1421572

Isono, M., Niimi, A., Oike, T., Hagiwara, Y., Sato, H., Sekine, R., Yoshida, Y., Isobe, S. Y., Obuse, C., Nishi, R., Petricci, E., Nakada, S., Nakano, T., & Shibata, A. (2017, Jan 10). BRCA1 Directs the Repair Pathway to Homologous Recombination by Promoting 53BP1 Dephosphorylation. *Cell Rep, 18*(2), 520-532. https://doi.org/10.1016/j.celrep.2016.12.042

Jackson, S. P., & Bartek, J. (2009, Oct 22). The DNA-damage response in human biology and disease. *Nature, 461*(7267), 1071-1078. https://doi.org/10.1038/nature08467

Jalal, S., Earley, J. N., & Turchi, J. J. (2011, Nov 15). DNA repair: from genome maintenance to biomarker and therapeutic target [Research Support, N.I.H., Extramural
Review]. *Clin Cancer Res, 17*(22), 6973-6984. https://doi.org/10.1158/1078-0432.CCR-11-0761

Janosi, I. M., Chretien, D., & Flyvbjerg, H. (2002, Sep). Structural microtubule cap: stability, catastrophe, rescue, and third state. *Biophys J, 83*(3), 1317-1330. https://doi.org/10.1016/S0006-3495(02)73902-7

Jasin, M., & Rothstein, R. (2013, Nov 01). Repair of strand breaks by homologous recombination [Research Support, N.I.H., Extramural
Review]. *Cold Spring Harb Perspect Biol, 5*(11), a012740. https://doi.org/10.1101/cshperspect.a012740

Johnson, V., Ayaz, P., Huddleston, P., & Rice, L. M. (2011, Oct 11). Design, overexpression, and purification of polymerization-blocked yeast αβ-tubulin mutants. *Biochemistry, 50*(40), 8636-8644. https://doi.org/10.1021/bi2005174

Juhász, S., Smith, R., Schauer, T., Spekhardt, D., Mamar, H., Zentout, S., Chapuis, C., Huet, S., & Timinszky, G. (2020). The chromatin remodeler ALC1 underlies resistance to PARP inhibitor treatment. *6*(51), eabb8626. https://doi.org/doi:10.1126/sciadv.abb8626

Kalantari, S., & Filges, I. (2020). 'Kinesinopathies': emerging role of the kinesin family member genes in birth defects. *57*(12), 797-807. https://doi.org/10.1136/jmedgenet-2019-106769 %J Journal of Medical Genetics

Kalra, A. P., Kar, P., Preto, J., Rezania, V., Dogariu, A., Lewis, J. D., Tuszynski, J. A., & Shankar, K. (2019). Behavior of α, β tubulin in DMSO-containing electrolytes [10.1039/C9NA00035F]. *Nanoscale Advances, 1*(9), 3364-3371. https://doi.org/10.1039/C9NA00035F

Kastenhuber, E. R., & Lowe, S. W. (2017, Sep 7). Putting p53 in Context. *Cell, 170*(6), 1062-1078. https://doi.org/10.1016/j.cell.2017.08.028

Kaverina, I., & Straube, A. (2011). Regulation of cell migration by dynamic microtubules. *Seminars in cell & developmental biology, 22*(9), 968-974. https://doi.org/10.1016/j.semcdb.2011.09.017

Kikkawa, M. (2008). The role of microtubules in processive kinesin movement. *Trends in Cell Biology, 18*(3), 128-135. https://doi.org/10.1016/j.tcb.2008.01.002

Kim, M. Y., Zhang, T., & Kraus, W. L. (2005, Sep 1). Poly(ADP-ribosyl)ation by PARP-1: 'PAR-laying' NAD+ into a nuclear signal. *Genes Dev, 19*(17), 1951-1967. https://doi.org/10.1101/gad.1331805

Kirli, K., Karaca, S., Dehne, H. J., Samwer, M., Pan, K. T., Lenz, C., Urlaub, H., & Gorlich, D. (2015, Dec 17). A deep proteomics perspective on CRM1-mediated nuclear export and nucleocytoplasmic partitioning. *Elife, 4*. https://doi.org/10.7554/eLife.11466

Kline-Smith, S. L., Khodjakov, A., Hergert, P., & Walczak, C. E. (2004, Mar). Depletion of centromeric MCAK leads to chromosome congression and segregation defects due to improper kinetochore attachments. *Molecular Biology of the Cell, 15*(3), 1146-1159. https://doi.org/10.1091/mbc.e03-08-0581

Knossow, M., Campanacci, V., Khodja, L. A., & Gigant, B. (2020). The Mechanism of Tubulin Assembly into Microtubules: Insights from Structural Studies. *iScience, 23*(9), 101511-101511. https://doi.org/10.1016/j.isci.2020.101511

Kolas, N. K., Chapman, J. R., Nakada, S., Ylanko, J., Chahwan, R., Sweeney, F. D., Panier, S., Mendez, M., Wildenhain, J., Thomson, T. M., Pelletier, L., Jackson, S. P., & Durocher, D. (2007, Dec 7). Orchestration of the DNA-damage response by the RNF8 ubiquitin ligase. *Science, 318*(5856), 1637-1640. https://doi.org/10.1126/science.1150034

Kolodner, R. D., Putnam, C. D., & Myung, K. (2002, Jul 26). Maintenance of genome stability in Saccharomyces cerevisiae. *Science, 297*(5581), 552-557. https://doi.org/10.1126/science.1075277

Krawczyk, P. M., Borovski, T., Stap, J., Cijsouw, T., ten Cate, R., Medema, J. P., Kanaar, R., Franken, N. A., & Aten, J. A. (2012, May 01). Chromatin mobility is increased at sites of DNA double-strand breaks. *J Cell Sci, 125*(Pt 9), 2127-2133. https://doi.org/10.1242/jcs.089847

Kueh, H. Y., & Mitchison, T. J. (2009, Aug 21). Structural plasticity in actin and tubulin polymer dynamics. *Science, 325*(5943), 960-963. https://doi.org/10.1126/science.1168823

Kumeta, M., Hirai, Y., Yoshimura, S. H., Horigome, T., & Takeyasu, K. (2013, Dec 10). Antibody-based analysis reveals "filamentous vs. non-filamentous" and "cytoplasmic vs. nuclear" crosstalk of cytoskeletal proteins. *Exp Cell Res, 319*(20), 3226-3237. https://doi.org/10.1016/j.yexcr.2013.07.021

Laan, L., Pavin, N., Husson, J., Romet-Lemonne, G., van Duijn, M., López, M. P., Vale, R. D., Jülicher, F., Reck-Peterson, S. L., & Dogterom, M. (2012). Cortical dynein controls microtubule dynamics to generate pulling forces that position microtubule asters. *Cell, 148*(3), 502-514. https://doi.org/10.1016/j.cell.2012.01.007

Langelier, M. F., & Pascal, J. M. (2013, Feb). PARP-1 mechanism for coupling DNA damage detection to poly(ADP-ribose) synthesis. *Curr Opin Struct Biol, 23*(1), 134-143. https://doi.org/10.1016/j.sbi.2013.01.003

Laporte, D., Courtout, F., Salin, B., Ceschin, J., & Sagot, I. (2013, Nov 25). An array of nuclear microtubules reorganizes the budding yeast nucleus during quiescence [Research Support, Non-U.S. Gov't]. *J Cell Biol, 203*(4), 585-594. https://doi.org/10.1083/jcb.201306075

Lavin, M. F., Kozlov, S., Gatei, M., & Kijas, A. W. (2015). ATM-Dependent Phosphorylation of All Three Members of the MRN Complex: From Sensor to Adaptor. *Biomolecules, 5*(4), 2877-2902. https://doi.org/10.3390/biom5042877

Lawrence, C. J., Dawe, R. K., Christie, K. R., Cleveland, D. W., Dawson, S. C., Endow, S. A., Goldstein, L. S., Goodson, H. V., Hirokawa, N., Howard, J., Malmberg, R. L., McIntosh, J. R., Miki, H., Mitchison, T. J., Okada, Y., Reddy, A. S., Saxton, W. M., Schliwa, M., Scholey, J. M., Vale, R. D., Walczak, C. E., & Wordeman, L. (2004, Oct 11). A standardized kinesin nomenclature. *J Cell Biol, 167*(1), 19-22. https://doi.org/10.1083/jcb.200408113

Lawrimore, J., Barry, T. M., Barry, R. M., York, A. C., Friedman, B., Cook, D. M., Akialis, K., Tyler, J., Vasquez, P., Yeh, E., & Bloom, K. (2017, Jun 15). Microtubule dynamics drive enhanced chromatin motion and mobilize telomeres in response to DNA damage. *Mol Biol Cell, 28*(12), 1701-1711. https://doi.org/10.1091/mbc.E16-12-0846

Lemaitre, C., & Soutoglou, E. (2015, Feb 13). DSB (Im)mobility and DNA repair compartmentalization in mammalian cells [Review]. *J Mol Biol, 427*(3), 652-658. https://doi.org/10.1016/j.jmb.2014.11.014

Lempiäinen, H., & Halazonetis, T. D. (2009, Oct 21). Emerging common themes in regulation of PIKKs and PI3Ks. *Embo j, 28*(20), 3067-3073. https://doi.org/10.1038/emboj.2009.281

Lesca, C., Germanier, M., Raynaud-Messina, B., Pichereaux, C., Etievant, C., Emond, S., Burlet-Schiltz, O., Monsarrat, B., Wright, M., & Defais, M. (2005, Aug 4). DNA damage induce gamma-tubulin-RAD51 nuclear complexes in mammalian cells [Research Support, Non-U.S. Gov't]. *Oncogene, 24*(33), 5165-5172. https://doi.org/10.1038/sj.onc.1208723

Lesca, C., Germanier, M., Raynaud-Messina, B., Pichereaux, C., Etievant, C., Emond, S., Burlet-Schiltz, O., Monsarrat, B., Wright, M., & Defais, M. (2005, 2005/08/01). DNA damage induce γ-tubulin–RAD51 nuclear complexes in mammalian cells. *Oncogene, 24*(33), 5165-5172. https://doi.org/10.1038/sj.onc.1208723

Levi, V., Ruan, Q., Plutz, M., Belmont, A. S., & Gratton, E. (2005, Dec). Chromatin dynamics in interphase cells revealed by tracking in a two-photon excitation microscope [Research Support, N.I.H., Extramural
Research Support, Non-U.S. Gov't]. *Biophys J, 89*(6), 4275-4285. https://doi.org/10.1529/biophysj.105.066670

Li, L.-y., Guan, Y.-d., Chen, X.-s., Yang, J.-m., & Cheng, Y. (2021, 2021-February-08). DNA Repair Pathways in Cancer Therapy and Resistance [Review]. *11*(2520). https://doi.org/10.3389/fphar.2020.629266

Li, L., & Zou, L. (2005, Feb 1). Sensing, signaling, and responding to DNA damage: organization of the checkpoint pathways in mammalian cells [Research Support, U.S. Gov't, P.H.S.
Review]. *Journal of Cellular Biochemistry, 94*(2), 298-306. https://doi.org/10.1002/jcb.20355

Lian, H.-Y., Jiao, G.-Z., Wang, H.-L., Tan, X.-W., Wang, T.-Y., Zheng, L.-L., Kong, Q.-Q., & Tan, J.-H. (2014). Role of Cytoskeleton in Regulating Fusion of Nucleoli: A Study Using the Activated Mouse Oocyte Model1. *Biology of Reproduction, 91*(3). https://doi.org/10.1095/biolreprod.114.120188

Liang, Y., Lin, S. Y., Brunicardi, F. C., Goss, J., & Li, K. (2009, Apr). DNA damage response pathways in tumor suppression and cancer treatment [Research Support, N.I.H., Extramural
Review]. *World J Surg, 33*(4), 661-666. https://doi.org/10.1007/s00268-008-9840-1

Lieber, M. R. (2010). The mechanism of double-strand DNA break repair by the nonhomologous DNA end-joining pathway [Review]. *Annu Rev Biochem, 79*, 181-211. https://doi.org/10.1146/annurev.biochem.052308.093131

Lisby, M., Barlow, J. H., Burgess, R. C., & Rothstein, R. (2004). Choreography of the DNA Damage Response: Spatiotemporal Relationships among Checkpoint and Repair Proteins. *Cell, 118*(6), 699-713. https://doi.org/10.1016/j.cell.2004.08.015

Lisby, M., Mortensen, U. H., & Rothstein, R. (2003, Jun). Colocalization of multiple DNA double-strand breaks at a single Rad52 repair centre [Research Support, Non-U.S. Gov't Research Support, U.S. Gov't, P.H.S.]. *Nat Cell Biol, 5*(6), 572-577. https://doi.org/10.1038/ncb997

Lloyd, C., & Chan, J. (2006, 2006/02/01). Not so divided: the common basis of plant and animal cell division. *Nature Reviews Molecular Cell Biology, 7*(2), 147-152. https://doi.org/10.1038/nrm1831

Locke, J., Joseph, A. P., Peña, A., Möckel, M. M., Mayer, T. U., Topf, M., & Moores, C. A. (2017). Structural basis of human kinesin-8 function and inhibition. *Proceedings of the National Academy of Sciences, 114*(45), E9539-E9548. https://doi.org/10.1073/pnas.1712169114

Lord, C. J., Tutt, A. N., & Ashworth, A. (2015). Synthetic lethality and cancer therapy: lessons learned from the development of PARP inhibitors. *Annu Rev Med, 66*, 455-470. https://doi.org/10.1146/annurev-med-050913-022545

Lottersberger, F., Karssemeijer, R. A., Dimitrova, N., & de Lange, T. (2015, Nov 5). 53BP1 and the LINC Complex Promote Microtubule-Dependent DSB Mobility and DNA Repair. *Cell, 163*(4), 880-893. https://doi.org/10.1016/j.cell.2015.09.057

Lou, Z., & Chen, J. (2005). Mammalian DNA damage response pathway [Review]. *Adv Exp Med Biol, 570*, 425-455. https://doi.org/10.1007/1-4020-3764-3_15

Lovejoy, C. A., & Cortez, D. (2009, Sep 2). Common mechanisms of PIKK regulation. *DNA Repair (Amst), 8*(9), 1004-1008. https://doi.org/10.1016/j.dnarep.2009.04.006

Lupardus, P. J., Van, C., & Cimprich, K. A. (2007, Feb). Analyzing the ATR-mediated checkpoint using Xenopus egg extracts. *Methods, 41*(2), 222-231. <Go to ISI>://000243758100010

Ma, N.-F., Hu, L., Fung, J. M., Xie, D., Zheng, B.-J., Chen, L., Tang, D.-J., Fu, L., Wu, Z., Chen, M., Fang, Y., & Guan, X.-Y. (2008). Isolation and characterization of a novel oncogene, amplified in liver cancer 1, within a commonly amplified region at 1q21 in hepatocellular carcinoma. *47*(2), 503-510. https://doi.org/https://doi.org/10.1002/hep.22072

MacNeal, R. K., & Purich, D. L. (1978, Jul 10). Stoichiometry and role of GTP hydrolysis in bovine neurotubule assembly. *J Biol Chem, 253*(13), 4683-4687.

Maddox, P., Straight, A., Coughlin, P., Mitchison, T. J., & Salmon, E. D. (2003). Direct observation of microtubule dynamics at kinetochores in Xenopus extract spindles: implications for spindle mechanics. *The Journal of cell biology, 162*(3), 377-382. https://doi.org/10.1083/jcb.200301088

Maekawa, H., & Schiebel, E. (2004). Cdk1-Clb4 controls the interaction of astral microtubule plus ends with subdomains of the daughter cell cortex. *Genes & development, 18*(14), 1709-1724. https://doi.org/10.1101/gad.298704

Maekawa, H., Usui, T., Knop, M., & Schiebel, E. (2003, Feb 3). Yeast Cdk1 translocates to the plus end of cytoplasmic microtubules to regulate bud cortex interactions. *Embo j, 22*(3), 438-449. https://doi.org/10.1093/emboj/cdg063

Mah, L. J., El-Osta, A., & Karagiannis, T. C. (2010, Apr). gammaH2AX: a sensitive molecular marker of DNA damage and repair. *Leukemia, 24*(4), 679-686. https://doi.org/10.1038/leu.2010.6

Maizels, Y., & Gerlitz, G. (2015, Sep). Shaping of interphase chromosomes by the microtubule network [Research Support, Non-U.S. Gov't
Review]. *FEBS J, 282*(18), 3500-3524. https://doi.org/10.1111/febs.13334

Malavazi, I., Lima, J. F., de Castro, P. A., Savoldi, M., de Souza Goldman, M. H., & Goldman, G. H. (2008). Genetic interactions of the Aspergillus nidulans atmAATM homolog with different components of the DNA damage response pathway. *Genetics, 178*(2), 675-691. https://doi.org/10.1534/genetics.107.080879

Malavazi, I., Semighini, C. P., Kress, M. R., Harris, S. D., & Goldman, G. H. (2006, May). Regulation of hyphal morphogenesis and the DNA damage response by the Aspergillus nidulans ATM homolog AtmA. *Genetics, 173*(1), 99-109. https://doi.org/10.1534/genetics.105.052704

Mandelkow, E. M., Mandelkow, E., & Milligan, R. A. (1991, Sep). Microtubule dynamics and microtubule caps: a time-resolved cryo-electron microscopy study. *J Cell Biol, 114*(5), 977-991. https://doi.org/10.1083/jcb.114.5.977

Maney, T., Hunter, A. W., Wagenbach, M., & Wordeman, L. (1998, Aug 10). Mitotic centromere-associated kinesin is important for anaphase chromosome segregation. *J Cell Biol, 142*(3), 787-801. https://doi.org/10.1083/jcb.142.3.787

Maney, T., Wagenbach, M., & Wordeman, L. (2001, Sep 14). Molecular dissection of the microtubule depolymerizing activity of mitotic centromere-associated kinesin. *J Biol Chem, 276*(37), 34753-34758. https://doi.org/10.1074/jbc.M106626200

Manning, A. L., Bakhoum, S. F., Maffini, S., Correia-Melo, C., Maiato, H., & Compton, D. A. (2010). CLASP1, astrin and Kif2b form a molecular switch that regulates kinetochore-

microtubule dynamics to promote mitotic progression and fidelity. *The EMBO Journal, 29*(20), 3531-3543. https://doi.org/10.1038/emboj.2010.230

Manning, A. L., Ganem, N. J., Bakhoum, S. F., Wagenbach, M., Wordeman, L., & Compton, D. A. (2007, 2007/08/01). The Kinesin-13 Proteins Kif2a, Kif2b, and Kif2c/MCAK Have Distinct Roles during Mitosis in Human Cells. *Molecular Biology of the Cell, 18*(8), 2970-2979. https://doi.org/10.1091/mbc.e07-02-0110

Mao, Z., Bozzella, M., Seluanov, A., & Gorbunova, V. (2008, Sep 15). DNA repair by nonhomologous end joining and homologous recombination during cell cycle in human cells. *Cell Cycle, 7*(18), 2902-2906. https://doi.org/10.4161/cc.7.18.6679

Mao, Z., Jiang, Y., Liu, X., Seluanov, A., & Gorbunova, V. (2009). DNA repair by homologous recombination, but not by nonhomologous end joining, is elevated in breast cancer cells. *Neoplasia (New York, N.Y.), 11*(7), 683-691. https://doi.org/10.1593/neo.09312

Marcomini, I., Shimada, K., Delgoshaie, N., Yamamoto, I., Seeber, A., Cheblal, A., Horigome, C., Naumann, U., & Gasser, S. M. (2018, Sep 4). Asymmetric Processing of DNA Ends at a Double-Strand Break Leads to Unconstrained Dynamics and Ectopic Translocation. *Cell Rep, 24*(10), 2614-2628 e2614. https://doi.org/10.1016/j.celrep.2018.07.102

Maréchal, A., & Zou, L. (2013). DNA damage sensing by the ATM and ATR kinases. *Cold Spring Harbor perspectives in biology, 5*(9), a012716. https://doi.org/10.1101/cshperspect.a012716

Marnef, A., & Legube, G. (2017, Jan 06). Organizing DNA repair in the nucleus: DSBs hit the road [Review]. *Curr Opin Cell Biol, 46*, 1-8. https://doi.org/10.1016/j.ceb.2016.12.003

Matsuoka, S., Ballif, B. A., Smogorzewska, A., McDonald, E. R., 3rd, Hurov, K. E., Luo, J., Bakalarski, C. E., Zhao, Z., Solimini, N., Lerenthal, Y., Shiloh, Y., Gygi, S. P., & Elledge, S. J. (2007, May 25). ATM and ATR substrate analysis reveals extensive protein networks responsive to DNA damage. *Science, 316*(5828), 1160-1166. https://doi.org/10.1126/science.1140321

Maurer, S. P., Bieling, P., Cope, J., Hoenger, A., & Surrey, T. (2011). GTPγS microtubules mimic the growing microtubule end structure recognized by end-binding proteins (EBs). *Proceedings of the National Academy of Sciences, 108*(10), 3988-3993. https://doi.org/10.1073/pnas.1014758108

Maurer, S. P., Fourniol, F. J., Bohner, G., Moores, C. A., & Surrey, T. (2012). EBs recognize a nucleotide-dependent structural cap at growing microtubule ends. *Cell, 149*(2), 371-382. https://doi.org/10.1016/j.cell.2012.02.049

Maynard, S., Schurman, S. H., Harboe, C., de Souza-Pinto, N. C., & Bohr, V. A. (2009, Jan). Base excision repair of oxidative DNA damage and association with cancer and aging. *Carcinogenesis, 30*(1), 2-10. https://doi.org/10.1093/carcin/bgn250

McAinsh, A. D., Tytell, J. D., & Sorger, P. K. (2003). Structure, function, and regulation of budding yeast kinetochores. *Annu Rev Cell Dev Biol, 19*, 519-539. https://doi.org/10.1146/annurev.cellbio.19.111301.155607

McCoy, A. J., Grosse-Kunstleve, R. W., Adams, P. D., Winn, M. D., Storoni, L. C., & Read, R. J. (2007, Aug 1). Phaser crystallographic software. *Journal of Applied Crystallography, 40*(Pt 4), 658-674. https://doi.org/10.1107/S0021889807021206

McIntosh, J. R., O'Toole, E., Morgan, G., Austin, J., Ulyanov, E., Ataullakhanov, F., & Gudimchuk, N. (2018, Aug 6). Microtubules grow by the addition of bent guanosine triphosphate tubulin to the tips of curved protofilaments. *J Cell Biol, 217*(8), 2691-2708. https://doi.org/10.1083/jcb.201802138

Mekhail, K. (2018, 2018-March-20). Defining the Damaged DNA Mobility Paradox as Revealed by the Study of Telomeres, DSBs, Microtubules and Motors [Perspective]. *9*(95). https://doi.org/10.3389/fgene.2018.00095

Melki, R., Carlier, M. F., Pantaloni, D., & Timasheff, S. N. (1989, Nov 14). Cold depolymerization of microtubules to double rings: geometric stabilization of assemblies. *Biochemistry, 28*(23), 9143-9152. https://doi.org/10.1021/bi00449a028

Melo, J. A., Cohen, J., & Toczyski, D. P. (2001, Nov 1). Two checkpoint complexes are independently recruited to sites of DNA damage in vivo. *Genes Dev, 15*(21), 2809-2821. https://doi.org/10.1101/gad.903501

Mennella, V., Rogers, G. C., Rogers, S. L., Buster, D. W., Vale, R. D., & Sharp, D. J. (2005, Mar). Functionally distinct kinesin-13 family members cooperate to regulate microtubule dynamics during interphase. *Nat Cell Biol, 7*(3), 235-245. https://doi.org/10.1038/ncb1222

Meunier, S., & Vernos, I. (2012, Jun 15). Microtubule assembly during mitosis - from distinct origins to distinct functions? *J Cell Sci, 125*(Pt 12), 2805-2814. https://doi.org/10.1242/jcs.092429

Miki, H., Okada, Y., & Hirokawa, N. (2005, Sep). Analysis of the kinesin superfamily: insights into structure and function. *Trends Cell Biol, 15*(9), 467-476. https://doi.org/10.1016/j.tcb.2005.07.006

Miller, R. K., Heller, K. K., Frisèn, L., Wallack, D. L., Loayza, D., Gammie, A. E., & Rose, M. D. (1998, 1998/08/01). The Kinesin-related Proteins, Kip2p and Kip3p, Function Differently in Nuclear Migration in Yeast. *Molecular Biology of the Cell, 9*(8), 2051-2068. https://doi.org/10.1091/mbc.9.8.2051

Mine-Hattab, J., & Rothstein, R. (2012, Apr 8). Increased chromosome mobility facilitates homology search during recombination [Research Support, N.I.H., Extramural

Research Support, Non-U.S. Gov't]. *Nat Cell Biol, 14*(5), 510-517. https://doi.org/10.1038/ncb2472

Mine-Hattab, J., & Rothstein, R. (2013, Nov). DNA in motion during double-strand break repair [Research Support, N.I.H., Extramural
Research Support, Non-U.S. Gov't
Review]. *Trends Cell Biol, 23*(11), 529-536. https://doi.org/10.1016/j.tcb.2013.05.006

Misu, S., Takebayashi, M., & Miyamoto, K. (2017). Nuclear Actin in Development and Transcriptional Reprogramming [Review]. *Front Genet, 8*, 27. https://doi.org/10.3389/fgene.2017.00027

Mitchison, T., & Kirschner, M. (1984a). Dynamic instability of microtubule growth. *Nature, 312*(5991), 237-242. https://doi.org/10.1038/312237a0

Mitchison, T., & Kirschner, M. (1984b). Microtubule assembly nucleated by isolated centrosomes. *Nature, 312*(5991), 232-237. https://doi.org/10.1038/312232a0

Mitra, A., & Sept, D. (2008). Taxol allosterically alters the dynamics of the tubulin dimer and increases the flexibility of microtubules. *Biophysical Journal, 95*(7), 3252-3258. https://doi.org/10.1529/biophysj.108.133884

Montoni, A., Robu, M., Pouliot, E., & Shah, G. M. (2013). Resistance to PARP-Inhibitors in Cancer Therapy. *Front Pharmacol, 4*, 18. https://doi.org/10.3389/fphar.2013.00018

Moore, A., & Wordeman, L. (2004, Oct). The mechanism, function and regulation of depolymerizing kinesins during mitosis. *Trends Cell Biol, 14*(10), 537-546. https://doi.org/10.1016/j.tcb.2004.09.001
S0962-8924(04)00233-8 [pii]

Moores, C. A., Cooper, J., Wagenbach, M., Ovechkina, Y., Wordeman, L., & Milligan, R. A. (2006, Aug). The role of the kinesin-13 neck in microtubule depolymerization. *Cell Cycle, 5*(16), 1812-1815. https://doi.org/10.4161/cc.5.16.3134

Moores, C. A., & Milligan, R. A. (2006, Oct 01). Lucky 13-microtubule depolymerisation by kinesin-13 motors. *J Cell Sci, 119*(Pt 19), 3905-3913. https://doi.org/10.1242/jcs.03224

Moores, C. A., & Milligan, R. A. (2008, Mar 28). Visualisation of a kinesin-13 motor on microtubule end mimics. *J Mol Biol, 377*(3), 647-654. https://doi.org/10.1016/j.jmb.2008.01.079

Moores, C. A., Perderiset, M., Kappeler, C., Kain, S., Drummond, D., Perkins, S. J., Chelly, J., Cross, R., Houdusse, A., & Francis, F. (2006). Distinct roles of doublecortin modulating the microtubule cytoskeleton. *The EMBO Journal, 25*(19), 4448-4457. https://doi.org/10.1038/sj.emboj.7601335

Moores, C. A., Yu, M., Guo, J., Beraud, C., Sakowicz, R., & Milligan, R. A. (2002, Apr). A mechanism for microtubule depolymerization by KinI kinesins. *Mol Cell, 9*(4), 903-909. https://doi.org/10.1016/s1097-2765(02)00503-8

Moritz, M., Braunfeld, M. B., Sedat, J. W., Alberts, B., & Agard, D. A. (1995). Microtubule nucleation by γ-tubulin-containing rings in the centrosome. *Nature, 378*(6557), 638-640. https://doi.org/10.1038/378638a0

Mukhtar, E., Adhami, V. M., & Mukhtar, H. (2014). Targeting microtubules by natural agents for cancer therapy. *Molecular cancer therapeutics, 13*(2), 275-284. https://doi.org/10.1158/1535-7163.MCT-13-0791

Mulder, A. M., Glavis-Bloom, A., Moores, C. A., Wagenbach, M., Carragher, B., Wordeman, L., & Milligan, R. A. (2009, Apr 06). A new model for binding of kinesin 13 to curved microtubule protofilaments. *J Cell Biol, 185*(1), 51-57. https://doi.org/10.1083/jcb.200812052

Müller-Reichert, T., Chrétien, D., Severin, F., & Hyman, A. A. (1998). Structural changes at microtubule ends accompanying GTP hydrolysis: information from a slowly hydrolyzable analogue of GTP, guanylyl (alpha,beta)methylenediphosphonate. *Proceedings of the National Academy of Sciences of the United States of America, 95*(7), 3661-3666. https://doi.org/10.1073/pnas.95.7.3661

Nawrotek, A., Knossow, M., & Gigant, B. (2011, Sep 9). The determinants that govern microtubule assembly from the atomic structure of GTP-tubulin. *J Mol Biol, 412*(1), 35-42. https://doi.org/10.1016/j.jmb.2011.07.029

Neumaier, T., Swenson, J., Pham, C., Polyzos, A., Lo, A. T., Yang, P., Dyball, J., Asaithamby, A., Chen, D. J., Bissell, M. J., Thalhammer, S., & Costes, S. V. (2012, Jan 10). Evidence for formation of DNA repair centers and dose-response nonlinearity in human cells [Research Support, N.I.H., Extramural
Research Support, Non-U.S. Gov't
Research Support, U.S. Gov't, Non-P.H.S.]. *Proc Natl Acad Sci U S A, 109*(2), 443-448. https://doi.org/10.1073/pnas.1117849108

Niederstrasser, H., Salehi-Had, H., Gan, E. C., Walczak, C., & Nogales, E. (2002, Feb 22). XKCM1 acts on a single protofilament and requires the C terminus of tubulin. *J Mol Biol, 316*(3), 817-828. https://doi.org/10.1006/jmbi.2001.5360

Nielsen, S. S., Toft, K. N., Snakenborg, D., Jeppesen, M. G., Jacobsen, J. K., Vestergaard, B., Kutter, J. P., & Arleth, L. (2009, Oct). BioXTAS RAW, a software program for high-throughput automated small-angle X-ray scattering data reduction and preliminary analysis. *Journal of Applied Crystallography, 42*, 959-964. https://doi.org/10.1107/S0021889809023863

Noda, Y., Niwa, S., Homma, N., Fukuda, H., Imajo-Ohmi, S., & Hirokawa, N. (2011). Phosphatidylinositol 4-phosphate 5-kinase alpha (PIPKÎ±) regulates neuronal microtubule depolymerase kinesin, KIF2A and suppresses elongation of axon branches. *Proceedings of the National Academy of Sciences, 109*(5), 1725-1730. https://doi.org/10.1073/pnas.1107808109

Noda, Y., Sato-Yoshitake, R., Kondo, S., Nangaku, M., & Hirokawa, N. (1995, Apr). KIF2 is a new microtubule-based anterograde motor that transports membranous organelles distinct from those carried by kinesin heavy chain or KIF3A/B. *J Cell Biol, 129*(1), 157-167. https://doi.org/10.1083/jcb.129.1.157

Nogales, E., Wolf, S. G., & Downing, K. H. (1998, Jan 8). Structure of the alpha beta tubulin dimer by electron crystallography. *Nature, 391*(6663), 199-203. https://doi.org/10.1038/34465

O'Brien, E. T., Salmon, E. D., & Erickson, H. P. (1997). How calcium causes microtubule depolymerization. *Cell motility and the cytoskeleton, 36*(2), 125-135. https://doi.org/10.1002/(sici)1097-0169(1997)36:2<125::aid-cm3>3.0.co;2-8

Ogawa, T., Nitta, R., Okada, Y., & Hirokawa, N. (2004, Feb 20). A common mechanism for microtubule destabilizers-M type kinesins stabilize curling of the protofilament using the class-specific neck and loops. *Cell, 116*(4), 591-602. https://doi.org/S0092867404001291 [pii]

Ogawa, T., Saijo, S., Shimizu, N., Jiang, X., & Hirokawa, N. (2017, Sep 12). Mechanism of Catalytic Microtubule Depolymerization via KIF2-Tubulin Transitional Conformation. *Cell Rep, 20*(11), 2626-2638. https://doi.org/10.1016/j.celrep.2017.08.067

Orr, G. A., Verdier-Pinard, P., McDaid, H., & Horwitz, S. B. (2003, 2003/10/01). Mechanisms of Taxol resistance related to microtubules. *Oncogene, 22*(47), 7280-7295. https://doi.org/10.1038/sj.onc.1206934

Osawa, F., & Asakura, S. (1975). *Thermodynamics of the polymerization of protein*. Academic Press.

Oshidari, R., Strecker, J., Chung, D. K. C., Abraham, K. J., Chan, J. N. Y., Damaren, C. J., & Mekhail, K. (2018, 2018/07/02). Nuclear microtubule filaments mediate non-linear directional motion of chromatin and promote DNA repair. *Nature Communications, 9*(1), 2567. https://doi.org/10.1038/s41467-018-05009-7

Otwinowski, Z., & Minor, W. (1997). Processing of X-ray diffraction data collected in oscillation mode. *Methods in Enzymology, 276*, 307-326.

Ovechkina, Y., Wagenbach, M., & Wordeman, L. (2002, Nov 25). K-loop insertion restores microtubule depolymerizing activity of a "neckless" MCAK mutant. *J Cell Biol, 159*(4), 557-562. https://doi.org/10.1083/jcb.200205089

Panda, D., Jordan, M. A., Chu, K. C., & Wilson, L. (1996, Nov 22). Differential effects of vinblastine on polymerization and dynamics at opposite microtubule ends. *J Biol Chem, 271*(47), 29807-29812. http://www.ncbi.nlm.nih.gov/pubmed/8939919

Panier, S., & Boulton, S. J. (2014, 2014/01/01). Double-strand break repair: 53BP1 comes into focus. *Nature Reviews Molecular Cell Biology, 15*(1), 7-18. https://doi.org/10.1038/nrm3719

Parke, C. L., Wojcik, E. J., Kim, S., & Worthylake, D. K. (2010, Feb 19). ATP hydrolysis in Eg5 kinesin involves a catalytic two-water mechanism. *J Biol Chem, 285*(8), 5859-5867. https://doi.org/M109.071233 [pii]
10.1074/jbc.M109.071233

Paull, T. T., & Gellert, M. (1998, Jun). The 3' to 5' exonuclease activity of Mre 11 facilitates repair of DNA double-strand breaks. *Mol Cell, 1*(7), 969-979. https://doi.org/10.1016/s1097-2765(00)80097-0

Pecqueur, L., Duellberg, C., Dreier, B., Jiang, Q., Wang, C., Plückthun, A., Surrey, T., Gigant, B., & Knossow, M. (2012). A designed ankyrin repeat protein selected to bind to tubulin caps the microtubule plus end. *109*(30), 12011-12016. https://doi.org/10.1073/pnas.1204129109 %J Proceedings of the National Academy of Sciences

Pettersen, E. F., Goddard, T. D., Huang, C. C., Couch, G. S., Greenblatt, D. M., Meng, E. C., & Ferrin, T. E. (2004, Oct). UCSF Chimera--a visualization system for exploratory research and analysis. *J Comput Chem, 25*(13), 1605-1612. https://doi.org/10.1002/jcc.20084

Piazza, A., Koszul, R., & Heyer, W.-D. (2018). Chapter Two - A Proximity Ligation-Based Method for Quantitative Measurement of D-Loop Extension in S. cerevisiae. In M. Spies & A. Malkova (Eds.), *Methods in Enzymology* (Vol. 601, pp. 27-44). Academic Press. https://doi.org/https://doi.org/10.1016/bs.mie.2017.11.024

Piazza, A., Shah, S. S., Wright, W. D., Gore, S. K., Koszul, R., & Heyer, W.-D. (2019, 2019/03/21/). Dynamic Processing of Displacement Loops during Recombinational DNA Repair. *Molecular Cell, 73*(6), 1255-1266.e1254. https://doi.org/https://doi.org/10.1016/j.molcel.2019.01.005

Plückthun, A. (2015, 2015/01/06). Designed Ankyrin Repeat Proteins (DARPins): Binding Proteins for Research, Diagnostics, and Therapy. *Annual Review of Pharmacology and Toxicology, 55*(1), 489-511. https://doi.org/10.1146/annurev-pharmtox-010611-134654

Polo, S. E., & Jackson, S. P. (2011, Mar 1). Dynamics of DNA damage response proteins at DNA breaks: a focus on protein modifications. *Genes Dev, 25*(5), 409-433. https://doi.org/10.1101/gad.2021311

Poon, B. P., & Mekhail, K. (2012). Effects of Perinuclear Chromosome Tethers in the Telomeric URA3/5FOA System Reflect Changes to Gene Silencing and not Nucleotide Metabolism. *Front Genet, 3*, 144. https://doi.org/10.3389/fgene.2012.00144

Porter, L. A., & Lee, J. M. (2001, Nov 01). alpha-, beta-, and gamma-Tubulin polymerization in response to DNA damage [Research Support, Non-U.S. Gov't]. *Exp Cell Res, 270*(2), 151-158. https://doi.org/10.1006/excr.2001.5322

Poruchynsky, M. S., Komlodi-Pasztor, E., Trostel, S., Wilkerson, J., Regairaz, M., Pommier, Y., Zhang, X., Kumar Maity, T., Robey, R., Burotto, M., Sackett, D., Guha, U., & Fojo, A. T. (2015). Microtubule-targeting agents augment the toxicity of DNA-damaging agents by disrupting intracellular trafficking of DNA repair proteins. *112*(5), 1571-1576. https://doi.org/10.1073/pnas.1416418112 %J Proceedings of the National Academy of Sciences

Prigozhina, N. L., Oakley, C. E., Lewis, A. M., Nayak, T., Osmani, S. A., & Oakley, B. R. (2004). γ-Tubulin Plays an Essential Role in the Coordination of Mitotic Events. *15*(3), 1374-1386. https://doi.org/10.1091/mbc.e03-06-0405

Prota, A. E., Bargsten, K., Zurwerra, D., Field, J. J., DÃaz, J. F., Altmann, K.-H., & Steinmetz, M. O. (2013). Molecular Mechanism of Action of Microtubule-Stabilizing Anticancer Agents. *Science, 339*(6119), 587-590. https://doi.org/10.1126/science.1230582

Ranaivoson, F. M., Gigant, B., Berritt, S., Joullie, M., & Knossow, M. (2012, Aug). Structural plasticity of tubulin assembly probed by vinca-domain ligands. *Acta Crystallogr D Biol Crystallogr, 68*(Pt 8), 927-934. https://doi.org/10.1107/S0907444912017143

Rastogi, R. P., Richa, Kumar, A., Tyagi, M. B., & Sinha, R. P. (2010, Dec 16). Molecular mechanisms of ultraviolet radiation-induced DNA damage and repair. *J Nucleic Acids, 2010*, 592980. https://doi.org/10.4061/2010/592980

Ravelli, R. B., Gigant, B., Curmi, P. A., Jourdain, I., Lachkar, S., Sobel, A., & Knossow, M. (2004). Insight into tubulin regulation from a complex with colchicine and a stathmin-like domain. *Nature, 428*(6979), 198-202.

Ray Chaudhuri, A., & Nussenzweig, A. (2017, Oct). The multifaceted roles of PARP1 in DNA repair and chromatin remodelling. *Nat Rev Mol Cell Biol, 18*(10), 610-621. https://doi.org/10.1038/nrm.2017.53

Reddy A.S.N., D. I. S. (2011). Microtubule Motor Proteins in the Eukaryotic Green Lineage: Functions and Regulation. *In: Liu B. (eds) The Plant Cytoskeleton. Advances in Plant Biology,, 2*.

Ren, D., Fisher, L. A., Zhao, J., Wang, L., Williams, B. C., Goldberg, M. L., & Peng, A. (2017, Apr 26). Cell Cycle-dependent Regulation of Greatwall Kinase by Protein Phosphatase 1 and Regulatory Subunit 3B. *J Biol Chem*. https://doi.org/10.1074/jbc.M117.778233

Ren, Y., Zhao, J., & Feng, J. (2003). Parkin Binds to α/β Tubulin and Increases their Ubiquitination and Degradation. *23*(8), 3316-3324. https://doi.org/10.1523/JNEUROSCI.23-08-03316.2003 %J The Journal of Neuroscience

Rice, L. M., Montabana, E. A., & Agard, D. A. (2008). The lattice as allosteric effector: structural studies of alphabeta- and gamma-tubulin clarify the role of GTP in microtubule assembly. *Proceedings of the National Academy of Sciences of the United States of America, 105*(14), 5378-5383. https://doi.org/10.1073/pnas.0801155105

Rickman, J., Duellberg, C., Cade, N. I., Griffin, L. D., & Surrey, T. (2017a). Steady-state EB cap size fluctuations are determined by stochastic microtubule growth and maturation. *Proceedings of the National Academy of Sciences, 114*(13), 3427-3432. https://doi.org/10.1073/pnas.1620274114

Rickman, J., Duellberg, C., Cade, N. I., Griffin, L. D., & Surrey, T. (2017b). Steady-state EB cap size fluctuations are determined by stochastic microtubule growth and maturation. *114*(13), 3427-3432. https://doi.org/10.1073/pnas.1620274114 %J Proceedings of the National Academy of Sciences

Ritter, A., Kreis, N. N., Louwen, F., Wordeman, L., & Yuan, J. (2015, Jul-Aug). Molecular insight into the regulation and function of MCAK [Review]. *Crit Rev Biochem Mol Biol, 51*(4), 228-245. https://doi.org/10.1080/10409238.2016.1178705

Robert, X., & Gouet, P. (2014, Jul). Deciphering key features in protein structures with the new ENDscript server. *Nucleic Acids Res, 42*(Web Server issue), W320-324. https://doi.org/10.1093/nar/gku316

Rogalska, A., & Marczak, A. (2015). Nuclear DNA Damage and Repair in Normal Ovarian Cells Caused by Epothilone B [Research Support, Non-U.S. Gov't]. *Asian Pac J Cancer Prev, 16*(15), 6535-6539. http://www.ncbi.nlm.nih.gov/pubmed/26434870

Roostalu, J., Cade, N. I., & Surrey, T. (2015). Complementary activities of TPX2 and chTOG constitute an efficient importin-regulated microtubule nucleation module. *Nature Cell Biology, 17*(11), 1422-1434. https://doi.org/10.1038/ncb3241

Roostalu, J., & Surrey, T. (2017, Nov). Microtubule nucleation: beyond the template. *Nat Rev Mol Cell Biol, 18*(11), 702-710. https://doi.org/10.1038/nrm.2017.75

Roostalu, J., Thomas, C., Cade, N. I., Kunzelmann, S., Taylor, I. A., & Surrey, T. (2020). The speed of GTP hydrolysis determines GTP cap size and controls microtubule stability. *eLife, 9*, e51992. https://doi.org/10.7554/eLife.51992

Roukos, V., Voss, T. C., Schmidt, C. K., Lee, S., Wangsa, D., & Misteli, T. (2013, Aug 9). Spatial dynamics of chromosome translocations in living cells. *Science, 341*(6146), 660-664. https://doi.org/10.1126/science.1237150

Roychowdhury, S., Panda, D., Wilson, L., & Rasenick, M. M. (1999). G Protein α Subunits Activate Tubulin GTPase and Modulate Microtubule Polymerization Dynamics *. *Journal of Biological Chemistry, 274*(19), 13485-13490. https://doi.org/10.1074/jbc.274.19.13485

Rutten, T., Chan, J., & Lloyd, C. W. (1997). A 60-kDa plant microtubule-associated protein promotes the growth and stabilization of neurotubules in vitro. *Proceedings of the National Academy of Sciences of the United States of America, 94*(9), 4469-4474. https://doi.org/10.1073/pnas.94.9.4469

Sancar, A., Lindsey-Boltz, L. A., Unsal-Kacmaz, K., & Linn, S. (2004). Molecular mechanisms of mammalian DNA repair and the DNA damage checkpoints [Research Support, Non-U.S. Gov't
Research Support, U.S. Gov't, P.H.S.
Review]. *Annu Rev Biochem, 73*, 39-85. https://doi.org/10.1146/annurev.biochem.73.011303.073723

Sandell, L. L., & Zakian, V. A. (1993, Nov 19). Loss of a yeast telomere: arrest, recovery, and chromosome loss. *Cell, 75*(4), 729-739. https://doi.org/10.1016/0092-8674(93)90493-a

Sandoval, I. V., Jameson, J. L., Niedel, J., MacDonald, E., & Cuatrecasas, P. (1978). Role of nucleotides in tubulin polymerization: effect of guanosine 5'-methylene diphosphonate. *Proceedings of the National Academy of Sciences of the United States of America, 75*(7), 3178-3182. https://doi.org/10.1073/pnas.75.7.3178

Sandoval, I. V., MacDonald, E., Jameson, J. L., & Cuatrecasas, P. (1977). Role of nucleotides in tubulin polymerization: effect of guanylyl 5'-methylenediphosphonate. *74*(11), 4881-4885. https://doi.org/10.1073/pnas.74.11.4881 %J Proceedings of the National Academy of Sciences

Sandoval, I. V., & Weber, K. (1980a, Oct 10). Different tubulin polymers are produced by microtubule-associated proteins MAP2 and tau in the presence of guanosine 5'-(alpha, beta-methylene)triphosphate. *J Biol Chem, 255*(19), 8952-8954.

Sandoval, I. V., & Weber, K. (1980b, Jul 25). Guanasone 5'-(alpha,beta-methylene)triphosphate enhances specifically microtubule nucleation and stops the treadmill of tubulin protomers. *J Biol Chem, 255*(14), 6966-6974.

Sanhaji, M., Friel, C. T., Wordeman, L., Louwen, F., & Yuan, J. (2011). Mitotic centromere-associated kinesin (MCAK): a potential cancer drug target. *Oncotarget, 2*(12), 935-947. https://doi.org/10.18632/oncotarget.416

Sarangapani, K. K., & Asbury, C. L. (2014, Apr). Catch and release: how do kinetochores hook the right microtubules during mitosis? *Trends Genet, 30*(4), 150-159. https://doi.org/10.1016/j.tig.2014.02.004

Savage, C., Hamelin, M., Culotti, J. G., Coulson, A., Albertson, D. G., & Chalfie, M. (1989, Jun). mec-7 is a beta-tubulin gene required for the production of 15-protofilament microtubules in Caenorhabditis elegans. *Genes Dev, 3*(6), 870-881. https://doi.org/10.1101/gad.3.6.870

Savoian, M. S., & Glover, D. M. (2010). Drosophila Klp67A binds prophase kinetochores to subsequently regulate congression and spindle length. *Journal of Cell Science, 123*(5), 767-776. https://doi.org/10.1242/jcs.055905

Schnitzer, M. J., & Block, S. M. (1997, 1997/07/01). Kinesin hydrolyses one ATP per 8-nm step. *Nature, 388*(6640), 386-390. https://doi.org/10.1038/41111

Scholey, J. M., Porter, M. E., Grissom, P. M., & McIntosh, J. R. (1985, 1985/12/01). Identification of kinesin in sea urchin eggs, and evidence for its localization in the mitotic spindle. *Nature, 318*(6045), 483-486. https://doi.org/10.1038/318483a0

Schrank, B. R., Aparicio, T., Li, Y., Chang, W., Chait, B. T., Gundersen, G. G., Gottesman, M. E., & Gautier, J. (2018, Jul). Nuclear ARP2/3 drives DNA break clustering for homology-directed repair. *Nature, 559*(7712), 61-66. https://doi.org/10.1038/s41586-018-0237-5

Schrodinger, LLC. (2010). *The PyMOL Molecular Graphics System, Version 1.3r1*.

Schwarzerová, K., Bellinvia, E., Martinek, J., Sikorová, L., Dostál, V., Libusová, L., Bokvaj, P., Fischer, L., Schmit, A. C., & Nick, P. (2019, 2019/04/05). Tubulin is actively exported from the nucleus through the Exportin1/CRM1 pathway. *Scientific Reports, 9*(1), 5725. https://doi.org/10.1038/s41598-019-42056-6

Seetapun, D., Castle, Brian T., McIntyre, Alistair J., Tran, Phong T., & Odde, David J. (2012). Estimating the Microtubule GTP Cap Size In Vivo. *Current Biology, 22*(18), 1681-1687. https://doi.org/https://doi.org/10.1016/j.cub.2012.06.068

Seetapun, D., Castle, B. T., McIntyre, A. J., Tran, P. T., & Odde, D. J. (2012, Sep 25). Estimating the microtubule GTP cap size in vivo. *Curr Biol, 22*(18), 1681-1687. https://doi.org/10.1016/j.cub.2012.06.068

Shi, X., & Sun, X. (2017, 2017/11/01). Regulation of paclitaxel activity by microtubule-associated proteins in cancer chemotherapy. *Cancer Chemotherapy and Pharmacology, 80*(5), 909-917. https://doi.org/10.1007/s00280-017-3398-2

Shilova, O. N., & Deyev, S. M. (2019, Oct-Dec). DARPins: Promising Scaffolds for Theranostics. *Acta naturae, 11*(4), 42-53. https://doi.org/10.32607/20758251-2019-11-4-42-53

Shimizu, Y., Shimizu, T., Nara, M., Kikumoto, M., Kojima, H., & Morii, H. (2013, Apr). Effects of the KIF2C neck peptide on microtubules: lateral disintegration of microtubules and beta-structure formation. *FEBS J, 280*(7), 1681-1692. https://doi.org/10.1111/febs.12182

Shiotani, B., & Zou, L. (2009, Mar 13). Single-stranded DNA orchestrates an ATM-to-ATR switch at DNA breaks. *Mol Cell, 33*(5), 547-558. https://doi.org/10.1016/j.molcel.2009.01.024

Shipley, K., Hekmat-Nejad, M., Turner, J., Moores, C., Anderson, R., Milligan, R., Sakowicz, R., & Fletterick, R. (2004, 2004/04/07). Structure of a kinesin microtubule depolymerization machine [https://doi.org/10.1038/sj.emboj.7600165]. *The EMBO Journal, 23*(7), 1422-1432. https://doi.org/https://doi.org/10.1038/sj.emboj.7600165

Sievers, F., Wilm, A., Dineen, D., Gibson, T. J., Karplus, K., Li, W., Lopez, R., McWilliam, H., Remmert, M., Soding, J., Thompson, J. D., & Higgins, D. G. (2011, Oct 11). Fast, scalable generation of high-quality protein multiple sequence alignments using Clustal Omega. *Mol Syst Biol, 7*, 539. https://doi.org/10.1038/msb.2011.75

Smolka, M. B., Albuquerque, C. P., Chen, S.-h., & Zhou, H. (2007). Proteome-wide identification of in vivo targets of DNA damage checkpoint kinases. *104*(25), 10364-10369. https://doi.org/10.1073/pnas.0701622104 %J Proceedings of the National Academy of Sciences

Snyder, J. P., Nettles, J. H., Cornett, B., Downing, K. H., & Nogales, E. (2001). The binding conformation of Taxol in β-tubulin: A model based on electron crystallographic density. *98*(9), 5312-5316. https://doi.org/10.1073/pnas.051309398 %J Proceedings of the National Academy of Sciences

Soppina, V., Norris, S. R., Dizaji, A. S., Kortus, M., Veatch, S., Peckham, M., & Verhey, K. J. (2014). Dimerization of mammalian kinesin-3 motors results in superprocessive motion. *111*(15), 5562-5567. https://doi.org/10.1073/pnas.1400759111 %J Proceedings of the National Academy of Sciences

Spiegelman, B. M., Penningroth, S. M., & Kirschner, M. W. (1977). Turnover of tubulin and the N site GTP in chinese hamster ovary cells. *Cell, 12*(3), 587-600. https://doi.org/https://doi.org/10.1016/0092-8674(77)90259-8

Stanton, R. A., Gernert, K. M., Nettles, J. H., & Aneja, R. (2011, May). Drugs that target dynamic microtubules: a new molecular perspective. *Med Res Rev, 31*(3), 443-481. https://doi.org/10.1002/med.20242

Stewart, R. J., Farrell, K. W., & Wilson, L. (1990). Role of GTP hydrolysis in microtubule polymerization: evidence for a coupled hydrolysis mechanism. *Biochemistry, 29*(27), 6489-6498.

Stokes, M., Newton, N., & Kaur, A. (2007, Nov). Stalking, and social and romantic functioning among adolescents and adults with autism spectrum disorder. *J Autism Dev Disord, 37*(10), 1969-1986. https://doi.org/10.1007/s10803-006-0344-2

Strachan, T. a. R., A.P. . (1999). Instability of Human Genome: Mutation and DNA Repair in Human Molecular Genetics. *John Wiley and Sons Inc.*

Strecker, J., Gupta, G. D., Zhang, W., Bashkurov, M., Landry, M. C., Pelletier, L., & Durocher, D. (2016, Mar). DNA damage signalling targets the kinetochore to promote chromatin mobility. *Nat Cell Biol, 18*(3), 281-290. https://doi.org/10.1038/ncb3308

Sukhanova, M. V., Abrakhi, S., Joshi, V., Pastre, D., Kutuzov, M. M., Anarbaev, R. O., Curmi, P. A., Hamon, L., & Lavrik, O. I. (2016, Apr 7). Single molecule detection of PARP1 and PARP2 interaction with DNA strand breaks and their poly(ADP-ribosyl)ation using high-resolution AFM imaging. *Nucleic Acids Res, 44*(6), e60. https://doi.org/10.1093/nar/gkv1476

Süsse, S., Scholz, C.-J., Bürkle, A., & Wiesmüller, L. (2004). Poly(ADP-ribose) polymerase (PARP-1) and p53 independently function in regulating double-strand break repair in primate cells. *Nucleic Acids Research, 32*(2), 669-680. https://doi.org/10.1093/nar/gkh227

Svergun, D., Barberato, C., & Koch, M. H. J. (1995, Dec 1). CRYSOL - A program to evaluate x-ray solution scattering of biological macromolecules from atomic coordinates. *Journal of Applied Crystallography, 28*, 768-773. https://doi.org/Doi 10.1107/S0021889895007047

Svergun, D. I. (1992, Aug 1). Determination of the Regularization Parameter in Indirect-Transform Methods Using Perceptual Criteria. *Journal of Applied Crystallography, 25*, 495-503. https://doi.org/Doi 10.1107/S0021889892001663

Svoboda, K., Schmidt, C. F., Schnapp, B. J., & Block, S. M. (1993, Oct 21). Direct observation of kinesin stepping by optical trapping interferometry. *Nature, 365*(6448), 721-727. https://doi.org/10.1038/365721a0

Symington, L. S. (2002, Dec). Role of RAD52 epistasis group genes in homologous recombination and double-strand break repair. *Microbiol Mol Biol Rev, 66*(4), 630-670, table of contents. https://doi.org/10.1128/mmbr.66.4.630-670.2002

Talapatra, S. K., Harker, B., & Welburn, J. P. I. (2015, 2015/04/27). The C-terminal region of the motor protein MCAK controls its structure and activity through a conformational switch. *eLife, 4*, e06421. https://doi.org/10.7554/eLife.06421

Talje, L., Ben El Kadhi, K., Atchia, K., Tremblay-Boudreault, T., Carreno, S., & Kwok, B. H. (2014, Jun 27). DHTP is an allosteric inhibitor of the kinesin-13 family of microtubule

depolymerases [Research Support, Non-U.S. Gov't]. *FEBS Lett, 588*(14), 2315-2320. https://doi.org/10.1016/j.febslet.2014.05.024

Tan, D., Asenjo, A. B., Mennella, V., Sharp, D. J., & Sosa, H. (2006, Oct 9). Kinesin-13s form rings around microtubules. *J Cell Biol, 175*(1), 25-31. https://doi.org/10.1083/jcb.200605194

Tan, D., Rice, W. J., & Sosa, H. (2008, Nov 12). Structure of the kinesin13-microtubule ring complex [Research Support, N.I.H., Extramural
Research Support, Non-U.S. Gov't]. *Structure, 16*(11), 1732-1739. https://doi.org/10.1016/j.str.2008.08.017

Tanaka, E. M., & Kirschner, M. W. (1991, Oct). Microtubule behavior in the growth cones of living neurons during axon elongation. *J Cell Biol, 115*(2), 345-363. https://doi.org/10.1083/jcb.115.2.345

Tanaka, K. (2012, Nov). Dynamic regulation of kinetochore-microtubule interaction during mitosis. *J Biochem, 152*(5), 415-424. https://doi.org/10.1093/jb/mvs109

Tanaka, K. (2013, Feb). Regulatory mechanisms of kinetochore-microtubule interaction in mitosis. *Cell Mol Life Sci, 70*(4), 559-579. https://doi.org/10.1007/s00018-012-1057-7

Tanaka, T. U., Stark, M. J., & Tanaka, K. (2005, Dec). Kinetochore capture and bi-orientation on the mitotic spindle. *Nat Rev Mol Cell Biol, 6*(12), 929-942. https://doi.org/10.1038/nrm1764

Tapley, E. C., & Starr, D. A. (2013, Feb). Connecting the nucleus to the cytoskeleton by SUN-KASH bridges across the nuclear envelope. *Curr Opin Cell Biol, 25*(1), 57-62. https://doi.org/10.1016/j.ceb.2012.10.014

Trofimova, D., Paydar, M., Zara, A., Talje, L., Kwok, B. H., & Allingham, J. S. (2018). Ternary complex of Kif2A-bound tandem tubulin heterodimers represents a kinesin-13-mediated microtubule depolymerization reaction intermediate. *Nature Communications, 9*(1), 2628. https://doi.org/10.1038/s41467-018-05025-7

Tubbs, A., & Nussenzweig, A. (2017, Feb 9). Endogenous DNA Damage as a Source of Genomic Instability in Cancer. *Cell, 168*(4), 644-656. https://doi.org/10.1016/j.cell.2017.01.002

Vadivel Gnanasundram, S., Bonczek, O., Wang, L., Chen, S., & Fahraeus, R. (2021). p53 mRNA Metabolism Links with the DNA Damage Response. *12*(9), 1446. https://www.mdpi.com/2073-4425/12/9/1446

Vagin, A., & Teplyakov, A. (2000). An approach to multi-copy search in molecular replacement. *Acta Crystallogr D Biol Crystallogr, 56*(Pt 12), 1622-1624.

Vale, R. D., & Fletterick, R. J. (1997). The design plan of kinesin motors. *Annu Rev Cell Dev Biol, 13*, 745-777. https://doi.org/10.1146/annurev.cellbio.13.1.745

Vale, R. D., Reese, T. S., & Sheetz, M. P. (1985). Identification of a novel force-generating protein, kinesin, involved in microtubule-based motility. *Cell, 42*(1), 39-50. https://doi.org/10.1016/s0092-8674(85)80099-4

Viscardi, V., Bonetti, D., Cartagena-Lirola, H., Lucchini, G., & Longhese, M. P. (2007, 2007/08/01). MRX-dependent DNA Damage Response to Short Telomeres. *Molecular Biology of the Cell, 18*(8), 3047-3058. https://doi.org/10.1091/mbc.e07-03-0285

Vleugel, M., Kok, M., & Dogterom, M. (2016). Understanding force-generating microtubule systems through in vitro reconstitution. *Cell adhesion & migration, 10*(5), 475-494. https://doi.org/10.1080/19336918.2016.1241923

Volkov, V. V., & Svergun, D. I. (2003, Jun). Uniqueness of ab initio shape determination in small-angle scattering. *Journal of Applied Crystallography, 36*, 860-864. https://doi.org/10.1107/S0021889803000268

Wagenbach, M., Domnitz, S., Wordeman, L., & Cooper, J. (2008). A kinesin-13 mutant catalytically depolymerizes microtubules in ADP. *Journal of Cell Biology, 183*(4), 617-623. https://doi.org/10.1083/jcb.200805145

Wagenbach, M., Domnitz, S., Wordeman, L., & Cooper, J. (2008, Nov 17). A kinesin-13 mutant catalytically depolymerizes microtubules in ADP. *J Cell Biol, 183*(4), 617-623. https://doi.org/10.1083/jcb.200805145

Wakida, N. M., Botvinick, E. L., Lin, J., & Berns, M. W. (2010, Dec 23). An intact centrosome is required for the maintenance of polarization during directional cell migration. *PLOS ONE, 5*(12), e15462. https://doi.org/10.1371/journal.pone.0015462

Walczak, C. E. (2003, Feb). The Kin I kinesins are microtubule end-stimulated ATPases. *Mol Cell, 11*(2), 286-288. https://doi.org/10.1016/s1097-2765(03)00067-4

Walczak, C. E., Gayek, S., & Ohi, R. (2013). Microtubule-depolymerizing kinesins. *Annu Rev Cell Dev Biol, 29*, 417-441.

Walczak, C. E., & Mitchison, T. J. (1996, 1996/06/28/). Kinesin-Related Proteins at Mitotic Spindle Poles: Function and Regulation. *Cell, 85*(7), 943-946. https://doi.org/https://doi.org/10.1016/S0092-8674(00)81295-7

Walker, R. A., Pryer, N. K., & Salmon, E. D. (1991, Jul). Dilution of individual microtubules observed in real time in vitro: evidence that cap size is small and independent of elongation rate. *J Cell Biol, 114*(1), 73-81. https://doi.org/10.1083/jcb.114.1.73

Wang, H. W., & Nogales, E. (2005, Jun 16). Nucleotide-dependent bending flexibility of tubulin regulates microtubule assembly. *Nature, 435*(7044), 911-915. https://doi.org/10.1038/nature03606

Wang, L., Luong, V. Q., Giannini, P. J., & Peng, A. (2014, Nov 30). Mastl kinase, a promising therapeutic target, promotes cancer recurrence. *Oncotarget, 5*(22), 11479-11489. http://www.ncbi.nlm.nih.gov/pubmed/25373736

Wang, L., Mosel, A. J., Oakley, G. G., & Peng, A. (2012, Nov). Deficient DNA damage signaling leads to chemoresistance to Cisplatin in oral cancer [Research Support, N.I.H., Extramural
Research Support, Non-U.S. Gov't]. *Molecular Cancer Therapeutics, 11*(11), 2401-2409. https://doi.org/10.1158/1535-7163.MCT-12-0448

Wang, W., Cantos-Fernandes, S., Lv, Y., Kuerban, H., Ahmad, S., Wang, C., & Gigant, B. (2017, 2017/07/10). Insight into microtubule disassembly by kinesin-13s from the structure of Kif2C bound to tubulin. *Nature Communications, 8*(1), 70. https://doi.org/10.1038/s41467-017-00091-9

Wang, W., Jiang, Q., Argentini, M., Cornu, D., Gigant, B., Knossow, M., & Wang, C. (2012, Apr 27). Kif2C minimal functional domain has unusual nucleotide binding properties that are adapted to microtubule depolymerization. *J Biol Chem, 287*(18), 15143-15153. https://doi.org/10.1074/jbc.M111.317859

Wang, W., Shen, T., Guerois, R., Zhang, F., Kuerban, H., Lv, Y., Gigant, B., Knossow, M., & Wang, C. (2015, Jul 24). New Insights into the Coupling between Microtubule Depolymerization and ATP Hydrolysis by Kinesin-13 Protein Kif2C. *J Biol Chem, 290*(30), 18721-18731. https://doi.org/10.1074/jbc.M115.646919

Wehland, J., & Sandoval, I. V. (1983, Apr). Cells injected with guanosine 5'-[alpha, beta-methylene]triphosphate, an alpha, beta-nonhydrolyzable analog of GTP, show anomalous patterns of tubulin polymerization affecting cell translocation, intracellular movement, and the organization of Golgi elements. *Proc Natl Acad Sci U S A, 80*(7), 1938-1941. https://doi.org/10.1073/pnas.80.7.1938

Weisenberg, R., Deery, W., & Dickinson, P. (1976). Tubulin-nucleotide interactions during the polymerization and depolymerization of microtubules. *Biochemistry, 15*(19), 4248-4254.

Westermann, S., Wang, H. W., Avila-Sakar, A., Drubin, D. G., Nogales, E., & Barnes, G. (2006, Mar 23). The Dam1 kinetochore ring complex moves processively on depolymerizing microtubule ends. *Nature, 440*(7083), 565-569. https://doi.org/10.1038/nature04409

Westermann, S., & Weber, K. (2003). Post-translational modifications regulate microtubule function. *Nature Reviews Molecular Cell Biology, 4*(12), 938-948. https://doi.org/10.1038/nrm1260

Williams, A. B., & Schumacher, B. (2016, May 2). p53 in the DNA-Damage-Repair Process. *Cold Spring Harb Perspect Med, 6*(5). https://doi.org/10.1101/cshperspect.a026070

Wloga, D., & Gaertig, J. (2010). Post-translational modifications of microtubules. *Journal of Cell Science, 123*(20), 3447-3455. https://doi.org/10.1242/jcs.063727

Wordeman, L., & Mitchison, T. J. (1995, Jan). Identification and partial characterization of mitotic centromere-associated kinesin, a kinesin-related protein that associates with centromeres during mitosis. *J Cell Biol, 128*(1-2), 95-104. http://www.ncbi.nlm.nih.gov/pubmed/7822426

Wordeman, L., Wagenbach, M., & Maney, T. (1999). Mutations in the ATP-binding domain affect the subcellular distribution of mitotic centromere-associated kinesin (MCAK). *Cell Biol Int, 23*(4), 275-286. https://doi.org/10.1006/cbir.1999.0359

Wu, G., Zhou, L., Khidr, L., Guo, X. E., Kim, W., Lee, Y. M., Krasieva, T., & Chen, P. L. (2008, Jul 1). A novel role of the chromokinesin Kif4A in DNA damage response. *Cell Cycle, 7*(13), 2013-2020. https://doi.org/10.4161/cc.7.13.6130

Xiao, H., Verdier-Pinard, P., Fernandez-Fuentes, N., Burd, B., Angeletti, R., Fiser, A., Horwitz, S. B., & Orr, G. A. (2006, Jul 5). Insights into the mechanism of microtubule stabilization by Taxol. *Proc Natl Acad Sci U S A, 103*(27), 10166-10173. https://doi.org/10.1073/pnas.0603704103

Xie, S., & Zhou, J. (2017, 2017-May-04). Harnessing Plant Biodiversity for the Discovery of Novel Anticancer Drugs Targeting Microtubules [Mini Review]. *8*. https://doi.org/10.3389/fpls.2017.00720

Yajima, H., Ogura, T., Nitta, R., Okada, Y., Sato, C., & Hirokawa, N. (2012, Aug 6). Conformational changes in tubulin in GMPCPP and GDP-taxol microtubules observed by cryoelectron microscopy. *J Cell Biol, 198*(3), 315-322. https://doi.org/10.1083/jcb.201201161

Yvon, A. M., Wadsworth, P., & Jordan, M. A. (1999). Taxol suppresses dynamics of individual microtubules in living human tumor cells. *Molecular Biology of the Cell, 10*(4), 947-959. https://doi.org/10.1091/mbc.10.4.947

Zanic, M., Stear, J. H., Hyman, A. A., & Howard, J. (2009). EB1 recognizes the nucleotide state of tubulin in the microtubule lattice. *PLoS ONE, 4*(10), e7585.

Zasadil, L. M., Andersen, K. A., Yeum, D., Rocque, G. B., Wilke, L. G., Tevaarwerk, A. J., Raines, R. T., Burkard, M. E., & Weaver, B. A. (2014, Mar 26). Cytotoxicity of paclitaxel in breast cancer is due to chromosome missegregation on multipolar spindles. *Sci Transl Med, 6*(229), 229ra243. https://doi.org/10.1126/scitranslmed.3007965

Zhang, R., Alushin, G. M., Brown, A., & Nogales, E. (2015, Aug 13). Mechanistic Origin of Microtubule Dynamic Instability and Its Modulation by EB Proteins. *Cell, 162*(4), 849-859. https://doi.org/10.1016/j.cell.2015.07.012

Zhang, R., LaFrance, B., & Nogales, E. (2018). Separating the effects of nucleotide and EB binding on microtubule structure. *115*(27), E6191-E6200. https://doi.org/10.1073/pnas.1802637115 %J Proceedings of the National Academy of Sciences

Zhou, B. B. S., & Elledge, S. J. (2000, Nov 23). The DNA damage response: putting checkpoints in perspective. *Nature, 408*(6811), 433-439. <Go to ISI>://000165429800038

Zhu, C., & Dixit, R. (2012, Oct). Functions of the Arabidopsis kinesin superfamily of microtubule-based motor proteins. *Protoplasma, 249*(4), 887-899. https://doi.org/10.1007/s00709-011-0343-9

Zhu, S., Fisher, L. A., Bessho, T., & Peng, A. (2017, Oct 13). Protein phosphatase 1 and phosphatase 1 nuclear targeting subunit-dependent regulation of DNA-dependent protein kinase and non-homologous end joining. *Nucleic Acids Res, 45*(18), 10583-10594. https://doi.org/10.1093/nar/gkx686

Zimmermann, M., & de Lange, T. (2014, Feb). 53BP1: pro choice in DNA repair. *Trends Cell Biol, 24*(2), 108-117. https://doi.org/10.1016/j.tcb.2013.09.003